Copyright Warning & Restrictions

The copyright law of the United States (Title 17, United States Code) governs the making of photocopies or other reproductions of copyrighted material.

Under certain conditions specified in the law, libraries and archives are authorized to furnish a photocopy or other reproduction. One of these specified conditions is that the photocopy or reproduction is not to be "used for any purpose other than private study, scholarship, or research." If a, user makes a request for, or later uses, a photocopy or reproduction for purposes in excess of "fair use" that user may be liable for copyright infringement,

This institution reserves the right to refuse to accept a copying order if, in its judgment, fulfillment of the order would involve violation of copyright law.

Please Note: The author retains the copyright while the New Jersey Institute of Technology reserves the right to distribute this thesis or dissertation

Printing note: If you do not wish to print this page, then select "Pages from: first page # to: last page #" on the print dialog screen

ABSTRACT

Title of Dissertation: Crystallization Kinetics and Polyblends of Poly(ethylene terephthalate) Recycled from Post-Consumer Beverage Bottles.

Peming (Peter) Hsu, Ph.D. in Chemical Engineering, 1991

Dissertation directed by:
Dr. Basil C. Baltzis
Associate Professor of Chemical Engineering

In order to reduce waste generation, and comply with state and federal laws, plastic beverage bottles are usually undergoing recycling. Poly(ethylene terephthalate) [PET], which is the main component the bottles are made of, cannot be used for manufacturing new food containers, and has to be used for manufacturing other end consumer products. The recycled PET is a cheap material, but its use is problematic due to the low crystallization rates of PET. The present study investigates ways of accelerating PET crystallization by using inorganic carbonate salts as nucleating agents. This study also explores the possibility of forming polymer blends based on recycled PET.

Crystallization kinetics of recycled PET were studied in the presence of Na_2CO_3, $NaHCO_3$, K_2CO_3, Li_2CO_3, $MgCO_3$, $CaCO_3$, $SrCO_3$, $BaCO_3$, $ZnCO_3$, $CdCO_3$, and $PbCO_3$ as nucleating agents. Based on results from Differential Scanning Calorimetry, Optical Microscopy, and thermal stability studies, it has been concluded that among the additives tried, Na_2CO_3 and $NaHCO_3$ are the most effective nucleating agents for recycled PET crystallization. From the results obtained during this study, and from published data on virgin PET crystallization, it has been concluded that the effectiveness of an additive as a nucleating agent for PET can be predicted based on the following general criteria: the additive

must have a good solubility in both water and alcohol and the resulting solution must be basic; the additive should be easily dispersed in the molten PET.

Processability of recycled PET in injection molding has been also investigated in the present study. It has been found that temperatures below $100^{o}C$ can be effectively used with low cycle times. More specifically, it has been found that a mold temperature of $40^{o}C$ can be used to produce amorphous specimens while at $90^{o}C$, and in the presence of either Na_2CO_3 or $NaHCO_3$, crystalline products with good properties can be formed.

Recycled PET has been also used for producing blends with polyester elastomers and low density polyethylene (LDPE). With polyester elastomers the blends resulted in products having a high degree of crystallinity, a good appearance, but relatively poor mechanical properties. With LDPE, blends of very good properties were produced but only in the presence of various ionomers which acted as compatibilizers.

CRYSTALLIZATION KINETICS AND POLYBLENDS OF POLY(ETHYLENE TEREPHTHALATE) RECYCLED FROM POST-CONSUMER BEVERAGE BOTTLES

by

Peming Peter Hsu

Dissertation submitted to the Faculty of the Graduate School

of the New Jersey Institute of Technology in partial fulfillment

of the requirements for the degree of

Doctor of Philosophy

1991

APPROVAL SHEET

Title of Dissertation:

Crystallization Kinetics and Polyblends of Poly(ethylene Terephthalate) Recycled from Post-Consumer Beverage Bottles

Name of Candidate: Peming Peter Hsu
Ph.D. in Chemical Engineering, 1991

Dissertation and
Abstract Approved:

Dr. Basil C. Baltzis — Date
Associate Professor
Department of Chemical Engineering,
Chemistry and Environmental Science

Signatures of other members
of the dissertation committee

Dr. David S. Kristol — Date
Professor
Department of Chemical Engineering,
Chemistry and Environmental Science.

Dr. George Y. Lei — Date
Associate Professor
Department of Chemical Engineering,
Chemistry and Environmental Science

Dr. James M. Grow — Date
Associate Professor
Department of Chemical Engineering,
Chemistry and Environmental Science

Dr. Neil Tai-Shung Chung — Date
Research Associate
Hoechst Celanese

VITA

Name: Peming Peter Hsu.

Degree and date to be conferred: Ph.D., 1991.

Collegiate institutions attended	Dates	Degree	Date of Degree
Chung Yuan University	1974-79	B.S.	1979
Chung Yuan University	1980-83	M.S.	1983
N. J. Institute of Technology	1985-91	Ph.D.	1991

Major: Chemical Engineering.

Publications/Research:

Master's Thesis, Chung Yuan University,
"Use of a Fluidized-bed in Conjunction with an Electrodialysis Machine: The Effects of the Operating Parameters of the Bed on the Limiting Current Density" (1983). Advisor: Dr. J. Y. Lai.

"Morphology and Mechanical Properties of Low Density Polyethylene / Recycled Poly(ethylene terephthalate) Blends containing Compatibilizers", P. P. Hsu, W. T. Wong, First Mini-technical Conference, SAMPE, New Jersey Institute Technology, Newark, N. J., April 1990.

"Crystallization Kinetics of Poly(ethylene terephthalate) Recycled from Post-Consumer Beverage Bottles", P. P. Hsu, Student Post Paper, CAAPCON, Sheraton Centre, New York, NY, 1990.

"Heterogeneous Nucleation of Poly(ethylene terephthalate): Factors Influencing the Nucleating Efficiency of Metal Salts", P. P. Hsu, B. C. Baltzis, Second Mini-technical Conference, SAMPE, New Jersey Institute Technology, Newark, N. J., April 1991.

Positions Held:

Spring 1989 Teaching Assistant
Department of Chemical Engineering, Chemistry and Environmental Science, N. J. Institute of Technology, Newark, New Jersey.

Fall 1986- Graduate Assistant
Fall 1988 Department of Chemical Engineering, Chemistry and Environmental Science, N. J. Institute of Technology, Newark, New Jersey.

Fall 1985- Research Assistant
Spring 1986 Department of Chemical Engineering, Chemistry and Environmental Science, N. J. Institute of Technology, Newark, New Jersey.

5/85-10/85 Project Engineer
Department of Environmental Protection, Trenton, New Jersey.

9/83-9/84 Lecturer
Department of Chemical Engineering, Chung Yuan University, Chung-li, Taiwan

9/81-9/83 Teaching Assistant
Department of Chemical Engineering, Chung Yuan University, Chung-li, Taiwan

5/80-9/80 Process Engineer
Ha Chen Chemical Company, Chung-li, Taiwan

This dissertation is dedicated to

my beloved parents

Chen-Shou and Chin-Chan Hsu

and

my wife

Linshowmay Hsu

ACKNOWLEDGEMENTS

I would like to express my sincere thanks and gratitude to Dr. Basil C. Baltzis, whose guidance and advice has been instrumental to the successful completion of this research work. His constructive criticism and his help with proper organization of the contents of this dissertation have been a valuable experience.

I would also like to thank my Dissertation Committee Members: Drs. David S. Kristol, George Y. Lei, James M. Grow, and Neil Tai-Shung Chung for their invaluable suggestions; the Divisions of Chemical Engineering and Chemistry at NJIT for awarding me various assistantships during my graduate studies; the Center for Plastics Recycling Research at Rutgers University for providing partial financial support to this project.

Special thanks to Drs. Wing Wong, Satish Baliga, K. W. Lem, and Thomas Yu for their invaluable suggestions, and to Dr. K. O'Brien for many helpful discussions and for having given me access to the facilities of his laboratory (DSC, Rheometer, Instron machine and injection molding machine). Special thanks should go to Dr. Neil Tai-Shung Chung for his help with the SEM experiments and for having donated many chemicals. I also wish to thank Dr. G. Lewandowski for encouraging me to finish this dissertation.

Above all, I would like to thank my parents, brothers, sisters, and my wife. Without their encouragement and support I would not have been able to complete this effort. As a small token of my gratitude I dedicate this dissertation to them.

TABLE OF CONTENTS

LIST OF TABLES

LIST OF FIGURES

LIST OF PICTURES

1. INTRODUCTION

An increasing public awareness and concern about environmental issues, and a rising number of state and federal laws have generated technological challenges for achieving reduction, if not prevention, of environmental pollution [97, 98]. One way to reduce pollution is to recycle the waste generated. The topic of this dissertation is related to the recycle of solid wastes. More specifically, it deals with problems of processing recycled polyethylene terephthalate (PET) from post consumer beverage bottles, and with the properties of the recycled material.

Thermoplastic resins such as polyethylene (either low density, LDPE, or high density, HDPE), polyethylene terephthalate (PET), polystyrene (PS), polyvinyl chloride (PVC), and polypropylene (PP) are widely used in consumer product packaging applications. The 1987 USA production of packaging resins consisted of 32% LDPE, 31% HDPE, 11% PS, 10% PP, 7% PET, 5% PVC, and 4% other resins [114].

The problem of municipal solid waste (MSW) generation in the United States is a very serious one. It is estimated that the annual production of MSW is 320 billion lbs, 7% of which consists of plastics [76, 121]. It has been reported [76], that 10% of MSW is currently recycled but only 1% of these recycled solids are plastics. The Environmental Protection Agency (EPA) has set a target for 25% of MSW to be recycled by 1992 [121].

The problem with plastics is that they cannot be landfilled, since they do not easily decompose and their volume creates problems; they cannot be incinerated either, since this is thought to be unsafe [121]. The ideal solution

would be that plastics ending up in the waste streams, are substituted for by biodegradable products. Such products either have not been developed yet, or their cost is still prohibitive for wide usage. The only remaining solution is, for the time being, recycling.

The use of PET in producing consumer beverage bottles was introduced in 1978. Almost immediately, nine states introduced "bottle bills" or deposit laws to prevent littering. In response, industry has introduced processes for reclaiming PET. In fact, 8 million lbs of PET bottles were recycled in 1979 and 150 million lbs in 1988 [121].

Although FDA regulations prohibit the use of recycled plastics for producing food containers, recycled PET can be used in a wide variety of applications in the end-use consumer market. More specifically, recycled PET is used for the production of fibers, engineering plastics, fillers for jackets and cushions, low cost items such as paint brushes and scouring pads, etc. [108, 109]. Recycled PET can be also converted, chemically, back to dimethylterephthalate (its building block), terephthalic acid, and ethylene glycol; furthermore it can be also used for producing aromatic polyols [108, 113]. It has been reported that in 1988 the potential market for recycled PET was 500 million lbs, and was anticipated to increase to 900 million lbs by 1993 [121].

There are other, non-conventional, uses for recycled PET and plastics in general. For example, the Center for Plastics Recycling Research (CPRR) at Rutgers University (which has been the main provider of recycled PET for the study presented in this dissertation), produces mixed, or commingled plastics by an extrusion process. One of the applications is to use these mixed plastics as plastic lumber in nonconstruction applications. In fact, lower-melting plastics in

the mixture form a continuous phase which carries other plastics (such as PET), as well as other contaminants (i.e. paper, metal, glass, and dirt) [97, 98, 121].

Further potential uses for recycled plastics could be found if the physical properties of recycled plastics improved. As an example, PET could be used in the formation of blends with other resins. This is not a trivial problem to solve. For instance, PET is not miscible with either HDPE or LDPE [115, 123]. However, with the use of suitable additives (known as compatibilizers), PET could form partially compatible blends with HDPE and/or LDPE. The possibility of forming such blends is one of the topics considered in this dissertation.

It becomes clear from the foregoing discussion that there are a lot of applications for recycled PET. This is due to the fact that PET (recycled or virgin) has some excellent physical properties. These properties include high flexural modulus, high heat-deflection temperature (HDT), high abrasion resistance, and good solvent resistance [83]. However, PET also presents some serious problems; it is susceptible to melt hydrolysis caused by moisture; PET products in the amorphous phase shrink and warp when heated to the crystallization temperature; plain PET crystallizes very slowly at normal mold temperatures and thus, high mold temperatures and long mold cycles are required in injection molding processing; crystallized PET is very brittle [35]. Hence, the technological challenge is to modify some of the PET properties, and to increase its crystallization rate.

This dissertation focuses on PET recycled from post consumer bottles. The production of these bottles is based on a bottle-grade PET which is primarily amorphous, i.e., it has a very low crystallinity. The first manufacturing step is to produce amorphous preforms by injection molding. The second step involves

heating the preforms, and expanding them under high pressure [83, 106]. It is clear then, that PET coming from bottles recycling is primarily amorphous. If this material is to be used for engineering plastics manufacturing, its crystallinity has to be increased. In fact, the uses of PET resins depends on their crystallinity and average molecular weight [83]. The main objective of this dissertation was to study ways that would increase the crystallinity of recycled PET, and produce the crystalline material at a fast rate.

Achieving an engineering-grade PET from the recycled material is not the end of problems. The material needs to be processed for manufacturing of consumer products, and this is usually done by injection molding. However, the use of this method of processing presents problems due to the slow crystallization rate of PET (virgin or recycled). In fact, it has been reported [41, 99], that the maximum radial growth of PET crystals is 10 μm/min. This growth rate is indeed very slow when compared, as an example, to that of polyethylene which is 5000 μm/min. To increase the crystallization rate, the mold temperature needs to be high. Actually, a mold temperature of at least 130^{o}C is needed for PET processing. Lower temperatures yield products which have a rough surface with poor gloss, and tend to stick to the mold [39, 44]. The requirement for high mold temperatures imposes a number of problems. The mold has to be heated either electrically or by using an oil, and this is not economical. Water cannot be used for heating the mold, since it cannot result in temperatures exceeding 85 to 110^{o}C. Furthermore, the high mold temperatures needed, are also translated to high molding times, i.e. high cycle times for the injection molding process, something which is not economical [94]. To deal with these problems, a possible solution is to increase the crystallization rate of PET so that lower molding temperatures and shorter molding times can be used. One way to increase the

crystallization rate is to use additives which can act as nucleating agents and thus promote crystallization. Various salts were examined in this study as potential nucleating agents for recycled PET.

In summary, the objectives of this study were the following:

- To evaluate various additives (inorganic carbonate salts, in particular) for their ability to act as effective nucleating agents for recycled PET. This evaluation was made based on crystallization kinetics studies. The analysis of data required the development of a software package.

- To investigate if nucleated recycled PET can be processed at mold temperatures below $100^{o}C$. A $90^{o}C$ mold temperature was found to be adequate for producing crystalline recycled PET.

- To examine if recycled PET can form blends with polyester elastomers. These blends were found to have mechanical properties worse than plain recycled PET, but the crystallization rate was enhanced.

- To examine if recycled PET can be blended with polyethylene at the presence of compatibilizers. In some cases the results were very encouraging.

2. LITERATURE REVIEW

Most of the recycled plastic material is from PET beverage bottles [97]. The Plastic Bottle Institute (PBI) publishes the Plastics Recycling Directory [108, 109] which is revised on an annual basis. This directory contains general information about plastics recycling and it also lists brokers, recyclers, and equipment producers involved in the recycling of post-consumer plastic bottles.

Recycling of PET from post-consumer bottles requires some separation steps to be taken first, since PET is not the only material making-up a bottle. In fact, a typical 2-liter beverage bottle contains PET (63 g), a base cup made of high density polyethylene (22g), label and adhesives (5 g), and an aluminum cup (1 g) [108]. Separation of these components can be achieved by a number of flotation and electrostatic systems such as those developed at the Center for Plastics Recycling Research (CPRR) at Rutgers University [97]. Separation of the two main components, PET and HDPE, is necessary because they form immiscible polyblends. Separation of PET and HDPE is not a major problem though, because PET has a density of about 1.37 g/cc, while HDPE has a density of less than 1 g/cc. Hence, water can be used as a separation medium since HDPE floats, while PET sinks in it [97].

The main incentives (legislation measures and wide use of the recycled PET in a variety of consumer product manufacturing), for the interest in PET recycling have been discussed in Chapter 1 (Introduction) of this work. It should be added here that plastics recycling is economical too. As an example, in November 1989, clean recycled PET sold for $0.19 to $0.40/lb (depending upon form and color), while the market price for virgin PET was around $0.60/lb.

Similarly, recycled HDPE sold for $0.20 to $0.33/lb, while the market price for the virgin material was 0.40/lb [97].

As discussed in the Introduction, this dissertation deals with the crystallization kinetics of recycled PET, the effects of nucleating agents on crystallization, and the possibility of forming PET-containing polyblends. The literature on recycled PET is by no means extensive, hence the literature review is mainly based on studies for virgin PET. The main body of this chapter is organized in three sections: Basic Theory of Polymer Crystallization, Studies on PET, and Polyblends with PET.

2.1 Basic Theory of Polymer Crystallization

Crystallization involves two distinct processes: nucleation and crystal growth. Usually, an overall crystallization rate, which is a combination of nucleation rate and crystal growth rate, is used. Measurements of the overall crystallization rate are primarily based on the development of crystallinity in the polymer as function of time. There are different equations relating crystallinity to time, but the one which is most commonly used is due to Avrami [8-10]. This equation has been used in interpreting the kinetic data obtained in this study, and is presented and discussed in detail in Chapter 4. It is an equation involving two parameters: an overall rate constant, and what is known as the Avrami exponent. The equation has been derived based on a theory which considers crystal growth from nuclei in a given number of dimensions until impingement.

The value of the overall crystallization rate constant (and thus, the rate itself), can be affected by either the nucleation rate, or the crystal growth rate. The present study deals with ways to affect (increase) the nucleation rate only.

The value of the Avrami exponent is indicative of the mechanism of crystallization. By mechanism, the growth geometry, the nucleation mode, and the rate-determining step of the crystallization process are implied. Detailed discussions of the factors affecting the mechanism of crystallization have been presented by Wunderlich [126] and Hiemenz [54]. Regarding the growth geometry, these authors have reported that crystal growth can be one-, two-, or three-dimensional. One-dimensional growth leads to rod-shaped crystals, two-dimensional to disk-shaped, and three dimensional growth to spherical crystals. Regarding the nucleation mode, the same authors have reported that it is either athermal, or thermal. Athermal nucleation occurs when all stable nuclei are simultaneously formed at the onset of crystallization. Thermal nucleation occurs when stable nuclei are sporadically (in space and time) created during the crystallization process. Finally, regarding the rate-determining step, the above mentioned authors have reported that it may or may not be diffusion. Crystallization occurs under diffusion control when the rate at which polymer segments deposit on the crystal surface is time dependent. Values for the Avrami exponent, and their implications are listed in Table 4.43.

As mentioned before, the Avrami equation is the one which has been used most. Nonetheless, there are also other equations expressing the development of crystallinity in a polymer as a function of time. These equations usually involve a number of constants significantly higher than the two involved in the Avrami equation. For example, Kim et al. [71] have proposed an equation which relaxes the assumption made by Avrami that crystal growth is a linear function of time; in this case, the three constants involved have a physical meaning. On the other hand, Malkin [80-82] has proposed an equation involving six constants none of which has a physical meaning. This equation involves a detailed temperature

dependence of crystallinity, and has been used in analyzing non-isothermal crystallization data, in conjunction with a heat transfer equation. Under isothermal conditions, Malkin's equation involves two constants, but its form is different from that of Avrami's equation.

2.2 Studies on PET

2.2.1 Crystallization of PET

Crystallization of PET can be achieved by the following processes: 1. Thermal-induced crystallization; this can happen either from the melt [47, 48], or from the glass state [34]. The temperature range for this type of crystallization is between the glass transition and the melt temperature. 2. Solvent-induced crystallization [38, 84], which can occur at temperatures lower than the glass transition temperature. 3. Strain-induced crystallization [112, 131].

In order to determine the overall crystallization rate, a number of parameters can be used [20, 75, 77, 117]. They are the following: 1. Size of polymer crystals; a small size indicates a high nucleation rate; 2. Time ($t_{1/2}$) needed to achieve a 50% crystallinity at a constant crystallization temperature; 3. The overall crystallization rate constant (k) which is one of the two parameters involved in the Avrami equation, discussed in the previous section; 4. The temperature (T_{ch}) at which the maximum of the exothermic peak occurs when crystallization is achieved while heating the polymer from the amorphous state; and 5. The temperature (T_{cc}) at which the maximum of the exothermic peak occurs when crystallization is achieved while cooling the polymer from the melt state.

Since the crystal size is, as mentioned above, an indicator of the overall crystallization rate, a few things need to be discussed regarding the morphology of PET.

It has been reported that the crystal structure of PET is triclinic, and the characteristics (axes, angles, density) of the unit cell have been measured [125].

In 1965, Yamashita [128] was able to obtain single PET crystals during crystallization from a dilute solution. These crystals were parallelogram-shaped lamellae. Depending on the crystallization conditions he also observed twin crystals (lath-shaped lamellae), dendritic crystals, as well as spherulites.

Most investigators have reported that PET forms spherulites. In an interesting study, Murphy et al. [93] have determined that spherulites are formed only if the polymer is melted at a temperature higher than the equilibrium melting temperature (T_m^o). Spherulites of PET have been studied by a number of researchers [66-69, 88]. Keller [66-69] studied microscopically (between crossed polarizers), the spherulites of PET. He reported that they could be recognized by the fourfold symmetry extinction pattern formation, known as Maltese cross. He also reported that individual spherulites were spherical-shaped, but they changed to polyhedral-shaped spherulites at the end of crystallization, when each spherulite is in contact with the ones adjacent to it. Misra et al. [88], concluded -based on light scattering studies- that each spherulite is developed from a rod-like nucleus formed at the onset of crystallization. Formation of irregular PET spherulites (called extraspherulites) have been reported by Jabarin [61] who used elaborate light techniques.

Thermal-induced crystallization of PET is a topic which is of interest in reference to the present study, and has been investigated by a number of

scientists [46-48, 50, 66, 90, 117]. Thermal-induced crystallization can occur either from the amorphous or from the melt state.

Amorphous PET, which is a transparent material, can crystallize when heated between its glass transition temperature ($80^{o}C$), and its melting temperature ($260^{o}C$). The crystallization rate is very slow near both ends of the aforementioned temperature range, and becomes maximum at about $175^{o}C$ [106]. Crystallized PET is an opaque white material.

When molten PET is quenched at a temperature between its glass transition and melt temperatures, stable nuclei are formed which then grow to final crystals. The time needed for the formation of the stable nuclei is called induction time, and can be predicted by using an equation proposed by Vilanova et al. [120].

After the induction time, the development of the crystallinity can be expressed by using the Avrami equation. It has been reported that the Avrami exponent varies form 2 (for crystallization between 90 and $160^{o}C$), to 4 (for crystallization above $230^{o}C$) [30, 45, 62, 63, 101, 126].

Van Antwerpen et al. [117], have proposed an equation for predicting the PET spherulites growth rate. In their expression, the growth rate is a function of the crystallization temperature, and also depends on the number average molecular weight of the polymer. According to these researchers, the PET growth rate at a given temperature, is practically the same for crystallization from the melt and the glassy state. In the same study, it was observed that in the presence of small quantities of liquid additives (0.92 wt% diphenylamine), the maximum growth rate increased. Since the radius of PET spherulites was found to be unaffected, the increased growth rate could not be attributed to an

increased nucleation rate. The increase was explained by arguing that the presence of liquid additives increases the mobility of the polymer molecules, and decreases the glass transition temperature of the polymer.

The maximum growth rate for PET spherulites has been reported to be 120 nm/sec at crystallization temperatures between 175 and 180^{o}C [117], 79 nm/sec at 190^{o}C [16], and 73 nm/sec at about 178^{o}C [99]. The difference can be attributed either to the different number average molecular weight (19,000 in [117] and [99], 13000 in [16]), or to different moisture contents and/or possible presence of organic impurities. The impact of these factors is reviewed in the next subsection.

From non-isothermal crystallization studies, Aharoni [3], has concluded that the temperature at which the maximum of the exothermic peak occurs upon cooling (T_{cc}) is linearly related to the viscosity average molecular weight. The same has been found to be true for the viscosity average molecular weight and melting point, as well as the temperature at which the maximum of the exothermic peak occurs upon heating (T_{ch}).

2.2.2 Moisture Effects and Thermal Stability of PET

PET is known to be a hygroscopic thermoplastic which absorbs moisture from its environment at a rapid rate. As discussed later in this subsection, absorbed moisture affects the thermal stability of PET since it induces hydrolysis at high temperatures.

In a comprehensive study, Jabarin et al. [60] have shown that the maximum (or equilibrium) moisture content of PET increases with the relative humidity of the environment in which PET is placed. Furthermore, they have

shown that at a given relative humidity, the equilibrium moisture content of PET increases with temperature, while it is independent of the molecular weight of the polymer. The same study has concluded that absorbed moisture has significant effects on the physical and mechanical properties of PET. For example, it has been found that the glass transition temperature decreases proportionally to the moisture content, something which indicates that water has a plasticizing effect on PET. The mechanical properties of PET samples have been found to deteriorate after prolonged storage in a humid environment. For this reason, in the present study all PET samples were vacuum dried before any experiments were performed. It should be mentioned that moisture may enhance the crystallization rate of PET, if crystallization occurs from the glassy state [64].

The presence of moisture in PET results in thermal instability. This is due to the fact that, especially in the melt state, water molecules attack and cleave ester linkages. As a result, PET undergoes hydrolytic degradation that is, its molecular weight is drastically reduced. In fact, it has been reported [106], that the molecular weight is directly proportional to the moisture content of the PET resin.

Because of the effects of water on the stability of PET, it has been recommended [59], that- even dried- PET is heated to temperatures higher than the melting point, under a nitrogen rather than air atmosphere. In fact, Lawton [75] has demonstrated, by using gel permeation chromatography, that the molecular weight of dried PET remains practically unchanged before and after heating the sample in a Differential Scanning Calorimeter under a nitrogen environment. This has been also the approach followed in the experiments performed within the context of the present study.

The PET resin is synthesized by a stepwise melt polymerization process [19]. This process involves transesterification, prepolymerization, and end polymerization steps. During synthesis, a large number of side reactions take place in the mixture [104]. Therefore, a quite complex mixture of side products is formed. These side products include acid- and vinyl-end group formations, acetaldehyde, diethylene glycol (DEG), and water [72]. The effect of water has been already discussed. Other side products though, may affect not only the thermal stability of the polymer, but its mechanical properties (strength, stiffness), and its chemical resistance as well. For example, the presence of 1% DEG in the final product reduces the polymer crystallinity. As a result, the melt point is lowered and the heat resistance of the polymer reduced [72].

2.2.3 Modification of PET Crystallization Characteristics

The crystallization rate of PET is relatively slow, and is unfavorable for using injection molding to manufacture consumer products. An increased crystallization rate reduces both molding time and temperature for injection molding. For these reasons, promotion of the PET crystallization rate has been of considerable interest to industry. To achieve this goal, nucleating agents and plasticizers have been simultaneously added to PET [30, 31, 33, 44, 52, 95, 96, 125]. The use of plasticizers increases the growth rate of spherulites, while nucleating agents are additives which induce heterogeneous nucleation by increasing the density of sites where PET can nucleate.

As has been already mentioned, moisture in PET has a plasticizing effect [60, 64]. In industrial applications the following substances have been used as plasticizers for PET: epoxidised soybean oil (i.e., products such as Drapex 68 and Estabex 2307); neopentyl glycol dibenzoate [32, 125]; and aliphatic glycol

phthalate [96]. Addition of plasticizers results in an increased mobility of the polymer chains, and a reduced glass transition temperature. As a result, the overall crystallization rate increases. It has been also reported [89], that carbon dioxide can act as plasticizer for PET. This occurs though at high pressures (50 atm), and may not be economical for industrial applications.

Since this study investigated the characteristics and promotion of recycled PET crystallization at the presence of additives, an extensive literature search was performed on heterogeneous nucleation in general, and nucleating agents for (virgin) PET in particular.

The mechanism of heterogeneous nucleation is not well understood. It is believed though, that nucleation occurs more easily in the presence of foreign particles when these particles reduce the free energy barrier which needs to be overcome in order to form nuclei having the required critical size. Many aspects of heterogeneous nucleation have been discussed in studies concerning polypropylene rather than PET. As an example, one can refer to the studies published by Binsbergen [20-24]. This investigator has suggested that good nucleating agents are insoluble in the polymer. A nucleating agent was classified as good, when it resulted in spherulites diameters equal to 10 to 20 % of the diameter values for the plain polymer. In general, the nucleating effect of an additive can be qualitatively judged by the decrease in size and increase in number of spherulites.

The mechanism of nucleation has been reported in some studies [12-15, 37, 43, 77-79, 87], to be chemical in nature. These studies were on PET and bisphenol-A polycarbonate (PC). The idea here is that the additive is not the actual nucleating agent. The actual nucleating agent is a product of a reaction

between the additive and the polymer. This mechanism has been proposed for PET crystallized in the presence of sodium salts of aromatic carboxylic acids, and is discussed later in more details.

The fact that solid additives promote PET crystallization, is well known. In the study of Van Antwerpen et al. [117], which was referred to earlier in a different context, it has been reported that small quantities (0.2 wt%), of solid additives led to a decrease in the maximum radius of PET spherulites. The same authors have argued that effective nucleating agents reduce the maximum radius of spherulites so drastically that even light-scattering methods cannot be used to accurately measure these radii. In the same study, it has been suggested that the crystallization half-time should be used in determining the effectiveness of nucleating agents. Legras [77] has argued that half-time measurements are not reliable either, and that the temperatures of the exothermic peaks (T_{ch} for heating; T_{cc} for cooling), should be used to judge the nucleating effectiveness of additives. Lawton [75] has reported that the presence of nucleating agents affects T_{cc} more than T_{ch}, hence T_{cc} is a more accurate indicator of the nucleating efficiency of additives.

PET synthesis requires the presence of a catalyst. Commonly used catalysts are based on Mn, Zn, Pb, Cd, Mg, Ca, Ce, Co, Li, Na, and Sb [75, 62]. Catalyst remnants, which are impurities in the PET resin, can act as nucleating agents for PET crystallization. As an example, Lawton [75] has demonstrated that an antimony based catalyst increases the PET crystallization rate. In fact, he has derived an expression which indicates that the PET crystallization rate is proportional to the antimony catalyst concentration. At the same time, his expression indicates that the crystallization rate decreases proportionally to the concentration of diethyl glycol, which is a side product from the synthesis of PET.

Inorganic compounds are widely used in industry as nucleating agents for PET. A variety of inorganic oxides and salts, such as antimony oxide (Sb_2O_3), sodium borohydride ($NaBH_4$), sodium nitrite ($NaNO_2$), $CaCO_3$, Na_2CO_3, $NaHCO_3$, K_2CO_3, Li_2CO_3, $(NH_4)_2HPO_4$, $Na_2HPO_4(12H_2O)$, $MgSO_4(12H_2O)$, NaCl, Na_2SiO_3, Na_2SO_4, even talc have been patented as promoters of fast PET crystallization [1, 29-31].

Groeninckx et al. [46], have reported crystallization, from the glassy state, of PET mixed with 0.2-0.3 vol% of talc, kaolin, silicon dioxide, or titanium dioxide. The particle size of the additives was about 1 μm. According to their findings, talc and titanium dioxide were the most effective nucleating agents.

Hydroxides of aluminum, copper(II), nickel(II), indium, barium, magnesium, cobalt (II), and lanthanum have been used by Aharoni [2, 3], as nucleating agents for PET. The conclusion from these studies was that nonalkali metal hydroxides capable of releasing water within the range of PET processing temperatures, are effective nucleating agents. It has been argued that the increased crystallization rates can be attributed to either a localized severe hydrolysis, or a localized supercooling of PET in the vicinity of the hydroxide particles. In either case, the effect is from the water released from the hydroxide. In these studies, alkali metal hydroxides were not considered, since it known that they induce severe hydrolytic degradation of the polyester.

Przygochi et al. [102], have measured PET crystallization kinetics in the presence of TiO_2, CaO, MgO, $BaSO_4$, SiO_2, and Al_2O_3 as nucleating agents. It was found that, with all additives, the crystallization rate was different (to a varying degree) from that of plain PET.

Use of nucleating agents at high concentrations may decrease rather than increase the crystallization rate. This was the case in a study on crystallization of polyester in the presence of MgO, reported by Szekely-pecsi et al. [111]. In this study, high MgO, concentrations yielded a large number of hydroxo-carboxylate complexes with magnesium ion. These complexes have a low mobility due to the coordination of the Mg ion within the complex, and this reduced mobility of polyester chains resulted in a crystallization rate decrease.

Organic salts is another large category of additives used as nucleating agents for PET in industrial applications. This category includes salts of hydrocarbon and polymeric carboxylic acids, alkali metal salts of ethylene terephthalate oligomers, alkali metal salts of benzoic acid [11, 39, 42, 44, 52, 96], and amine carboxylate which has been reported to act not only as a nucleant, but as a plasticizer as well [52].

Although the mechanisms of crystal nucleation are not well understood, it was believed for years that nucleating agents are insoluble, and unreactive substrates. There are more and more studies now which suggest that solubility and a chemical reaction may be involved, and may play a key role for nucleation. Some of these studies are for PET.

Legras et al. [77-79], studied the crystallization of PET in the presence of additives such as sodium o-chlorobenzoate, sodium p-chlorobenzoate, sodium benzoate, sodium p-hydroxy-benzoate, and disodium terephthalate. These investigators have suggested that a reaction occurs between the salt and the molten polyester chains. This reaction produces species having ionic end groups, and these species are the actual nucleating agents for PET. More specifically, it has been suggested that in these studies the actual nucleating

agent was the sodium-PET salt (Na-PET). Comparing the various additives tested in their studies, these authors suggested that the solubility of the additive in the (molten) polymer is an important factor. More soluble additives lead to an increased probability for reaction, and thus, formation of the actual nucleant.

Using IR spectroscopy, Dekoninck et al. [37], have been able to confirm the suggestions regarding chemical nucleation. Using sodium o-chlorobenzoate (which had been tried by Legras et al.), they have been able to identify chains having sodium carboxylate ends. They have also shown that these ionic chains precipitate in the PET melt as ionic aggregates, and have concluded that these precipitated aggregates act as nuclei for crystallization. They have also reported that the efficiency of an additive as a nucleant may decrease as the processing time increases. This is due to the fact that sodium in particular, when given enough time, forms disodium terephthalate which is not an effective nucleant. These authors have proposed a series of reaction steps, to describe the overall phenomenon.

If a chemical reaction is involved, one should be thinking along the lines of homogeneous rather than heterogeneous nucleation. Further confirmation of the homogeneous nature of PET nucleation with sodium-organic acid salts has been given by Garcia [43]. This author has concluded that the key factors determining the efficiency of an additive for PET nucleation, are: the alkalinity of the salt, its solubility and ability to disperse in PET, and finally, the purity and thermal stability of the additive.

Other substances that have been tried as nucleating agents for PET, involve some sodium type ionomers and some polymers. Among ionomers, Surlyn S8920 [40], AClyn 285A [4], and polyethylene ionomer [11], have been

reported as highly efficient nucleating agents. These claims have been made by the producers of the ionomers. Among polymers, low density polyethylene (1.5% to 4%), linear low density polyethylene (3%), conventional polypropylene (3%), low-molecular-weight isotactic polypropylene (3%), polyamide-6,6, and Poly(butylene terephthalate) have been used as nucleating agents for PET [25, 33, 65, 88, 95, 130].

2.2.4 Recycled PET from Beverage Bottles

It is clear from the foregoing discussion that there is a very large number of studies on PET. It should be emphasized that all these studies are for virgin PET. Recycled PET, recycled from beverage bottles in particular, is a material quite different from virgin PET. Some differences between recycled and virgin PET have been reported by Muller [92], in the only published study on crystallization of PET recycled from beverage bottles. The lack of sufficient information on recycled PET was the reason for undertaking the present study.

It should be mentioned here that beverage bottles are manufactured from pellets of virgin PET as follows: First, the bottle preform is produced by injection molding at a mold temperature of 5^{o}C in order to have an amorphous material. The preform is heated to a temperature just above the glass transition temperature of PET, and expanded under high pressure into a cold bottle mold. Because of this expansion, part of the amorphous material gets crystallized. In fact, some biaxially oriented crystals are obtained and as a result, the bottle is transparent and has good mechanical properties (e.g. strength) [92, 106]. Due to this type of processing, the thermal and mechanical history of PET in bottles is drastically different from that of PET in the original pellets. This is what makes the two types of PET (recycled and virgin), quite different.

2.3 Polyblends of PET and Polyethylene

It is well known that blending of two polymers can lead to the formation of an economical material possessing good mechanical properties. Recycled PET could then be used for producing polyblends. This is not a trivial problem though, since PET is incompatible with a good number of other polymers. Incompatible polymers when blended, lead to products of poor quality (e.g. they fracture easily) mainly due to phase separation.

The presence of multiple phases in immiscible blends result in injection-molded parts which may show opacity, swirl, and other surface imperfections. Furthermore, poor dispersion of the components of a blend affects the physical and mechanical properties of the final material. In fact, poor dispersion can severely affect the ductility of the material [17, 116]. To alleviate the problems of immiscible blends one could try to increase the interfacial area of the two components (phases) by using blending techniques based on flow processing. Another way is to improve adhesion between the two phases by using compatibilizers [17]. Methods to improve adhesion between two immiscible phases have been reviewed by Xanthos [127].

Recycled PET has been used for producing polyblends with high density polyethylene (HDPE) in the presence of elastomeric substances acting as compatibilizers [27, 35, 115]. It has been shown that some elastomers can improve the impact strength, the ductility, and toughness of PET/HDPE blends.

Linear low density polyethylene (LLDPE) has been used for producing blends with virgin PET [e.g., 123]. There is no study on the formation of blends of recycled PET with low density polyethylene. This subject is studied in the present dissertation.

3. MATERIALS AND EXPERIMENTAL METHODS

In this chapter, the materials used in this study are briefly discussed, and a detailed discussion is offered regarding the methodologies followed in the experimental procedures.

3.1 Materials

In this study, the objective was to study the properties of PET recycled from post-consumer bottles. This material was provided by the Center for Plastics Recycling Research at Rutgers University. For comparison purposes one more, commercially available, recycled PET grade was examined, as well as a grade of virgin PET. The appearance of those materials (as received), and their suppliers are listed in Table 3.1.

The crystallization kinetics of recycled PET were studied for pure (plain) PET as well as PET with inorganic carbonate salts which acted as nucleating agents. The salts used in this study as potential effective nucleating agents are listed in Table 3.2.

Recycled PET was also studied for its ability to be used in the production of blends which could have improved properties. The properties of blends of PET with either polyester elastomers or polyethylene were examined. The types of polyethylene and elastomers used, are listed in Table 3.1. Blends of PET with polyethylene were formed either with PE and PET alone or PE, PET and another additive which could act as compatibilizer for the blend. The substances used as compatibilizers were either ionomers (listed in Table 3.1) or coupling agents (listed in Table 3.3).

3.2 Sample Preparation

The materials were dried in vacuum oven before they were used for sample preparation. Drying was necessary due to the fact that PET is prone to hydrolysis at high temperatures. PET was dried at a moderate temperature of 110^{o}C over a period of 15 hours. Polyethylene, elastomers, and other additives were dried at 80^{o}C for at least 12 hours. The temperature of 80^{o}C was selected in order to avoid decomposition of the various chemicals.

Samples were prepared either by mixing desired quantities of each compound (to achieve a certain composition), in a Brabender Plastic-Corder Torque mixer, or by injection molding. Injection molding was used mainly to prepare specimens for testing the mechanical properties. For all other studies, the samples were prepared mainly by mixing.

3.2.1 Mixing

Mixing of PET with various additives was done under a nitrogen atmosphere. The Brabender mixer [26] was operated at 280^{o}C and 40 RPM. Figure 3.1 shows a schematic representation of the mixing process. The polymer (PET) was first added to the mixing head area and allowed to mix for about 4 minutes. Samples (reference samples) were taken at that instant, and about 1 minute later the additive was introduced. Mixing of PET and additive was allowed to occur typically for 1 minute and then a number of samples were taken; each sample was used in a different measurement. The samples from the mixer (irregularly shaped melts) were placed on a cold plate and pressed to form a film. These films were then used in the actual experiments. Typically, 80 grams of PET were needed each time in the Brabender mixer.

3.2.2 Injection Molding

A Van Dorn 50, single screw, injection molding machine was used to prepare the specimens (bars) for the flexural and tensile tests. The machine was equipped with a Hunkar process controller [56, 57]. The conditions under which the injection molding machine was operated are shown in Table 3.4. Typically, 800 grams of material were needed for the production of a batch from the injection molding machine. Each batch consisted of 40 specimens (2 specimens per cycle). The shape and the dimensions of the specimens (determined by the type of mold used), were such that the ASTM D638 method could be used for the tensile measurement, and the ASTM D790 method for the flexural measurement [5, 6].

3.3 Experimental Plan

In order to study the crystallization kinetics of recycled PET, with or without nucleating agents, the procedure was as follows:

First, the thermal stability of nucleating agents was studied by thermogravimetric analysis.

Second, PET, alone or with nucleating agents was introduced in a Brabender mixer, and samples were produced as described in section 3.2.1. These samples were used for studying the thermal properties of the material via Differential Scanning Calorimetry (DSC), its intrinsic viscosity via rheological studies, and its texture via optical microscopy. Specific procedures for the methods mentioned above are described in subsequent subsections.

Third, PET and its additive (nucleating agent) were subjected to injection molding to produce specimens as described in section 3.2.2. These specimens

were used for testing the mechanical properties, and shrinkage of the product. Some specimens were cut to smaller pieces which were used in determining the melt viscosity of the material. In some cases, small parts (actually the end parts) of the specimen were used in further DSC studies.

The plan described above, is shown schematically in Figure 3.2.

PET was mixed with polyester elastomers to form blends. The two components were subjected to injection molding and the produced specimens were tested for their mechanical properties. Small parts of the molded specimens were used in DSC for determining the thermal properties of the blend. The procedure is depicted schematically in Figure 3.3.

PET was also used in forming blends with low density polyethylene (LDPE) with or without compatibilizers (ionomers or coupling agents). The procedure is shown in Figure 3.4, and is essentially identical with the procedure followed for PET/polyester elastomer blends. Specimens of PET/LDPE blends were subjected to an additional test. Namely, specimens of the blends were fractured by tensile force and the surfaces at the points of fracture were examined by Scanning Electron Microscopy (SEM).

3.3.1 Thermogravimetric Analysis (TGA) for Nucleating Agents

All carbonate salts which were used in this study as potential nucleating agents for recycled PET, were subjected to thermogravimetric analysis in order to check their thermal stability. A Perkin-Elmer Thermogravimetric Analyzer (TGA-7) was used to monitor the weight loss of the salts as a function of temperature. The temperature was increased at a scan rate of 20 °C/min, from 60 to 300°C during the experiment. This test was made in order to insure that the nucleating

agents do not decompose in the temperature range which was used in this study for PET processing and the PET crystallization kinetics determination.

3.3.2 Differential Scanning Calorimetry (DSC)

In order to study the crystallization kinetics and the thermal properties of recycled PET the method of differential scanning calorimetry (DSC) was employed [51].

A Perkin-Elmer DSC-2 instrument was used [100]. Temperature calibration was carried out by using standard samples of pure indium (In) and zinc (Zn).

A dried sample (3-14 mg) was used for each experiment. The sample was encapsulated in an aluminum pan which was then introduced in a special cell in the instrument. The atmosphere of the cell consisted of nitrogen only, in order to prevent any possible oxidation of the material in the sample. Every sample was first melted (around 280^{o}C) in the aluminium pan and kept in the liquid phase for at least 5 minutes before an actual experimental run started. This was done in order to eliminate effects of the past thermal and mechanical history of the material.

The instrument gives an output (thermogram) which indicates energy changes in the sample as a function of either temperature (nonisothermal conditions), or time (isothermal conditions). The areas under the peaks of a thermogram, were measured by using a Lasico L20M compensating polar planimeter. The areas under the peaks of nonisothermal scans were converted ("translated") to energy (enthalpy), by comparison to the area under a peak of a DSC curve produced by a standard sample of indium. This reference area corresponds to 28.45 J/g or 6.8 cal/g [100]. Exothermic peaks in a nonisothermal

DSC thermogram of a polymer can be thus converted to crystallization enthalpies, while endothermic peaks can be used to determine the energy (enthalpy) required for melting the polymer crystals.

DSC studies were made for isothermal and nonisothermal crystallization.

3.3.2.1 Isothermal Crystallization

Isothermal crystallization studies were made at temperatures between 170 and 240^{o}C. The melted sample (see section above) was quenched to the desired temperature at a rate of 320 ^{o}C/min. The quenching rate was selected from a range available in the DSC instrument.

The area of the peak appearing in the isothermal DSC thermogram was measured as a function of time. These data were then fitted to the Avrami equation (as discussed in detail in Chapter 4), in order to determine the kinetic parameters for the crystallization process.

The isothermally crystallized sample was then quenched to 100^{o}C and subsequently heated to about 280^{o}C at a rate of 20 ^{o}C/min. From the nonisothermal thermogram the melting temperature was determined as well as the enthalpy required for melting the polymer crystals. This enthalpy was divided by 120 J/g which is the enthalpy required for melting 100% crystalline PET [105]. The resulting number indicated the crystallinity of the PET sample.

3.3.2.2 Nonisothermal Crystallization

For nonisothermal crystallization studies the sample underwent two heating and two cooling scans. The sample was introduced in the DSC instrument, and the system was allowed to equilibrate at 60^{o}C which was the

minimum temperature the DSC equipment could operate in the controlled mode. The first heating scan was from 60 to 280^{o}C at a rate of 20 ^{o}C/min. The melted sample was left at 280^{o}C for at least 5 minutes for the reasons discussed in section 3.3.2. The first cooling scan consisted of either cooling the sample at a rate of 20 ^{o}C/min or quenching it at a rate of 320 ^{o}C/min. In either case the sample was cooled from 280 to 60^{o}C. The second heating scan was a repetition of the first, while the second cooling scan was from 280 to 60^{o}C at a rate of 20 ^{o}C/min, i.e. the second cooling scan never involved quenching of the sample.

The thermograms from the nonisothermal DSC runs were used to determine the thermal properties of the material, as discussed in detail in Chapter 4 of this dissertation.

3.3.3 Intrinsic Viscosity Measurements

The intrinsic viscosity was determined based on kinematic viscosity measurements as follows. A mixture of phenol (60 wt%) and 1,1,2,2 tetrachloroethane (TCE, 40 wt%) was used as solvent for the polymer. The kinematic viscosity of the solvent (η_S) was measured by a Cannon-Ubbelohde dilution viscometer (model T5). The polymer samples (dried) were accurately weighed and dissolved in solvent to obtain solutions of concentration between 0.5 to 0.8 g/dl. The solutions were allowed to cool to room temperature and then filtered before viscosity measurements. The kinematic viscosity of the solution (η_p) was measured by the viscometer mentioned above. This was done at different concentrations (up to 1 g/dl) of polymer in the solvent. All measurements were made at 25.00±0.02 ^{o}C. The intrinsic viscosity ($[\eta]$) was determined by using the following equation [19, 54]:

$$\frac{\eta_{sp}}{C} = [\eta] + K' [\eta]^2 C \qquad \text{(Huggins equation)}$$

$$\frac{\ln \eta_r}{C} = [\eta] - K'' [\eta]^2 C \qquad \text{(Kraemer equation)}$$

where $\eta_r = \eta_p / \eta_s$; $\eta_{sp} = \eta_r - 1$; C is the concentration of the polymer in the solution (g/dl).

The two equations above represent straight lines when the quantities in the left hand side are plotted versus C. The intercept of both lines is the intrinsic viscosity.

The intrinsic viscosity values can be used to determine the viscosity-average molecular weight (m_v) of PET, via the Mark-Houwink [54] equation:

$$[\eta] = K_W (m_v)^a$$

where, $k_W = 2.37 \times 10^{-4}$ dl/g and $a = 0.73$ [53].

3.3.4 Methods for Optical Microscopy Studies

Thin films of the polymer were observed under the microscope. These films were prepared as follows. About 10 mg of dried polymer material were sandwiched between two glass plates one of which was maintained at 290°C. The material was allowed to melt at that temperature under nitrogen atmosphere, and then squeezed between the two plates. About 5 minutes later the plates were brought to room temperature and the film was formed.

A Bristoline optical microscope was used. The microscope was equipped with a rotating and a fixed analyzer, and a hot-stage mounted to the metal platform of the instrument. The hot-stage was connected to a temperature indicator. A Nikon Microflex AFX-II camera was connected to the eyepiece of the microscope and was used to record (photograph) the texture of material under observation.

Optical microscopy was used in observing the whole process of isothermal and non-isothermal crystallization of a given sample.

For non-isothermal studies, a thin film (see first paragraph) was placed on the hot-stage mounted to the microscope. The hot-stage was heated by using an electrical resistance, to about 300^{O}C. The heating rate from 60 to 300^{O}C was 13 ^{O}C/min. Subsequently, the power supply was cut and the hot stage was allowed to cool down to about 200^{O}C before heating started again. The cooling rate was found to be about 12 ^{O}C/min from 300 to 260^{O}C, and 8.5 ^{O}C/min from 260 to 200^{O}C. Typically, each sample underwent two heating and two cooling scans. The first cooling scan was to about 200^{O}C because it was observed that all processes (crystallization, phase transition) are completed before the temperature drops below 200^{O}C. During the second (or final, if there were more than two) cooling scan, the sample was allowed to reach room temperature, and at that point its texture was photographed. The process of heating and cooling was monitored by eye observation under the microscope and the recorded observations (changes and at what temperature they occurred), are reported in Chapter 4. It should be added that the heating and cooling rates are comparable to the controlled rate (20 ^{O}C/min) used in the DSC studies and thus, the results from the two studies can be easily compared.

About 10 mg of the material was placed between two glass plates, and then put on a hot-stage maintained at 300^{o}C. When the material was melted, the plates were pressed so that the material formed a thin film between them. The sample was then transferred on another hot-plate which was maintained at a desired temperature (values from 215 to 240^{o}C) for crystallization. It was held there for about 2 hours, and then transferred to a plate held at room temperature. A few hours later, the material was observed under the microscope and its texture was photographed. The hot-stages were kept under a nitrogen atmosphere.

3.3.5 Melt Viscosity Measurements

A highly automated Kayeness Capillary Rheometer was used in order to measure the melt viscosity of various types of PET. Measurements were made at 260, 270, and 280^{o}C for various values of shear rate which ranged from 10 to 3000/sec. For the measurements, around 15 g of material were needed. This material came from injection molding. Actually the bars used for mechanical tests were subsequently cut to smaller pieces and used for the melt viscosity determination. The procedure for measuring the melt viscosity followed the one described in the manual accompanying the instrument [7]. The values of melt viscosity were given on the printout from the computerized rheometer.

3.3.6 Shrinkage Determination

Bars of the polymer material produced by injection molding (at 40 and 90^{o}C) were annealed in a vacuum oven at 130^{o}C for at least 40 hours. The length (distance between the center points of the two ends) was measured before and after annealing. The purpose of this test was to examine whether the material can be used at high temperatures without compromising the product

quality. If an amorphous polymeric material spends a prolonged time at temperatures above its glass transition temperature, it can crystallize. High temperatures may result in warping due to polymer relaxation while the induced crystallinity may result in shrinkage of the product. The test was performed since molded PET is not necessarily completely crystalline. Part of the product may be amorphous.

3.3.7 Mechanical Tests

Mechanical properties of PET and PET blends were tested in an Instron Floor Model TT-B [58], testing instrument. The stress-strain curves were obtained at constant rate according to ASTM methods. For tensile testing, method D638 was used, while for flexural testing, method D790 was followed [5, 6].

4. RESULTS AND DISCUSSION

4.1 Nucleation of PET by Inorganic Carbonate Salts

Inorganic carbonate salts were investigated in this dissertation, for their ability to act as effective nucleating agents for poly(ethylene terephthalate) (PET) crystallization. The choice of inorganic over organic salts was made because organic salts sometimes decompose to liquid compounds at high temperatures. These liquid compounds may act as plasticizers and therefore, affect the crystallization process.

Some physical properties of the salts tried as nucleating agents are listed in Table 4.1 while properties of the cations of the salts are listed in Table 4.2. These physical properties are from data published in the literature [122].

Polyethylene terephthalate was classified into V-PET (aV-PET, bV-PET), R-PET (aR-PET, bR-PET), and G-PET (aG-PET, bG-PET). V-PET represents the material donated by the Eastman Kodak company. R-PET and G-PET represent the clear and green types of poly(ethylene terephthalate) obtained from recycled post-consumer beverage bottles. The physical properties of V-PET are listed in Table 4.3. R-PET and G-PET were donated by the Center for Plastics Recycling Research (CPRR) at Rutgers University. The properties of R-PET are listed in Table 4.4 [36]. Properties of PET were studied on the material as was received (this is indicated by the prefix b), as well as after thermal and mechanical processing of the original material (this is indicated by the prefix a).

4.1.1 Studies on Nucleating Agents.

The inorganic carbonate salts were scanned by a Thermogravimetric Analyzer (TGA) from 60 to 300^{o}C at a scan rate of 20 ^{o}C/min.

Figures 4.1 through 4.10 and Table 4.5 show the results of TGA studies on nucleating agents. The weight loss (solid line), and first derivative of weight loss (broken line) versus temperature were recorded on the plots.

Figure 4.1 shows that the weight of Li_2CO_3 (Melting Point: 723^{o}C) did not change at all.

Figure 4.2 shows that the weight of Na_2CO_3 (M.P.=857^{o}C) decreased as the temperature was increased from 90 to 180^{o}C. The maximum rate of weight loss was at 175^{o}C. The total weight loss of Na_2CO_3 was 15%.

Figure 4.3 shows that the weight of $NaHCO_3$ decreased as the temperature was increased from 108 to 250^{o}C. The weight loss rate exhibited peaks at 110 and 215^{o}C. The total weight loss of $NaHCO_3$ was 36.4%. As indicated in Table 4.1, sodium bicarbonate decomposes at the temperature of 270^{o}C before it melts. The reaction can be represented as follows:

$$2\,NaHCO_{3(s)} \xrightarrow[270^{o}C]{} Na_2CO_{3(s)} + CO_{2(g)} + H_2O_{(g)}$$

Weight	168	106	44	18
wt%		63.1	26.2	10.7

The weight loss from carbon dioxide and water for this system is 36.9%, and the residual Na_2CO_3 corresponds to 63.1%. Therefore, the weight loss indicated by TGA is obviously the result of carbon dioxide and water loss. The first small temperature peak could be attributed to the absorbed water in sodium bicarbonate. The second large temperature peak is the dominant one for this process, and corresponds to the chemical decomposition, i.e., loss of carbon

dioxide and water. It should be noted that the 215°C finding is different from the 270°C value reported in the literature (Table 4.1).

Figure 4.4 shows that the weight of K_2CO_3 (M.P.=891°C) decreased as the temperature was increased from 95 to 245°C. The maximum rate of weight loss was at 200°C. The total weight loss of K_2CO_3 was 9%.

Figure 4.5 shows that the weight of $MgCO_3$ decreased as the temperature was increased from 60 to 300°C. The total weight loss of $MgCO_3$, between 60 and 175°C, was 1.6%, and between 175 and 300°C, 6%. Decomposition of $MgCO_3$ occurs at 350°C according to Table 4.1. It is speculated then, that the maximum rate of weight loss occurs at a temperature higher than 300°C.

Figure 4.6 shows that the weight of $CaCO_3$ (M.P.=520°C) changed insignificantly as the temperature was increased from 60 to 300°C. The total weight loss of $CaCO_3$ was 0.03%.

Figure 4.7 shows that the weight of $SrCO_3$ (M.P.=1700°C) changed insignificantly as the temperature was increased from 60 to 300°C. The total weight loss of $SrCO_3$ was 0.026%.

Figure 4.8 shows that the weight of $BaCO_3$ (M.P.=1740°C) changed insignificantly as the temperature was increased from 102 to 125°C. The total weight loss of $BaCO_3$ was 0.19%. The peak in the weight loss rate (at 115°C) is attributed to loss of moisture.

Figure 4.9 shows that the weight of $ZnCO_3$ changed as the temperature was increased from 60 to 300°C. The total weight loss of $ZnCO_3$, between 60 and 205°C, was 0.83%, and between 205°C and 300°C, 3.8%. Decomposition of $ZnCO_3$ occurs at 300°C according to Table 4.1.

Figure 4.10 shows that between 134 and 300^{o}C the weight of $PbCO_3$ decreased by 0.92%. As indicated in Table 4.1, decomposition of $PbCO_3$ occurs at 315^{o}C.

The weight losses of Li_2CO_3, $CaCO_3$, $SrCO_3$, and $BaCO_3$ are very small (0.03-0.2%), when these materials are heated up to 300^{o}C, something which implies that insignificant water is released. Furthermore, it should be noted that the melting temperatures of these compounds are well beyond 300^{o}C.

$NaHCO_3$, Na_2CO_3, and K_2CO_3 showed significant weight losses between 90 and 270^{o}C.

$MgCO_3$, $ZnCO_3$, and $PbCO_3$ showed insignificant weight losses at temperatures below 200^{o}C. After 200^{o}C, the weight loss of these carbonates increased and it is anticipated that a maximum rate of weight loss should be observed beyond 300^{o}C.

The decomposition temperatures (reported in the literature), for $ZnCO_3$, $PbCO_3$, and $MgCO_3$ are 300, 315, and 350^{o}C, respectively. Nonetheless, the TGA analysis has indicated a relatively substantial weight loss even at temperatures below 300^{o}C. These changes could be attributed to the fact that some decomposition occurs even in that temperature range. Decomposition would lead to the formation of oxides. The oxide of magnesium in water is basic, while those of zinc and lead are amphoteric [122]; as a result, the physical properties of these nucleating agents are expected to change when decomposition starts to occur, in an environment which contains moisture.

4.1.2 Intrinsic Viscosity (I.V.) Studies

Values for the intrinsic viscosity (I.V.) of R-PET with or without nucleating agents are listed in Table 4.6. An I.V. value divided by the I.V. value of bR-PET is defined as the reduced I.V. Reduced I.V. values are also listed in Table 4.6. As can be seen from the table, mechanically processed R-PET (i.e., aR-PET), as well as R-PET nucleated with K_2CO_3, $SrCO_3$, $CaCO_3$, $MgCO_3$, $CdCO_3$, and $BaCO_3$, have reduced I.V. values higher than 90%. The reduced I.V. values for R-PET nucleated with $ZnCO_3$ and $PbCO_3$ are below 75%. R-PET nucleated with Na_2CO_3 or $NaHCO_3$ has reduced I.V. values between 75% to 90 %.

The I.V. values of R-PET, G-PET, and V-PET with Na_2CO_3, $CaCO_3$, $PbCO_3$ are listed in Table 4.7. The I.V. of PET with nucleating agents decreased as the weight percentage of the agent increased. This could be attributed to the water content of nucleating agents, since water could cause a reduction of average molecular weight due to hydrolysis of ester (R_1COOR_2) linkages in PET.

According to Thermogravimetric analysis, the water content of $NaHCO_3$ and Na_2CO_3 is 10.7 wt% and 15 wt%, respectively. Therefore the reduced I.V. of $NaHCO_3$ and Na_2CO_3 nucleated PET samples decreased to 79.3 and 83.2%, respectively. As indicated by the weight losses shown in Table 4.5, the water content of $CaCO_3$, $SrCO_3$, $BaCO_3$, and $MgCO_3$ is small; consequently, the reduced I.V. decreased only slightly to 91, 91.5, 90.2, and 90.9%, respectively.

The reduced I.V. of PET with K_2CO_3 nucleant is 91.9%. When examining injection molded PET specimens with K_2CO_3 nucleant, coarse particles were seen. These K_2CO_3 particles, which were not broken during processing, released water locally in certain areas. Therefore, the effect of hydrolysis was reduced.

$CdCO_3$ decomposes at 500^{o}C as indicated in Table 4.1. The reduced I.V. of $CdCO_3$ nucleated PET was 90.6% indicating minor effects of hydrolysis when processing occurs at temperatures up to 270^{o}C.

$ZnCO_3$ and $PbCO_3$ decompose at 300, and 315^{o}C, respectively to form amphoteric oxides. The reduced I.V. of $ZnCO_3$ and $PbCO_3$ nucleated PET are 69.9 and 62.2%, respectively, indicating that both amphoteric oxides caused serious molecular breakdown, probably due to hydrolysis and/or reduction [91].

The reduced I.V. of aR-PET, aG-PET and aV-PET decreased because of chain scission due to shear and possibly, hydrolysis.

4.1.3 Melt Viscosity Studies

Melt viscosity values (η_m) for PET with or without nucleating agents are listed in Tables 4.8 through 4.25. Measurements were made at different temperatures and shear rates.

The melt viscosity (η_m) of PET with or without nucleating agents as a function of shear rate is shown in Figures 4.11 through 4.30.

As can be seen from Table 4.8, at 270^{o}C the melt viscosity of bV-PET (before shear) is higher (as expected), than that of aV-PET (after shear). The melt viscosity of R-PET and G-PET showed similar results as that of V-PET. The lower the average molecular weight of a polymer, the lower is its melt viscosity. The shearing process breaks down the polymer molecular chain. Therefore, the melt viscosity decreases after any mechanical processing. The melt viscosity of R-PET and G-PET was found to be slightly higher than that of V-PET. These results comply with the findings from I.V. studies shown in Table 4.7. Regarding temperature, the higher it is, the lower is the melt viscosity. The results shown in

Figures 4.11, 4.12, 4.13 and Table 4.8, show the types of behavior described above.

The addition of small amounts (0.5 wt%) of a nucleating agent in PET should somewhat affect the melt viscosity. Figures 4.14 through 4.24 are logarithmic plots showing the viscosity of PET with 0.5% nucleating agents at 270^{o}C. Except for $MgCO_3$, $PbCO_3$, and $ZnCO_3$ nucleated PET samples, all other nucleated PET samples exhibited a linear power law relationship for viscosity. Table 4.26 shows the power law parameters for melts of PET (with or without nucleating agents) at temperatures of 260, 270, and 280^{o}C. The value of power law index was found to be about 0.8 for plain PET as well as nucleated PET. When the value of power law index approaches unity, the behavior of viscosity is like the one expected of Newtonian fluids. The data indicate that the higher the Na_2CO_3 content in R-PET, the higher is the melt viscosity. The viscosity of 1.0 wt% of Na_2CO_3 in R-PET (1369 poise at 1000/sec) was higher than that of aR-PET (1295 poise at 1000/sec). This indicates that a high Na_2CO_3 content in PET can affect the mobility of the polymer chains and greatly increase the melt viscosity, thereby causing serious processing problems.

It is interesting to observe the difference between PET/$NaHCO_3$ and PET/Na_2CO_3, from Figures 4.25 to 4.27, and 4.28 to 4.30. For PET/Na_2CO_3, one can say that the melt viscosity dependence on shear rate is roughly the same at all temperatures. In contrast, for PET/$NaHCO_3$ the melt viscosity is less dependent on shear rate at high temperatures. This seems to be more pronounced in the case of V-PET.

Most melt viscosities of PET with 0.5 wt% nucleating agents were found to be less than that of plain PET as shown in Table 4.27. The melt viscosity dropped

considerably for PET nucleated with $NaHCO_3$, $MgCO_3$, $ZnCO_3$, and $PbCO_3$. On the contrary, an increase in melt viscosity was observed in the cases of V-PET/$CaCO_3$, V-PET/$SrCO_3$, and R-PET/$CdCO_3$. Furthermore, the melt viscosity did not change in the cases of V-PET/Na_2CO_3, V-PET/$BaCO_3$, G-PET/$BaCO_3$, R-PET/$CdCO_3$, and V-PET/$CdCO_3$.

To summarize, even small amounts (as low as 0.5 wt%), of nucleating agents in PET, affected the melt viscosity. Nucleating agents like $MgCO_3$, $PbCO_3$, and $ZnCO_3$ which decomposed upon heating, caused a larger decrease in melt viscosities of PET because they probably initiated a molecular chain breakdown. The melt viscosity of PET after processing decreased due to molecular chain breakdown caused by shear. Increasing contents of nucleating agents like 1% Na_2CO_3 in PET, causes higher flow resistance; therefore the viscosity increased.

4.1.4 Differential Scanning Calorimetry (DSC) Studies

DSC can operate under either isothermal or nonisothermal conditions. Typical nonisothermal thermograms are shown in Figure 4.34 for heating, and 4.35 for cooling. Typical isothermal thermograms are shown in Figure 4.52.

4.1.4.1 Reproducibility of Thermal Data

The question addressed in this section is whether the thermal properties depend on processing time and/or source (batch) of sample. Before measurements, PET was processed at 280^{o}C and 40 RPM in a Brabender mixer. The thermal properties were subsequently obtained via DSC. As shown below, the data were reproducible regardless of time of processing and source of sample.

4.1.4.1.1 Isothermal crystallization:

Three samples of aV-PET weighing 10.00, 8.37, and 4.98 mg, respectively, were cut from injection molding bars. The samples were isothermally scanned on the DSC at 200^{o}C and the results were examined for reproducibility. Table 4.28 shows values based on data from the DSC recorder. Results shown in Table 4.29, and Figures 4.31 and 4.32 indicate that when values from all samples are considered, the relative error in $t_{1/2}$, t_{max}, n, and k was 3, 3.4, 3, and 4%, respectively.

The 10.00 mg sample was scanned nine times (three times at 200^{o}C) on the DSC to examine the possibility of thermal degradation of polyethylene terephthalate. The sample pan was then opened and its contents were examined. Absence of any visible change in color indicated that the sample had not degraded in spite of multiple thermal scans. Figure 4.32, and Table 4.29 show that the data were highly reproducible. The relative error of $t_{1/2}$ (1.93±0.02) and n (2.64±0.03) was found to be 1% (in the case of 10.00mg sample).

4.1.4.1.2 Nonisothermal scan:

Three samples of aV-PET weighing 10.00, 8.37, and 4.98 mg respectively, which were used for isothermal scans, were also scanned non-isothermally at a rate of 20 ^{o}C/min from 280 to 60^{o}C. The results from these tests were examined for reproducibility.

As an example, the 10.00 mg sample was subjected to heating, cooling, and annealing for about 100 minutes. The value of T_{cc} was 174^{o}C in the first run, and 174.5^{o}C in the last run. Figure 4.33 shows that the data were highly

reproducible. From Table 4.30, it can be seen that the relative error in the average T_{cc} values was 0.6%.

R-PET was mixed in a Brabender mixer for a total time of 15 minutes at 280^{o}C and 40 RPM under a nitrogen atmosphere. The values of T_{cc} for samples from the same batch, mixed for different amounts of time in the Brabender are shown in Table 4.31. The average value of T_{cc} was found to be 181.1±1.8 ^{o}C for the whole range of mixing times.

Table 4.32 shows the T_{cc} values of R-PET from different batches, for the case where the samples were mixed for the same amount of time (about 5 minutes) in the Brabender mixer. The average value of T_{cc} was found to be 181.1±1.9 ^{o}C.

To summarize, the relative error in the T_{cc} value of V-PET and R-PET is within 1% irrespective of the batch from which samples are taken and mixing time. This is an expected result which confirms that the method of thermal testing (DSC) is a reliable one for getting thermal properties of polymers.

4.1.4.2 Nonisothermal Scan

4.1.4.2.1 Thermogram, T_g, T_{ch}, T_m, T_{cc}

Under thermal treatment, semi-crystalline polymers principally crystallize between glass transition temperature, T_g, and melting temperature, T_m. Below T_g, the thermal energy is inadequate to allow much relative motion between chains. The location of T_g depends on the rate of cooling [54]. Therefore, the range of crystallization for plain polyethylene terephthalate is theoretically from 80 to 260^{o}C. Crystallization occurs at a significant rate between 110 and 230^{o}C, while the maximum rate occurs at a temperature of 175^{o}C [106].

While slowly heating a an amorphous PET sample from below T_g to above T_m, the following transitions were typically obtained: 1) endothermal peak for glass transition, T_g; 2) exothermal peak indicating a change from the amorphous phase to crystalline phase, T_{ch}; 3) endothermal peak for melting transition, T_m. While slowly cooling a PET sample from melt to room temperature, an exothermal peak corresponding to a change from the isotropic phase to the crystalline phase, was obtained. If the heating or cooling rate is too fast, the exothermal peak might be absent because of the slow crystallization rate of PET. The scan rate chosen in this study was 20 ^{o}C/min.

The temperature at which the peak of the exotherm occurs is designated as T_{ch} for the heating scan and as T_{cc} for the cooling scan. These temperatures also indicate where the maximum rate of crystallization occurs [3, 77]. T_{ch} is mostly affected by the molecular mobility, whereas T_{cc} is mostly affected by the rate of nucleation. Plasticizers favor the rate of crystal growth, and nucleating agents enhance the nucleation rate. Therefore, the T_{ch} decreases in the direction of T_g with increasing rate of crystal growth, and the T_{cc} increases in the direction of T_m with increasing nucleation rate [27].

The crystallization rate is controlled by two factors: rate of crystal growth and nucleation rate. Therefore, a fast crystallization rate could be achieved by adding plasticizers and/or nucleating agents. The value of T_{cc}, however, is the index of the effectiveness of nucleation. A high value of T_{cc} indicates a better nucleating agent.

It has been found in this study that the rate of PET crystallization is very slow. In fact, when samples were cooled at a very high rate, i.e. quenched, the material was amorphous. In some experiments, samples were quenched from

melt to 60^{o}C at a rate of 320 ^{o}C/min in the DSC. Under these conditions, the polymer chains are frozen, and do not have enough time to crystallize. The fact that the material was in the amorphous phase became evident from the following observations:

(1) When the DSC pan was opened after quenching, the entire polymer was transparent, something which happens only if the material is amorphous.

(2) Material held for 3-5 minutes at 280^{o}C under nitrogen atmosphere, and then quenched in the air (not the DSC) to room temperature, appeared transparent even when observed under an optical microscope.

(3) The thermogram of DSC indicated no sign of crystallization during quenching at 320 ^{o}C/min.

(4) When the quenched sample was heated, it showed a crystallization exotherm after T_g, which has been termed as "cold crystallization". This phenomenon is easily explained; as the mobility of frozen chains is activated after T_g, the molecules rearrange to a lower energy state. Therefore, the process is exothermic.

4.1.4.2.2 Polyethylene Terephthalate

4.1.4.2.2.1 R-PET

The thermal properties of R-PET, as received chips (bR-PET), and samples sheared in the Brabender mixer (aR-PET), are listed in Table 4.33. The thermograms of aR-PET and bR-PET are shown in Figure 4.34 for the heating scan, and Figure 4.35 for the cooling scan. The T_{cc} of aR-PET (181^{o}C) is higher than that of bR-PET (168^{o}C), indicating that the crystallization rate of aR-PET was

higher than that of bR-PET. The breakdown of molecules of aR-PET caused by mechanical shearing, increased the crystallization rate of aR-PET. The crystallization rate of aV-PET (T_{CC}=173°C) is slight higher than that of bR-PET (T_{CC}=168°C) because of the different history of the materials. In fact, while aV-PET is a virgin material subjected only to shear (Brabender mixer or extruder) during this study, bR-PET has a certain degree of crystallinity because of the various processing steps involved in the manufacturing and recycling of bottles.

Some experiments were made with R-PET which had not been subjected to mechanical shearing (woR-PET), in order to see if the extent of thermal treatment time has any impact on the thermal properties. A test tube containing the material under a nitrogen atmosphere, placed in a constant temperature oil bath (280^{O}C). At different instants of time a sample was taken out of the tube, quenched, and its thermal properties were measured. The results are shown in Table 4.34. From Tables 4.33 and 4.34 one can see that the T_{CC} value of bR-PET is almost the same as that of woR-PET which is thermally treated for a short period of time. The results also indicate that the T_{CC} value of woR-PET increases with the thermal treatment time, probably due to molecular breakdown caused by hydrolysis.

Samples of amorphous aR-PET were annealed at 100^{O}C for 30 minutes, and 130^{O}C for 3 minutes. Each sample was quenched and then scanned from 60 to 280^{O}C at a rate of 20 ^{O}C/min. The thermal properties of annealed R-PET are listed in Table 4.35. Figure 4.36 indicates that the areas under the exotherm and endotherm of R-PET annealed at 100^{O}C for 30 minutes were approximately equal. This implies that the material was primarily amorphous. However, this is not the case for aR-PET annealed at 130^{O}C even for three minutes only, as can be concluded from the following. Figure 4.36 also shows the heating thermogram

for aR-PET (annealed at 130^{o}C) at a scan rate of 20 ^{o}C/min. An small endothermal peak (at 145^{o}C) is present instead of the exothermal peak. This endothermal peak can be attributed to the melting of small crystals that were formed at the annealing temperature [131]. This indicates that the sample had developed a high degree of crystallinity at the annealing period.

The values of thermal properties of PET were affected by the scan rate of DSC. Table 4.36 indicates that the value of T_{cc} for aR-PET decreases with increasing scan rate. This is due to the fact that a slow scan rate allows for a longer crystallization time. Although the results reported here are for T_{cc} only, all thermal properties are affected by the scan rate. Therefore, values for thermal properties are meaningless if the scan rate at which they were measured is not reported. Furthermore, if comparisons are to be made, the same scan rate has to be used in all experiments. A scan rate of 20 ^{o}C/min was chosen for this study.

It should be mentioned that it was difficult to determine the T_g of PET from the first heating scan if the material was dried under vacuum at high temperature. In fact, samples dried under vacuum at 120^{o}C, had a thermal behavior similar to that of samples annealed at 130^{o}C. Samples dried over a long period of time, develop a high degree of crystallinity. Since T_g is a property of amorphous polymer, the high crystallinity of dried PET made it difficult to determine T_g from the first heating scan since, the curve around T_g in a thermogram was smooth [104, 110]. During the second heating, the curve around T_g in the thermogram, showed clearly an endothermic peak. This was due to the fact that before the second heating, the polymer was held at 280^{o}C for five minutes and then quenched to room temperature to obtain an amorphous structure. Therefore, the T_g from the second heating scan was reliable and invariant among samples which had undergone the same heat treatment.

4.1.4.2.2.2 V-PET

Some physical properties of Kodapak PET (7352) polyesters, supplied by Eastman Kodak Company are listed in Table 4.3. The Kodapak PET (7352) is used to produce bottles for carbonated beverages, distilled spirits, and cosmetics. Kodapak PET was supplied as opaque 0.1-in., cube-cut pellets. The opacity is derived from the high level of crystallinity that develops during solid-state polymerization.

The thermal properties of V-PET, as received chips (bV-PET) and shear treated by injection molding (aV-PET), are listed in Table 4.33. DSC thermograms of aV-PET are shown in Figure 4.37 for heating scan, and Figure 4.38 for cooling scan.

The T_{cc} of aV-PET (173^{o}C) is clearly higher than that of bV-PET (162^{o}C). Therefore, the crystallization rate of aV-PET is higher than that of bV-PET. The breakdown of molecules of aV-PET caused by mechanical shearing, increases the crystallization rate for aV-PET as was also discussed previously for the case of R-PET.

The thermograms of bV-PET shown in Figures 4.34 and 4.35 indicate a broad crystallization peak, something which implies that crystallization of bV-PET is slow [95].

Figures 4.37 and 4.38 show a total of seven scans for the same sample (aV-PET). In Figure 4.37, the first heating scan (indicated as run 1) is somewhat different from other heating scans, such as runs 3, 5, and 11. The values of T_g (74^{o}C) and T_{ch} (138^{o}C) from run 1, are less than those obtained from other runs (80 and 141^{o}C, respectively), because of the different thermal history. The higher

melting temperature (252^{o}C) in run 1 is attributed to the crystal structure that is drastically affected by high pressure at injection molding. Run 3 corresponds to the heating scan after the cooling scan from 280 to 60^{o}C at a rate of 20 ^{o}C/min (run 2). In this run, there was no detectable exothermic peak due to the fact that the polymer crystallized while being cooled slowly from 280 to 60^{o}C (during run 2). All PET samples showed a similar thermal behavior. Runs 5 and 11 are the heating scans for a sample which was quenched from 280 to 60^{o}C at a scan rate of 320^{o}C/min. Most of the reliable data for PET are obtained from quenched samples. Figure 4.38 depicts the same T_{cc} in all runs because of the fact that they have the same thermal history. During the cooling scan, the sample was held at 280^{o}C for five minutes, and cooled from 280 to 60^{o}C at a scan rate of 20 ^{o}C/min. Figure 4.33 shows the reproducibility of T_{cc} values for aV-PET obtained from different batches of aV-PET.

4.1.4.2.2.3 G-PET

The thermal properties of G-PET, as received chips (bG-PET) and shear treated at Brabender mixer (aG-PET), are listed in Table 4.33. Thermograms of aG-PET and bG-PET are shown in Figure 4.39 for heating scan and in Figure 4.40 for cooling scan. The T_{cc} of aG-PET (182^{o}C) was higher than that of bG-PET (153^{o}C), indicating that the crystallization rate of aG-PET was higher than that of bG-PET. This can be attributed to the breakdown of molecules of aG-PET due to mechanical shearing. These observations are the same with those made for V-PET and R-PET.

4.1.4.2.3 R-PET with Nucleating Agents

The thermal properties of R-PET with nucleating agents (inorganic salts of carbonate) are listed in Table 4.37. A DSC scan rate of 20 ^{o}C/min was used. The weight percentages of nucleating agents were controlled at 0.3, 0.5, and 1.0%.

The crystallization rate is theoretically improved by adding nucleating agents which increase the value of T_{cc} or lower the value of T_{ch}.

For aR-PET, the value of T_{cc} was found to be 181^{o}C, while that of T_{ch} 138^{o}C. All nucleating agents, except $CaCO_3$, $SrCO_3$, and $BaCO_3$, improved the crystallization rate to some extent. The value of T_{cc} increased with the concentration of nucleating agent in R-PET, except in the cases of $CaCO_3$, $SrCO_3$, and $BaCO_3$.

When a polymer is subjected to heating, it melts at a temperature T_m. The value of T_m may vary with the method used to measure it. On the other hand, the equilibrium melting temperature, T_m^o [55, 117, 120, 131] is constant for a given polymer. The value of T_m^o is always higher than that of T_m. Upon cooling, a polymer exhibits an exothermal peak (corresponding to crystallization), the maximum of which occurs at a temperature T_{cc}. The value of T_{cc} is lower than that of T_m, indicating that there is a hysteresis in the crystallization process. In fact, the difference between T_m^o and T_{cc} (designated as ΔT_c) is known as the supercooling of the polymer melt [126, 120]. Supercooling is the result of the lack of stable nuclei for crystallization to get initiated [74]. From the foregoing discussion, it becomes clear that an additive is an efficient nucleating agent for a polymer, if its presence in the polymer melt causes a drop in the ΔT_c value. Values for ΔT_c of R-PET nucleated with various inorganic carbonate salts are listed in Table 4.37 and presented in graphical form in Figure 4.41.

Another indicator of the effectiveness of an additive as a nucleating agent is ΔT_{ch} which is defined as the difference between the values of T_{cc} and T_{ch} [52, 118]. Actually, ΔT_{ch} indicates the temperature range over which crystallization can occur. A polymer melt which is cooled at a certain (constant) rate, spends more time in the crystallization temperature range if ΔT_{ch} is large. This is important especially for slowly crystallizing polymers such as PET. Hence, an additive which causes ΔT_{ch} to increase can be viewed as an efficient nucleating agent. Values for ΔT_{ch} of R-PET nucleated with various additives are listed in Table 4.37 and also shown in Figure 4.42.

Based on the T_{ch}, T_{cc}, ΔT_c, and ΔT_{ch} values, the results of this study indicate that sodium carbonate (Na_2CO_3) is the most effective nucleating agent for R-PET. The results also indicate that $CaCO_3$, $SrCO_3$, $BaCO_3$, Li_2CO_3, and $CdCO_3$ are not effective nucleating agents for R-PET. Furthermore, using higher concentrations of ineffective nucleating agents does not lead to a sufficient improvement of the overall crystallization rate.

4.1.4.2.4 G-PET with Nucleating Agents

The thermal properties of G-PET with nucleating agents (inorganic carbonate salts) are listed in Table 4.38. A DSC scan rate of 20 ^{o}C/min was used. The weight percentage of nucleating agents was controlled at 0.5 wt%.

The results are very similar to those obtained for R-PET. For aG-PET, the T_{cc} value was found to be 182^{o}C, while that of T_{ch} 136^{o}C. As the results shown in Table 4.38 indicate that all additives used, except $CaCO_3$ and $SrCO_3$, resulted in some decrease in the T_{ch} value, and some increase in the T_{cc} value. These results indicate that -theoretically, at least- all tried additives , except $CaCO_3$ and $SrCO_3$, improve crystallization to a certain extent.

As discussed in the previous section, ΔT_{ch} and ΔT_c values can be used as indicators of the effectiveness of an additive as a nucleating agent. Values of ΔT_{ch} and ΔT_c for G-PET nucleated with various carbonate salts are listed in Table 4.38 and plotted in the graphs of Figures 4.43 and 4.44.

The results indicate that sodium carbonate is the most effective nucleating agent for G-PET. The results also indicate that $CaCO_3$, $SrCO_3$, $BaCO_3$, and $CdCO_3$ are not at all effective nucleating agents for G-PET.

4.1.4.2.5 V-PET with Nucleating Agents

The thermal properties of V-PET with nucleating agents are listed in Table 4.39. A DSC scan rate of 20 ^{o}C/min was used. The weight percentage of nucleating agents was controlled at 0.5 wt%.

The results for V-PET are practically the same as for R-PET and G-PET. Based on T_{cc} and T_{ch} values, one could say that all additive tried, improve the crystallization rate. Values for ΔT_{ch} and ΔT_c are also plotted in Figures 4.45 and 4.46.

As in the cases of R-PET and G-PET, the results indicate that sodium carbonate is the most effective nucleating agent for V-PET. Base on the results, one can also conclude that $CaCO_3$, $SrCO_3$, $BaCO_3$, K_2CO_3, and $CdCO_3$ are not at all effective nucleating agents for V-PET.

4.1.4.2.6 Discussion

The rate of crystallization of bR-PET, bG-PET, and bV-PET is slow according to the analysis of thermal properties. The crystallization rate of PET after processing was faster than that of PET before any processing treatment.

The breakdown of molecules of PET caused by mechanical shearing, increased the crystallization rate for PET.

The thermal properties of aV-PET were found to be similar to those of bR-PET. This can be attributed to the fact that the two materials had a similar processing history.

The results indicate that for any type of PET, Li_2CO_3, $CaCO_3$, $SrCO_3$, $BaCO_3$, and $CdCO_3$ are ineffective nucleating agents, while the most effective ones are Na_2CO_3 and $NaHCO_3$. The thermal properties of PET nucleated by Li_2CO_3, $CaCO_3$, $SrCO_3$, $BaCO_3$, and $CdCO_3$ are similar to these of plain PET.

$PbCO_3$ and $ZnCO_3$ should be the good nucleating agents according to the analysis of thermal properties. However, as discussed later in Optical Microscopy Studies, $PbCO_3$ and $ZnCO_3$ actually proved to be ineffective nucleating agents for PET.

4.1.4.3 Isothermal Crystallization

The DSC has two cells in which the sample pan and reference pan were placed. The polymer, as a thin film, was placed in the sample pan, and nothing was placed in the reference pan. The isothermal crystallization process in the DSC cell involves quenching the PET sample from the $290^{o}C$ isotropic state to a crystallization temperature, and allowing crystal formation after an induction period.

The crystallinity of the polymer is proportional to the heat evolution of the polymer during isothermal crystallization. The isothermal curve obtained from DSC is a plot of the rate of heat evolution, dQ/dt, as a function of time. Therefore, the heat of crystallization can be obtained by measuring the area under the

thermogram peak [85]. In order to calculate the integral, the baseline of the curve should be determined first. If the induction time of crystallization is longer than the time needed for the system to reach thermal equilibrium, the baseline is simple and calculable, whereas in other cases the baseline is difficult to determine. The system is said to attain thermal equilibrium when the polymer reaches the isothermal temperature. The induction time is the time for obtaining a stable nucleus at steady state.

Before actual DSC runs were made with PET samples, control runs were made with the sample pan being empty. The pan was heated at 290^{o}C. Subsequently, the temperature for the machine was set at a temperature T_c which was lower than 290^{o}C. If a PET sample were present on the pan, this change would imply that the melt is quenched from 290^{o}C to the temperature T_c. The output ("thermogram") was recorded. Such outputs for different T_c values are shown in Figure 4.47. Figure 4.48 shows the features of a typical output. For this diagram, x_1 represents the time for machine transition; x_2 represents the time needed for the machine to reach temperature T_c; x_3 represents the time needed for the cell of DSC to reach temperature T_c; x_4 represents the time needed for the polymer to reach temperature T_c (thermal equilibrium). The time span for the system to reach thermal equilibrium equals the time interval from 0 to x_4. The time span for the system to reach thermal equilibrium, depends on the isothermal temperature T_c. The higher the isothermal temperature, the smaller is the time span for thermal equilibrium of system (as shown in Figure 4.47).

Another series of control runs were made by having only the reference pan in the DSC cell. The sample pan was taken out of the cell. DSC curves for these control experiment are shown in Figure 4.49. The time span needed for the system to reach thermal equilibrium for T_c = 443 K or 503 K was found to be the

same whether the sample pan was present (Figure 4.47) or removed (Figure 4.49). It was concluded that the presence of the sample pan does not affect the time needed for the system to reach thermal equilibrium.

Figure 4.50 shows the DSC curves for the case where the sample pan contained 3 mg of PET. The solid line is from the recorded data, while the broken line is the assumed baseline. The arrow indicators represent the polymer crystallization peak. The induction time appeared before the system reached thermal equilibrium. Furthermore, at 413, 433, and 443 complete crystallization occurred before thermal equilibrium.

Figure 4.51 shows the details of a typical DSC curve for isothermal crystallization. The time designated as t_0 is the induction time. Actual DSC curves for aR-PET are shown in Figure 4.52. From the diagrams shown in this figure, one can see that as the temperature for isothermal crystallization decreases, it becomes more and more difficult to identify the onset of the exothermic (crystallization) peak. This is due to the fact that at low temperatures thermal equilibrium is not completely attained before crystallization starts. Therefore, one should select the crystallization temperature, depending on the polymer and nucleating agents. The crystallization temperature chosen in this study was primarily between 200 and 230^{o}C.

4.1.4.3.1 Kinetics of Crystallization

The Avrami Equation

In general, the development of crystallinity in isothermal crystallization can be represented by the following equation:

$$1\text{-}x(t) = \exp[-kt^{n}] \qquad 4.1$$

Equation 4.1 is commonly called the Avrami equation. The fraction of the material which is in crystallized form, is represented by x(*t*), and is also known as reduced crystallinity; k is the rate constant; n is called the Avrami exponent, and depends on the diffusion, nucleation, and growth of the polymer.

The time needed to achieve a reduced crystallinity of 50% is represented by $t_{1/2}$. Setting $x(t_{1/2})$ to be 0.5, Equation 4.1 yields:

$$t_{1/2} = [\ln 2/k]^{1/n} \qquad 4.2$$

t_{max} represents the time needed to attain a maximum rate of crystallization. Therefore,

$$d^2x(t)/dt^2 = 0 \qquad \text{at } t=t_{max} \qquad 4.3$$

Setting the second derivative of x(t) from the Avrami equation, to be zero, one gets

$$t_{max}=[(n-1)/nk]^{1/n} \qquad 4.4$$

From Equations 4.2 and 4.4, one gets

$$t_{max}/t_{1/2} = [(n-1)/n/\ln(2)]^{1/n} \qquad 4.5$$

The ratio of t_{max} to $t_{1/2}$ is less than 1, if the Avrami exponent, n, is less than 3.2588. This implies that a 50% crystallinity is achieved at a time beyond the one where the crystallization rate is maximum. Figure 4.53. shows the ratio of t_{max} to $t_{1/2}$ as a function of the Avrami exponent, n.

Khanna and Taylor [70] found that the validity of the Avrami equation is better, if k is substituted by $k_n^{(1/n)}$. The modified Avrami equation becomes:

$$1\text{-}x(t) = \exp[-(k_n t)^n] \qquad 4.6$$

where k_n is the modified rate constant.

4.1.4.3.2 Data Processing and Development of Computer Code

The DSC was interfaced with a digital computer for data acquisition. A continuous curve (see Figure 4.54), was interpolated through the data points which were acquired by the computer. This curve was obtained as follows: a Fast Fourier transformation (FFT) was performed, and the high frequencies were deleted since they were attributed to noise. Subsequently, the remaining frequencies were used for an inverse FFT in order to go to the time domain, and the curve was generated. The software for the analysis of data as described above, was developed in the course of the present study, and is given in the Appendix.

The DSC records the rate of heat release (*dQ/dt*) which comes from the exothermal process associated with crystallization of the polymer. The integral of dQ/dt equals the heat evolution from the polymer, and it approximately equals the enthalpy of crystal formation. The enthalpy of formation of crystals is a measure of crystallinity. The weight fraction of crystalline material x(t) at time t, has been calculated according to the equation:

$$x(t) = \frac{\int_0^t (dH/dt)dt}{\int_0^\infty (dH/dt)dt} \qquad 4.7$$

One can also write:

$$x(t) = \frac{A_X(t)}{A_\infty} \qquad 4.8$$

Crystallization starts at time t=0, and ends at time t=∞. $A_X(t')$ is the area under the DSC curve from t=0 to t=t', and A_∞ is the total area under the crystallization curve. A_∞ is also called the equilibrium degree of crystallization.

One can see that x(t) is a measure of the extent of crystallization at time, t; x(t) is also called reduced crystallinity which is the ratio of the instantaneous crystallinity to the total crystallinity that can be attained under the experimental conditions. Therefore, the range of x(t) is between 0 and 1.

In order to calculate $A_X(t)$ and A_∞, one needs to determine the time at which crystallization starts (t_0 in Figure 4.51). One also needs to determine the baseline of the isothermal crystallization exotherm. The area under the curve can be then calculated and thus, x(t) versus t data are generated. In this study, x(t) versus t data (for x values between 0.1 and 0.6), were regressed to the Avrami equation and thus, the values of k and n were obtained. Parameter k is like an inverse Arrhenius type function of temperature, i.e.

$$k=k_0\exp[E_k/RT] \qquad 4.9$$

where E_k is a parameter resembling activation energy.

When the modified Avrami equation is used, k_n is a function of temperature, given as

$$k_n=k_{n0}\exp[E_n/RT] \qquad 4.10$$

where now E_n is like an activation energy.

In the literature [66, 70], the time needed for achieving 50% crystallinity, i.e. $t_{1/2}$, has been expressed as a function of temperature, as follows

$$(1/t_{1/2})=k_t\exp[E_t/RT] \qquad 4.11$$

E_t is again like an activation energy.

The following is an outline of the computer program used to obtain the Avrami parameters, k, n, and E_k, E_n, E_t.

1. The data acquisition card was connected to the DSC recorder, to get the voltage signal which represents the rate of heat change, d(DH)/dt, or heat capacity, d(DH)/dT.

2. The Fast Fourier Transformation (FFT) technique was employed to filter the noise from the data and make the curve smoother. Figure 4.54 shows the result of FFT technique. The points represent the recorded data, and the solid curve represents the curve after an inverse FFT.

3. The filtered curve is divided into five parts and the division points are t_1, through t_5, as shown in Figure 4.55. Curves f_1, f_2, and f_3 represent fittings of data for intervals t_1-t_2, t_4-t_5, and t_3-t_4, respectively. The procedure ensures that all data are above the baseline, which is determined as shown in Figure 4.51. The following equations have been used for generating the f_1, f_2, and f_3 curves:

$$f_1(t)=a_{10} + a_{11}t + a_{12}t^2 + a_{13}t^3 \qquad 4.12$$

$$f_2(t)=a_{20} + a_{21}t \qquad 4.13$$

$$f_3(t)=a_{30} + a_{31}t \qquad 4.14$$

4. Under isothermal conditions, the crystalline phase is obtained from the amorphous phase. The baseline of crystallizing polymer is a weighted average of the baselines corresponding to the amorphous and crystalline phases. The baseline corresponding to the amorphous phase is assumed to be a line parallel to the time axis, and is drawn from a point on the curve corresponding to the initial crystallization time, t_o. The crystalline baseline is assumed to be the f_2 line. The system baseline is in actuality a curve, as shown in Figure 4.51. The equation for the system baseline is [51, 107]:

$$\text{baseline}_{(\text{system})} = (1\text{-}x)\,[\text{baseline}_{(\text{amorphous})}] + x\,[\,\text{baseline}_{(\text{crystalline})}\,] \qquad 4.15$$

5. By subtracting the system baseline from the recorded data, a new curve (known as optimized curve) is generated as shown in Figure 4.56. $A_X(t')$ is the area under the optimized curve from t=0 to t=t', and A_∞ is the total area under the optimized curve.

6. The optimized curve is used to determine the reduced crystallinity, x(t), which is defined as the ratio of $A_X(t)$ to A_∞. A typical x(t) versus t curve is shown in Figure 4.57.

7. The kinetic analysis for the isothermal crystallization is carried out on the basis of the Avrami equation, which can be also written as:

$$\ln[-\ln(1\text{-}x)] = \ln(k) + n\ln(t) \qquad 4.16$$

The x(t) data are then regressed to a straight line by using the least squares method. This way, k, n, as well as k_n, are determined as shown in

Figure 4.58. It should be noted here, that t in equation 4.16 is the recorded time minus t_0.

8. Since it is not easy to exactly determine t_0, steps 4 through 7, above, are repeated for different values of t_0. The values of t_0 which are tried are from a probable range (see next page), and the value which gives the highest confidence in step 7 is taken as the actual t_0 value.

9. The filtered curve (derived at step 2 above) has a maximum which occurs at time t_{max}. From the x(t) curve (see step 6), the time corresponding to x=0.5 is $t_{1/2}$.

10. The values of k, n, k_n, and $t_{1/2}$ which have been calculated by now, are used for getting the values of E_k, E_t, and E_n, as shown graphically in Figures 4.59, 4.60, and 4.61 .

The procedure to choose t_0 is as follows:

1) The first (guess) and last values for t_0, t_{00} are set as following:

$$t_{00} = t_s \qquad 4.17$$

$$t_{00} = t_{in} \qquad 4.18$$

where t_s is the time needed for the system to reach thermal equilibrium and t_{in} the time corresponding to the inflection point of $f_1(t)$,

$$t_{in} = (1/3)\,(a_{12}/a_{13}) \qquad 4.19$$

2) The probable range for t_0 values, discussed in step 8 above, is taken to be from t_s to t_{in}.

4.1.4.3.3 Polyethylene Terephthalate

The kinetic parameters for isothermal crystallization of R-PET, G-PET, and V-PET are listed in Tables 4.40, through 4.42. These parameters are based on the Avrami equation. The tables also indicate the time at which the peak of the exotherm, t_{max}, occurs, as well as $t_{1/2}$, i.e. the time needed to achieve 50% crystallinity. The $t_{1/2}$ and k versus T values shown in these tables are also plotted in Figures 4.62 through 4.64.

In most cases, the Avrami exponent, n, of PET is not an integer. Its values range between 1.8 at lower temperatures, and 3.0 at higher temperatures. One can conclude then, that the Avrami exponent increases with the isothermal crystallization temperature. The value of n can be used as an indicator for the mechanism of crystallization [126]. Values of n and their implications are listed in Table 4. 43. As discussed later in this chapter, at high temperatures, all types of PET showed a Maltese cross under microscope. This observation has lead to the conclusion that PET crystals formed at high temperatures, are spherulites. In the temperature range from 200 to 215^{O}C, the Avrami exponents for aR-PET, aG-PET, and aV-PET (shear treated PET) were close to 3, while those of bR-PET, bG-PET, and bV-PET (as received materials) were close to 2.5. Knowing the value of the Avrami exponent and the shape of the crystals formed, one can use Table 4.43 to possibly deduce what is the mechanism which governs crystallization. The conclusion made here is that most likely the mechanism for crystallization shear treated PET is athermal nucleation, while that of unprocessed PET is thermal nucleation and diffusion control. The conclusion is based on Table 4.43 as well as, on the following arguments. Shear processing causes molecular breakdown in the polymer and it also produces contaminants (dirt). The contaminants in processed PET may play a role as dominant nuclei,

while the molecular breakdown results in an increased mobility of PET segments. Therefore, the mechanism of crystallization could be athermal nucleation. Unprocessed PET does not contain contaminants from shear processing, hence contaminants cannot play a dominant role as nuclei, and one can conclude that crystallization of this material is controlled by thermal nucleation and diffusion.

Figure 4.64 shows half time values plotted versus isothermal crystallization temperatures. As one can easily see from this figure, the half times of bV-PET, bR-PET, and bG-PET are higher than those of aV-PET, aR-PET, and aG-PET, respectively. This implies that processed PET has an overall crystallization rate higher than that of unprocessed PET. The higher crystallization rate can be attributed to molecular breakdown and contaminants formed during the processing of the material. The half times of bR-PET and aV-PET were found to be almost equal, something which implies that the two materials have approximately the same overall crystallization rate. This could be attributed to the fact that both materials had a similar thermal history. Based on the half-time values, Figure 4.64 also indicates that the overall crystallization rate of bR-PET was higher than that of bG-PET. This result seems opposite to what one would anticipate based on the intrinsic viscosity values. In fact, the I.V. of bR-PET was found to be higher than that of bG-PET (as shown in Table 4.7), and thus, bG-PET should have a higher crystallization rate. This discrepancy can be attributed to the dyes present in G-PET which may suppress the crystallization rate. Based on the I.V. values for aR-PET and aG-PET (shown in Table 4.7), one would had again anticipated that aG-PET should crystallize at a faster rate. Nonetheless, as Figure 4.64 indicates, the crystallization rates for aR-PET and aG-PET are practically equal. So, again the presence of dyes may have an inhibitory effect on the crystallization rate. The fact that the crystallization rate of bG-PET is so much

inhibited that it becomes lower than that of bR-PET, while this does not happen for the case of these materials after processing, may be attributed to some decomposition of the dye during processing resulting in a less intense inhibitory effect on the crystallization rate.

It should be mentioned that the experimentally determined values of $t_{1/2}$, t_{max}, and n (shown in Tables 4.40 through 4.42) do not necessarily satisfy equation 4.5. This may be attributed to the following: (1) possibility of secondary crystallization; (2) inaccurate estimation of the crystalline baseline [21].

From Tables 4.40 through 4.42 one can see that in all cases, the values of k and k_n, for processed PET (a-PET) are higher than those of unprocessed PET (b-PET). The values of k and k_n are a measure of the crystallization rate. This rate depends on the crystal growth and nucleation rates. Crystal growth rate increases as the molecular weight decreases. Shear processed polymers are expected to have a higher crystal growth rate due to molecular breakdown which occurs during processing. Nonetheless, this cannot be the dominating factor for the observed high values of k and k_n for shear processed PET. For example, at 200^{o}C the value of k for aR-PET is 3.5 times higher than that of bR-PET. This cannot be (at least mainly) due to molecular weight difference, since the I.V. value of aR-PET is 98.6% (see Table 4.6)). It is concluded then that the increased k and k_n values for shear processed PET are mainly due to increased nucleation rates. These rates are high probably due to the presence of contaminants (which act as nucleating sites) in the processed PET. It can be also observed from the tables, that the values of k and k_n decreased as the temperature for isothermal crystallization increased; these trends are consistent with theoretical predictions (see for example Equation 4.10).

The E_k, E_t, and E_n values for PET are listed in Tables 4.44 through and 4.46. E_t and E_n for PET were found to be almost equal, something which is expected.

In conclusion, it has been found that the crystallization characteristics of shear processed PET are different from those for the unprocessed material. More specifically, the spherulite growth under thermal nucleation and diffusion control for PET (as received) changed to that of athermal nucleation control for processed PET. These changes can be attributed to molecular breakdown and the presence of contaminants in the processed PET.

4.1.4.3.4 R-PET with Nucleating Agents

The kinetic parameters (based on the Avrami equation) for isothermal crystallization of R-PET with nucleating agents are listed in Tables 4.40 and 4.44.

Figures 4.65 and 4.66 show crystallization half times against isothermal crystallization temperature for R-PET with $CaCO_3$ and Na_2CO_3, respectively. Both graphs also show the values for aR-PET. As can be seen from Figure 4.65, $CaCO_3$ is not an effective nucleating agent for R-PET. In fact, the curve corresponding to 0.3% $CaCO_3$ is almost identical to that for aR-PET. On the contrary, the curves for Na_2CO_3 in Figure 4.66 are far away from the curve for aR-PET, indicating that Na_2CO_3 is a very effective nucleating agent for R-PET. From both graphs one can see that as the concentration of the nucleating agent increases, the half-time decreases, or in other words the crystallization rate increases. This can be also seen from the k_n values listed in Table 4.40.

For comparison purposes, the half time for R-PET with 0.5% of different nucleating agents are plotted against temperature in Figure 4.67. From this figure

it becomes clear that amongst the nucleating agents for R-PET tried in this study, Na_2CO_3 is the most effective and $NaHCO_3$ is the second best. The same information is also shown in Figures 4.68 and 4.69 where lnk and $\ln(1/t_{1/2})$, respectively, are plotted against inverse temperature. From these graphs, one can also see that mechanical processing alone can substantially increase the crystallization rate. For example, at 210^{o}C the half time of bR-PET is 4.57 minutes while that of aR-PET is 2.55 minutes. If instead of mechanical processing an effective nucleating agent is added to bR-PET, the results are much better. For example, at 210^{o}C the value of 4.57 drops to 0.62 minutes when 0.5% Na_2CO_3 is added to the material.

Table 4.44 shows E_k, E_n, and E_t, values for R-PET with various nucleating agents. These values were obtained by regressing the data to Equations 4.9, 4.10, and 4.11, respectively. E_t is the slope of $\ln(1/t_{1/2})$ versus 1/T. It should be noted here that the solid lines shown in Figure 4.69 are not the regressed lines. These lines were simply drawn to show the trend in the data points. The value of E_t for R-PET with Na_2CO_3 was found to be above 200 kJ/mole while for R-PET with any other nucleating agents, E_t values were found to be between 155 and 190 kJ/mole. A large value of E_t implies that a small temperature decrease results in a large decrease in $t_{1/2}$, or in a large increase in crystallization rate. Since at high temperatures the growth rate is expected to be low one could argue that a large E_t value implies a high nucleation rate. Thus, it was thought that E_t (or E_n) could be used as an indicator of the effectiveness of an additive as a nucleating agent for R-PET. If this argument were correct, the values shown in Table 44 would lead to conclusions which contradict the results from other parts of this dissertation. For example, a conclusion would be that $PbCO_3$ is the second best nucleating agent, while in reality (from other measurements and microscopy

The E_k, E_t, and E_n values for PET are listed in Tables 4.44 through and 4.46. E_t and E_n for PET were found to be almost equal, something which is expected.

In conclusion, it has been found that the crystallization characteristics of shear processed PET are different from those for the unprocessed material. More specifically, the spherulite growth under thermal nucleation and diffusion control for PET (as received) changed to that of athermal nucleation control for processed PET. These changes can be attributed to molecular breakdown and the presence of contaminants in the processed PET.

4.1.4.3.4 R-PET with Nucleating Agents

The kinetic parameters (based on the Avrami equation) for isothermal crystallization of R-PET with nucleating agents are listed in Tables 4.40 and 4.44.

Figures 4.65 and 4.66 show crystallization half times against isothermal crystallization temperature for R-PET with $CaCO_3$ and Na_2CO_3, respectively. Both graphs also show the values for aR-PET. As can be seen from Figure 4.65, $CaCO_3$ is not an effective nucleating agent for R-PET. In fact, the curve corresponding to 0.3% $CaCO_3$ is almost identical to that for aR-PET. On the contrary, the curves for Na_2CO_3 in Figure 4.66 are far away from the curve for aR-PET, indicating that Na_2CO_3 is a very effective nucleating agent for R-PET. From both graphs one can see that as the concentration of the nucleating agent increases, the half-time decreases, or in other words the crystallization rate increases. This can be also seen from the k_n values listed in Table 4.40.

For comparison purposes, the half time for R-PET with 0.5% of different nucleating agents are plotted against temperature in Figure 4.67. From this figure

- Among the nucleating agents studied here, Na_2CO_3 and $NaHCO_3$ proved to be the most effective. The conclusions above are valid for any type of PET, and are identical with those reached for the non-isothermal crystallization case.

4.1.5 Optical Microscopy Studies

4.1.5.1 Nucleating Agents

In order to be able to distinguish (at high temperature), the characteristics of nucleating agents from those of PET, all nucleating agents were observed under the microscope. Samples were observed between crossed polarizers and without analyzer at a magnification of 100. The observations are shown in Tables 4.47 (a) and (b). The color of all nucleating agents is white to the naked eye. Two sets of observations were made; one in which the samples were not thermally treated, and one in which they were thermally treated to 300^{o}C. Thermal treatment implies that the sample was heated to 300^{o}C for 10 minutes, and then cooled for the observations at room temperature. Most samples had almost identical characteristics before and after thermal treatment. Small changes may be attributed to the loss of water due to heating. Some agents, such as $PbCO_3$, $ZnCO_3$, and $NaHCO_3$ were drastically different after thermal treatment; this is because they decompose to other materials when heated to a temperature of 300^{o}C or less. The fact that decomposition does occur, can be also seen from Table 4.1 as well as from the TGA graph shown in Figure 4.3.

4.1.5.2 Nonisothermal Scan of Polymer

In all cases, approximately 5 mg of PET with or without additives were sandwiched between clean, thin glass cover slips. This was done on a plate heated at 300^{o}C and under nitrogen atmosphere. The samples were then

brought into the air, and thus quenched to room temperature, in order to obtain the amorphous phase. Subsequently, the samples were heated and cooled on the hot stage of the microscope between temperatures of 100 and 300^{o}C. The phase transitions as a function of temperature were recorded by visual observations of the texture of the polymer melt. The heating rate was about 13 ^{o}C/min, while the cooling rate was about 8.5-12 ^{o}C/min. Samples were examined under both normal illumination and cross polarized light at a magnification of 200. Most recorded observations were examined between crossed polarizers, except where indicated.

4.1.5.2.1 R-PET

Samples of bR-PET after they were quenched from 300^{o}C to room temperature, showed a totally black background between crossed polarizers, and a clear background when observed without an analyzer. These observations indicated that the polymer was amorphous. It should be added that between crossed polarizers, a small number of white particles was also observed. These particles could be detected even after heating to temperatures as high as 330^{o}C. This possibly indicates that these particles were from some unknown impurities.

The amorphous bR-PET was heated from 40 to 300^{o}C at a rate of 13 ^{o}C/min, and the following observations were made: at 144^{o}C a large number of white points appeared suddenly; at 152^{o}C the entire sample indicated a white pattern; at 163^{o}C the white pattern changed to a colorful brown one, which again started turning white at 245^{o}C; when the colorful brown vanished completely, the white pattern endured up to 254^{o}C, and then vanished while the sample indicated a totally dark background.

The amorphous segments of PET commence to crystallize at about 144^{o}C. Spherulite patterns were formed as the crystals grew. At a temperature of 261^{o}C, the sample suddenly became completely isotropic with no visible textures under normal polarized light. It was completely dark when examined between crossed polarizers, and clear when observed without an analyzer, indicating a total elimination of the light intensity. From the DSC scan, Figure 4.34, one can see that the end of the main endothermal peak corresponds to this temperature (259^{o}C). The melting of PET is associated with complete disordered orientation of the chains (amorphous or liquid state). That is also why no changes were observed while the sample was heated beyond that temperature.

The power supply to the hot stage of the microscope was turned off when the temperature reached 300^{o}C. The sample was then allowed to cool from 332 to 100^{o}C at a rate of about 15 ^{o}C/min. The texture of the polymer showed no changes between crossed polarizers when the temperature passed through the 260^{o}C mark. This indicates that no phase transition occurred around 260^{o}C while cooling the sample. In fact, the texture showed no changes until the temperature reached 222^{o}C. This indicates that there is a supercooling of PET. Above 223^{o}C, the texture of the polymer melt was similar to a dark sky with no stars. At 222^{o}C, it looked like a few stars appeared in the dark sky. As cooling continued below 222^{o}C, stars increased abruptly both in number and size. At 217^{o}C, Maltese crosses were evident, something which indicated the presence of spherulites. At 212^{o}C, the Maltese cross pattern began to change to colorful brown. At 209^{o}C, banding Maltese crosses (ringed spherulites) were seen. This indicated the twisting of lamellar ribbons along the radial direction [86]. At 202^{o}C, large size textures were seen. At 190^{o}C, the colorful brown texture

occupied almost the entire sample. Below 190^{O}C, no further changes in the texture of the polymer were observed.

The same sample was heated again from 75 to 290^{O}C and observed between crossed polarizers. There was only brown color to be seen below 210^{O}C. Above 210^{O}C, the intensity of brown color decreased. At 247^{O}C, the color rapidly vanished, and only the black and white banding Maltese crosses remained. At 257^{O}C, all banding Maltese crosses disappeared and a dark color appeared (indicating an isotropic material).

The results from the two heating scans described above, have shown that the temperature range for the colorful brown texture to change to a dark one was between 210 and 260^{O}C. This range corresponds to the melting range from the DSC scan shown in Figure 4.34 at scan rate of 20 ^{O}C/min. Therefore, the change of color corresponds to the melting of crystals. At 247^{O}C, the color rapidly vanished and only the black and white banding Maltese crosses remained. This corresponds to the peak of melting temperature of 248^{O}C shown the in the thermogram of Figure 4.34.

As shown in Picture 4.1, the polymer chains crystallize to form spherulites or ring spherulites as indicated by the Maltese cross pattern which is characteristic of this morphological texture. Similar spherulites have been reported in the literature [67, 68].

Observations were also made with aR-PET. After the original heating at 300^{O}C and subsequent quenching to room temperature, the sample was dark between crossed polarizers, and clear when observed without an analyzer, indicating that the material was in an amorphous state.

The amorphous material was then heated from 33 to 300°C. Crystallization started around 138°C. At 146°C, white points appeared in the dark background. The colorful brown texture appeared at 221°C, and it totally disappeared at 250°C. There was no further change up to 300°C.

The sample was cooled from 340 to 115°C. Crystallization started around 221°C (white points in the dark). At 213°C, the white pattern occupied all the sample. At 209°C the white pattern changed to colorful brown. At 206°C, the intensity of colorful brown texture was maximum. There was no much change below this temperature. At this temperature the sample was bright brown when observed without an analyzer.

The same sample was heated again from 115 to 300°C. It was colorful golden brown between crossed polarizers, and brown when observed without an analyzer. At 207°C, the intensity of colorful brown started to decrease. At 243°C, white points were observed in a blue background. At 257°C, all patterns disappeared, and the background turned dark.

The sample was then cooled again from 330 to 180°C. This time, crystallization started at 223°C, the colorful brown texture started at 213°C, and the intensity of colorful brown texture increased to a maximum at 203°C. Picture 4.2 shows ring Maltese crosses of aR-PET produced by cooling from 300 to 100°C.

Comparing the observations for aR-PET and bR-PET, one could conclude that the crystallization process occurs via spherulites in both cases. Changes in texture corresponding to crystallization occurred at temperature values that are different but consistent with those obtained from the DSC studies discussed earlier. Due to processing, aR-PET is expected to crystallize faster due to

presence of more nuclei, something which is confirmed from Pictures 4.1 and 4.2.

4.1.5.2.2 G-PET

Microscopy studies with G-PET were also performed, following the methodology described in the preceding section.

For bG-PET, there were indications of impurities being present, as in the case bR-PET. The polymer started crystallizing at 134^{O}C (showing white points in a blue background under the microscope), and melted completely at 257^{O}C in the first heating scan which was from 50 to 300^{O}C. During cooling, crystallization started at around 224^{O}C. At 217^{O}C, the characteristics of banding Maltese crosses were first observed. At 215^{O}C, the texture of polymer was of a colorful brown. The intensity of the colorful brown became maximum at 210^{O}C. At 205^{O}C a golden brown texture was observed.

When the same sample was heated again, the golden brown color started decreasing in intensity, and was completely lost at 254^{O}C. At 260^{O}C, no texture could be detected. Picture 4.3 shows a characteristic texture of bG-PET at room temperature, from a sample which was cooled from 300^{O}C.

Observations of aG-PET indicated that during heating, crystallization started around 137^{O}C, while complete melting occurred at 256^{O}C. During cooling, crystallization started at 222^{O}C, while the colorful brown texture was first observed at about 213^{O}C. Picture 4.4 shows a characteristic texture of aG-PET from a sample cooled from 300^{O}C to room temperature.

In general, the morphology of aG-PET and bG-PET was practically the same, although (as can be seen from Pictures 4.3 and 4.4), the number of

crystals was higher, and their size smaller, for the case of aG-PET due to processing.

4.1.5.2.3 V-PET

bV-PET

A sample of bV-PET (before injection molding) was heated from 50 to 330^{o}C. The sample was then quenched to room temperature, and appeared transparent when observed without an analyzer, and dark between crossed polarizers. Crystallization of bV-PET started around 147^{o}C, showing a white cloud in a dark background under the microscope. At 167^{o}C, large and clear Maltese crosses were observed. At 190^{o}C, the spherulites next to the cover glass were colorful brown, while those away from glass were still black and white. At 248^{o}C, the entire pattern was black and white. At 259^{o}C, the texture completely disappeared. At 330^{o}C, the sample was very clear when observed without an analyzer, and dark between crossed polarizers.

While cooling the same sample from 330^{o}C, crystallization started at 218^{o}C. At 209^{o}C, Maltese crosses were clearly seen, and occupied all sample. Close to the glass surface, some Maltese crosses changed from blue to a colorful brown, and at 208^{o}C their texture changed to banding Maltese crosses.

The same sample was heated again from 100 to 285^{o}C. Banding Maltese crosses were clearly seen at 233^{o}C. The intensity of colorful brown texture decreased after 246^{o}C. The color of all crosses changed to black and white at 251^{o}C. At 260^{o}C all Maltese crosses disappeared. It was possible to actually see under the microscope, small crosses disappearing first, followed by the larger ones.

After the heating scan described above, the sample was cooled again. Crystallization started at 219^{o}C; this temperature is the same (218^{o}C) as in the first cooling scan. Below 211^{o}C, all sample was filled with colorful banding Maltese crosses, the larger ones of which were observed close to the glass surface.

Pictures 4.5 and 4.6 show the Maltese crosses of bV-PET while melting. Pictures 4.7 and 4.8 show the colorful Maltese crosses for bV-PET obtained during nonisothermal crystallization from 300 to 100^{o}C.

bV-PET without top glass cover

As discussed in the preceding section, the size of spherulites near the glass cover was larger than that of spherulites in the bulk material and the color was different. In order to find out if the cover affected the size and color of spherulites, the procedure followed in the previous section, was repeated without the top glass cover of the sample. The sample was heated from 25 to 300^{o}C. The amorphous material started crystallizing at 148^{o}C. The Maltese cross patterns were clearly seen at 171^{o}C. The color of patterns changed from black and white to colorful brown at 175^{o}C. The intensity of color started decreasing at 250^{o}C. The color changed again to black and white at 263^{o}C. The texture disappeared completely at 266^{o}C.

The sample was then cooled from 280^{o}C. It started crystallizing at 238^{o}C. The colorful brown texture was seen at 229^{o}C. The Maltese cross pattern was not observed during this run.

The sample was subsequently heated for a second time. The intensity of color started decreasing at 240^{o}C. Clear and large Maltese crosses were seen at

250^{O}C. This indicated that the spherulites were present in the sample at the end of the cooling run described in the previous paragraph. The fact that they were not observed is probably due to the presence of abnormal crystals at the surface of the material. When these crystals melted during the heating scan discussed in this paragraph, the pattern could be easily observed. The color of the texture was totally black and white at 252^{O}C. The texture disappeared at 258^{O}C.

The sample was then cooled a second time from 335^{O}C. It crystallized at about 225^{O}C; a few spherulites were seen. Small Maltese cross patterns were observed at 215^{O}C. The color of these patterns changed to yellow brown at 212^{O}C. The yellow brown texture covered all sample at 206^{O}C.

The sample was heated again for a third time. The intensity of color started decreasing at 239^{O}C. All Maltese crosses were black and white at 250^{O}C. The texture disappeared at 256^{O}C.

Large spherulites were seen close to the free surface of the material. A colorful brown texture was seen while the temperature changed. These observations are identical with those made in the previous section. Therefore, the possibility of the top glass cover affecting the size and color should be ruled out. One could had speculated that the nucleation rate close to the glass surface should be higher due to flint. This would had resulted in smaller crystals. But this was not the case. Hence, the glass cover does not affect the crystallization of bV-PET.

The Maltese crosses of bV-PET are very large and easily recognizable. Hence, this material can be recommended for studying spherulite texture.

aV-PET

A sample of amorphous aV-PET was heated from 45 to 300^{o}C. Crystallization started at 133^{o}C; the pattern of the texture could not be recognized. All texture disappeared at 259^{o}C.

The sample was then cooled from 300^{o}C. Crystallization started at 227^{o}C; few white points appeared. At 220^{o}C, a pattern of small Maltese crosses was observed. At 215^{o}C, a colorful brown texture appeared. At 200^{o}C, the entire sample had a colorful brown texture.

The same sample was heated again; the loss of intensity of colorful brown texture began at 222^{o}C, and the texture completely disappeared at 251^{o}C leaving only a black and white color. At 254^{o}C, banding Maltese cross patterns were clearly seen. At 258^{o}C, all patterns disappeared.

Picture 4.9 shows a characteristic banding Maltese cross for aV-PET produced by cooling from 300 to 100^{o}C.

The size of spherulites of bV-PET was much larger than that of aV-PET (see Pictures 4.8 and 4.9); the T_{mch} (133^{o}C) of aV-PET was smaller than that (147^{o}C) of bV-PET. These facts indicate that aV-PET has a faster crystallization rate. This can be attributed to the molecular breakdown due to shear and thermal degradation during the injection molding process.

4.1.5.2.4 PET with Na_2CO_3

The crystallization temperature, the melting point and texture of pattern for PET with Na_2CO_3 as nucleating agent, are listed in Tables 4.48, 4.49, and 4.50.

Samples of R-PET with different concentrations of Na_2CO_3 nucleant, were observed under the microscope between crossed polarizers.

Samples of R-PET containing Na_2CO_3 were quenched from 300°C to room temperature. Under the microscope the material appeared to have a certain degree of crystallinity. It was also observed that the samples contained some small particles the number of which, increased as the concentration of Na_2CO_3 increased. These particles were identified as Na_2CO_3 . Identification was made by comparing these particles to those of pure Na_2CO_3 which were observed under the microscope as discussed in an earlier section of this chapter.

The procedure always was to heat the quenched sample from 50 to 300°C, cool it from 300 to 180°C, and heat it again from 180 to 300°C.

As discussed in the previous sections, PET without a nucleant consists of large (identifiable) crystals. An effective nucleant is expected to increase the crystallization rate (due to increased nucleation), and form a large number of small crystals. This was actually observed for R-PET nucleated with Na_2CO_3, when Na_2CO_3 was added at concentrations of 0.3% and higher. In fact, in these cases the texture of the observed patterns was tiny and ambiguous. On the other hand, when Na_2CO_3 was added at 0.06%, some Maltese crosses could be observed. This indicated that the amount of Na_2CO_3 used was not enough to completely preclude the formation of at least some spherulites. One can conclude then, that the minimum effective Na_2CO_3 concentration is between 0.063 and 0.3%.

For G-PET and V-PET nucleated with Na_2CO_3, a 0.5% concentration of Na_2CO_3 was enough to preclude a clear Maltese cross pattern formation. In fact, in these cases the texture of the observed patterns was tiny and ambiguous.

The colors of the observed patterns during the first and second heating were similar at low temperatures, as was not the case of plain PET. This is a further confirmation of the fact that Na_2CO_3 is a very good nucleating agent. That is to say, Na_2CO_3 results in a certain degree of crystallinity even when the polymer crystallizes abruptly (is quenched); or, in other words, when Na_2CO_3 is used, PET cannot be completely amorphous even if the polymer is quenched at room temperature . This may not be the case if quenching occurs at an extremely high rate, such as the one achieved with liquid nitrogen.

In the section where the DSC studies were discussed, it was argued that the higher the T_{cc} value, the more effective the nucleating agent is. One would think that the analogue of T_{cc} in microscopy studies would be T_{mcc}, and thus this value could be used as an indicator of the effectiveness of nucleation. Nonetheless, T_{mcc} seems not to be a safe indicator. For example, looking at Table 4.48, one could erroneously conclude that 1% Na_2CO_3 is less effective than 0.063% something which is contradicted by the observed texture of patterns. The problem is that T_{mcc} cannot be accurately found, and in actuality the recorded value is the temperature where crystallization is completed especially when the size of crystals is very small. Thus, if microscopy is to be used for determining the effectiveness of a nucleating agent, decisions should be based only on the size of the observed patterns.

Pictures 4.10 through 4.13, show the textures of R-PET with different weight percentages of Na_2CO_3, while Pictures 4.14 and 4.15 show the texture of

G-PET with 0.5% Na_2CO_3 nucleant, observed after cooling from 300 to 100^{o}C. Pictures 4.14 and 4.15 show a particular (and same) location in the sample. The difference is that Pictures 4.15 was taken without an analyzer, while 4.14 was taken from an observation made between crossed polarizers. As can be seen from all pictures (4.10-4.14) the observed textures were grainy, with the exception of R-PET with 0.063% Na_2CO_3.

In order to further understand the role of Na_2CO_3 as nucleant for PET crystallization, powder of Na_2CO_3 was spread on two separate molten V-PET samples which were then covered with glass plates. One sample was mixed up (locally) by gently pressing and twisting the glass plates whereas, the other one was not, for the purpose of comparison. For the unmixed sample, large size Maltese cross patterns were predominant, indicating that the presence of Na_2CO_3 did not efficiently enhance crystallization. However, in the locally mixed sample, the Maltese cross patterns were significantly smaller and much more numerous close to the mixed area. In regions where Na_2CO_3 was absent larger Maltese cross patterns were observed. It is thus obvious that when Na_2CO_3 in uniformly mixed with PET, the nucleation rate is enhanced.

4.1.5.2.5 PET with $NaHCO_3$

Samples of PET containing $NaHCO_3$ were quenched from 300^{o}C to room temperature. When the samples were observed, they indicated the presence of a few particles, which were colorful between crossed polarizers. These particles were identified as $NaHCO_3$, after comparisons with pure $NaHCO_3$ particles which had been examined earlier under the microscope.

The texture of crystallized R-PET, G-PET, and V-PET with 0.5% $NaHCO_3$ nucleant was tiny and ambiguous, and it could not be identified as Maltese cross.

From these observations, it is concluded that $NaHCO_3$ when added to 0.5%, effectively nucleates PET crystallization.

4.1.5.2.6 PET with K_2CO_3

As in the cases of Na_2CO_3 and $NaHCO_3$, quenched samples of PET containing K_2CO_3 showed a few particles (white between crossed polarizers, dark without an analyzer), and these particles were identified as K_2CO_3.

The texture of crystallized R-PET and G-PET with 0.5% K_2CO_3 nucleant was tiny and ambiguous, and it could not be identified as Maltese cross. It is then concluded that 0.5% of K_2CO_3 effectively nucleates PET crystallization. However, the textures of V-PET with 0.5% K_2CO_3 were of Maltese cross type indicating that K_2CO_3 is not an effective nucleating agent for V-PET.

4.1.5.2.7 PET with $CaCO_3$, $BaCO_3$, $SrCO_3$, $CdCO_3$

As with other agents, $CaCO_3$, $BaCO_3$, $SrCO_3$, and $CdCO_3$ particles were observed in quenched PET samples. $CaCO_3$ was studied at a number of different concentrations as shown in Table 4.48, while $BaCO_3$, $SrCO_3$, and $CdCO_3$ were only studied at 0.5%. In all cases, spherulites (Maltese crosses) of large size were observed. It was then concluded that none of these substances is an effective nucleating agent for PET.

4.1.5.2.8 PET with $MgCO_3$, $ZnCO_3$, $PbCO_3$

In the quenched samples, particles of $ZnCO_3$, $PbCO_3$, and $MgCO_3$ could be easily identified under the microscope. Identification was made after comparing these particles to those the pure components.

Except for $MgCO_3$ added at 0.5% in R-PET, large spherulites were observed in any PET crystallized in the presence of $MgCO_3$, $ZnCO_3$, or $PbCO_3$. The conclusion is again that $MgCO_3$, $ZnCO_3$, and $PbCO_3$ are not effective nucleating agents.

It should be added that the microscopy studies with all nucleating agents confirmed the results of DSC analysis and intrinsic viscosity measurements which were discussed in an earlier section of the present thesis.

4.1.5.3 Isothermal Crystallization from Melt

In all cases, approximately 5 mg of PET with or without additives were sandwiched between clean, thin, glass cover slips on the top of hot plate at a temperature of 300^{o}C, under a nitrogen atmosphere. The samples, after pressing to form a film, were quickly transferred onto another plate held at 240^{o}C. The samples were allowed to isothermally crystallize at 240^{o}C for time periods which varied from 2 minutes up to 2 hours.

Samples of the following systems were chosen for this study:

aV-PET	bV-PET	V-PET/Na_2CO_3	V-PET/$CaCO_3$
aR-PET	bR-PET	R-PET/Na_2CO_3	R-PET/$CaCO_3$
aG-PET	bG-PET	G-PET/Na_2CO_3	G-PET/$CaCO_3$

Picture 4.16 shows the texture of bV-PET crystallized at 240^{o}C for 1 hr. The colored and the black and white Maltese cross pattern, typical of spherulites, can be clearly seen. It can be also observed that the size of spherulites is large.

Pictures 4.17 and 4.18, show the texture of aV-PET crystallized for 1 hour. Picture 4.17 shows the colored and black and white Maltese cross patterns. Picture 4.18 shows the ring Maltese cross pattern. These two pictures are from two different locations of a single sample.

Picture 4.19 shows the texture of bR-PET crystallized for 30 minutes. The Maltese cross pattern can be clearly seen.

Pictures 4.20 and 4.21 show the texture of aR-PET (1 hr). Both pictures show the Maltese cross pattern, while Picture 4.21 shows regions where a ring formation may be occurring.

Pictures 4.22 and 4.23 show the texture of bG-PET (2 hrs). Picture 4.22 shows colored as well as black and white Maltese cross patterns. Picture 4.23 clearly shows ring Maltese cross patterns. Again, both pictures are from different locations in the same sample.

Picture 4.24 shows the texture of aG-PET (2 hrs). Colored and black and white ring Maltese cross patterns are clearly visible.

The spherulites of unprocessed PET (b-PET) were larger than those of PET after mixing (a-PET); see for example, Pictures 4.16 and 4.17. The reason could be attributed to chain breakdown and presence of impurities after processing.

Pictures 4.25 through 4.28 show the texture of PET with Na_2CO_3. Picture 4.25 is for R-PET/0.063% Na_2CO_3, (41 mins) and shows some spherulites. Picture 4.26 shows the grainy texture of R-PET/1.0% Na_2CO_3 (40 mins). Picture 4.27 shows the grainy texture for G-PET/0.5% Na_2CO_3 (90 mins). Picture 4.28 is for V-PET/0.5% Na_2CO_3 (40 mins), and shows a tiny texture that could be of

Maltese cross type. The tiny textures indicate that Na_2CO_3 is a good nucleating agent.

Pictures 4.29, 4.30, and 4.31 show the texture of PET with $CaCO_3$. Picture 4.29 shows the Maltese cross pattern for R-PET/0.5% $CaCO_3$ (51 mins). Picture 4.30 shows the Maltese cross pattern for G-PET/0.5% $CaCO_3$ (40 mins). Picture 4.31 shows the ring Maltese cross pattern for V-PET/1.0% $CaCO_3$ (40 mins). The large size of spherulites indicates the ineffectiveness of $CaCO_3$ as a nucleating agent for PET.

Lastly, it should added that it is a good idea to always use both DSC and microscopy studies in order to make safe conclusions about the effectiveness of a substance as a nucleating agent. As an example, the T_{cc} value from DSC studies for PET with $PbCO_3$ indicated that $PbCO_3$ was a good nucleating agent; on the other hand, analysis of texture size (Picture 4.32), indicated that it was an ineffective nucleating agent. In this case, the fast crystallization rate determined via DSC studies should really be attributed to the low average molecular weight of PET due to molecular chain breakdown, and not to the effectiveness of the nucleating agent.

4.1.6 Studies on the Mechanical Properties

4.1.6.1 Tensile Properties

Tables 4.51 through 4.53 list the tensile properties of PET with and without nucleating agents.

The tensile modulus of PET with nucleating agents was found to be higher than that of plain PET, indicating that PET with nucleating agents had higher crystallinity. This could be attributed to the improved nucleation rate. It is known

that the crystallization rate increases with temperature up to an optimal value which for PET has been reported to be 175^{o}C; at higher temperatures, the crystallization rate decreases [106]. Therefore, 90^{o}C is closer to the optimal temperature than 40^{o}C. Consequently, at 90^{o}C crystallization is better and thus, the observed higher tensile modulus. The results indicate that Na_2CO_3 and $NaHCO_3$ nucleated PET has the highest tensile modulus. Hence, this test confirms once again that sodium carbonates are the best nucleating agents.

With regard to tensile strength, the results indicate that most nucleating agents do not alter the strength of non-nucleated PET. Furthermore, they indicate that when Na_2CO_3 is used at high concentrations the tensile strength is lower than that of plain R-PET. Thus, a nucleating agent, even if it is good, has to be used with caution so that other properties are not severely affected. It should be added that the tensile strength depends on the average molecular weight of PET. Therefore, low tensile strengths correspond to low intrinsic viscosity values. This can be seen by comparing Tables 4.51 through 4.53, and 4.6 and 4.7.

4.1.6.2 Flexural Properties

Tables 4.54 through 4.56 list the flexural properties of PET with and without nucleating agents. As the results indicate, the flexural properties improve substantially as the crystallinity of the polymer increases. Once again, sodium carbonates prove to be the best to use as nucleating agents.

6.1.6.3 Shrinkage Properties

For these experiments, tensile bars were placed in a vacuum oven at about 130^{o}C for 40 hours or more. With the exception of Na_2CO_3 and $NaHCO_3$

nucleated PET, all tensile bars were observed to warp, indicating that the material was thermally unstable.

Tables 4.57 through 4.59 list the shrinkage of PET with and without nucleating agents. As the data indicate, the shrinkage of nucleated PET is much less than that of plain PET. As expected, the percent shrinkage decreases as the crystallinity increases. One can easily see from the tables that Na_2CO_3 and $NaHCO_3$ result in an almost insignificant shrinkage, implying that they are very good nucleating agents. On the other hand, other substances such as $SrCO_3$ or $CdCO_3$ reduce the shrinkage observed in plain PET, but still the measured shrinkage is considerable. It is also interesting to observe that the shrinkage in PET nucleated with different concentrations of Na_2CO_3 is practically constant. Hence a 0.3% addition of Na_2CO_3 seems enough to achieve perfect crystallinity. Furthermore, it can be also observed that the shrinkage at 90^{o}C is lower that at 40^{o}C mold temperature. This (as also discussed earlier), is due to the fact that at 90^{o}C mold temperature the crystallinity is higher. In fact, this could be also observed when the tensile bars were produced for the experiments. The average length of bars produced at 40^{o}C was 12.80 cm while bars produced at 90^{o}C mold temperature were 12.70 cm in length. This is again due to the higher crystallinity of the material molded at 90^{o}C.

4.1.6.3 Molded specimen appearance

Molded parts were also evaluated for apparent crystallinity, surface appearance, and thermal stability on a scale of 1 (poor) to 5 (good). The results are shown in Tables 4.60 through 4.62.

Parts rated 5 for crystallinity were uniformly opaque, with no observable amorphous regions. Parts rated 1 were nearly uniformly amorphous. Parts rated

3 had a thin amorphous surface, but otherwise appeared crystalline. A surface appearance rating of 5 was assigned to parts with uniformly smooth, glossy surfaces. Badly blistered or scarred parts were rated 1. Dull parts were rated 3. Thermal stability was examined on final thermal shrinkage at 130^{o}C; "Y" represents good thermal stability in which the shape of molded parts did not change; "N" represents bad thermal stability in which the shape of molded parts changed and warped.

Small black dots were observed in molded bars of PET with $PbCO_3$ nucleant due to decomposition of the nucleant.

Clear, distributed particles were observed in molded bars of PET with K_2CO_3 nucleant. Before adding K_2CO_3 to the polymer, it has attempted to reduce its particle size via milling by hand. This proved to be very difficult as opposed to cases of Na_2CO_3 and $NaHCO_3$. It seems that fine K_2CO_3 particles could not be produced even by the shear applied through the extruder. The large size of K_2CO_3 particles resulted in poor dispersion, and thus improved nucleation rates only locally.

4.1.7 Discussion

The primary technical challenge in developing a PET-based engineering thermoplastic resin is to sufficiently increase the rate of crystallization in order to allow injection molding in short cycle times and at low mold temperatures. The present study investigated inorganic carbonate salts as nucleating agents with the objective being to improve crystallization rates in recycled PET.

For comparison purposes the properties of PET without additives were first studied. It was found that mechanically processed PET has crystallization

rates higher than those of unprocessed (virgin) PET. This is due to the fact that molecular breakdown occurs as a result of the applied shear and thus, the average molecular weight of PET reduces. Furthermore, due to the presence of moisture, hydrolysis occurs leading to molecular breakdown. Finally, during mechanical processing PET becomes contaminated with unknown species which probably act as nucleating sites. As explained before, crystallization of processed PET is controlled by athermal nucleation, while crystallization of virgin PET is diffusion and thermal nucleation controlled. Improvement of crystallization rate by mechanical processing cannot be viewed as a solution to the problems mentioned in the preceding paragraph, because the crystallinity achieved at low temperatures (e.g. $90^{o}C$) is too low.

A number of inorganic carbonate salts were used as nucleants. Among them, $CaCO_3$, $SrCO_3$, $BaCO_3$, $CdCO_3$ proved to be ineffective. Their ineffectiveness was established by the thermal properties, and can be attributed to the large sizes of spherulites formed in the material. These spherulites were observed under the microscope.

For K_2CO_3/PET, the values of k and $t_{1/2}$ indicate that its crystallization rate was improved. However, the large spherulites observed in V-PET, and the appearance of molded PET bars showing poor K_2CO_3 dispersion, indicated that this carbonate is not an effective nucleating agent for PET

Based on k and $t_{1/2}$ values for PET nucleated with $PbCO_3$, $ZnCO_3$, and $MgCO_3$ one can conclude that these salts lead to high crystallization rates. However, when the material is observed under the microscope large spherulites are seen. Hence, the nucleation rate is low and the increased crystallization rate

can be attributed only to a higher growth rate due to low average molecular weight. These salts are actually ineffective nucleating agents.

Samples of PET nucleated with Na_2CO_3 or $NaHCO_3$ had a tiny size texture morphology; they had the largest overall crystallization rate (based on k_p and $t_{1/2}$) amongst all additives; they showed the largest shrinkage of dimensions in mold; they had the smallest shrinkage of dimensions for the annealed tensile bar. All these results lead to the conclusion that Na_2CO_3 and $NaHCO_3$ are the most effective nucleating agents for PET, amongst the additives studied in this dissertation.

Reaction of PET with nucleating agents

As has been discussed in the preceding sections of this thesis, the experimental results indicate that among the inorganic carbonate salts studied, sodium carbonate and sodium bicarbonate proved to be the best nucleating agents. Furthermore, some salts - such as calcium carbonate - proved to be completely ineffective agents. In this section, an effort is made to understand and explain this difference in nucleating effectiveness of inorganic carbonate salts.

Sodium salts (mainly organic), have been studied by other researchers, and have proved to be very good nucleating agents for (not recycled) PET. The effectiveness of these salts as nucleating agents has been attributed to the formation of sodium-PET which has been claimed to be the actual nucleating agent. It has been further claimed that nucleating agents should have a good solubility in PET probably in order to promote reaction between PET and the cation, thus forming the actual nucleating agent [37, 43].

The explanations offered within the context of the present dissertation follow a different approach. The key arguments are as follows:

The basic unit of Polyethylene terephthalate contains ester groups which are susceptible to nucleophilic attacks. The ester reactions which are important to the arguments made here, are hydrolysis, transesterification (alcoholysis), and reduction to alcohols.

From organic chemistry, it is known that hydrolysis of carboxylic esters can occur under either acidic or basic conditions. Under acidic conditions, the products are an alcohol and a carboxylic acid (via a reversible reaction), while under basic conditions, the reaction is irreversible and produces an alcohol and a salt of a carboxylic acid. Alcohols react with esters resulting in transesterification and/or reduction. Reduction is known to occur at high temperatures and pressures, and is promoted by the presence of metal oxides [91].

During injection molding, a polymer (PET in this particular case) is subjected to high temperature and pressure. The material contains small amounts of moisture, and this probably starts hydrolysis. When a nucleating agent is used, two things can happen. First, due to heating and/or decomposition further amounts of water are released (see weight loss in Table 4.3), thus promoting hydrolysis. Second, depending on the solubility of the additive (nucleating agent) in water, hydrolysis occurs under either acidic or basic conditions. If the environment is basic, a PET salt is formed with the cation, and this salt is the actual nucleating agent. If the environment is acidic, the result of hydrolysis is simply molecular breakdown of the polymer. Based on the foregoing discussion, one could understand why sodium carbonate is a good

nucleating agent. It is water soluble, and forms a basic environment. Calcium carbonate is almost water insoluble, and thus one can understand why it proved to be an ineffective nucleating agent. But, the arguments presented up-till now, cannot explain why potassium carbonate (which is more water soluble, and forms a stronger basic environment than sodium carbonate), turned out to be an ineffective agent. Additional arguments are then needed.

Hydrolysis produces an alcohol. Furthermore, alcohols are produced either due to transesterification or reduction. The argument made here, is the following. If a salt used as a nucleating agent is soluble in alcohols, the cations are available for reaction with PET to form a PET salt (which is the actual nucleating agent), provided that (as in the case of hydrolysis) the environment is basic. Minute amounts of alcohols start to be produced due to hydrolysis (which occurs because of the presence of moisture either in the polymer of the salt). As soon as some alcohol is produced, transesterification takes place, and further amounts of alcohol (probably ethylene glycol and diethylene glycol) are produced. Sodium salts are soluble in alcohols (as well as water), and produce a basic environment. Hence, this is an extra reason for sodium carbonate and sodium bicarbonate to be good nucleating agents. On the other hand, lithium carbonate dissolves slightly in hot water ($100^{o}C$), but it is not alcohol soluble (see Table 4.1), indicating that there is a very low probability for forming Li-PET, which would be the nucleating agent. Potassium carbonate, which proved to be an ineffective nucleating agent, is not soluble in alcohols either [122]. On the contrary, potassium benzoate has been reported to be a good nucleating agent [43], and one can see from data available in the literature [122] that this organic salt is soluble in alcohols. Of course, potassium carbonate is much more water soluble than sodium carbonate (see Table 4.1). Nonetheless, as can be seen

from Table 4.5, it seems that potassium carbonate contains less moisture than sodium carbonate. Thus, there is not enough water for potassium carbonate to get dissolved, and the K-PET salt to be formed. One extra reason for potassium carbonate to be an ineffective nucleating agent, is the fact that it proved very difficult to reduce the size of its particles, something which implies that the salt cannot be nicely distributed in the polymer melt. As a result, poor dispersion of K_2CO_3 particles in molded bars was observed.

Among the salts studied in this dissertation, $CaCO_3$, $SrCO_3$, $BaCO_3$, and $CdCO_3$ are slightly soluble in water and insoluble in alcohols. All of them, proved to be ineffective nucleating agents. Their ineffectiveness was confirmed from the high reduced intrinsic viscosity values, the thermal properties as well as the texture of the material observed under the microscope.

Regarding $PbCO_3$ and $ZnCO_3$, one can say the following. These substances are neither water nor alcohol soluble. Furthermore, as can be seen from Table 4.1, and Figures 4.9 and 4.10, these substances decompose in the range of the temperatures used, and produce the corresponding metal oxides. These oxides may act as catalysts for reduction of PET. Reduction of esters implies formation of smaller molecules, and this is in fact confirmed by the low reduced intrinsic viscosity values (see Table 4.6). A low average molecular weight increases the growth rate of the polymer crystal, resulting in the observed high crystallization rates. Nonetheless, nucleation was not improved, as was confirmed by microscopic observations which indicated the formation of large spherulites.

Finally, $MgCO_3$ is again neither water nor alcohol soluble. The obtained reduced intrinsic viscosity values are high. It could be that the magnesium oxide

is formed from decomposition, and that it promotes reduction of PET. But this effect may be counterbalanced by the formation of larger molecules due to PET-magnesium complexes [111, 119].

In conclusion, the theory offered here is that for a salt to be a good nucleating agent, it has to be water and alcohol soluble, in order to form a PET salt (with the cation), which acts as the actual nucleating agent. Furthermore, the additive needs to be nicely dispersed in the polymer.

4.2 Polymer Blends

Within the context of this dissertation, some preliminary studies were made regarding polymer blends involving recycled PET. The findings are presented and discussed in the following sections.

4.2.1 Blending R-PET with Polyester Elastomers

The main objective of this preliminary study was to modify the crystallization kinetics of reclaimed PET (R-PET) by blending it with another polymer so that the resulting polyblend either has a higher rate of crystallization or is predominantly amorphous. Thermoplastic elastomers were deemed as potential candidates that may be effective in achieving this goal, because the soft and flexible segments of the elastomer molecules could have either a plasticizing effect to facilitate, or an inhibiting effect to suppress, the alignment of PET molecules in forming crystals. Furthermore, because of the high melting point ($260^{o}C$) and molecular polarity of PET, any possible candidate must also be polar in order to be more compatible with PET and be thermally stable in the temperature range from 260 to $280^{o}C$ for at least a short period of time.

Elastomers belonging to the class of polyester elastomers were of particular interest to the present study, because of their possible miscibility with PET, due to similarity in molecular structure. Two types of polyester elastomers were employed in this study. The first type was the GAFLEX series manufactured by GAF. According to the data provided by the company, GAFLEX is a block copolymer consisting of hard and soft segments which contain the characteristic ester linkage, -C(=O)-O-. It was found to be thermally stable in the melt state of PET (among 250 and 280^{O}C) during a typical injection molding cycle. There is the possibility of transesterification reaction between PET and polyester elastomer. However, while this reaction is relevant and important, it has not been investigated in this preliminary study. Three different grades of GAFLEX (547ZS, 555ZS, and 572ZS), spanning a wide range of hardness, were considered. A second type of polyester elastomer considered was the HYTREL series of resins made by DuPont. Only one grade, G4056, was used in this study. Some physical and mechanical properties of these polyester elastomers, as furnished by the companies, are listed in Table 4.63.

4.2.1.1 Thermal Properties

Clear reclaimed PET and the polyester elastomers were dried overnight in a vacuum oven at about 100^{O}C. Dry mixtures of R-PET and polyester elastomer, with composition of 10% and 20% by weight of elastomers, were prepared in the form of 80 g batches and loaded into a Brabender Plasti-Corder Mixer. The mixing head was electrically heated and maintained at 270-280^{O}C. The mixture was kept in the melt state at 60 RPM for about five minutes and then tiny samples were taken from the mixer and immediately immersed in liquid nitrogen. In such rapid quenching, any crystallization activity would be completely stopped and the samples were amorphous. The samples were analyzed in the Perkin-Elmer DSC-

2. In all cases, the DSC scans showed only one glass transition, one crystallization exotherm and one melting endotherm. Some important characteristics (T_g, T_{ch}, T_{cc}, T_m) of these scans are summarized in Tables 4.64 through 4.67. For comparison purposes, the corresponding data for reclaimed PET are also shown. The following observations are immediately evident from Tables 4.64 through 4.67:

(l) there is a reduction (by a few degrees), in the glass transition temperatures of the blends;

(2) the temperature of the crystallization (exotherm) peak, T_{ch}, of the blends on heating from glassy state is lowered by as much as 19^{o}C;

(3) the temperature of the crystallization (exotherm) peak, T_{cc} of the blends on cooling from melt (isotropic) state is raised by as much as 16^{o}C;

(4) the melting endotherm peaks of the blends are similar (with respect to both the peak temperature, T_m, and the range of melting) to that of R-PET; no separate melting peak of the elastomer is evident.

The first three observations imply that the crystallization kinetics of PET molecules have been substantially modified and that the blends evidently crystallize more readily and have a rate of crystallization faster than R-PET. In particular, the considerably higher T_{cc} for the R-PET/elastomer blends would have the practical significance that parts made from these blends in a normal injection molding cycle will possess a higher degree of crystallinity.

4.2.1.2 Mechanical Properties

Heterogeneous mixtures of R-PET flakes and elastomer pellets, which had been pre-dried overnight in an oven at 100^{o}C, were prepared at specific composition (10% and 20% by weight of elastomers) by simply vigorously shaking them in a covered container. These mixtures were directly loaded into the hopper of the Van Dorn injection molding machine. The operating settings of the machine were the same as those listed in Table 3.4. The colors of the specimens resembled closely those of the elastomers, muddy brown for GAFLEX and white for HYTREL. The tensile and flexural properties were measured according to ASTM D638 and D790, respectively and are summarized in Tables 4.64 through 4.67. In general, there is a gradual degradation in tensile and flexural strength of the blends as the content of the elastomers increases. The tensile bars did not break until strain reached 300 to 500 %. Stress-induced crystallization in the stretched tensile bars was evident to the naked eye. However, on closer examination, it was observed that the morphology of the stress-induced crystal structure in specimens made from reclaimed PET alone, was entirely different from those made from the blends. The stress-induced crystal structure for reclaimed PET was fibrous in nature, whereas those for the polyblends were in the form of layered flat filaments. Evidently, the presence of the elastomer molecules affects the alignment of the PET molecules during stress-induced crystallization.

4.2.1.3 Shrinkage

The flexural test specimens (5"x1/2"x1/8" bars) made from the blends, were placed in an oven at about 150^{o}C for a period of about 20 hours. The changes in the dimensions of the specimens after prolonged thermal annealing

were measured, and are listed in Tables 4.64 through 4.67. It is of interest to note from these tables that the shrinkage of parts made from the blends are much lower than that of parts made from reclaimed PET alone. Furthermore, for blends, the shrinkage decreases as the amount of the elastomer in the blend increases. These shrinkage results, together with those of the DSC scans, imply that the presence of polyester elastomer accelerates the crystallization of PET molecules upon cooling from the melt state. Therefore, parts made from the blends in a normal injection molding cycle have a degree of crystallinity considerably higher than would be obtained from reclaimed PET alone.

4.2.2 Polyblends of LDPE/R-PET with Compatibilizers.

A potential answer to the question as to how to produce low cost consumer items from recycled PET, processed by injection molding, is to treat R-PET as a filler for polyethylene (PE). This could improve the mechanical properties of PE. However, PET and PE are immiscible, and the only way to get a product (blend) with good mechanical properties is to use a compatibilizer. Within the scope of the present dissertation, some studies were performed in an attempt to improve the adhesion stress between PET and PE. To achieve this objective, coupling agents and ionomers were tested as compatibilizers. The results with coupling agents such as LICA-12, LICA-44 (obtained from Kenrich Petrochemicals, Inc.), and Prosil 2020 (obtained from PCR Incorporated), were negative and no further work with coupling agents was done within the context of this study.

For the studies with ionomers, R-PET was classified into two grades: R-PET-1 and R-PET-2. R-PET-1 is the material studied in the main body of this thesis, and was obtained from the Center for Plastics Recycle Research at

Rutgers University. R-PET-2 (which proved to have a crystallization rate higher than R-PET-1), was obtained from the St. Jude Polymer company. The polyethylene used was of low density (LDPE), and was classified into two grades LDPE-1 (high melting point), and LDPE-2 (low melting point). One set of experiments involved high density polyethylene (HDPE). The mechanical and thermal properties of the pure resins (PET, PE, ionomers), are listed in Tables 4.68, 4.69, and 4.70. The percentage of ionomer reported in the tables is based on polyethylene only (not the entire blend). The specimens used for the study were produced by injection molding. The machine was operated at a hold pressure of 800 psi, and a back pressure of 50 psi. The results are discussed in the following sections.

4.2.2.1 PE/PET

4.2.2.1.1 Melt Temperature Effect

4.2.2.1.1.1 LDPE

Table 4.71, and Figures 4.76 and 4.77 show the mechanical properties of LDPE-1 processed at different barrel temperatures of the injection molding machine. The tensile strength and tensile modulus decreased with increasing barrel temperature. However, both the elongation at break and toughness, increased with increasing barrel temperature. The higher the barrel temperature, the lower is the crystallinity. Therefore, as the barrel temperature increases, the molded bar is more amorphous, something which results in enhanced toughness.

As Table 4.72 indicates, the thermal properties of LDPE-1 are independent of barrel temperature.

4.2.2.1.1.2 LDPE/PET

Mechanical Properties:

Table 4.73, and Figures 4.78 through 4.80 show the mechanical properties of blends containing 10% fine particles of R-PET-1 and 90% LDPE-1 processed at different barrel temperatures of the injection molding machine. The mechanical properties improved as the barrel temperature increased from 360^{O}F to 460^{O}F. The tensile modulus is constant up to 420^{O}F, and then increases linearly with barrel temperature. The elongation at break and the tensile strength increase with barrel temperature up to 440^{O}F, and 420^{O}F, respectively, and remain constant thereafter. PET particles could be easily seen in bars molded at barrel temperatures below 380^{O}F, indicating that PET had not melted. PET particles could be also observed in bars molded at barrel temperatures between 380^{O}F and 440^{O}F; the size of these particles decreased as the temperature increased, indicating that PET had partially melted. Above 440^{O}F, the molded bar was homogeneous to the naked eye, indicating that PET had melted completely. Complete melting of PET is necessary for good mechanical properties as indicated in Table 4.73.

Thermal analysis:

Table 4.74 shows the thermal properties of a 90% LDPE-1/10% R-PET-1 blend, molded at different barrel temperatures. The thermal properties were measured by DSC as follows: a sample from the bar was melted and then quenched to a low temperature; the quenched material was then heated up slowly, and then cooled at a slow scan rate of 20 ^{O}C/min. Upon heating, the quenched sample shows two endothermic peaks corresponding to melting of PE and PET, and -possibly- an exothermic peak (between the two endotherms),

corresponding to crystallization of amorphous PET. The first endothermic peak occurs at T_m(PE), the exothermic peak occurs (if at all) at T_{ch}(PET), and the third peak (endothermic) occurs at T_m(PET). The area of each peak is a measure of the amount of enthalpy involved. Correspondingly, these enthalpies are designated as ΔH_m(PE), ΔH_{ch}(PET), and ΔH_m(PET). Upon cooling, two exothermic peaks are observed. First (at high temperature), the exotherm ΔH_{cc}(PET) of PET crystallization at T_{CC}(PET), and at low temperature the exotherm ΔH_{cc}(PE) of PE crystallization at T_{CC}(PE). During the second heating, only two endotherms are observed, since (after slow cooling) PET is crystalline and the exotherm at T_{ch}(PET) does not occur. The enthalpies referred to above were used in getting a quantitative index for the quality of the blend formed. The following quantities have been defined:

$$W_m(PET) = \Delta H_m(PET)/[\Delta H_m(PET) + \Delta H_m(PE)]$$

$$W_m(PE) = \Delta H_m(PE)/[\Delta H_m(PET) + \Delta H_m(PE)]$$

$$W_{ch}(PET) = \Delta H_{ch}(PET)/[\Delta H_m(PET)]$$

$$W_{cc}(PET) = \Delta H_{cc}(PET)/[\Delta H_{cc}(PET) + \Delta Hcc(PE)]$$

$$W_{cc}(PE) = \Delta H_{cc}(PE)/[\Delta H_{cc}(PET) + \Delta Hcc(PE)]$$

W_m(PET) is a measure of the percentage of PET crystals in the blend; W_m(PE) is a measure of the percentage of PE crystals in the blend; W_{cc}(PET) is a measure of the percentage of PET crystals in the crystallized blend; W_{cc}(PE) is a measure of the percentage of PE crystals in the crystallized blend; W_{ch}(PET) is a measure of the amount of amorphous PET in the quenched blend which can undergo cold crystallization. Since the DSC test is based on a small part of the molded bar, [a sample which is selected from the main phase, if two phases are seen to be

formed], W_m(PET) can be viewed as a measure of PET contained in the main phase. In fact, as the barrel temperature increases (and approaches the melting temperature of PET), W_m(PET) increases towards the value which could be calculated assuming perfect mixing of the PET- and PE-phases. Hence, W_m(PET) can be used as a measure of the quality of the blend formed.

For barrel temperatures below 400^{O}F no thermal properties of PET could be measured, This can be attributed to the fact that the (small) part of the molded bar used for DSC, did not contain any detectable amount of PET. This implies that practically, no blend was actually formed.

From the experimental data obtained, it seems that a processing temperature of 440^{O}F is the minimum required for producing an acceptable blend.

Morphology:

SEM (scanning electron microscopy) micrographs of tensile fractured surfaces of 90% LDPE-1/10% R-PET-1 material at different barrel temperatures, are shown in Pictures 4.33 through 4.38.

In Pictures 4.33 and 4.34, large irregularly shaped PET particles can be easily observed indicating that PET did not melt yet. In Pictures 4.35 and 4.36 the more regular shape of PET particles is due to partial melting of PET. In Pictures 4.37 and 4.38, small spheres of PET can be seen, indicating that PET has melted substantially, and the remaining small spheres are completely dispersed in the LDPE matrix.

4.2.2.1.2 Composition effect

4.2.2.1.2.1 Mechanical Properties

Stress-strain curves for LDPE-1/PET blends measured at room temperature with crosshead speed of 1 in/min are shown in Figures 4.81 and 4.82. PET had sharp yielding, and upon an increase in LDPE composition, the yield peak decreased and became broadened.

For LDPE-1/PET blends, the 60/40 blends show a considerably broadened yield peak and in the 80/20 blends the yield peak is almost invisible and a flat plateau results; this is typically called "gradual yielding" [73].

Tables 4.75 and 4.76 show the results of mechanical properties of LDPE-1/PET blends. Tensile strength, tensile modulus, elongation at break, and toughness are plotted against weight fraction for the LDPE/PET blends in Figures 4.83, 4.84, 4.85, and 4.86, respectively. Tensile strength and tensile modulus increase with increasing PET composition. Elongation and toughness increase reaching a maximum and then decrease with increasing PET composition. Maximum elongation and toughness are located at about 30% PET. The tensile strength and tensile modulus of LDPE-1/R-PET-2 blends were slightly higher than those of LDPE-1/R-PET-1; whereas, the elongation at break and toughness of LDPE-1/R-PET-1 blends were slightly higher than those of LDPE-1/R-PET-2. These results can be attributed to the fact that R-PET-2 has a fast crystallization rate.

4.2.2.1.2.2 Thermal Analysis (DSC)

As the values in Table 4.69 indicates, T_m and T_{cc} of LDPE-1 are higher than the corresponding values of LDPE-2. T_{cc} of R-PET-2 was 213^{o}C, indicating

a fast crystallization rate, whereas, T_{cc} of R-PET-1 was 181^{o}C, indicating a slow crystallization rate.

Tables 4.77 and 4.78 show the thermal properties of LDPE/PET blends.

Typical DSC cooling thermograms for LDPE/PET blends are shown in Figure 4.87. Cooling from 280^{o}C first resulted in crystallization of PET, followed by crystallization of PE. This behavior was typical for PE/PET blends for a cooling rate of 20 ^{o}C/min. The crystallization exotherm for PET in the cooling thermograms was broader when PET composition was below 20%.

Typical DSC heating thermograms for LDPE/PET blends are shown in Figure 4.88. Starting from low temperatures the thermogram reveals the glass transition temperature of PET, the melting of PE, followed by cold crystallization of PET, and finally melting of PET. The absence of cold crystallization of R-PET-2 in the case of the quenched sample (curve A2), indicates that R-PET-2 has a fast crystallization rate. In the case of the 90/10 (LDPE/PET) composition, cold crystallization of PET was not observed due to the small sample size utilized, but was clearly seen in other compositions.

A decrease in the T_{cc} (when the LDPE percentage is more than 20) and T_{ch} values of R-PET-2 blended with PE was observed, as shown in Table 4.78. The decrease in T_{cc} indicates that the overall crystallization rate (from cooling) of PET decreases. The olefin particles do not act as nucleating agents during PET crystallization from the melt. A decrease in crystallization growth rate has been reported for PE/PET blends and it is thought that expenditure of energy in rejection and/or occlusion of the olefin particles by the growing spherulitic front, results in the observed depression of the crystallization growth rate [123]. An increase in T_{cc} for higher composition (above 80%) of PET was also observed.

This increased overall crystallization rate can be attributed to the increase in nucleation rate caused by PE; nucleation compensates the depression of growth rate [123].

The decrease in T_{ch} of PET in blends, indicates that the overall crystallization rate (from heating) of PET increases. Since LDPE melts before the onset of cold crystallization, it has been suggested that the volume expansion associated with LDPE melting, creates stress concentrations which induce PET crystallization [123].

4.2.2.1.2.3 Morphology

Scanning Electron Microscopy (SEM) micrographs of tensile fractured surfaces of LDPE/PET blends are shown in Pictures 4.39 through 4.42.

The tensile bar of 20%LDPE-1/80%R-PET-2 shows two layers; a surface layer which is LDPE-rich and a core which is PET-rich. The core morphology consists of spherical LDPE particles distributed throughout a PET matrix, as shown in Picture 4.39. PET crystallizes completely when LDPE is still a liquid (molten material); liquid droplets of LDPE are entrapped in the PET matrix; when LDPE crystallizes, its volume gets reduced and thus, the LDPE inclusions are sitting loosely in the holes of the PET matrix (Picture 4.39). The existence of a large number of LDPE particles in the core may be the result of different melt viscosities for LDPE and PET. In fact, it is highly likely that during processing (in the injection molding machine), the LDPE component is masticated into small droplets by the shearing force caused by the highly viscous PET melt. Regarding the surface layer (Picture 4.40), the morphology shows few PET particles in the LDPE matrix.

The morphology of 50%LDPE-1/50%R-PET-2 is shown in Picture 4.41. In this case, LDPE and PET seem to form co-continuous phases. In fact, it is a challenge to identify the components in the micrograph.

The morphology of 80%LDPE-1/20%R-PET-2 is shown in Picture 4.42. LDPE forms lamellar structures. The spherical PET particles are distributed on the surface of the LDPE lamellar matrix.

Discussion:

Based on the morphology and thermal properties of LDPE/PET blends one can conclude that these two components form incompatible blends. An improvement in toughness for blends containing 30% to 40% PET is not the result of compatibility, rather it is due to the formation of co-continuous phases.

The fact that LDPE/PET form incompatible blends, is resulting in the formation of two layers in the molded bars. Actually, LDPE which has lower viscosity tends to accumulate in areas of high shear, thus the LDPE matrix constitutes the surface of the molded bar [49].

4.2.2.2 LDPE/PET Blends with AClyn Ionomers

Some physical properties of AClyn ionomers (which are sodium salts [4]), are shown in Table 4.70. These ionomers were investigated as compatibilizers for LDPE/PET blends.

4.2.2.2.1 Mechanical Properties

Stress-strain curves for LDPE/PET blends with AClyn ionomers measured at room temperature at a crosshead speed of 1 in/min are shown in Figure 4.89. Table 4.79 shows tensile properties of the blends. As can be seen from the table,

the elongation for polyblends of 90% LDPE-2/10% R-PET-2 containing the ionomers is higher than the blends produced without the AClyn resin. This can be attributed to the fact that the ionomer increases the adhesion between LDPE and PET.

It should be noted that according to the company producing AClyn, the grades used in this study are efficient nucleating agents for PET [4]. In fact, the cation (sodium) of the ionomer, reacts with PET at the carboxylic positions as discussed in earlier parts of this thesis, and produces a PET-Na salt. As the concentration of the ionomer increases, one should expect that PET is attacked at many carboxylic position, something which results in a molecular breakdown. This may be the reason for lower toughness and elongation in the blend produced with 6% AClyn relative to the blend prepared with 2% of the ionomer (see Table 4.79).

4.2.2.2.2 Thermal Analysis (DSC)

Table 4.80 shows the thermal properties of LDPE/PET blends produced with AClyn ionomers. As discussed in the previous section, AClyn is an efficient nucleating agent for PET. This is confirmed by the T_{cc} values for PET which -as the values in Table 4.80 indicate- are higher when PET is mixed with AClyn (expect for grade 262A).

4.2.2.2.3 Morphology

Picture 4.43 shows a SEM micrograph of a blend which is 90% LDPE-2/10% R-PET-2 with 2% AClyn A285 based on LDPE. It seems that the presence of the ionomer increases the interfacial adhesion between the LDPE and PET phases. This can be seen by comparing Pictures 4.38 and 4.43.

Picture 4.44 shows a SEM micrograph of a polyblend which is 20% LDPE-1/80% R-PET-2 with 6% AClyn 285A based on LDPE. The broken spherical LDPE particles, attributed to an increased interfacial adhesion, are in contrast to the perfect spherical LDPE particles shown in Picture 4.39. Picture 4.45 shows in magnification a detail of Picture 4.44, and shows the linkage between PET and LDPE. This picture confirms that AClyn A285 does in fact increase interfacial adhesion in the polyblend.

Discussion:

Using AClyn for producing LDPE/PET blends, resulted in better mechanical properties. Nonetheless, as the SEM pictures indicate, one can easily distinguish the two phases. Thus, AClyn resin is not a good compatibilizer, but it increases the interfacial adhesion between the two phases.

4.2.2.3 LDPE/PET Blends with Surlyn Ionomers

Surlyn ionomers are another class of substances tested in this study as potential compatibilizers for LDPE/PET blends. Some of the physical properties of these ionomers are shown in Table 4.70. One of the main differences between Surlyn and AClyn ionomers is in the average molecular weight. Actually, Surlyn has a average molecular weight much higher than AClyn.

4.2.2.3.1 Mechanical Properties

Stress-strain curves for LDPE/PET blends with Surlyn ionomers measured at room temperature at a crosshead speed of 1 in/min are shown in Figures 4.90 through 4.92. Table 4.81 shows tensile properties of the blends. As the values in the table indicate, the toughness of a 50% LDPE-2/50% R-PET-1 blend is almost doubled when 2% Surlyn S8920 is added. The results for the 20% LDPE-1/

80% R-PET-2 blends indicate that the mechanical properties of the blend improve as the concentration of Surlyn S8527 ionomer increases. In fact, the toughness of the blend with 6% ionomer is almost 4 times higher than that of the blend without Surlyn S8527.

Since S8527 gave the best results for LDPE/PET blends (see next sections too), an experiment was performed with high density polyethylene (HDPE) as well. The results indicate that S8527 does not seem to substantially improve the mechanical properties of HDPE/PET blends.

4.2.2.3.2 Thermal Analysis (DSC)

Figures 4.93 through 4.96 show the heating and cooling thermograms for LDPE/PET blends with Surlyn ionomers. Table 4.82 also shows the thermal properties of LDPE/PET blends with Surlyn ionomers.

The T_{cc} value for R-PET-2 increased with increasing content of Surlyn S8527 as shown in Figure 4.94.

From Figure 4.95, one can see that the 50% LDPE-2/50% R-PET-1 blend without the ionomer showed a peak for cold crystallization at 137^{o}C (curve A1). The same blend with 2% Surlyn S8920 ionomer did not show any cold crystallization, (curve A2), implying that S8920 is a very good nucleating agent for PET. One should also recall that R-PET-1 is a material undergoing slow crystallization. The fact that S8920 is a good nucleating agent for PET, can be also seen from curves A1 and A2 in Figure 4.96; as these thermograms indicate, the T_{cc} value increases when S8920 is added.

4.2.2.3.3 Morphology

Picture 4.46 shows a SEM micrograph of a polyblend which is 90% LDPE-2/10% R-PET-1 with 2% Surlyn S8920 based on LDPE. This picture indicates that Surlyn S8920 acts as a good compatibilizer for LDPE/PET blends, since very few PET particles can be distinguished. This is in contrast to the situation where no ionomer is used (Picture 4.38), as well as to the situation where an AClyn ionomer is used (Picture 4.43).

Pictures 4.47 and 4.48 show SEM micrographs for blends containing 50% and 80% PET, respectively. These pictures can be compared with Pictures 4.41 and 4.39, respectively, for cases where no ionomer is used. The difference in morphology can be attributed to enhanced adhesion between the LDPE and PET phases in the presence of the ionomer. This enhanced adhesion (or homogeneity) is also reflected by the values for toughness shown in Table 4.81.

Discussion:

The results indicate that the mechanical properties of LDPE/PET blends improve drastically when Surlyn ionomers are used. The morphology from SEM confirms that Surlyn is a good compatibilizer. Comparing Surlyn to AClyn resin, Surlyn ionomers proved much better, and this can be attributed to its higher average molecular weight.

5. CONCLUSIONS

5.1 PET

The main conclusions from this study are the following:

1. The crystallization rate of recycled PET is well improved when Na_2CO_3 or $NaHCO_3$ is used as nucleating agent. Other inorganic carbonate salts tried in this study proved to be ineffective nucleating agents. Nucleation of PET is of chemical nature. In general, an additive proves to be an effective nucleating agent for PET crystallization if it has a high enough solubility in both water and alcohol, and if the resulting solution is basic. Furthermore, the additive must be easily dispersed in PET.

2 Kinetic and microscopy data have indicated that recycled PET which has not been mechanically processed, crystallizes under diffusion and thermal nucleation control. The crystallization mechanism of mechanically processed recycled PET is controlled by athermal nucleation.

3. Plain PET can be injection molded at $40^{o}C$ mold temperature to produce an amorphous material. A mold temperature of $90^{o}C$ cannot be used. Nucleated PET can be processed at a $90^{o}C$ mold temperature in injection molding, but only Na_2CO_3 and $NaHCO_3$ give good results from the point of view of appearance, crystallinity, and thermal stability.

The general criteria that can be used in determining the effectiveness of an additive as a nucleating agent are:

a) The additive should enhance the crystallization rate. The crystal size should be as small as possible.

b) The injection molded product should have good, uniform appearance.

c) Nucleated PET resins should retain sufficient mechanical properties so that they could have practical end-use applications.

The present study has concluded that Na_2CO_3 and $NaHCO_3$ satisfy all the criteria mentioned above when applied to recycled PET crystallization.

5.2 Polyblends of PET

A. PET with Thermoplastic Polyester Elastomers

Two types (GAFLEX and HYTREL), of polyester elastomers have been tested for their ability to produce blends with reclaimed PET. The results have indicated that small amounts of polyester elastomers (up to 20% by weight) accelerate the crystallization of PET. Products made from the blend (in a typical injection molding cycle), possess a relatively high degree of crystallinity. They also exhibit negligible shrinkage after thermal annealing. The results have also indicated that the blend products have a tensile and flexural strength lower than PET, but this loss of mechanical strength is not significant. Of the two grades of polyester elastomers tested, GAFLEX appears to be better than HYTREL, in terms of both, ease of processability and appearance of the blends.

B. LDPE/PET blends with compatibilizers

Some studies were made in order to explore the possibility of using reclaimed PET as a filler for LDPE. When no compatibilizer was used, LDPE/PET blends resulted in products having mechanical properties better than LDPE. It was found that if PET is present at 30-40%, one gets the best results.

Nonetheless, LDPE and PET are immiscible and, as the SEM studies have indicated, there are always two distinct phases. This can lead to phase separation, and consequently the material may have a short life span (may break). For this reason, compatibilizers were used. Studies with AClyn and Surlyn ionomers showed that the mechanical properties of LDPE/PET blends improve (drastically in the case of Surlyn), when these ionomers are used. This improvement is due to enhanced adhesion between the LDPE and PET phases. Surlyn ionomers give a rather homogeneous material and thus, can be considered as good compatibilizers for LDPE/PET blends.

6. RECOMMENDATIONS FOR FUTURE WORK

Although the present study has provided a number of answers to questions relating to PET recycling, there are still a number of subjects which need further research. Some of them are listed below:

1. Determination of the crystallization induction time has proved to be a difficult task during this study. Development of a model which could predict the induction time would be of extreme importance for future studies.

2. Modelling and simulation work for predicting transient temperature and crystallinity profiles in a finite polymeric slab could provide useful insight regarding what additives and at what temperatures could be used as efficient promoters of PET crystallization.

3. It has been established here that sodium salts are very effective nucleating agents. It stills remains to be determined which sodium salts (i.e. sodium salt of which acids) are the most effective. The target should be to find a salt which can lead to very short cycle times for injection molding, and which can allow for low mold temperatures to be used.

4. Morphology studies on LDPE/PET blends (at the presence of ionomers) can be improved if chemical etching techniques are used.

5. Efforts to form polyblends of recycled PET with polymeric materials other than polyethylene should be continued.

NOMENCLATURE

t_0:	Minute	Starting time of crystallization.
$t_{1/2}$:	Minute	Time span between t_0 and the time needed to achieve a 50% crystallinity.
t_{max}:	Minute	Time span between t_0 and the time at which the maximum of the crystallization peak occurs.
t_∞:	Minute	Ending time of crystallization.
T_{cc}:	°C	Temperature at which the maximum of the crystallization exotherm peak occurs in a cooling scan.
T_{ch}:	°C	Temperature at which the maximum of the crystallization exotherm peak occurs in a heating scan.
T_g:	°C	Glass transition temperature of polymer.
T_m:	°C	Temperature at which the minimum of the melting endotherm peak occurs in a heating scan.
T_m^o:	°C	Equilibrium melting temperature of polymer.
$\triangle T_c$:	°C	Supercooling (temperature span between T_m^o and T_{cc}.)
$\triangle T_{ch}$:	°C	Temperature span between T_{cc} and T_{ch}.
X(t'):	%	Crystallinity of polymer at time, t'.
X_∞:	%	Crystallinity of polymer at time t_∞.

APPENDIX A:

```
C       Avrami equation is used to analyze the isothermal
C       crystallization of poly(ethylene terephthalate). The
C       obtained parameters of the Avrami equation is based
C       on the best confidence of regression.
C       The crystallinity of PET is obtained as described in
C       Chapter 4. The area under curve from thermogram of
C       DSC is integrated by simpson's rule.
C       Area = (Y1+4*Y2+Y3)*H/3
C       Where Y1, Y2, and Y3 are the heights of y-axis
C       (dQ/dt), and H is the stepsize of time.
C
C       ************************************************
C       Name:          Sample code for PET with or without
C                      nucleating agents
C       T:             Isothermal Crystallization temperature
C       NDATA:         Number of data pairs to be analyzed from
C                      computer acquisition
C       X(I):          Crystallization time
C                      XS1: Initial time of F1(t)
C                      XE1: Ending time of F1(t)
C                      XS2: Initial time of F2(t) and ending
C                           time of F3(t)
C                      XE2: Ending time of F2(t)
C                      XS3: Initial time of F3(t)
C       Y(I):          Rate of heat flow at time X(I)
C       AREA(I):       %CRYST*
C       RANGE(I):      RANGE(1): Minimum of x-axis for plot
C                      RANGE(2): Maximum of x-axis for plot
C                      RANGE(3): Minimum of y-axis for plot
C                      RANGE(4): Maximum of y-axis for plot
C       STAT(I)        Parameters as described in subroutine
C                      RCURV in IMSL (FORTRAN subroutines)
C                      STAT(5):  Confidence of regression
C       OUT:           New zero time for system to use FFT
C                      technique
C       CONTROL        Frequency to be deleted whenever the
C                      values are greater than CONTROL
C       STEPSIZE:      Increment time of t_o
C       Ya:            Amorphous baseline
C       Ye:            Crystalline baseline
C       tmax:          Time corresponding to the maximum rate
C                      of heat flow
C       t(half):       Time corresponding to the 50% of
C                      crystallinity
C       n:             Avrami exponent
C       kp(plot):      Rate constant of the Avrami equation
C                      obtained by using regression
C       kp(1/2):       Rate constant of the Avrami equation
C                      obtained by using t(half)
C       kpn(plot):     Rate constant of the modified Avrami
C                      equation obtained by using regression
```

```
C       kpn(1/2):     Rate constant of the modified Avrami
C                     equation obtained by using t(half)
C       TS:           New starting time, t_o, of isothermal
C                     crystallization
C       CON:          Best confidence of regression
C       CONXX1:       Estimate the best time of t_o based on
C                     best confidence
C       CONYA:        Estimate the best amorphous baseline
C                     based on best confidence
C       CONYE:        Estimate the best crystalline baseline
C                     based on best confidence
C       ************************************************

        DIMENSION X(1000), Y(1000), AREA1(1000), XDATA(1000),
           YDATA(1000), B(6), XDATA1(1000), YDATA1(1000),
           Y1(1000), STAT(10), AVDATA(100,15), DATA(15),
           CONDATA(15), RANGE(4)

        EXTERNAL  PAGE, PLOTP, FFTRF, UMACH
        CHARACTER NAME*40

        OPEN(1,STATUS='OLD')
        OPEN(6,STATUS='NEW',RECORDSIZE=132)
        OPEN(7,STATUS='NEW',RECORDSIZE=132)

        READ(1,*)ANYTHING
        READ(1,*)RANGE(3)
        READ(1,*)XS1, XE1, XS2, XE2, XS3
        READ(1,1)NAME
        READ(1,*)T
        READ(1,*)OUT
        READ(1,*) NDATA
        READ(1,*) CONTROL
        DO 100 I=1,NDATA
        READ(1,*)X(I),Y(I)
100     CONTINUE

C       FILTER THE NOISE OF DATA ACQUISITION
        CALL FFTDSC(OUT,CONTROL,XS1,XE1,XS2,XE2,XS3,NDATA,X,
                    Y,Y1)
        STEPSIZE=(XE1-XS1)/100
C       WRITE THE HEADING OF THE RESULTS
        WRITE(7,2)NAME
        WRITE(7,3)T
        WRITE(7,72)
        WRITE(7,*)'ts, Ya, Ye, tmax, t(half), n, kp(plot),',
                  'kp(1/2), kpn(plot)'
C       ESTIMATE THE BEST STARTING CRYSTALLIZATION TIME, t_o,
C       WHICH IS BASED ON THE BEST CONFIDENCE OF REGRESSION
        CON=0.
        DO 3333 IMP=1,100
        TS=XS1+STEPSIZE*(IMP-1)
C       OPTIMIZED BASELINE FOR CRYSTALLIZATION
        CALL NORM3(XS1,XE1,XS2,XE2,XS3,NDATA,X,Y1,TS,YA,YE,
```

```
                XMAX,MDATA,XDATA,YDATA,AREA1)
C       CALCULATE THE PARAMETERS OF THE AVRAMI EQUATION
        CALL AVRAMI1(MDATA,XDATA,YDATA,AREA1,TS,XMAX,T,STAT,
                     DATA)
        DO 87 J=1,12
        AVDATA(IMP,J)=DATA(J)
87      CONTINUE
        WRITE(7,71)TS,YA,YE,(AVDATA(IMP,L),L=1,12),STAT(5)
C       BEST RESULT OF t_o
        IF(CON .GE. STAT(5) ) GO TO 3333
        =STAT(5)
        CONXX1=TS
        CONYA=YA
        CONYE=YE
        DO 89 K=1,12
        CONDATA(K)=DATA(K)
89      CONTINUE
3333    CONTINUE

        WRITE(7,*)'BEST CONFIDENCE '
        WRITE(7,72)
        WRITE(7,*)'ts, Ya, Ye, tmax, t(half), n,',
                  'kp(plot),kp(1/2), kpn(plot)'
1       FORMAT(A)
2       FORMAT(5X,A)
3       FORMAT(2X,F10.1,T40'TEMP')
72      FORMAT(59X,'kpn(1/2),temp,(1000/temp+273.1),
              ln(1/t(1/2)),',','ln(kp),ln(kpn), confidence')
        WRITE(7,71)CONXX1,CONYA,CONYE,(CONDATA(J),J=1,12),CON
71      FORMAT(1X,F6.4,1X,4(F6.2,1X),F4.2,1X,4(F8.3,1X),F6.1,
              1X,F6.2,1X,3(E10.2,1X),F8.4)
        STOP
        END



C       ************************************************
C       SUBROUTINE NORM3(...)
C          PURPOSE:  Optimizing baseline of thermogram
C          INPUT:    XS1,XE1,XS2,XE2,XS3,NDATA,X,Y,TS,YA,
C          OUTPUT:   YE,tmax,MDATA,XDATA,YDATA,AREA1
        SUBROUTINE NORM3(XS1,XE1,XS2,XE2,XS3,NDATA,X,Y,TS,YA,
                         YE,XMAX,MDATA,XDATA,YDATA,AREA1)

        DIMENSION X(1000),Y(1000),AREA1(1000),XDATA(1000),
                  YDATA(1000),YNEW(1000),Y0(1000),B(6),
                  XDATA1(400), YDATA1(400)
C       F1, F2, AND F3 ARE THE CURVE FITTING AS DESICRIBED IN
C       CHAPTER 4, AND A0, A1, A2, AND A3 ARE THE CONSTANTS
C       OF POLYNOMIAL FUNCTION
        F1(Z)=A0+A1*Z+A2*Z*Z+A3*Z*Z*Z
        F2(Z)=A20+A21*Z
        F3(Z)=A30+A31*Z
C       CURVE FITTING FOR F2(Z).
```

```
C       PRINT THE SLOPE, IF IT IS NEGATIVE
        NDEG=1
        DO 2000 I=1,100
        CALL CURVE1(NDATA,X,Y,XDATA1,YDATA1,NDEG,B,XS2,XE2,
                    NOBS)
        A20=B(1)
        A21=B(2)
        IF(A21 .LE. 0.) GO TO 905
        XS2=XS2-0.01
2000    CONTINUE
        WRITE(*,*)'NDEG=',NDEG,'  THE SLOPE OF F2 IS +'
        GO TO 1002
C       CURVE FITTING FOR F3(Z).
C       PRINT THE SLOPE, IF IT IS NEGATIVE
905     DO 3000 I=1,100
        CALL CURVE1(NDATA,X,Y,XDATA1,YDATA1,NDEG,B,XS3,XS2,
                    NOBS)
        A30=B(1)
        A31=B(2)
        IF(A31 .LE. 0.) GO TO 906
        XS3=XS3-0.01
3000    CONTINUE
        WRITE(*,*)'NDEG=',NDEG,'   THE SLOPE OF F3 IS +'
        GO TO 1002
906     KDATA=0

        DO 3300 I=1,NDATA
        IF(X(I) .LE. XE2) GO TO 3300
        KDATA=KDATA+1
3300    CONTINUE
        NDATA=NDATA-KDATA

C       ESTIMATE THE AMORPHOUS BASELINE
        CALL NEWT0(NDATA,X,Y,TS,YA)
        CALL XS3XE2(NDATA,X,Y,XS3,XS2,XE2,A20,A21,A30,A31,
                    YNEW)
        YE=F2(XE2)
C       OPTIMIZED CURVE FITTING
C       REDUCED CRYSTALLINITY, AREA1(I) AT TIME OF X(I)
        CALL BASELINE(NDATA,X,YNEW,TS,YA,YE,A20,A21,
      *               K,XDATA,YDATA,AREA1,XMAX,YMAX)
        DO 4000 I=1,K,2
        MDATA=I/2.+1.
        YDATA(MDATA)=YDATA(I)
        XDATA(MDATA)=XDATA(I)
        AREA1(MDATA)=AREA1(I)
4000    CONTINUE
1002    RETURN
        END
```

```
C       ***************************************************
        SUBROUTINE BASELINE(N,X,Y,TS,YA,YE,A20,A21,M,X0,Y00,
                            AREA0,XMAX,YMAX)
        DIMENSION X(1000),Y(1000),AREA0(1000),X0(1000),
                  Y0(1000), Y00(1000)
C       F2(Z) IS CRYSTALLINE BASELINE
C       BASELINE1 IS SYSTEM BASELINE OF CRYSTALLIZATION
        F2(Z)=A20+A21*Z
        BASELINE1(Z)=(1.-CRYST)*YA+CRYST*F2(Z)
        DO 100 I=1,N
        IF(X(I) .LE.  TS) GO TO 101
        M=I-IXXS+1
        X0(M)=X(I)
        Y0(M)=Y(I)
        GO TO 100
101     IXXS=I
100     CONTINUE
        X0(1)=0
        Y0(1)=0
        Y00(1)=0
        YMAX=0
        XMAX=0
        DO 200 I=2,M
        IF(YMAX .GT. Y0(I)) GO TO 200
        YMAX=Y0(I)
        XMAX=X0(I)
200     CONTINUE
C       CALCULATE THE RATE OF HEAT FLOW, Y00(I), BASED ON YA
C       AND YE
        DO 400 I=2,M
        IF(XMAX .GT. X0(I)) GO TO 450
        BASELINE0=YE
        GO TO 460
450     BASELINE0=YA
460     Y00(I)=Y0(I)-BASELINE0
        IF(Y00(I) .GE. 0.) GO TO 400
        Y00(I)=0.
400     CONTINUE
C       INTEGRATE THE REDUCED CRYSTALLINITY, AREA0(I), BASED
C       ON YA AND YE
        CALL CRYSTAL(M,X0,Y00,AREA0)
        DO 500 I=2,M
        CRYST=AREA0(I)/AREA0(M)
C       CALCULATE THE RATE OF HEAT FLOW, Y00(I), BASED ON
C       OPTIMIZED BASELINE
        Y00(I)=Y0(I)-BASELINE1(X0(I))
        IF(Y00(I) .GE. 0.) GO TO 500
        Y00(I)=0.
500     CONTINUE
C       INTEGRATE THE REDUCED CRYSTALLINITY, AREA0(I), BASED
C       ON OPTIMIZED BASELINE
        CALL CRYSTAL(M,X0,Y00,AREA0)
        RETURN
        END
```

```
C       ****************************************************
        SUBROUTINE CRYSTAL(N,X,Y,AREA)
        DIMENSION X(1000),Y(1000),AREA(1000)

C       AREA, AREA(I), IS INTEGRATED FROM CURVE OF (X, Y) BY
C       USING SIMPSON'S RULE
C       H IS THE STEPSIZE OF TIME

        H=(X(N)-X(1))/(N-1)
        Z=N/2.
        NN=N/2
        NE=N
        IF(Z .GT. NN) GO TO 102
        NE=N+1
        Y(NE)=Y(N)
102     L=N/2
        SUM=0.
        DO 10 I=1,L
        M=2*I+1
        SUM=SUM+(Y(M-2)+4*Y(M-1)+Y(M))*H/3
        AREA(M)=SUM
10      CONTINUE
        AREA(1)=0.
        DO 20 I=1,L
        M=2*I+1
        M1=M-1
        AREA(M1)=(AREA(M)+AREA(M-2))/2
20      CONTINUE
        RETURN
        END


C       ****************************************************
        SUBROUTINE CURVE1(NDATA,X,Y,XDATA,YDATA,NDEG,B,XXS,
                          XXE, NOBS)
        DIMENSION XDATA(1000),YDATA(1000),X(1000),Y(1000),
                  B(6)

C       NDEG IS THE ORDER OF POLYNOMIAL CURVE FITTING IN THE
RANGE
C       BETWEEN XXS AND XXE
        K=0
        IXXS=0
        DO 100 I=1,NDATA
        IF(X(I) .LT. XXS) GO TO 1100
        IF(X(I)  .GT. XXE) GO TO 101
        K=I-IXXS
        XDATA(K)=X(I)
        YDATA(K)=Y(I)
        GO TO 100
1100    IXXS=I
100     CONTINUE
101     NOBS=K
C       POLYNOMIAL CURVE FITTING IN IMSL
```

```
      CALL RCURV(NOBS,XDATA,YDATA,NDEG,B,SSPOLY,STAT)
      RETURN
      END


C     ****************************************************
      SUBROUTINE FFTDSC(OUT,CONTROL,XS1,XE1,XS2,XE2,XS3,N,
                        X,Y,Y1)
      DIMENSION X(1000),Y(1000),Y1(1000),COEF(1000)
C     NEW COORDINATE FOR TIME TO USE FFT TECHNIQUE IN IMSL
      XS1=XS1-OUT
      XE1=XE1-OUT
      XS2=XS2-OUT
      XE2=XE2-OUT
      XS3=XS3-OUT
      M=0
      DO 100 I=1,N
      IF(X(I)  .LT. OUT) GO TO 600
      K=I-M
      X(K)=X(I)-OUT
      Y(K)=Y(I)
      GO TO 100
600   M=I
100   CONTINUE
      N=N-M
C     FFT BY IMSL
      CALL FFTRF(N,Y,COEF)
      DO 900 I=1,N
      COEF(I)=COEF(I)/N
900   CONTINUE
      DO 400 I=CONTROL,N
      COEF(I)=0
400   CONTINUE
C     INVERSE OF FFT BY IMSL
      CALL FFTRB(N,COEF,Y1)
      RETURN
      END


C     ****************************************************
      SUBROUTINE VALUE(K,XDATA,YDATA,Y1,X1)
      DIMENSION XDATA(1000),YDATA(1000)
C     LAGRANGE'S  INTERPOLATION  TO  OBTAIN  Y-VALUE  FOR  A
C     GIVEN X-VALUE
      YY=0.
      DO 100 I=1,K
      TERM=XDATA(I)
      DO 200 J=1,K
      IF(I-J) 1,200,1
1     SA=(Y1-YDATA(J))/(YDATA(I)-YDATA(J))
      TERM=TERM*SA
200   CONTINUE
100   YY=YY+TERM
      X1=YY
```

```
      RETURN
      END


C     ***************************************************
      SUBROUTINE XS3XE2(N,X,Y,XS3,XS2,XE2,A20,A21,A30, A31,
                        YNEW)
      DIMENSION X(1000),Y(1000),YNEW(1000)
      F2(Z)=A20+A21*Z
      F3(Z)=A30+A31*Z
      DO 200 I=1,N
      YNEW(I)=Y(I)
200   CONTINUE
      DO 100 I=1,N
      IF( X(I) .LT. XS2 .OR. X(I) .GT. XE2) GO TO 100
      YNEW(I)=F2(X(I))
100   CONTINUE
      RETURN
      END


C     ***************************************************
C     Ln(-Ln(1-cryst%))=Ln(k)+n*Ln(t)  Avrami Equation

      SUBROUTINE AVRAMI1(N,X,Y,AREA,XX1,TMAX1,T,STAT,DATA)
      DIMENSION X(1000),Y(1000),AREA(1000),U(1000),V(1000),
               Q(1000),V1(1000),U1(1000),V2(1000),B1(2),
               STAT(10), DATA(15)
      DOUBLE PRECISION YY,TERM, Z1(200),Z2(200)
      F4(XZ)=YK3+SLOPE*(XZ)
      Y(I)=Y(I)*100.
C     XX1 REPRESENTS t_o
C     TMAX1 REPRESENTS THE TIME WHICH CORRESPONDS TO
C     THE MAXIMUM RATE OF HEAT FLOW
      CON=0.
C     YY : HALF TIME, t_1/2, OF CRYSTALLIZATION
      IF(XX1 .GT. TMAX1) GO TO 3335
      TMAX=TMAX1-XX1
      DO 1000 I=2,N
      X(I)=X(I)-XX1
1000  CONTINUE
      DO 2000 I=1,N
      AREA(I)=100*AREA(I)/AREA(N)
2000  CONTINUE
C     AREA(I) REPRESENTS THE REDUCED CRYSTALLINITY
      IF(AREA(2) .GT. 5) GO TO 3334
      K=0
      DO 20 I=2,N
      IF(AREA(I) .LT. 40) GO TO 20
      IF(AREA(I) .GT. 60) GO TO 20
      K=K+1
      Z1(K)=X(I)
      Z2(K)=AREA(I)
20    CONTINUE
```

```
C       CALL VALUE(K,Z1,Z2,50,YY)
        YY=0
        DO 500 I=1,K
        TERM=Z1(I)
        DO 600 J=1,K
        IF(I-J)1,600,1
1       TERM=TERM*(50-Z2(J))/(Z2(I)-Z2(J))
600     CONTINUE
500     YY=YY+TERM
        YY1=1./YY
        TYY1=ALOG(YY1)
C       YY : t(half)
C       YY1 : 1/[t(half)]
C       tyy1 : ln{ 1/[t(half)] }

        KK=0
        DO 40 I=2,N
        IF(AREA(I) .LE. 1E-4) GO TO 41
        IF(AREA(I) .LE. 99.99999  ) GO TO 42
        AREA(I)=99.99999
42      U(I)=ALOG(X(I))
        Q(I)=-1.0*ALOG(1.0-(AREA(I)/100.0))
        V(I)=ALOG(Q(I))
C       LEAST SQUARES METHOD TO OBTAIN THE PARAMETERS OF
C       AVRAMI EQUATION IN A REDUCED CRYSTALLINITY RANGE
C       BETWEEN 10 TO 60
        IF(AREA(I) .LT. 10) GO TO 40
        IF(AREA(I) .GT. 60) GO TO 40
        KK=KK+1
        U1(KK)=U(I)
        V1(KK)=V(I)
        GO TO 40
41      IY0=I
40      CONTINUE
        NDEG=1
        CALL RCURV(KK,U1,V1,NDEG,B1,SSPOLY,STAT)
        SLOPE=B1(2)
        YK3=B1(1)
        YK1=EXP(YK3)

C       AVRAMI EQUATION:  1-x=exp[-kpt^n]
C       MODIFIED AVRAMI EQUATION:  1-x=exp[-(kpn*t)^n]

C       SLOPE:  AVRAMI EXPONENT, n
C       YK1:    RATE CONSTANT, kp(plot), OF AVRAMI EQUATION
                FROM PLOT
C       YK2:    RATE CONSTANT, kp(t(half)), OF AVRAMI
C               EQUATION FROM t(half)
C       YK3:    INTERCEPT
C       YK4:    RATE CONSTANT, kpn(plot), OF MODIFIED AVRAMI
C               EQUATION FROM PLOT
C       YK5:    RATE CONSTANT, kpn(t(half), of MODIFIED
                AVRAMI EQUATION FROM t(half)
        YK2=-1*ALOG(0.5)/(YY**SLOPE)
```

```
      YK4=EXP(YK3/SLOPE)
      S=YY
      G=ALOG(-ALOG(0.5))/SLOPE
      H=ALOG(S)
      YK6=G-H
      YK5=EXP(YK6)
C     V2 : REDUCED CRYSTALLINITY FROM AVRAMI EQUATION
      DO 401 I=1,N
401   V2(I)=F4(U(I))

C     TKP     =     ln [kp]
C     TKPN    =     ln [kpn]
C     TEMP    =     1000 /(T+273.150)
      TKP=ALOG(YK1)
      TKPN=ALOG(YK4)
      TEMP=1000./(T+273.15)
      AREA(1)=0.0
      DATA(1)=TMAX
      DATA(2)=YY
      DATA(3)=SLOPE
      DATA(4)=YK1
      DATA(5)=YK2
      DATA(6)=YK4
      DATA(7)=YK5
      DATA(8)=T
      DATA(9)=TEMP
      DATA(10)=TYY1
      DATA(11)=TKP
      DATA(12)=TKPN
      GO TO 3335
3334  WRITE(*,*)'AREA(2) > 5',AREA(2),'%'
3335  RETURN
      END


C     ************************************************
C     SUBROUTINE:  FIND AMORPHOUS BASELINE, YA, FROM
                   F1(XS1) CURVE
      SUBROUTINE NEWT0(NDATA,X,Y,XS1,YA)
      DIMENSION X(1000),Y(1000),XDATA(30),YDATA(30),B(6)
      F1(Z)=A0+A1*Z+A2*Z*Z+A3*Z*Z*Z
      NDEG=3
      DO 1230 I=1,NDATA
      M=I
      IF(X(I) .LT. XS1 ) GO TO 1230
      GO TO 1231
1230  CONTINUE
      WRITE(*,*)'COULD NOT FIND YA, FROM CALL NEWT0'
      GO TO 1002
C     DETERMINE THE RANGE TO CALCULATE THE t_o AND YA
1231  K=0
      ME=0
      YMAXX=0
      DO 301 I=1,NDATA
```

```
      IF(YMAXX .GT. Y(I) ) GO TO 301
      YMAXX=Y(I)
      XYMAXX=X(I)
301   CONTINUE
      DO 303 I=M,NDATA
      ME=I
      IF(X(I) .GT. XYMAXX) GO TO 304
      MEI=ME-M
      IF(MEI .GT. 11) GO TO 304
303   CONTINUE
304   IF(M .GT. 1) GO TO 1232
      DO 21 I=1,ME
      K=K+1
      XDATA(K)=X(I)
      YDATA(K)=Y(I)
21    CONTINUE
      GO TO 1233
1232  DO 20 I=M-1,ME
      K=K+1
      XDATA(K)=X(I)
      YDATA(K)=Y(I)
20    CONTINUE
1233  NOBS=K
C     THE RANGE STARTS FROM 'M'  TO 'ME'
      CALL RCURV(NOBS,XDATA,YDATA,NDEG,B,SSPOLY,STAT)
      A0=B(1)
      A1=B(2)
      A2=B(3)
      A3=B(4)
      YA=F1(XS1)
1002  RETURN
      END
```

REFERENCES:

1 Aharoni, S.M., "Polyester Compositions Containing Sodium Nitrite," US Patent No. 4,349,503 (1982).

2 Aharoni, S.M., "Injection Moldable PET," US Patent No. 4,390,649 (1983).

3 Aharoni, S.M., "Nucleation of PET Crystallization by Metal Hydroxides," J. Appl. Polym. Sci., 29, 853 (1984).

4 Allied-signal Inc., "Introducing a Whole New Breed of Problem-Solvers: AClyn Low Molecular Weight Ionomers," ACL-200 (1987).

5 ASTM "Tensile Properties of Plastics," Part 35, D638, p. 228-244, 1981 Annual Book of ASTM Standards, Philadelphia, Pa 1981.

6 ASTM "Flexural Properties of Plastics and Electrical Insulating Materials," Part 35, D790, p. 327-337, 1981 Annual Book of ASTM Standards, Philadelphia, Pa 1981.

7 ASTM "Rheological Properties of Thermoplastics with a Capillary Rheometer," Part 35, D3835, p. 954-961, 1981 Annual Book of ASTM Standards, Philadelphia, Pa 1981.

8 Avrami, M., "Kinetics of Phase Change. I. General Theory," J. Chem. Phys., 7, 1103 (1939).

9 Avrami, M., "Kinetics of Phase Change. II. Transformation-Time Relations for Random Distribution of Nuclei," J. Chem. Phys., 8, 212 (1940).

10 Avrami, M., "Kinetics of Phase Change. III. Granulation, Phase Change, and Microstructure," J. Chem. Phys., 9, 177 (1941).

11 Axelrod, R.J., F.N. Liberti, and J. Semen, "Process for Increasing the Rate of Crystallization of Polyesters," US Patent No. 4,401,792 (1983).

12 Bailly, CH., M. Daumerie, R. Legras, and J.P. Mercier, "Crystallization of Bisphenol-A Polycarbonate Induced by Organic Salts: Chemical Modification of the Polymer. I. Model Reactions," J. Polym. Sci. Polym. Phys. Ed., 23, 343 (1985).

13 Bailly, CH., M. Daumerie, R. Legras, and J.P. Mercier, "Crystallization of Bisphenol-A Polycarbonate Induced by Organic Salts: Chemical Modification of the Polymer. II. Model Reactions," J. Polym. Sci. Polym. Phys. Ed., 23, 355 (1985).

14 Bailly, CH., M. Daumerie, R. Legras, and J.P. Mercier, "Crystallization of Bisphenol-A Polycarbonate Induced by Organic Salts: Chemical Modification of the Polymer. III. Reactions Mechanism," J. Polym. Sci. Polym. Physics Ed., 23, 493 (1985).

15 Bailly, CH., M. Daumerie, R. Legras, and J.P. Mercier, "Crystallization of Bisphenol-A Polycarbonate Induced by Organic Salts; Physical Aspects. I. Crystallization Rate, Melting Behavior, and Morphology," J. Polym. Sci. Polym. Phys. Ed., 23, 751 (1985).

16 Baranov, V.G., A.V. Kanarov, and T.I. Volkov, "Morphology and Kinetics Studies of Spherulitization of PET," J. Polym. Sci. Part C, Polym. Symp. No. 30, 271 (1970).

17 Barlow, J.W., and D.R. Paul, "Mechanical Compatibilization of Immiscible Blends," Polym. Eng. Sci., 24, No. 8, 525 (1984).

18 Besnoin J.M., and K.Y. Choi, "Identification and Characterization of Reaction Byproducts in the Polymerization of Poly(ethylene terephthalate)," JMS-Rev. Macromol. Chem. Phys., C29(1), 55 (1989).

19 Billmeyer, F.W., Jr., "Textbook of Polymer Science," John Wiley and Sons, Inc, 1962.

20 Binsbergen, F.L.,"Heterogeneous Nucleation in the Crystallization of Polyolefins: Part I. Chemical and Physical Nature of Nucleating Agents," Polymer, 11, 253 (1970).

21 Binsbergen, F.L., and B.M. De Lange "Heterogeneous Nucleation in the Crystallization of Polyolefins: Part II," Polymer, 11, 309 (1970).

22 Binsbergen, F.L., "Heterogeneous Nucleation of Crystallization," in Progress in Solid State Chemistry, Vol. 8, p. 189-238, Pergamon, Oxford, 1973.

23 Binsbergen, F.L., "Heterogeneous Nucleation in the Crystallization of Polyolefins. III. Theory and Mechanism," J. Polym. Sci. Polym. Phys. Ed., 11, 117 (1973).

24 Binsbergen, F.L., "Heterogeneous Nucleation," J. Polym. Sci. Polym. Symp. No. 59, 11 (1977).

25 Bourland, L., "Ultra-High-Flow PP Speeds up PET Crystallization," Plastics Engineering, 43, No. 7, 39 (1987).

26 Brabender, C.W., "Plasti-Corder Torque Rheometer: Manual," Bulletin, PC-78, South Hackensack, N.J. 1980.

27 Chen, I.M. and C.M. Shiah, "Thoughening of PET/HDPE Polyblends from Recycled Beverage Bottles," SPE, ANTEC 89, Technical Papers XXXV, 1802 (1989).

28 Chen, L., W. Chiu, and W.Yu, "A Study on Improving the Crystallization Rate of PET", J. Chin. Chem. Soc., 32, 135 (1985).

29 Christiansen, J. and S.Z. Lu, "High Gloss PET Reinforced Resin Compositions," US Patent No. 4,483,955 (1984).

30 Coleman, E.A., "Fast Crystallizing Ethylene Terephthalate Polymer Composition Containing sodium borohydride," UK Patent Application GB 2108968A (1982).

31 Coleman, E.A., "Fast Crystallizing Ethylene Terephthalate Polymer Composition Containing Antimony Oxide," UK Patent Application GB 2108969A (1982).

32 Coleman, E.A., "Fast Crystallizing PET Containing Neopentyl Dibenzoate," US Patent No. 4,368,285 (1983).

33 Coleman, E.A., K.J. Cronin, J.K. Chu, and W. Kirwan, "Fast Crystallizing PET Composition," US Patent No. 4,448,913 (1984).

34 Coppola, P., G. Fabbri, B. Pallesi, G.C. Alfonso, G. Dondero, and E. Pdedmonte, "Viscosity and Optical Observation of PET During Annealing and Thermal Scanning," Makromo. Chem. 176, 767 (1975).

35 Curry, J. and A. Kiani, "Compounding Recycled PET into Impact-Resistant Plastic," Plastics Engineering, 46, No. 11, 37 (1990).

36 Data sheet, "New Engineering Polymer Source: Recycled PET from Post-Consumer Soft Drink Bottles," Center for Plastics Recycling Research at Rutgers, The State University of New Jersey, (1989).

37 Dekoninck, J.M., R. Legras and J.P. Mercier, "Nucleation of PET by Sodium Compounds: a Unique Mechanism," Polymer, 30, 910 (1989).

38 Desai, A.B., and G.L. Wilkes, "Solvent-Induced Crystallization of PET," J. Polym. Sci., C46, 291 (1974).

39 Deyrup, E.J., "Molding Resins," US Patent No. 4,352,904 (1982).

40 Du Pont Company, "Surlyn Ionomer Resin," H-04376, (1989).

41 Gallez, F., R. Legras and J.P. Mercier, "Some New Aspects of the Crystallization of Bisphenol-A Polycarbonate," Polym. Eng. Sci., 16, No. 4, 276 (1976).

42 Garcia, D.S., "Alkali Metal Salts of Low Molecular Weight PET as Nucleating Agents for PET," US Patent No. 4,425,470 (1984).

43 Garcia, D.S., "Heterogeneous Nucleation of Poly(ethylene terephthalate)," J. Polym. Sci. Polym. Phys. Ed., 22, 2063 (1984).

44 Garrison, W.E. Jr., "Fast Crystallizing Polyester Resin Containing Three-Component Crystallization System," US Patent No. 4,548,978 (1985).

45 Gilbert, M. and F.J. Hybart, "Effect of Chemical Structure on Crystallization Rates and Melting of Polymers: Part 1. Aromatic Polyesters," Polymer, 13, 327 (1972).

46 Groeninckx, G., H. Berghmans, N. Overbergh, and G. Smets, "Crystallization of Polyethylene Terephthalate Induced by Inorganic Compounds," J. Polym. Sci. Polym. Phys. Ed. 12, 303 (1974).

47 Groeninckx, G., H. Reynaers, H. Berghmans, and G. Smets, "Morphology and Melting Behavior of Semicrystalline PET. (I). Isothermally Crystallized PET," J. Polym. Sci. Polym. Phys. Ed., 18, 1311 (1980).

48 Groeninckx, G., and H. Reynaers, "Morphology and Melting Behavior of Semicrystalline PET. (II). Annealed PET," J. Polym. Sci. Polym. Phys. Ed., 18, 1325 (1980).

49 Han, C.D., Rheology in Polymer Processing, Academic Press, New York, 1976.

50 Hartley, F.D., F.W. Lord, L.B. Morgan, "Crystallization Phenomena in Polymers. (III). Effect of Melt Condition and the Temperature of Crystallization on the Course of Crystallization in Poly(ethylene terephthalate)," Phil. Trans. Roy. Soc. London, A247, 23 (1954).

51 Hay, J.N. and P.J. Mills, "The Use of Differential Scanning Calorimetry to Study Polymer Crystallization Kinetics," Polymer, 23, 1380 (1982).

52 Haylock, J.C., and N. Vanderkooi, Jr., "Polyester Composition Containing Tertiary and Quaternary Amine Carboxylate Salts," US Patent No. 4,551,507 (1985).

53 Hergenrother, W.L., and C.J. Nelson, "Viscosity-Molecular Weight Relationship for Fractionated PET," J. Polym. Sci. Polym. Chem. Ed., 12, 2905 (1974).

54 Hiemenz, P.C., Polymer Chemistry, Marcel Dekker, Inc. New York, 1984.

55 Hoffman, J.D., J.J. Weeks, and W. M. Murphey, "Experimental and Theoretical Study of Kinetics of Bulk Crystallization in Poly(Chlorotrifluoro ethylene)," Journal of Research of the National Bureau of Standards-A. Physics and Chemistry, 63A, No. 1, 67 (1959).

56 Hunkar Laboratories Inc., "315 Control System Instruction Manual 98041," Hunkar Laboratories Inc. Ohio, 1978.

57 Hunkar Laboratories Inc., "Molding with the Hunkar Series 700," Part number 98060, Hunkar Laboratories Inc. Ohio, 1986.

58 Instron Engineering Corporation, "Operating Instructions for the Instron Testing Instruments Type TT-B," Manual #10-29-1, Instron Engineering Corporation, Canton, Massachusetts, 1975.

59 Jabarin, S.A., and E.A. Lofgren," Thermal Stability of Polyethylene Terephthalate," Polym. Eng. Sci., 24, No. 13, 1056 (1984).

60 Jabarin, S.A., and E.A. Lofgren, "Effects of Water Absorption on Physical Properties and Degree of Molecular Orientation of PET," Polym. Eng. Sci., 26, No. 9, 620 (1986).

61 Jabarin, S.A., "Crystallization Behavior of PET," Polymer Engineering and Science, 29, No. 18, 1259 (1989).

62 Jabarin, S.A., "Crystallization Kinetics of PET. I. Isothermal Crystallization from the Melt," J. Appl. Polym. Sci., 34, 85 (1987).

63 Jabarin, S.A., "Crystallization Kinetics of PET. II. Dynamic Crystallization of PET," J. Appl. Polym. Sci., 34, 97 (1987).

64 Jabarin, S.A., "Crystallization Kinetics of PET. III. Effect of Moisture on the Crystallization Behavior of PET from the Glassy State," J. Appl. Polym. Sci., 34, 103 (1987).

65 Kamal, M.R., and P.G. Lafleur, "Computer Simulation of Injection Molding", Polym. Eng. Sci., 22, No. 17, 1066 (1982).

66 Keller, A., and G.R. Lester, and L.B. Morgan, "Crystallization Phenomena in Polymers, (I). Preliminary Investigation of the Crystallization Characteristics of Poly(ethylene Terephthalate)," Phil. Trans. Roy. Soc. London, A247, 1 (1954).

67 Keller, A., "The Spherulitic Structure of Crystalline Polymers. Part I. Investigations with the Polarizing Microscope," J. Polym. Sci. 17, 291 (1955).

68 Keller, A., "The Spherulitic Structure of Crystalline Polymers. Part III. Geometrical Factors in Shperulitic Growth and the Fine-Structure," J. Polym. Sci., 17, 447 (1955).

69 Keller, A., and A. O'Connor, "Study of Single Crystals and Their Associations in Polymers?," Discuss. Farady Soc., 25, 114 (1958).

70 Khanna, Y.P., and T.J. Taylor, "Comments and Recommendations on the Use of the Avrami Equation for Physico-Chemical Kinetics," Polym. Eng. Sci., 28, 1042 (1988).

71 Kim, S.P., and S.C. Kim, "Crystallization Kinetics of PET. Part I. Kinetic Equation with Variable Growth Rate," Polym. Eng. Sci., 31, No. 2, 110 (1991).

72 Kumar, A., V.K. Sukthankar, C.P. Vaz and S.K. Gupta, "Optimization of the Transesterification Stage of PET Reactors," Polym. Eng. Sci., 24, No, 3, 185 (1984).

73 Kunori, T., and P.H. Geil, "Morpholoty-Property Relationships in Polycarbonate-Based Blends. I. Modulus," J. Macromol. Sci. Phys., B18(1), 93 (1980).

74 Lauritzen, Jr., J.I., and J.D. Hoffman, "Theory of Formation of Polymer Crystals with Folded Chains in Dilute Solution," J. of Research of the National Bureau of Standards-A. Physics and Chemistry, 64A, No. 1, 73 (1960).

75 Lawton, E.L., "Nucleation of Crystallization of Polyester by Catalyst Remnants-A Review," Polym. Eng. Sci., 25, No.6, 348 (1985).

76 Leaversuch, R.D., "Industry Begins to Face up to the Crisis of Recycling," Modern Plastics, 64, No. 3, 44 (1987).

77 Legras, R., J.P. Mercier, and E. Nield, "Polymer Crystallization by Chemical Nucleation," Nature (London), 304, 432 (1983).

78 Legras, R., C. Bailly, M. Daumerie, J.M. Dekoninck and J.P. Mercier, V. Zichy and E. Nield, "Chemical Nucleation, a New Concept Applied to the Mechanism of Action of Organic Acid Salts on the Crystallization of Poly(ethylene Terephthalate) and Bisphenol-A Polycarbonate," Polymer, 25, 835 (1984).

79 Legras, R., J.M. Dekoninck, A. Vanzieleghem and J. P. Mercier, and E. Nield, "Crystallization of PET Induced by Organic Salts: Model Compound Study of the Mechanism of Action of the Nucleating Agent," Polymer, 27, 109 (1986).

80 Malkin, A.Y., V.P. Beghishev, and I.A. Keapin, "Macrokinetics of Polymer Crystallization," Polymer, 24, 81 (1983).

81 Malkin, A.Y., V.P. Beghishev, I.A. Keapin , and S.A. Bolgov, "General Treatment of Polymer Crystallization Kinetics-Part 1. A New Macrokinetic Equation and its Experimental Verification," Polym. Eng. Sci., 24, No. 18, 1396 (1984).

82 Malkin, A.Y., V.P. Beghishev, I.A. Keapin , and Z.S. Andrianova, "General Treatment of Polymer Crystallization Kinetics-Part 2. The Kinetics of Nonisothermal Crystallization," Polym. Eng. Sci., 24, No. 18, 1402 (1984).

83 Margolis, J.M., Engineering Thermoplastics: Properties and Applications, Marcel Dekker, Inc., New York, 1983.

84 Makarewicz, P.J., and G.L. Wilkes, "Morphology Studies of the Liquid-Induced Crystallization of PET: Effects of Polymer Blending, Nucleating Agents, and Molecular Weight," J. Appl. Polym. Sci., 23, 1619 (1979).

85 McNaughton, J.L., and C.T. Mortimer, "Differential Scanning Calorimetry," Order Number: L-604, The Perkin-Elmer Corporation, Norwalk, Connecticut, (Reprinted from "IRS; Physical Chemistry Series 2, 10, 1975").

86 Meeten, G.H., Optical Properties of Polymers, Elsevier Applied Science Publishers, London and New York, 1986.

87 Mercier, J.P. "Nucleation in Polymer Crystallization: A Physical or a Chemical Mechanism?," Polym. Eng. Sci., 30, No. 5, 270 (1990).

88 Misra, A., and S.N. Garg, "Block Copolymers of Poly(ethylene Terephthalate - Polybutylene Terephthalate). I. Preparation and Crystallization Behavior," J. Polym. Sci. Part B Polym. Phys., 24, 983 (1986).

89 Mizoguchi, K., T. Hirose, Y. Naito, and Y. Kamiya, "CO_2-Induced Crystallization of PET," Polymer, 28, 1298 (1987).

90 Morgan, L.B., "Crystallization Phenomena in Polymers. (II). The Course of the Crystallization," Phil. Trans Roy. Soc. London, A247, 13 (1954).

91 Morrison, R.T., and R.N. Boyd, Organic Chemistry, 3rd edition, Allyn and Bacon, Inc., Boston, 1976.

92 Muller, A.J., J.L. Feijoo, M.E. Alvarez, and A.C. Febles, "The Calorimetric and Mechanical Properties of Virgin and Recycled PET from Beverage Bottles," Polym. Eng. Sci., 27, No 11, 796 (1987).

93 Murphy, C.J., G.V. S.Henderson, Jr., E.A. Murphy, and L.H. Sperling, "The Relationship Between the Equilibrium Melting Temperature and the Supermolecular Structure of Several Polyoxetanes and Polyethylene Oxide," Polym. Eng. Sci., 27, No. 11, 781 (1987).

94 Muzzy, J.D., D.G. Bright, and G.H. Hoyos, "Solidification of PET with Incomplete Crystallization," Polym. Eng. Sci., 18, No. 6, 437 (1978).

95 Nakamura, K., K. Neki, "Polyester Composition and Production Thereof," US Patent No. 4,524,191 (1985).

96 Nelsen, S.B.,"PET Molding Composition," US Patent No. 4,539,356 (1985).

97 Nir, M.M, "Implications of Post-Consumer Plastic Waste: Part Two," Plastics Engineering, 46, No. 9, 29 (1990).

98 Nir, M.M, "Implications of Post-Consumer Plastic Waste: Part Two," Plastics Engineering, 46, No. 10, 21 (1990).

99 Palys, L.H., and P.J. Phillips, "Microkinetics of Crystallization in Polyethylene Terephthalate," J. Polym. Sci. Polym. Phys. Ed., 18, 829 (1980).

100 Perkin-Elmer, "DSC-2 manual," 1978.

101 Pratt, C.F. and S.Y. Hobbs, "Comparative Study of Crystallization Rates by DSC and Depolarization Microscopy," Polymer, 17, 12 (1976).

102 Przygocki, W., and A. Wlochowicz, "Effect of Nucleating Agents Upon the Kinetics of PET Crystallization," J. Appl. Polym. Sci., 19, 2683 (1975).

103 Ravindranath, K., and R.A. Mashelkar, "Modeling of PET Reactors," Chem. Eng. Sci., 41(9), 2197 (1986).

104 Rao, M.V.S., R. Kumar, and N.E. Dweltz, "Studies on the Structural Dependence of Melting Behavior of PET by Differential Scanning Calorimetry," J. Appl. Polym. Sci., 32, 4439 (1986).

105 Roberts, R.C., "PET; I. Heat of Fusion," Polymer 10, 113 (1969).

106 Schaul, J.S., "Drying and Injection Molding PET for Beverage Bottle Preforms," Polym. Plast. Technol. Eng., 16(2), 209 (1981).

107 Scott, M.G., and P. Ramachandrarao, "The Kinetics of Crystallization of an Fe-P-C Glass," Materials Science and Enginerring, 29, 137 (1977).

108 SPI, "Plastics Bottle Recycling Directory and Reference Guide 1985," Plastic Bottle Institute, Division of the Society of the Plastics Industry, Inc., Washington, D.C., 1985.

109 SPI, "1989 Plastics Recycling Directory," SPI, Plastic Bottle Institute, The Society of the Plastics Industry, Inc., Washington, D.C., (1989).

110 Sun, D.C. and J.H. Magill, "Thermal Interactions in Oriented Polymeric Materials: Shrinkage, Crystallization, and Melting," Polym. Eng. Sci., 29, No. 21, 1503 (1989).

111 Szekely-pecsi, Z., I. Vancso-szmercsanyi, and F. Cser, "Metal-Containing Corrdination Polymers. XI. Crystallization and Melting Behavior of a Semicrystalline Polyester and Its Mg(II) Complexes," J. Polym. Sci., 19, 703 (1981).

112 Tan, V., "On the Kinetics of Flow Induced Crystallization of Polyethylene Melt Above Its Normal Melting Point," PhD Dissertation, Stevens Institute of Technology, Castle Point Station, Hoboken, New Jersey, 1975.

113 Tesoro, G., "Recycling of Synthetic Polymers for Energy Conservation-The State of the Art," Polymer News, 12, 265 (1987).

114 Thayer, A.M., "Solid Waste Concerns Spur Plastic Recycling Efforts," Chemical & Engineering News, 67, 7 1989.

115 Traugott, T.D., J.W. Barlow, and D.R. Paul, "Mechanical Compatibilization of HDPE/PET Blends," J. Appl. Polym. Sci. 28, 2947 (1983).

116 Utracki, L.A., "Economics of Polymer Blends," Polym. Eng. Sci., 22, No. 17, 1166 (1982).

117 Van Antwerpen, F., and D.W.V. Krevelen, "Influence of Crystallization Temperature, Molecular Weight, and Additives on the Crystallization Kinetics of PET," J. Polym. Sci. Polym. Phys. Ed., 10, 2423 (1972).

118 Vanderkooi, N., and H.W. Tuller, "PET Composition Containing Aliphatic Plasticizer and Nucleating Agent," U.S. Patent, No. 4,327,007 (1982).

119 Vancso-szmercsanyi, I., and A. Szilagyi, "Coordination Polymers form Polycondensates and Metal Oxides. II. Effect of Water Molecules on the Reactions of Polyesters with MgO and ZnO," J. Polym. Sci. Polym. Chem. Ed., 12, 2155 (1974).

120 Vilanova, P.C., and S.M. Ribas, "Isothermal Crystallization PET of Low Molecular Weight by Differential Scanning Calorimetry: 1. Crystallization Kinetics," Polymer, 26, 423 (1985).

121 Voss, D., and S. Spring, "Plastics Recycling," Chemical Engineering Progress, 85, No. 10, 67 (1989).

122 Weast, R.C., CRC, Handbook of Chemistry and Physics, 64th Edition, CRC Press, Florida, 1984.

123 Wilfong, D.L., A. Hiltner, and E. Baer, "Toughening of Polyester Resins Through Blending with Polyolefins," J. of Materials Science, 21, 2014 (1986).

124 Williams, R., "Polyester Moulding Compositions," US Patent No. 4,540,729 (1985).

125 Wunderlich, B., Macromolecular Physics, Vol. 1, Academic Press, New York, 1976.

126 Wunderlich, B., Macromolecular Physics, Vol. 2, Academic Press, New York, 1976.

127 Xanthos, M., "Interfacial Agents for Multiphase Polymer Systems: Recent Advances," Polym. Eng. Sci., 28, No. 21, 1392 (1988).

128 Yamashita, Y., "Single Crystals of Poly(ethylene Terephthalate)," J. Polym. Sci.: Part A, 3, 81 (1965).

129 Yeh, G.S.Y., and P.H. Geil, "Strain-Induced Crystallization of PET, "J. Macromol. Sci. (Phys.), B1(2), 251 (1967).

130 Zeilstra, J.J., "Influencing the Crystallization Behavior of PET-Based Segmented Copoly(ether Ester)," J. Appl. Polym. Sci., 31, 1977 (1986).

131 Zhou, C. and S.B. Clough, "Multiple Melting Endotherms of PET," Polym. Eng. Sci., 28, No. 2, 65 (1988).

Table 3.1 *Resins Used in this Study. R represents recycled material; V represents virgin material.*

Resin	Sample Code Used	V/R	Appearance of Material	Supplier
PET	V-PET	V	Opaque, 0.1" Pellet	Eastman Kodak Co. (Kodapak PET 7352)
	R-PET or R-PET-1	R	Clear, Transparent Flakes	CPRR (Rutgers University)
	R-PET-2	R	Opaque Pellet	St. Jude Polymer
	G-PET	R	Green, Transparent Flakes	CPRR (Rutgers University)
	RR-PET	R	Green Flakes & Clear Flakes	CPRR (Rutgers University)
PE	LDPE-1	V	White Chip	Mobil
	LDPE-2	V	White Chip	US Industrial, (LDPE,NA140)
	HDPE	V	White Chip	Phillips 66 Company, HHM TR-140 Company
Polyester Elastomer	GAFLEX 547ZS 555ZS 572ZS	V	Muddy Brown	GAF
	HYTREL 4056	V	White	Du Pont Co.
Ionomer	Surlyn S8527 S8920	V	Muddy Brown	Du Pont Co.
	Aclyn 262A 272A 276A 285A	V	White Powder	Allied-Signal Inc.

Table 3.2 Inorganic Carbonates Salts Used as Potential Nucleating Agents

Carbonate	Chemical Name	Supplier
Na_2CO_3	Sodium Carbonate	Brothers Chemical Co.
$NaHCO_3$	Sodium Bicarbonate	Brothers Chemical Co.
K_2CO_3	Potassium Carbonate	Fisher Scientific Co.
$MgCO_3$	Magnesium Carbonate	J. T. Baker Chemical Co.
$CaCO_3$	Calcium Carbonate	Fisher Scientific Co.
$SrCO_3$	Strontium Carbonate	J. T. Baker Chemical Co.
$BaCO_3$	Barium Carbonate	Brothers Chemical Co.
$ZnCO_3$	Zinc Carbonate	Fisher Scientific Co.
$CdCO_3$	Cadmium Carbonate	Merck & Company Inc.
$PbCO_3$	Lead Carbonate	Fisher Scientific Co.

Table 3.3 Coupling Agents Used in LDPE/PET Blends.

Coupling Agent	Supplier	Formula
LICA 12	Kenrich Petrochemicals Inc.	$ROTi[OP(O)(OC_8H_{17})_2]_3$
LICA 44	Kenrich Petrochemicals Inc.	$ROTi(OC_2H_4NHC_2H_4NH_2)_3$
Prosil 2020	PCR Inc.	Silane coupling agents, $R'\text{-}SiR_3$

R' is an organofunctional group attached to silicon.
R group is a hydrolyzable group that converts to a silanol group or reacts readily with silanols or metal oxides

Table 3.4. Operating Conditions for Injection Molding.

Cylinder Temperature rear zone front zone nozzle	(^{o}C)	 260 278 280
Injection Pressure	(psi)	1100 to 1350
Shot Size	(in)	1.5-2.0
Cushion	(in)	0.1
Pullback	(in)	0.7
Injection Forward Time	(sec)	10
Mold Cooling Time	(sec)	10 to 60
Mold Temperature	(^{o}C)	10 to 90

Table 4.1 Physical Properties of Carbonate Salts used as Nucleating Agents for PET.

Chemical	Mol. wt.	Form	Density g/cc	T_m °c	Solubility g/100 cc of H_2O Cold	Hot	Other solvents
Li_2CO_3	73.89	wh	2.11	723	1.54^{0}	0.72^{100}	i al; acet
Na_2CO_3	105.99	wh powd	2.532	851	7.1^{0}	45.54^{100}	sl s abs al; i acet
$NaHCO_3$	84.00	wh	2.159	$-CO_2$, 270	6.9^{0}	16.4^{60}	sl s al
K_2CO_3	138.21	col	2.428	891	112^{20}	156^{100}	i al, acet
$MgCO_3$	84.32	wh	2.958	d 350	0.0106		s a, aq+CO_2; i acet,NH_3
$CaCO_3$	100.09	col	2.930	520	0.00153^{25}	0.00190^{75}	s a, NH_4Cl
$SrCO_3$	147.63	wh powd	3.70	>1700	0.0011^{18}	0.065^{100}	0.12 aq CO_2; s a, NH_4 salts
$BaCO_3$	197.35	wh	4.43	1740	0.002^{20}	0.006^{100}	s a, NH_4Cl; i al
$ZnCO_3$	125.39	col	4.398	$-CO_2$, 300	0.001^{15}		s a, alk, NH_4 salt i NH_3, acet, pyr
$CdCO_3$	172.41	wh	4.258	d < 500	i	i	s a, KCN, NH_4 salts
$PbCO_3$	267.2	col	6.6	d 315	0.00011^{20}	d	s a, alk; i NH_3, al

a: acid, abs: absolute, acet: acetone, al: alcohol, alk: alkali, aq: aqua, water, col: colorless, d: decomposes, i: insoluble, powd: powder, pyr: pyridine, s: soluble, sl: slightly, wh: white.

Table 4.2 Properties of Cations of Nucleating Agents.

Symbol	Li	Na	K	Mg	Ca	Sr	Ba	Zn	Cd	Pb	Uint
Group	IA	IA	IA	IIA	IIA	IIA	IIA	IIB	IIB	IVB	
Atomic Number	3	11	19	12	20	38	56	30	48	82	
Atomic Weight	6.9	22.9	39.1	24.3	40.1	87.6	137	65.3	112	207	
Oxidation States	1	1	1	2	2	2	2	2	2	2,4	
Density	0.53	0.97	0.86	1.74	1.55	2.6	3.5	7.14	8.65	11.4	g/cm^3
Melting Point	453	371	336	922	1112	1041	1002	692	594	600	^oK
Boiling Point	1615	1156	1032	1363	1757	1650	2171	1180	1040	2023	^oK
Covalent Radius	1.23	1.54	2.03	1.36	1.74	1.91	1.98	1.25	1.48	1.47	Å
Atomic Radius	2.05	2.23	2.77	1.72	2.23	2.45	2.78	1.53	1.71	1.81	Å
Atomic Volume	13.1	23.7	45.5	14.0	29.9	33.7	39.2	9.2	13.1	18.2	cm^3/mol
Electronegativity	0.98	0.93	0.82	1.31	1.0	0.95	0.89	1.65	1.69	2.33	Pauling's
Frist Ionization Potential	5.39	5.14	4.34	7.65	6.11	5.70	5.21	9.39	8.90	7.42	Volt
Heat of Fusion	3.00	2.60	2.33	8.95	8.54	8.30	7.75	7.32	6.19	4.80	KJ/mol
Specific Heat Capacity	3.6	1.23	0.75	1.02	0.63	0.30	0.20	0.39	0.23	0.13	J/g/K
Thermal Conductivity	0.85	1.41	1.02	1.56	2.00	0.35	0.18	1.16	0.97	0.35	W/cm/K
Electrical Conductivity	0.11	0.21	0.14	0.23	0.30	0.08	0.03	0.17	0.14	0.05	10^6/cm/oh

Table 4.2 Continued.

Symbol	Li	Na	K	Mg	Ca	Sr	Ba	Zn	Cd	Pb	Uint
Acid-Base Properties	B	B	B	B	B	B	B	AB	WB	AB	Symbol
Crystal Structure	BCC	BCC	BCC	HG	FCC	FCC	BCC	HG	HG	FCC	

BCC: Body Centered Cubic
FCC: Face Centered Cubic
HG : Hexagonal
B : Oxide is Basic
A : Oxide is Acidic
WB : Oxide is Week Basic
AB : Oxide is Amphoteric

Table 4.3 Typical Physical Data of Kodapak PET-7352 Supplied by Eastman Kodak Company.

Property of pellets	Test Method	Value
IV[a] (g/dl)	ECD-A-AC-G-V-1	0.74
Density (g/cm^3) Crystalline) Amorphous Melt at 285 ^oC	 ASTM D 1505 ASTM D 1238-79	 less 1.40 1.33 less 1.2
Molecular weight Number avg (M_n) Weight avg (M_w)		 23,000 46,000
Crystalline peak melting point, T_m, ^oC	ASTM D3418	about 245
Heat of fusion (cal/g)	ASTM E 793	14
Thermal Conductivity (10^{-4}cal/cm /^oC/s)	ASTM C 177	6.5
Specific heat (cal/g/^oC) 23 ^oC 80 ^oC 100 ^oC 200 ^oC 280 ^oC	ASTM D 2766	 0.27 0.34 0.36 0.45 0.49
Acetaldehyde (ppm)		about 3
Pellets, size and shape, in		1/10 cube
Crystallinity (%)		about 50%
Properties of oriented bottle molded in Eastman's Laboratory		
Crystallinity		about 25%
Tensile strength at yield (psi)		10,000
Tensile modulus of elasticity (10^5 psi)		3.2

[a] IV represents the intrinsic viscosity.

Table 4.4 Properties of R-PET from Center for Plastics Recycling Research at Rutgers University.

a: Purity from recycling stream	
Material	Percent
PET	99.9
PE	0.03
Aluminum	0.01
Other	0.06

b: Molecular Weight Distribution*	
R-PET	Pounds/Pound-Mole
Number Average	39,832
Weight Average	86,688
Z Average	155,445

* gel permeation chromatography

Table 4.5 Weight Loss of Inorganic Carbonate Salts by TGA from 60 to 300 ^{o}C at a scan rate of 20 ^{o}C/min

Name	T_m	Weight loss,	Peak 1		Weight loss,	Peak 2	
	^{o}C	wt%	Temp range ^{o}C	^{o}C	wt%	Temp range ^{o}C	^{o}C
Li_2CO_3	723				0	60-300	
Na_2CO_3	851				15	90-180	175
$NaHCO_3$	270d		108-125	110	36.4	125-250	215
K_2CO_3	891				9	95-245	200
$MgCO_3$	350d	1.6	60-175		6	175-300	
$CaCO_3$	520				.03	60-300	
$SrCO_3$	1700				.026	60-300	
$BaCO_3$	1740				.19	102-125	115
$ZnCO_3$	300d	.83	60-205		3.8	205-300	
$PbCO_3$	315d				.92	134-300	

Table 4.6 I.V. of R-PET with 0.5% of Various Nucleating Agents Measured at 25 ^{o}C.

Nucleating Agent	wt% dl/g	I.V. %	I.V.reduced
bR-PET		0.715	100
aR-PET		0.705	98.6
Na_2CO_3	0.5	0.595	83.2
$NaHCO_3$	0.5	0.567	79.3
K_2CO_3	0.5	0.657	91.9
$MgCO_3$	0.5	0.650	90.9
$CaCO_3$	0.5	0.651	91.0
$SrCO_3$	0.5	0.654	91.5
$BaCO_3$	0.5	0.645	90.2
$ZnCO_3$	0.5	0.500	69.9
$CdCO_3$	0.5	0.648	90.6
$PbCO_3$	0.5	0.445	62.2

Table 4.7 I.V. of R-PET, G-PET, and V-PET with Different Concentrations of Na_2CO_3, $CaCO_3$, and $PbCO_3$ Measured at 25 ^oC.

Nucleating Agent	wt%	R-PET [dl/g]	G-PET [dl/g]	V-PET [dl/g]
b, PET		0.715	0.655	0.625
a, PET		0.705	0.560	
Na_2CO_3	0.3 0.5 1.0	0.687 0.595 0.525		 0.588 0.530
$CaCO_3$	0.3 0.5 1.0	0.700 0.651 0.635	 0.62	 0.605
$PbCO_3$	0.3 0.5 1.0	0.585 0.445 0.390	 0.481	 0.380

Table 4.8 Melt Viscosity of PET at Different Temperatures and Shear Rates.

Shear rate 1/sec	bV-PET 270 °C poise	bV-PET 280 °C poise	aV-PET 270 °C poise
30	3326	3302	2255
100	3025	2659	1830
300	2597	2206	1562
1000	1904	1658	1233
2000	1423	1258	979

Shear rate 1/sec	bR-PET 270 °C	bR-PET 280 °C	aR-PET 270 °C
30	3503	2474	2760
100	3039	2001	1934
300	2699	1785	1605
1000	1930	1378	1295
2000	1445	1067	1052

Shear rate 1/sec	bG-PET 270 °C	bG-PET 280 °C	aG-PET 270 °C
30	3977	3432	2462
100	3206	2269	1625
300	2684	1734	1300
1000	1942	1256	1059
2000	1448	894	871

Table 4.9 Melt Viscosity of PET with 0.5 wt% Na_2CO_3 at 270 ^oC and Different Shear Rates.

Shear rate 1/sec	R-PET poise	V-PET poise	G-PET poise
30		2237	
100		1775	
300		1646	
1000		1345	
2000		1107	
58.6	2290		1740
106			1233
199	1736		1339
504	1135		1151
820			865
996	888		970
1992	1003		824
2930	1083		569

Table 4.10 Melt Viscosity of R-PET with 0.5% $NaHCO_3$ at 270 ^oC and Different Shear Rates.

Shear rate 1/sec	R-PET poise	G-PET poise	V-PET poise
30		1242	2308
100		720	1843
300		466	1108
1000		418	878
2000		356	736
199.25	924		
504	989		
996	833		
1992	578		

Table 4.11. Melt Viscosity of R-PET with 0.5% K_2CO_3 at 270 ^oC and Different Shear Rates.

Shear rate 1/sec	R-PET poise	G-PET poise	V-PET poise
30		1077	1894
100	1034	992	1375
300	804	875	1169
1000	650	756	979
2000	545	618	830

Table 4.12 Melt Viscosity of R-PET with 0.5% $MgCO_3$ at 270 ^oC and Different Shear Rates.

Shear rate 1/sec	R-PET poise	G-PET poise	V-PET poise
30	1445	1396	3124
100	532	612	1200
300	306	418	606
1000	230	375	469
2000	209	347	412

Table 4.13. The melt Viscosity of R-PET with 0.5% $CaCO_3$ at 270 ^oC and Different Shear Rates.

Shear rate 1/sec	R-PET poise	G-PET poise	V-PET poise
30	1935	1822	3030
100	1311	1295	2123
300	1000	1003	1742
1000	822	807	1361
2000	691	670	1088

Table 4.14 Melt Viscosity of R-PET with 0.5% $SrCO_3$ at 270 ^oC and Different Shear Rates.

Shear rate 1/sec	R-PET poise	G-PET poise	V-PET poise
30	2757		2947
100	1490	1358	2203
300	1145	1263	1863
1000	958	1050	1451
2000	805	875.6	1141

Table 4.15. Melt Viscosity of R-PET with 0.5% $BaCO_3$ at 270 ^oC and Different Shear Rates.

Shear rate 1/sec	R-PET poise	G-PET poise	V-PET poise
30	2935	2722	2639
100	1723	1688	1918
300	1384	1272	1560
1000	1128	994	1233
2000	918	807	986

Table 4.16 Melt Viscosity of R-PET with 0.5% $ZnCO_3$ at 270 ^{o}C and Different Shear Rates.

Shear rate 1/sec	R-PET poise	G-PET poise	V-PET poise
30	2272	1704	1408
100	766	701	772
300	340	448	567
1000	268	386	496
2000	242	345	442

Table 4.17 Melt Viscosity of R-PET with 0.5% $CdCO_3$ at 270 ^{o}C and Different Shear Rates.

Shear rate 1/sec	R-PET poise	G-PET poise	V-PET poise
30		2817	2557
100	2109	1333	1939
300	1541	892	1600
1000	1226	718	1262
2000	989	598	1005

Table 4.18 Melt Viscosity of R-PET with 0.5% $PbCO_3$ at 270 ^oC and Different Shear Rates.

Shear rate 1/sec	R-PET poise	G-PET poise	V-PET poise
30	1680	2956	2000
100	710	1344	992
300	430	808	709
1000	363	663	592
2000	331	596	508

Table 4.19. Melt Viscosity of R-PET with 0.3%, 0.5%, and 1.0% Na_2CO_3 at 270 ^oC and Different Shear Rates.

Shear rate 1/sec	0.3 wt% Na_2CO_3 poise	0.5 wt% Na_2CO_3 poise	1.0 wt% Na_2CO_3 poise
30	1829		2787
100	1462		2255
300	1127		1745
1000	912		1369
2000	750		1113
58.6		2290	
199.3		1736	
504		1135	
996		888	
1992		1003	
2930		1083	

Table 4.20 Melt Viscosity of R-PET with 0.5% $NaHCO_3$ at 260, 270, and 280 ^{o}C, and Different Shear Rates.

Shear rate 1/sec	260 ^{o}C poise	270 ^{o}C poise	280 ^{o}C poise
58.6	1633		
105	1854		
199		924	
504		989	
820	981		
996	708	833	
1992	869	578	
2930	730		
11			799
58			479
292			507
703			507
1464			420
2929			401
7031			312

Table 4.21 Melt Viscosity of G-PET with 0.5% $NaHCO_3$ at 260, 270, and 280 ^{o}C, and Different Shear Rates.

Shear rate 1/sec	260 ^{o}C poise	270 ^{o}C poise	280 ^{o}C poise
11.7			621
58.6			434
105			641
199			280
504			305
820			374
996			286
1992			299
2930			249
30	1609	1242	
100	874	720	
300	625	466	
1000	527	418	
2000	457	356	

Table 4.22 Melt Viscosity of V-PET with 0.5% $NaHCO_3$ at 260, 270, and 280 ^{o}C, and Different Shear Rates.

Shear rate 1/sec	260 ^{o}C poise	270 ^{o}C poise	280 ^{o}C poise
58.6			692
105			522
199			574
504			576
996			569
1992			465
30	3089	2308	
100	1552	1843	
300	1166	1108	
1000	926	878	
2000	768	736	

Table 4.23 Melt Viscosity of R-PET with 0.5% Na_2CO_3 at 260, 270, and 280 ^oC, and Different Shear Rates.

Shear rate 1/sec	260 ^oC poise	270 ^oC poise	280 ^oC poise
11.7	3817		1997
58.6	4243	2290	870
105	3373		976
199	1533	1736	952
504	1663	1135	910
820	2231		
996	1367	888	855
1992	1358	1003	680
2930	1215	1083	

Table 4.24 Melt Viscosity of G-PET with 0.5% Na_2CO_3 at 260, 270, and 280 °C and Different Shear Rates.

Shear rate 1/sec	260 °C poise	270 °C poise	280 °C poise
11.7			621
58.6			434
105			641
199			280
504			305
820			374
996			286
1992			299
2930			249
30	1609	1242	
100	874	720	
300	625	466	
1000	527	418	
2000	457	356	

Table 4.25 Melt Viscosity of V-PET with 0.5% Na_2CO_3 at 260, 270, and 280 ^oC, and Different Shear Rates.

Shear rate 1/sec	260 ^oC poise	270 ^oC poise	280 ^oC poise
11.7	3196		2485
58.6	2574		1428
105	2377		1015
199	1987		1148
504	1467		701
820	1748		
996	1128		853
1992	1115		743.5
2930	1072		
30		2237	
100		1775	
300		1646	
1000		1345	
2000		1107	

Table 4.26 Parameters of Power Law for Melt Viscosity of Polymer ($\eta_m = k\,\gamma^{(n-1)}$ or $\tau = \eta_m\,\gamma$ and $\tau = k\,\gamma^n$).

Material	Temp °C	n-1	Consist. k	Index n
bR-PET,	270	-0.20	7603.09	0.80
bR-PET,	280	-0.19	4863.39	0.81
aR-PET,	270	-0.22	5573.59	0.78
bG-PET,	270	-0.23	9261.95	0.77
bG-PET,	280	-0.30	9607.82	0.70
aG-PET,	270	-0.23	5142.85	0.77
bV-PET,	270	-0.20	7157.70	0.80
bV-PET,	280	-0.22	7321.66	0.78
aV-PET,	270	-0.19	4422.33	0.81
R-PET/0.5% Na_2CO_3	270	-0.23	5592.04	0.77
G-PET/0.5% Na_2CO_3	270	-0.23	4275.64	0.77
V-PET/0.5% Na_2CO_3	270	-0.16	3799.17	0.84
R-PET/0.5% $NaHCO_3$	270	-0.20	2954.11	0.80
G-PET/0.5% $NaHCO_3$	270	-0.29	2899.54	0.71
V-PET/0.5% $NaHCO_3$	270	-0.28	6176.95	0.72
R-PET/0.5% K_2CO_3	270	-0.21	2681.28	0.79
G-PET/0.5% K_2CO_3	270	-0.13	1733.37	0.87
V-PET/0.5% K_2CO_3	270	-0.19	3423.96	0.81
R-PET/0.5% $CaCO_3$	270	-0.24	4094.51	0.76
G-PET/0.5% $CaCO_3$	270	-0.23	3872.91	0.77
V-PET/0.5% $CaCO_3$	270	-0.23	6504.18	0.77
R-PET/0.5% $BaCO_3$	270	-0.26	6367.27	0.74
G-PET/0.5% $BaCO_3$	270	-0.28	6524.37	0.72
V-PET/0.5% $BaCO_3$	270	-0.22	5574.43	0.78
R-PET/0.5% $SrCO_3$	270	-0.27	6068.68	0.73
G-PET/0.5% $SrCO_3$	270	-0.14	2741.34	0.86
V-PET/0.5% $SrCO_3$	270	-0.21	6119.23	0.79
R-PET/0.5% $CdCO_3$	270	-0.24	6400.29	0.76
G-PET/0.5% $CdCO_3$	270	-0.35	7804.16	0.65
V-PET/0.5% $CdCO_3$	270	-0.21	5289.05	0.79

Table 4.26 Continued.

R-PET/0.3% Na_2CO_3	270	-0.21	3774.38	0.79
R-PET/0.5% Na_2CO_3	270	-0.22	5233.05	0.78
R-PET/1.0% Na_2CO_3	270	-0.22	5974.28	0.78
R-PET/0.5% Na_2CO_3	260	-0.24	8036.03	0.76
R-PET/0.5% Na_2CO_3	270	-0.22	5160.12	0.78
R-PET/0.5% Na_2CO_3	280	-0.16	2294.03	0.84
G-PET/0.5% Na_2CO_3	260	-0.29	3675.86	0.71
G-PET/0.5% Na_2CO_3	270	-0.29	2899.54	0.71
G-PET/0.5% Na_2CO_3	280	-0.16	909.73	0.84
V-PET/0.5% Na_2CO_3	260	-0.21	5910.85	0.79
V-PET/0.5% Na_2CO_3	270	-0.16	3799.17	0.84
V-PET/0.5% Na_2CO_3	280	-0.23	3713.66	0.77
R-PET/0.5% $NaHCO_3$	260	-0.24	4757.66	0.76
R-PET/0.5% $NaHCO_3$	270	-0.20	2951.20	0.80
R-PET/0.5% $NaHCO_3$	280	-0.12	957.17	0.88
G-PET/0.5% $NaHCO_3$	260	-0.29	3675.86	0.71
G-PET/0.5% $NaHCO_3$	270	-0.29	2899.54	0.71
G-PET/0.5% $NaHCO_3$	280	-0.16	909.73	0.84
V-PET/0.5% $NaHCO_3$	260	-0.31	7623.21	0.69
V-PET/0.5% $NaHCO_3$	270	-0.28	6176.95	0.72
V-PET/0.5% $NaHCO_3$	280	-0.07	824.55	0.93

where g_m (g/cm/sec) is the melt viscosity of polymer, c (1/sec) the shear rate, k= consistency, and n power law index, Ó shear stress.

Table 4.27 Comparison of Melt Viscosity of PET with 0.5 wt% Nucleating Agents to that of Plain PET.

Nucleating Agent	R-PET with	G-PET with	V-PET with
Na_2CO_3	-	-	=
$NaHCO_3$	--	--	--
K_2CO_3	-	-	-
$MgCO_3$	---	---	---
$CaCO_3$	-	-	+
$SrCO_3$	-	-	+
$BaCO_3$	-	=	=
$ZnCO_3$	---	---	---
$CdCO_3$	=	+	=
$PbCO_3$	---	---	---

+ represents the melt viscosity of PET/nucleating agent larger than that of plain PET.
= represents the same of the melt viscosity between PET/ nucleating agent and Plain PET.
- represents the melt viscosity of PET/nucleating agent less than that of plain PET.
More symbols (+++ or ---) represent high values.

Table 4.28 Data Sheet for Isothermal Crystallization of aV-PET at 200 ^{o}C

Table 4.28(a): T_{iso}= 200.0 ^{o}C, Wt:(10.0 mg), Run No. 5th.

t, min	ln(t),	x%, Reduced Crystallinity	ln(-ln(1-x))
0.075	-2.590	0.033	-8.020
0.175	-1.743	0.205	-6.191
0.275	-1.291	0.546	-5.207
0.375	-0.981	1.091	-4.513
0.475	-0.744	1.882	-3.964
0.575	-0.553	2.913	-3.521
0.675	-0.393	4.212	-3.146
0.775	-0.255	5.807	-2.816
0.875	-0.134	7.758	-2.516
0.975	-0.025	10.085	-2.241
1.075	0.072	12.773	-1.990
1.175	0.161	15.844	-1.757
1.275	0.243	19.280	-1.541
1.375	0.318	23.077	-1.338
1.475	0.389	27.218	-1.147
1.575	0.454	31.643	-0.966
1.675	0.516	36.318	-0.796
1.775	0.574	41.165	-0.634
1.875	0.629	46.094	-0.481
1.975	0.681	51.084	-0.335
2.075	0.730	56.057	-0.196
2.175	0.777	60.929	-0.062
2.275	0.822	65.632	0.066
2.375	0.865	70.139	0.189
2.475	0.906	74.297	0.306
2.575	0.946	78.083	0.417
2.675	0.984	81.558	0.525
2.775	1.021	84.667	0.629
2.875	1.056	87.379	0.727
2.975	1.090	89.748	0.823
3.075	1.123	91.761	0.915
3.175	1.155	93.471	1.004
3.275	1.186	94.885	1.090
3.375	1.216	96.028	1.171
3.475	1.246	97.044	1.259
3.575	1.274	97.865	1.347
3.675	1.302	98.459	1.429
3.775	1.328	98.926	1.512
3.875	1.355	99.273	1.594
3.975	1.380	99.510	1.671
4.075	1.405	99.697	1.758
4.175	1.429	99.814	1.838
4.275	1.453	99.892	1.922

Table 4.28(b): T_{iso}= 200.0 ^{o}C, Wt:(10.0 mg), (A), Run No. 8th.

t,	ln(t),	x%,	ln(-ln(1-x))
0.087	-2.436	0.113	-4.789
0.187	-1.674	0.395	-5.533
0.287	-1.247	0.850	-4.763
0.387	-0.948	1.512	-4.184
0.488	-0.718	2.391	-3.722
0.588	-0.532	3.520	-3.329
0.687	-0.375	4.898	-2.991
0.787	-0.239	6.587	-2.686
0.887	-0.119	8.628	-2.405
0.988	-0.013	11.054	-2.144
1.088	0.084	13.832	-1.905
1.188	0.172	16.959	-1.683
1.288	0.253	20.458	-1.475
1.388	0.328	24.327	-1.277
1.487	0.397	28.551	-1.090
1.588	0.462	33.054	-0.913
1.688	0.523	37.805	-0.745
1.788	0.581	42.724	-0.585
1.888	0.635	47.754	-0.432
1.987	0.687	52.809	-0.286
2.088	0.736	57.833	-0.147
2.188	0.783	62.735	-0.013
2.288	0.827	67.442	0.115
2.388	0.870	71.847	0.237
2.487	0.911	75.945	0.354
2.588	0.951	79.662	0.465
2.688	0.989	83.007	0.572
2.788	1.025	85.973	0.675
2.888	1.060	88.557	0.774
2.987	1.094	90.787	0.869
3.088	1.127	92.676	0.961
3.188	1.159	94.255	1.050
3.288	1.190	95.558	1.136
3.388	1.220	96.608	1.219
3.487	1.249	97.444	1.299
3.587	1.277	98.099	1.377
3.688	1.305	98.617	1.454
3.788	1.332	99.001	1.527
3.888	1.358	99.313	1.606
3.987	1.383	99.533	1.680
4.087	1.408	99.697	1.758
4.188	1.432	99.804	1.830
4.287	1.456	99.890	1.918
4.387	1.479	99.942	2.007
4.487	1.501	99.976	2.118
4.587	1.523	99.994	2.278
4.688	1.545	99.999	2.426
4.787	1.566	99.999	2.494
4.887	1.587	100.000	2.580

Table 4.28(c): T_{iso}= 200.0 ^{o}C, Wt:(10.0 mg), (AA), Run No. 9th.

t,	ln(t),	x%,	ln(-ln(1-x))
0.075	-2.590	0.086	-7.054
0.175	-1.743	0.353	-5.644
0.275	-1.291	0.826	-4.792
0.375	-0.981	1.469	-4.213
0.475	-0.744	2.327	-3.749
0.575	-0.553	3.454	-3.348
0.675	-0.393	4.863	-2.999
0.775	-0.255	4.601	-2.684
0.875	-0.134	8.665	-2.401
0.975	-0.025	11.098	-2.140
1.075	0.072	13.895	-1.900
1.175	0.161	17.059	-1.676
1.275	0.243	20.596	-1.467
1.375	0.318	24.525	-1.268
1.475	0.389	28.788	-1.080
1.575	0.454	33.369	-0.901
1.675	0.516	38.156	-0.733
1.775	0.574	43.125	-0.572
1.875	0.629	48.206	-0.419
1.975	0.681	53.301	-0.273
2.075	0.730	58.359	-0.132
2.175	0.777	63.261	0.001
2.275	0.822	67.932	0.129
2.375	0.865	72.317	0.250
2.475	0.906	74.322	0.365
2.575	0.946	80.022	0.477
2.675	0.984	83.317	0.583
2.775	1.021	84.228	0.684
2.875	1.056	88.777	0.783
2.975	1.090	90.969	0.877
3.075	1.123	92.817	0.968
3.175	1.155	94.369	1.057
3.275	1.186	95.641	1.142
3.375	1.216	94.643	1.222
3.475	1.246	97.470	1.302
3.575	1.274	98.132	1.381
3.675	1.302	98.652	1.460
3.775	1.328	99.056	1.540
3.875	1.355	99.341	1.614
3.975	1.380	99.559	1.691
4.075	1.405	99.706	1.763
4.175	1.429	99.816	1.840
4.275	1.453	99.907	1.944
4.375	1.476	99.958	2.052
4.475	1.499	99.989	2.211
4.575	1.521	99.998	2.382
4.675	1.542	99.999	2.450
4.775	1.563	100.000	2.518
4.875	1.584	100.000	2.600

Table 4.28(d): T_{iso}= 200.0 ^{o}C Wt:(8.37 mg), (B), Run No. 1st.

t,	ln(t),	x%,	ln(-ln(1-x))
0.096	-2.343	0.056	-7.484
0.196	-1.630	0.305	-5.792
0.296	-1.217	0.749	-4.891
0.396	-0.926	1.404	-4.258
0.496	-0.701	2.256	-3.780
0.596	-0.518	3.328	-3.386
0.696	-0.362	4.671	-3.040
0.796	-0.228	6.290	-2.734
0.896	-0.110	8.226	-2.455
0.996	-0.004	10.507	-2.198
1.096	0.092	13.097	-1.963
1.196	0.179	15.974	-1.748
1.296	0.259	19.182	-1.547
1.396	0.334	22.711	-1.356
1.496	0.403	26.523	-1.177
1.596	0.468	30.572	-1.008
1.696	0.528	34.819	-0.849
1.796	0.586	39.268	-0.696
1.896	0.640	43.843	-0.550
1.996	0.691	48.489	-0.410
2.096	0.740	53.149	-0.277
2.196	0.787	57.755	-0.149
2.296	0.831	62.230	-0.027
2.396	0.874	66.569	0.091
2.496	0.915	70.679	0.204
2.596	0.954	74.535	0.313
2.696	0.992	78.079	0.417
2.796	1.028	81.310	0.517
2.896	1.063	84.256	0.615
2.996	1.097	86.880	0.709
3.096	1.130	89.168	0.799
3.196	1.162	91.179	0.887
3.296	1.193	92.920	0.974
3.396	1.223	94.396	1.058
3.496	1.252	95.628	1.141
3.596	1.280	96.655	1.223
3.696	1.307	97.489	1.304
3.796	1.334	98.169	1.386
3.896	1.360	98.738	1.475
3.996	1.385	99.161	1.565
4.096	1.410	99.491	1.664
4.196	1.434	99.739	1.783
4.296	1.458	99.891	1.921
4.396	1.481	99.970	2.093
4.496	1.503	99.999	2.416
4.596	1.525	99.999	2.480
4.696	1.547	100.000	2.557
4.796	1.568	100.000	2.650
4.896	1.588	100.000	2.743

Table 4.28 (e): T_{iso}= 200.0 ^{o}C, Wt:(4.98 mg), (C), Run No. 1st.

t,	ln(t),	x%,	ln(-ln(1-x))
0.058	-2.847	0.029	-8.141
0.158	-1.845	0.224	-6.101
0.258	-1.355	0.621	-5.078
0.358	-1.027	1.243	-4.382
0.458	-0.781	2.078	-3.863
0.558	-0.583	3.110	-3.455
0.658	-0.419	4.376	-3.107
0.758	-0.277	5.941	-2.793
0.858	-0.153	7.784	-2.513
0.958	-0.043	9.934	-2.257
1.058	0.056	12.382	-2.024
1.158	0.147	15.146	-1.806
1.258	0.230	18.213	-1.604
1.358	0.306	21.593	-1.414
1.458	0.377	25.240	-1.235
1.558	0.443	29.154	-1.065
1.658	0.506	33.281	-0.905
1.758	0.564	37.604	-0.751
1.858	0.620	42.041	-0.606
1.958	0.672	46.580	-0.467
2.058	0.722	51.179	-0.333
2.158	0.769	55.757	-0.204
2.258	0.814	60.259	-0.080
2.358	0.858	64.646	0.039
2.458	0.899	68.870	0.154
2.558	0.939	72.867	0.266
2.658	0.978	76.588	0.373
2.758	1.015	80.007	0.476
2.858	1.050	83.127	0.576
2.958	1.085	85.882	0.672
3.058	1.118	88.322	0.764
3.158	1.150	90.496	0.856
3.258	1.181	92.391	0.946
3.358	1.211	93.974	1.033
3.458	1.241	95.312	1.118
3.558	1.269	96.418	1.203
3.658	1.297	97.308	1.285
3.758	1.324	98.027	1.368
3.858	1.350	98.593	1.450
3.958	1.376	99.014	1.530
4.058	1.401	99.348	1.616
4.158	1.425	99.606	1.711
4.258	1.449	99.781	1.812
4.358	1.472	99.902	1.936
4.458	1.495	99.978	2.129
4.558	1.517	99.995	2.297
4.658	1.539	99.998	2.375
4.758	1.560	99.999	2.470
4.858	1.581	100.000	2.600

Table 4.29 Characteristic Constants Obtained from Different Runs of DSC Isothermal Crystallization at 200 ^{o}C for aV-PET.

Weights	Run No	$t_{1/2}$ mins	t_{max} mins	n	k
10.00	5th 8th (A) 9th (AA)	1.95 1.93 1.91	2.03 1.99 1.97	2.68 2.63 2.62	0.114 0.121 0.126
8.17	1st (B)	2.03	2.10	2.57	0.112
4.98	1st (C)	2.03	2.16	2.51	0.116
Average		1.97 ±0.06	2.05 ±0.07	2.60 ±0.08	0.118 ±0.005

Table 4.30. T_{cc} Values for aV-PET form DSC Nonisothermal Crystallization (scan rate 20 ^{o}C/min).

(aV-PET)	
Weights	T_{cc}
mg	^{o}C
10.00	174 174.5
8.17	173 172
4.98	172
Average	173.1±1.0

Table 4.31 Variation of Thermal Properties of R-PET with Mixing Time. The scan rate of DSC was 20 ^{o}C/min. Samples of R-PET were from the same batch.

Batch 1 (R-PET)				
Mixing time (min)	T_{cc} ^{o}C	T_{ch} ^{o}C	T_{g} ^{o}C	T_{m} ^{o}C
0.5-1	180 180 180 180	135.5	78	249
1	184	136.5	80	248
2	181	136.5	79.5	248
3	182	136.2	78	248
4	180	136	79	250
5	180.5 180 180	136	79	250 246
6	184.5	136.5	78	248
7	180.5	136.5	80	248
8	185	136.5	78	248
9	185	136.5 137.5	79 80	250 249
10	180	136.5	78	249
11	181	137	76	248
12	182	136	78	249
13	179 179 180	135	78	248
14	182	135	76	249
15	180.5	135	78	248
Average	181.1±1.8	136±0.7	78.3±1.2	248.5±1.0

Table 4.32 Thermal Properties of R-PET Based on Samples from Different Batches. The scan rate of DSC was 20 ^{o}C/min.

R-PET	T_{cc} ^{o}C	T_{ch} ^{o}C	T_g ^{o}C	T_m ^{o}C
Batch 2	181 180	136 138	82	251 250
Batch 3	180	137	81	248
Batch 4	183	132	79	250
Batch 5	178	137	75	249
Batch 6	178	134	73 80 81	247
Batch 7	182 182 182			
Batch 8	185 180	135 138	80 82	250 249
Batch 9		138	81	251
Batch 10	183	137	77	246
Average*	181.1±1.9			

*The value of T_{cc} is the average from batchs 1 through 10.

Table 4.33 Thermal Properties of R-PET, G-PET, and V-PET. The scan rate of DSC was 20 ^{o}C/min.

Material	T_g ^{o}C	T_{ch} ^{o}C	T_{cc} ^{o}C	T_m ^{o}C
bR-PET	80	158	168	248
aR-PET	80	138	181	248
bV-PET	80	185	162	247
aV-PET	80	142	173	248
bG-PET	80	160	153	247
aG-PET	80	136	182	248

Prefixed "a" represents the material after processing in the extruder. Prefixed "b" represents the material before any shearing process (material as received).

Table 4.34 Thermal Properties of woR-PET. The scan rate of DSC was 20 ^{o}C/min.

Batch 11: R-PET in the tube at 280 ^{o}C.			
Time min.	T_g ^{o}C	T_{cc} ^{o}C	T_m ^{o}C
1	76 80	170 168	244
9	78	173	248

woR-PET: Non-mechanically processed R-PET.

Table 4.35 Thermal Properties of Annealed R-PET. The scan rate of DSC was 20 ^{o}C/min.

Batch 12: aR-PET					
Annealing time min	Annealing temperature ^{o}C	T_g ^{o}C	T_{ch} ^{o}C	T_m ^{o}C	Endotherm Peak ^{o}C
30	100	80	138	254	none
3	130			242	145

Table 4.36. T_{cc} values of aR-PET at Different Scan Rates.

aR-PET (batch 7)	
Scan rate ^{o}C/min.	T_{cc} ^{o}C
0.31	225.15
0.62	220.78
1.25	215.5
2.50	209.5
5.0	203
10.0	194
20.0	182 182 182
40.0	166
80.0	146

Table 4.37 Thermal Properties of R-PET with Nucleating Agents (scan rate of 20 ^{o}C/min).

Nucleating Agents	wt%	T_g ^{o}C	T_{ch} ^{o}C	T_{cc} ^{o}C	T_m ^{o}C	ΔTc^a ^{o}C	ΔTch^b ^{o}C
bR-PET		80	158	168	248	132	10
aR-PET		80	138	181	248	119	43
Li_2CO_3	0.5	85	138	180	249	120	42
Na_2CO_3	0.3 0.5 1.0	78 79 76	134 129 122	197 201 203	249 248 247	103 99 97	63 72 81
$NaHCO_3$	0.3 0.5 1.0	77 77 76	134 134 130	193 194 200	249 250 249	107 106 100	59 60 70
K_2CO_3	0.3 0.5 1.0	74 75 76	136 132 129	183 187 198	249 249 249	117 113 102	47 55 69
$MgCO_3$	0.3 0.5 1.0	78 79 79	135 136 136	184 186 189	248 248 250	116 114 111	49 50 53
$CaCO_3$	0.3 0.5 1.0	81 80 80	140 144 142	181 181 181	247 248 248	119 119 119	41 37 39
$SrCO_3$	0.3 0.5 1.0	81 80 81	144 142 142	181 182 181	247 247 247	119 118 119	37 40 39
$BaCO_3$	0.3 0.5 1.0	80 76 81	142 135 145	180 181 180	248 249 248	120 119 120	38 46 35

Table b. 4.37. Continue.

$ZnCO_3$	0.5	82	140	192	250	108	52
$CdCO_3$	0.3 0.5 1.0	80 80 80	145 141 141	178 183 183	246 246 247	122 117 117	33 42 42
$PbCO_3$	0.3 0.5 1.0	80 80 81	143 141 143	186 192 197	249 248 250	114 108 103	43 51 54

[a] $\Delta T_c = T_m^o - T_{cc}$, where T_m^o, the equilibrium melting temperature of polyethylene terephthalate, is 300 ^oC [117].
[b] $\Delta T_{ch} = T_{cc} - T_{ch}$

Table 4.38 Thermal Properties of G-PET with Nucleating Agents (scan rate of 20 ^{o}C/min).

Nucleating Agents	wt%	T_g ^{o}C	T_{ch} ^{o}C	T_{cc} ^{o}C	T_m ^{o}C	ΔTc^a ^{o}C	ΔTch^b ^{o}C
bG-PET		80	160	153	247	142	-
aG-PET		80	136	182	248	118	46
Na_2CO_3	0.5	80	124	206	249	94	82
$NaHCO_3$	0.5	80	126	200	253	100	74
K_2CO_3	0.5	79	135	190	249	110	55
$MgCO_3$	0.5	80	134	192	252	108	58
$CaCO_3$	0.5	79	139	181	248	119	42
$SrCO_3$	0.5	80	136	181	252	119	45
$BaCO_3$	0.5	80	136	183	248	117	47
$ZnCO_3$	0.5	79	134	189	250	111	55
$CdCO_3$	0.5	79	136	185	250	115	49
$PbCO_3$	0.5	80	138	196	251	104	58

[a] $\Delta T_c = T_m^o - T_{cc}$, where T_m^o, the equilibrium melting temperature of polyethylene terephthalate, is 300 ^{o}C [117].
[b] $\Delta T_{ch} = T_{cc} - T_{ch}$

Table 4.39 Thermal Properties of V-PET with Nucleating Agents (scan rate of 20 ^{o}C/min).

Nucleating Agents	wt%	T_g ^{o}C	T_{ch} ^{o}C	T_{cc} ^{o}C	T_m ^{o}C	ΔTc^a ^{o}C	ΔTch^b ^{o}C
bV-PET		80	185	162	247	138	-
aV-PET		80	142	173	248	127	31
Na_2CO_3	0.5	82	118	204	250	96	86
$NaHCO_3$	0.5	81	128	203	250	97	75
K_2CO_3	0.5	80	139	183	250	117	44
$MgCO_3$	0.5	78	134	187	250	113	53
$CaCO_3$	0.5	80	137	184	250	116	47
$SrCO_3$	0.5	80	135	184	250	116	49
$BaCO_3$	0.5	79	135	182	250	118	47
$ZnCO_3$	0.5	78	131	191	251	109	60
$CdCO_3$	0.5	80	139	178	248	122	39
$PbCO_3$	0.5	82	140	200	252	100	60

[a] $\Delta Tc = T_m^{o} - T_{cc}$, where T_m^{o}, the equilibrium melting temperature of polyethylene terephthalate, is 300 ^{o}C [117].
[b] $\Delta Tch = T_{cc} - T_{ch}$

Table 4.40 Avrami Parameters for R-PET with and without Nucleating Agents at Different Temperatures.

bR-PET					
T ^{o}C	$t_{1/2}$ Min	t_{max} Min	n	k	k_n
160.00	0.66	0.60	1.9	1.5050	1.2400
170.00	0.71	0.52	1.8	1.2660	1.1410
180.00	0.78	0.69	2.1	1.1710	1.0790
190.00	1.14	1.10	2.3	0.5160	0.7500
200.00	2.09	1.77	2.3	0.1250	0.4090
210.00	4.57	4.24	2.4	0.0180	0.1880

aR-PET					
T ^{o}C	$t_{1/2}$ Min	t_{max} Min	n	k	k_n
200.	1.17	1.17	2.8	0.4527	0.7526
205.	1.65	1.63	3.0	0.1548	0.5363
210.	2.55	2.55	3.0	0.0420	0.3465
215.	4.21	4.35	3.0	0.0091	0.2104

Table 4.40 Continued.

0.3% Na_2CO_3 + R-PET					
T ^oC	$t_{1/2}$ Min	t_{max} Min	n	k	k_n
200.00	0.32	0.20	1.8	5.3510	2.5260
210.00	0.80	0.67	3.2	1.4470	1.1220
220.00	2.96	2.72	4.0	0.0090	0.3080
0.5% Na_2CO_3 + R-PET					
T ^oC	$t_{1/2}$ Min	t_{max} Min	n	k	k_n
200.	0.29	0.21	2.0	7.9410	2.8320
202.	0.32	0.24	2.0	6.8950	2.6220
205.	0.40	0.30	2.0	4.3680	2.1010
207.	0.49	0.41	2.1	3.0810	1.7020
210.	0.62	0.58	2.2	1.9710	1.3590
212.	0.76	0.59	2.5	1.3780	1.1370
215.	1.00	0.70	2.0	0.6930	0.8360
217.	1.28	1.26	2.7	0.3610	0.6820
220.	1.98	1.49	2.2	0.1600	0.4270
1.0% Na_2CO_3 + R-PET					
T ^oC	$t_{1/2}$ Min	t_{max} Min	n	k	k_n
190.00	0.15	0.12	1.6	13.8760	5.3570
200.00	0.23	0.15	1.8	10.0120	3.5070
210.00	0.57	0.42	2.3	2.6020	1.5020
215.00	1.03	0.75	2.2	0.6450	0.8210
220.00	1.87	1.44	2.5	0.1450	0.4620
230.00	7.05	7.10	2.5	0.0050	0.1230

Table 4.40 Continued.

0.5% $NaHCO_3$ + R-PET					
T ^oC	$t_{1/2}$ Min	t_{max} Min	n	k_p	k_{pn}
190.	0.18	0.12	2.0	21.6650	4.5870
200.	0.39	0.32	2.5	7.0460	2.2040
210.	0.84	0.72	2.8	1.1120	1.0390
215.	1.45	0.81	2.1	0.3110	0.5800
220.	2.61	2.39	3.2	0.0330	0.3410

0.5% K_2CO_3 + R-PET					
T ^oC	$t_{1/2}$ Min	t_{max} Min	n	k	k_n
180.	0.29	0.25	2.2	11.0690	2.9280
190.	0.45	0.43	2.1	3.7440	1.8670
195.	0.58	0.49	2.5	2.8170	1.5010
200.	0.79	0.60	2.2	1.1580	1.0710
205.	1.08	0.89	2.2	0.5810	0.7800
210.	1.52	1.12	2.3	0.2640	0.5610
215.	2.38	1.82	2.5	0.0800	0.3630
220.	4.07	3.22	2.3	0.0270	0.2100

Table 4.40 Continued.

0.5% $MgCO_3$ + R-PET					
T ^oC	$t_{1/2}$ Min	t_{max} Min	n	k	k_n
170.	0.24	0.13	1.7	7.9480	3.3920
180.	0.26	0.22	1.8	7.6920	3.1120
190.	0.39	0.29	2.0	4.4740	2.1500
200.	0.72	0.62	2.5	1.5850	1.2030
210.	1.36	1.11	2.5	0.3200	0.6330
220.	3.65	2.93	2.4	0.0310	0.2350

0.3% $CaCO_3$ + R-PET					
T ^oC	$t_{1/2}$ Min	t_{max} Min	n	k	k_n
190.	0.60	0.60	2.1	2.0600	1.4080
200.	1.09	1.11	2.6	0.5600	0.8000
210.	2.48	2.37	3.4	0.0310	0.3620
220.	6.64	6.80	3.0	0.0020	0.1340

0.5% $CaCO_3$ + R-PET					
T ^oC	$t_{1/2}$ Min	t_{max} Min	n	k	k_n
170.	0.25	0.13	1.9	10.3480	3.3310
180.	0.28	0.12	2.0	9.0490	2.9660
190.	0.60	0.46	2.2	2.2120	1.4260
200.	1.02	0.84	2.5	0.6610	0.8480
210.	2.14	2.14	3.4	0.0530	0.4190
220.	5.81	5.41	3.2	0.0020	0.1540

Table 4.40 Continued.

1.0% $CaCO_3$ + R-PET					
T ^oC	$t_{1/2}$ Min	t_{max} Min	n	k	k_n
190.	0.56	0.69	1.8	1.9460	1.4520
200.	0.95	0.84	2.5	0.7790	0.9050
210.	1.88	1.70	2.5	0.1430	0.4600
215.	3.21	2.26	2.1	0.0630	0.2610

0.5% $SrCO_3$ + R-PET					
T ^oC	$t_{1/2}$ Min	t_{max} Min	n	k	k_n
170.	0.37	0.29	1.9	4.3860	2.2180
180.	0.42	0.39	2.0	3.9390	1.9720
190.	0.57	0.50	2.2	2.4410	1.4930
200.	0.92	0.85	2.3	0.8510	0.9340
210.	2.10	1.99	2.7	0.0910	0.4170
220.	5.49	5.36	2.4	0.0110	0.1570

0.5% $BaCO_3$ + R-PET					
T ^oC	$t_{1/2}$ Min	t_{max} Min	n	k	k_n
170.	0.36	0.35	1.8	4.4590	2.2660
180.	0.42	0.39	2.0	4.0190	2.0010
190.	0.57	0.48	2.2	2.3410	1.4760
200.	0.99	0.85	2.5	0.7110	0.8750
210.	2.13	1.99	3.2	0.0640	0.4190
220.	5.78	5.10	2.5	0.0080	0.1500

Table 4.40 Continued.

0.5% $ZnCO_3$ + R-PET					
T ^oC	$t_{1/2}$ Min	t_{max} Min	n	k	k_n
170.	0.22	0.15	1.5	6.7820	3.6100
180.	0.25	0.15	1.6	6.4210	3.2150
190.	0.34	0.26	1.8	4.8960	2.3850
200.	0.59	0.51	2.4	2.4190	1.4510
210.	1.18	1.00	2.6	0.4510	0.7320
220.	2.93	2.57	2.5	0.0460	0.2950

0.5% $CdCO_3$ + R-PET					
T ^oC	$t_{1/2}$ Min	t_{max} Min	n	k	k_n
170.	0.34	0.29	2.0	6.0890	2.4770
180.	0.42	0.36	2.0	4.0760	2.0080
190.	0.56	0.49	2.2	2.4770	1.5060
200.	0.89	0.78	2.5	0.9210	0.9680
210.	1.94	1.75	2.7	0.1140	0.4500
220.	5.37	4.48	2.3	0.0150	0.1590

0.5% $PbCO_3$ + R-PET					
T ^oC	$t_{1/2}$ Min	t_{max} Min	n	k	k_n
170.	0.22	0.11	1.6	8.0170	3.6820
180.	0.21	0.11	1.7	9.5180	3.8930
190.	0.27	0.25	1.8	6.8590	2.9930
200.	0.40	0.34	2.1	4.8210	2.0870
210.	0.98	0.83	2.6	0.7250	0.8840
220.	2.86	2.57	2.5	0.0480	0.3030

Table 4.41 Avrami Parameters for G-PET with and without Nucleating Agents at Different Temperatures.

bG-PET					
T ^{o}C	$t_{1/2}$ Min	t_{max} Min	n	k	k_n
160.	1.36	1.13	2.2	0.3570	0.6210
170.	0.98	0.97	2.0	0.7190	0.8480
175.	1.05	0.92	2.3	0.6170	0.8070
180.	1.22	0.94	2.0	0.4690	0.6850
190.	1.76	1.55	2.2	0.2010	0.4790
200.	3.65	3.17	2.0	0.0520	0.2280
210.	9.12	8.11	2.4	0.0030	0.0940

aG-PET					
T ^{o}C	$t_{1/2}$ Min	t_{max} Min	n	k	k_n
190.	0.70	0.60	2.4	1.6292	1.2259
200.	1.12	1.03	2.7	0.5160	0.7798
205.	1.62	1.51	2.8	0.1763	0.5442
210.	2.52	2.35	3.0	0.0430	0.3515
215.	4.25	4.20	2.9	0.0103	0.2075

Table 4.41 Continued.

G-PET + 0.5% Na_2CO_3					
T ^oC	$t_{1/2}$ Min	t_{max} Min	n	k	k_n
200.	0.21	0.11	1.7	9.2990	3.8440
205.	0.28	0.21	2.1	9.8960	3.0280
210.	0.44	0.34	2.6	5.7660	1.9770
215.	0.69	0.59	2.8	1.9540	1.2660
220.	1.17	0.99	2.8	0.4480	0.7470

G-PET + 0.5% $NaHCO_3$					
T ^oC	$t_{1/2}$ Min	t_{max} Min	n	k	k_n
200.	0.21	0.16	2.4	29.0350	4.1710
205.	0.30	0.26	2.8	21.4920	2.9710
210.	0.44	0.38	3.3	10.5500	2.0540
215.	0.75	0.62	3.1	1.6560	1.1770
220.	1.34	1.17	3.1	0.2820	0.6650

G-PET + 0.5% K_2CO_3					
T ^oC	$t_{1/2}$ Min	t_{max} Min	n	k	k_n
180.	0.30	0.26	1.9	6.5090	2.7130
190.	0.40	0.38	2.6	7.0990	2.1510
200.	0.66	0.57	2.3	1.7770	1.2890
210.	1.30	1.27	2.4	0.3720	0.6600
220.	4.01	4.38	2.7	0.0170	0.2180

Table 4.41 Continued

G-PET + 0.5% $MgCO_3$					
T ^oC	$t_{1/2}$ Min	t_{max} Min	n	k	k_n
190.	0.31	0.25	2.2	8.7210	2.7410
200.	0.50	0.41	2.3	3.2920	1.6980
205.	0.70	0.58	2.3	1.5730	1.2160
210.	1.00	0.82	2.3	0.6950	0.8500
215.	1.79	1.49	2.3	0.1840	0.4760

G-PET + 0.5% $CaCO_3$					
T ^oC	$t_{1/2}$ Min	t_{max} Min	n	k	k_n
190.	0.54	0.53	2.4	3.0790	1.5860
200.	0.90	0.82	2.5	0.9040	0.9600
205.	1.23	1.16	2.5	0.4150	0.6980
210.	2.01	1.95	3.0	0.0880	0.4390
215.	3.47	3.38	2.9	0.0200	0.2540

G-PET + 0.5% $SrCO_3$					
T ^oC	$t_{1/2}$ Min	t_{max} Min	n	k	k_n
190.	0.57	0.47	2.4	2.6060	1.4940
200.	0.90	0.82	2.5	0.8910	0.9540
205.	1.25	1.16	2.5	0.3990	0.6930
210.	2.06	1.97	2.7	0.1000	0.4240
215.	3.48	3.11	2.6	0.0260	0.2500

Table 4.41 Continued

G-PET + 0.5% $BaCO_3$					
T ^oC	$t_{1/2}$ Min	t_{max} Min	n	k	k_n
190.	0.48	0.45	2.4	3.8960	1.7770
200.	0.78	0.67	2.3	1.2460	1.0990
205.	1.05	0.94	2.4	0.6200	0.8170
210.	1.66	1.52	2.5	0.1950	0.5200
215.	2.93	2.78	2.6	0.0440	0.2960

G-PET + 0.5% $ZnCO_3$					
T ^oC	$t_{1/2}$ Min	t_{max} Min	n	k	k_n
190.	0.33	0.30	2.1	7.3590	2.5620
200.	0.54	0.48	2.3	2.9240	1.5930
205.	0.77	0.67	2.4	1.3240	1.1220
210.	1.07	1.00	2.7	0.5820	0.8200
215.	1.90	1.65	2.4	0.1500	0.4510

G-PET + +0.5% $CdCO_3$					
T ^oC	$t_{1/2}$ Min	t_{max} Min	n	k	k_n
190.	0.47	0.36	2.2	3.5420	1.7970
200.	0.76	0.71	2.4	1.3490	1.1310
210.	1.56	1.41	2.6	0.2160	0.5590
215.	2.82	2.59	2.5	0.0510	0.3060

Table 4.41 Continued

G-PET + +0.5% $PbCO_3$					
T ^oC	$t_{1/2}$ Min	t_{max} Min	n	k	k_n
190.	0.29	0.24	2.0	8.0650	2.8330
200.	0.49	0.43	2.4	3.6440	1.7300
205.	0.68	0.64	2.5	1.8510	1.2790
210.	0.98	0.84	2.3	0.7320	0.8720
215.	1.74	1.45	2.2	0.2000	0.4870

Table 4.42 Avrami Parameters for V-PET with and without Nucleating Agents at Different Temperatures.

bV-PET					
T ^{o}C	$t_{1/2}$ Min	t_{max} Min	n	k	k_n
160	2.78	2.58	2.0	0.0900	0.3000
180	1.85	1.73	2.4	0.1560	0.4650
190	2.55	2.09	2.0	0.1060	0.3260
200	4.36	3.39	2.5	0.0180	0.1980

aV-PET (MOLDED BAR)					
T ^{o}C	$t_{1/2}$ Min	t_{max} Min	n	k	k_n
170.	0.70	0.75	2.2	1.5481	1.2150
180.	0.83	0.84	2.2	1.0479	1.0211
190.	1.16	1.17	2.5	0.4832	0.7474
200.	1.95	2.05	2.7	0.1150	0.4469
205.	2.73	2.83	2.8	0.0427	0.3214
210.	4.16	4.07	2.8	0.0120	0.2111
215.	6.32	6.55	2.9	0.0031	0.1398

Table 4.42 Continued.

V-PET + 0.5% Na_2CO_3 (MOLDED BAR)					
T ^oC	$t_{1/2}$ Min	t_{max} Min	n	k	k_n
210.	0.40	0.33	2.5	7.0890	2.1760
215.	0.66	0.64	3.1	2.5020	1.3480
220.	1.37	1.24	3.1	0.2590	0.6500
225.	2.53	2.58	3.2	0.0350	0.3520

V-PET + 0.5% $NaHCO_3$ (MOLDED BAR)					
T ^oC	$t_{1/2}$ Min	t_{max} Min	n	k	kn
210.	0.40	0.36	3.6	18.6420	2.2690
215.	0.69	0.66	3.8	2.7910	1.3150
220.	1.38	1.35	4.0	0.1910	0.6610
225.	2.99	2.91	4.0	0.0090	0.3050

V-PET + 0.5% K_2CO_3 (MOLDED BAR)					
T ^oC	$t_{1/2}$ Min	t_{max} Min	n	k	k_n
200.	1.25	1.26	2.7	0.3760	0.7000
205.	1.85	1.85	2.9	0.1140	0.4760
210.	2.82	2.78	3.0	0.0310	0.3140
215.	4.38	4.38	3.0	0.0090	0.2020

Table 4.42 Continued

V-PET + 0.5% $MgCO_3$ (MOLDED BAR)					
T ^oC	$t_{1/2}$ Min	t_{max} Min	n	k	k_n
200.00	0.86	0.79	2.3	0.9960	0.9980
210.00	1.64	1.58	2.3	0.2190	0.5230
220.00	4.67	4.55	2.5	0.0150	0.1850

V-PET + 0.5% $CaCO_3$ (MOLDED BAR)					
T ^oC	$t_{1/2}$ Min	t_{max} Min	n	k	k_n
200.	0.99	0.99	2.4	0.7110	0.8650
205.	1.43	1.45	2.5	0.2850	0.6030
210.	2.20	2.12	2.7	0.0840	0.3970
215.	3.34	3.34	2.7	0.0270	0.2610

V-PET + 0.5% $SrCO_3$ (MOLDED BAR)					
T ^oC	$t_{1/2}$ Min	t_{max} Min	n	k	k_n
200.	1.10	1.09	2.7	0.5380	0.7920
205.	1.55	1.52	2.7	0.2130	0.5650
210.	2.33	2.33	2.8	0.0670	0.3770
215.	3.50	3.65	2.8	0.0200	0.2510

Table 4.42 Continued

V-PET + 0.5% $BaCO_3$ (MOLDED BAR)					
T ^oC	$t_{1/2}$ Min	t_{max} Min	n	k	k_n
200.	1.23	1.20	2.5	0.4150	0.7040
205.	1.68	1.66	2.6	0.1780	0.5180
210.	2.45	2.49	2.8	0.0600	0.3580
215.	3.84	3.88	2.8	0.0160	0.2280

V-PET + 0.5% $ZnCO_3$ (MOLDED BAR)					
T ^oC	$t_{1/2}$ Min	t_{max} Min	n	k	k_n
200.	0.65	0.64	2.2	1.8070	1.3020
205.	0.99	0.91	2.3	0.7060	0.8570
210.	1.44	1.49	2.2	0.3100	0.5890
215.	2.26	2.32	2.2	0.1150	0.3750

V-PET + 0.5% $CdCO_3$ (MOLDED BAR)					
T ^oC	$t_{1/2}$ Min	t_{max} Min	n	k	k_n
200.	1.51	1.50	2.6	0.2340	0.5760
205.	2.17	2.17	2.6	0.0910	0.4010
210.	3.24	3.21	2.8	0.0270	0.2700
215.	5.02	4.97	2.7	0.0080	0.1740

Table 4.42 Continued

V-PET + 0.5% $PbCO_3$ (MOLDED BAR)					
T ^{o}C	$t_{1/2}$ Min	t_{max} Min	n	k	k_n
200.	0.33	0.30	2.4	9.4640	2.5970
205.	0.44	0.40	2.4	5.2420	1.9710
210.	0.65	0.58	2.8	2.3010	1.3530
215.	0.96	0.88	2.9	0.7840	0.9190

Table 4.43 Avrami Exponents and Their Implications.

Type of crystallization	Nucleation	n
A. Linear problem:		
Line	Athermal	1
Line	Thermal	2
B. Two-dimensional:		
Ribbon	Athermal	≤ 1
Ribbon	Thermal	≤ 2
Circular	Athermal	2
Circular	Thermal	3
Circular, diffusion control	Athermal	1
Circular, diffusion control	Thermal	2
Circular	Thermal, exhaustion	3 to 2
C. Three-Dimensional Problem:		
Filbrillar	Athermal	≤ 1
Filbrillar	Thermal	≤ 2
Circular lamellar	Athermal	≤ 2
Circular lamellar	Thermal	≤ 3
Spherical	Athermal	3
Spherical	Thermal	4
Spherical, diffusion control	Athermal	3/2
Spherical, diffusion control	Thermal	5/2
Spherical	Thermal, exhaustion	4 to 3
Two-stage	Athermal/thermal	fractional
Branching fibrillar	Athermal/thermal	1, 2 large
Solid sheaf	Athermal	≥ 5
Solid sheaf	Thermal	≥ 6
Truncated sphere	Athermal	2-3
Truncated sphere	Thermal	3-4
Volume decrease on cryst.	Athermal/thermal	fractional increase
Perfection after initial cryst.	Athermal/thermal	decrease

Reproduced from B.Wunderlich, "Macromolecular physics", Academic Press, New York, Vol 2, p147, 1976.

Table 4.44 Constants for the Inverse Arrhenius-type Expressions (Eq. 6.9, 6.10, and 6.11) for R-PET.

Material	Range* ^{o}C	k_{to}	k_{no}	k_{o}	E_t	E_n	E_k
bR-PET	190-210	2.54E-15	2.44E-15	0.39E-35	129.0	128.5	311.7
aR-PET	200-215	6.8E-19	6.97E-19	0.33E-55	164.1	163.5	499.8
0.5% Na_2CO_3/R-PET	205-220	2.57E-22	4.22E-22	0.11E-45	201.4	198.7	426.9
0.5% $NaHCO_3$/R-PET	200-220	2.14E-20	2.88E-20	0.11E-53	182.1	180.3	497.4
0.5% K_2CO_3/R-PET	200-220	5.41E-18	7.17E-18	0.32E-40	157.6	155.8	368.0
0.5% $MgCO_3$/R-PET	200-220	6.54E-18	4.45E-18	0.15E-41	157.1	158.1	381.0
0.5% $CaCO_3$/R-PET	200-220	2.53E-19	5.10E-19	0.67E-62	168.5	165.2	562.0
0.5% $SrCO_3$/R-PET	200-220	8.55E-20	8.02E-20	0.22E-46	173.1	172.8	421.8
0.5% $BaCO_3$/R-PET	200-220	1.40E-19	1.26E-19	0.58E-48	170.9	170.8	435.4
0.5% $ZnCO_3$/R-PET	200-220	1.26E-17	1.37E-17	0.11E-41	155.2	154.3	383.9
0.5% $CdCO_3$/R-PET	200-220	6.97E-20	4.87E-20	0.75E-44	174.1	175.0	399
0.5% $PbCO_3$/R-PET	200-220	2.31E-21	4.90E-21	0.28E-48	190.6	187.0	446.5

Table 4.44 continued.

0.3% Na_2CO_3/R-PET	200-220	5.44E-24	8.79E-23	0.77E-67	215.4	203.7	617.0
0.5% Na_2CO_3/R-PET	205-220	2.57E-22	4.22E-22	0.11E-45	201.4	198.7	426.9
1.0% Na_2CO_3/R-PET	200-230	5.36E-25	1.38E-24	0.26E-54	226.2	221.7	506.2
0.3% $CaCO_3$/R-PET	200-220	4.38E-20	6.36E-20	0.25E-60	175.1	173.1	546.6
0.5% $CaCO_3$/R-PET	200-220	2.53E-19	5.10E-19	0.67E-62	168.5	165.2	562.0
1.0% $CaCO_3$/R-PET	200-215	1.81E-17	8.00E-18	0.22E-35	151.9	154.6	322.0

Table 4.45 Constants for the Inverse Arrhenius-type Expressions (Eq. 6.9, 6.10, and 6.11) for G-PET.

Material	Range* ^{o}C	k_{t0}	k_{n0}	k_0	E_t	E_n	E_k
bG-PET	200-210	1.66E-20	5.83E-20	0.72E-61	174.0	168.4	542.2
aG-PET	205-215	2.27E-21	2.03E-21	0.12E-60	187.1	187.0	550.7
0.5% Na_2CO_3/G-PET	210-220	2.65E-21	2.91E-21	0.12E-53	193.6	192.7	505.8
0.5% $NaHCO_3$/G-PET	210-220	3.26E-24	1.45E-24	0.27E-76	220.5	223.3	717.5
0.5% K_2CO_3/G-PET	200-220	8.49E-20	1.40E-19	0.49E-49	174.6	172.0	449.9
0.5% $MgCO_3$/G-PET	205-215	1.92E-20	1.71E-20	0.60E-45	182.0	181.8	416.0
0.5% $CaCO_3$/G-PET	205-215	8.55E-23	2.67E-22	0.21E-64	201.2	196.1	588.5
0.5% $SrCO_3$/G-PET	205-215	1.59E-22	1.70E-22	0.50E-58	198.6	197.8	529.9
0.5% $BaCO_3$/G-PET	205-215	1.74E-22	2.54E-22	0.57E-56	199.0	196.9	513.1
0.5% $ZnCO_3$/Gpet	205-215	1.00E-19	5.89E-20	0.10E-45	175.1	176.6	422.2
0.5% $CdCO_3$/G-PET	200-215	1.31E-18	1.39E-18	0.11E-44	163.1	162.3	408.6
0.5% $PbCO_3$/G-PET	205-215	1.90E-20	4.64E-21	0.14E-46	182.1	187	431.5

Table 4.46 Constants for the Inverse Arrhenius-type Expressions (Eq. 6.9, 6.10, and 6.11) for V-PET.

Material	Range* °C	k_{t0}	k_{n0}	k_0	E_t	E_{kn}	E_k
bV-PET	190-200	3.72E-12	1.84E-11	0.39E-37	97.728	90.850	323.054
aV-PET	190-215	4.38E-15	5.45E-15	0.21E-42	127.0	125.7	377.0
0.5% Na_2CO_3/V-PET	215-225	1.24E-29	1.16E-29	0.99E-92	271.75	271.55	863.37
0.5% $NaHCO_3$/V-PET	215-225	2.82E-32	3.30E-32	0.24E-123	296.4	295.37	1159.6
0.5% K_2CO_3/V-PET	205-215	2.91E-19	3.24E-19	0.16E-54	167.2	166.3	492.7
0.5% $MgCO_3$/V-PET	200-220	1.02E-18	1.02E-18	0.17E-44	163.8	163.2	406.1
0.5% $CaCO_3$/V-PET	205-215	7.24E-19	1.06E-18	0.30E-50	164.6	162.5	457.3
0.5% $SrCO_3$/V-PET	205-215	3.49E-18	3.56E-18	0.15E-50	158.0	157.4	459.0
0.5% $BaCO_3$/V-PET	205-215	1.82E-18	2.13E-18	0.16E-51	160.3	159.1	467.3
0.5% $ZnCO_3$/Vpet	205-215	3.29E-18	2.64E-18	0.25E-38	160.1	160.3	352.0
0.5% $CdCO_3$/V-PET	205-215	7.75E-19	8.14E-19	0.26E-52	162.7	161.9	471.8
0.5% $PbCO_3$/V-PET	205-215	6.58E-17	1.32E-16	0.30E-39	151.3	148.0	368.5

Table 4.47 Characteristics of the Texture of Nucleating Agents from Observations Under the Microscope.

(a) No thermal treatment.

	+ (*)	= (**)
Na_2CO_3	bright grey	dark
$NaHCO_3$	colorful white	colorful particle
K_2CO_3	white	dark
$MgCO_3$	white	dark
$CaCO_3$	colorful white	dark
$SrCO_3$	white	grey
$BaCO_3$	grey	dark
$ZnCO_3$	grey	dark
$PbCO_3$	grey	dark
$CdCO_3$	grey	dark

Table 4.47 Continued

(b) After thermal treatment at 300 ^{o}C.

	+ (*)	= (**)
Na_2CO_3	white grey	dark
$NaHCO_3$	white grey	dark
K_2CO_3	white	dark
$MgCO_3$	white	dark
$CaCO_3$	colorful white	dark
$SrCO_3$	white	dark
$BaCO_3$	grey	dark
$ZnCO_3$	grey	dark
$PbCO_3$	brown red (***)	dark
$CdCO_3$	brown red (***)	dark

*: + represents the cross polars.

**: = represents the no cross polars.

*** The color changes to red from white while heating.

Table 4.48 Characteristics of Texture and Thermal Properties of R-PET with and without Nucleating Agents from Microscopy Studies.

Additive	wt%	T_{mch}	T_{mm}	T_{mcc}	Note
bR-PET		144, MC	260	222, RM	Pic. 4.1
aR-PET		138, MC	257	221, RM	Pic. 4.2
Na_2CO_3	.063 0.3 0.5 1.0	143 135 130 135	253 250 255 254	222, MC 215, TG 220, TG 217 TG	Pic. 4.10 Pic. 4.11 Pic. 4.12 Pic. 4.13
$CaCO_3$	0.3 0.5 1.0	141 141 140	252 254 250	219 MC 217 MC 216 MC	
$NaHCO_3$	0.5	137	250	223 TG	
K_2CO_3	0.5	140	251	219 TG	
$MgCO_3$	0.5	144	267	233 TG	
$SrCO_3$	0.5	140	259	217 RM	
$BaCO_3$	0.5	148	260	223 RM	
$ZnCO_3$	0.5	134	255	223 RM	
$CdCO_3$	0.5	141	255	218 RM	
$PbCO_3$	0.5		254	223 RM	Pic. 4.32

(1) T_{mch} is the temperature at which texture (indicating the onset of crystallization) was first observed under the microscope during the heating scan.

(2) T_{mm} is the temperature at which birefrigence of the polymer crystals was observed to totally disappear.

(3) T_{mcc} is the temperature at which texture (crystallization) was first observed during the cooling scan.

RM: Ring Maltese cross pattern. MC: Maltese cross pattern.

TG: Tiny grainy.

Table 4.49 Characteristics of Texture and Thermal Properties of G-PET with and without Nucleating Agents from Microscopy Studies.

Additive	wt%	T_{mch}	T_{mm}	T_{mcc}	Note
bG-PET		134	257	224, RM	Pic. 4.3
aG-PET		137	256	222, RM	Pic. 4.4
Na_2CO_3	0.5	133	252	228, TG	Pic. 4.14, 4.15
$NaHCO_3$	0.5	125	256	227, TG	
K_2CO_3	0.5	135	261	227, TG	
$MgCO_3$	0.5	135	257	227, RM	
$CaCO_3$	0.5	137	258	223, RM	
$SrCO_3$	0.5	142	252	220, RM	
$BaCO_3$	0.5	136	256	222, RM	
$ZnCO_3$	0.5	138	253	221, RM	
$CdCO_3$	0.5	137	256	222, RM	
$PbCO_3$	0.5	137	258	231, RM	

Remarks as those made in Table 4.48.

Table 4.50 Characteristics of Texture and Thermal Properties of V-PET with and without Nucleating Agents from Microscopy Studies.

Additive	wt%	T_{mch}	T_{mm}	T_{mcc}	Note
bV-PET		147, MC	259	218, MC	Pic. 4.5, 4.6, 4.7, 4.8
aV-PET		133	259	227, RM	Pic. 4.9
Na_2CO_3	0.5	123	255	228, TG	
$NaHCO_3$	0.5	135	257	225, TG	
K_2CO_3	0.5	137	262	226, MC	
$MgCO_3$	0.5	131	260	229, MC	
$CaCO_3$	0.5	143	258	220, RM	
$SrCO_3$	0.5	138	260	221, RM	
$BaCO_3$	0.5	136	257	221, RM	
$ZnCO_3$	0.5	135	264	229, MC	
$CdCO_3$	0.5	137	260	229, MC	
$PbCO_3$	0.5	139	260	224, RM	

Remarks as those made in Table 4.48.

Table 4.51 Tensile Properties of R-PET with, and without Nucleating Agents. The rate of cross head is 0.2 in/min at room temperature.

R-PET with nucleating agents			
Nucleating Agent	Mold Temp	Tensile Strength	Tensile Modulus
	^{o}C	psix10^3	psix10^5
R-PET	40	7.078	1.19680
0.5% Na_2CO_3	40	5.648	1.33056
0.5% $CaCO_3$	40	7.002	1.18613
0.5% Na_2CO_3	90	4.340	1.48806
0.5% $NaHCO_3$	90	6.716	1.44819
0.5% K_2CO_3	90	8.106	1.39265
0.5% $MgCO_3$	90	4.410	1.31875
0.5% $CaCO_3$	90	7.770	1.35731
0.5% $SrCO_3$	90	7.637	1.33182
0.5% $BaCO_3$	90	7.244	1.30831
0.5% $ZnCO_3$	90	7.008	1.02641
0.5% $CdCO_3$	90	7.952	1.22343
0.5% $PbCO_3$	90	6.346	1.10400
0.3% Na_2CO_3	90	6.288	1.44586
0.5% Na_2CO_3	90	4.340	1.48806
1.0% Na_2CO_3	90	4.614	1.48480

Table 4.52 Tensile Properties of G-PET with, and without Nucleating Agents. The rate of cross head is 0.2 in/min at room temperature.

G-PET with nucleating agents			
Nucleating Agent	Mold Temp	Tensile Strength	Tensile Modulus
	^{o}C	psix10^3	psix10^5
G-PET	40	7.312	1.19592
0.5% Na_2CO_3	40	5.948	1.39817
0.5% $CaCO_3$	40	7.416	1.22876
0.5% Na_2CO_3	90	5.051	1.43424
0.5% $NaHCO_3$	90	3.652	1.33647
0.5% K_2CO_3	90	6.720	1.21333
0.5% $MgCO_3$	90	5.328	1.22300
0.5% $CaCO_3$	90	6.992	1.19333
0.5% $SrCO_3$	90	7.056	1.20666
0.5% $BaCO_3$	90	7.018	1.22533
0.5% $ZnCO_3$	90	6.484	1.20400
0.5% $CdCO_3$	90	7.640	1.24984
0.5% $PbCO_3$	90	6.266	1.22666

Table 4.53 Tensile Properties of V-PET with, and without Nucleating Agents. The rate of cross head is 0.2 in/min at room temperature.

V-PET with nucleating agents			
Nucleating Agent	Mold Temp	Tensile Strength	Tensile Modulus
	^{o}C	psix10^3	psix10^5
V-PET	40	7.642	1.24819
0.5% Na_2CO_3	40	6.796	1.43311
0.5% $CaCO_3$	40	7.674	1.28329
0.5% Na_2CO_3	90	6.916	1.41431
0.5% $NaHCO_3$	90	6.734	1.43398
0.5% K_2CO_3	90	7.210	1.27155
0.5% $MgCO_3$	90	5.040	1.21583
0.5% $CaCO_3$	90	6.116	1.24405
0.5% $SrCO_3$	90	6.341	1.26682
0.5% $BaCO_3$	90	7.776	1.32969
0.5% $ZnCO_3$	90	6.848	1.19120
0.5% $CdCO_3$	90	8.128	1.36791
0.5% $PbCO_3$	90	6.853	1.24373

Table 4.54 Flexural Properties of R-PET with, and without Nucleating Agents.

R-PET with nucleating agents			
Nucleating Agent	Mold Temp	Flexural Strength	Modulus of Flexural
	^{o}C	psix10^3	psix10^5
R-PET	40	12.787	3.64428
0.5% $CaCO_3$	40	12.403	3.52090
0.5% Na_2CO_3	40	13.240	3.65077
0.5% Na_2CO_3	90	15.674	5.12747
0.5% $NaHCO_3$	90	15.634	4.47434
0.5% K_2CO_3	90	13.785	4.10275
0.5% $MgCO_3$	90	11.123	4.32522
0.5% $CaCO_3$	90	13.875	4.33619
0.5% $SrCO_3$	90	13.027	3.79997
0.5% $BaCO_3$	90	12.940	4.07324
0.5% $ZnCO_3$	90	11.942	3.54011
0.5% $CdCO_3$	90	12.979	3.94444
0.5% $PbCO_3$	90	12.505	4.05164
0.3% Na_2CO_3	90	15.544	4.04274
0.5% Na_2CO_3	90	15.674	5.12747
1.0% Na_2CO_3	90	15.767	4.59651

The rate of cross head is 0.05 in/min at room temperature.

Table 4.55 Flexural Properties of G-PET with, and without Nucleating Agents.

G-PET with nucleating agents			
Nucleating Agent	Mold Temp	Flexural Strength	Modulus of Flexural
	^{o}C	psix10^3	psix10^5
G-PET	40	11.660	3.37489
0.5% Na_2CO_3	40	13.201	3.63226
0.5% $CaCO_3$	40	11.724	3.33947
0.5% Na_2CO_3	90	13.482	4.36900
0.5% $NaHCO_3$	90	10.380	4.50410
0.5% K_2CO_3	90	10.905	3.49580
0.5% $MgCO_3$	90	12.556	3.76987
0.5% $CaCO_3$	90	11.123	3.47075
0.5% $SrCO_3$	90	10.956	3.36475
0.5% $BaCO_3$	90	10.931	3.45612
0.5% $ZnCO_3$	90	11.942	3.82995
0.5% $CdCO_3$	90	11.980	3.54829
0.5% $PbCO_3$	90	11.315	3.70846

The rate of cross head is 0.05 in/min at room temperature.

Table 4.56 Flexural Properties of V-PET with, and without Nucleating Agents. The rate of cross head is 0.05 in/min at room temperature.

V-PET with nucleating agents			
Nucleating Agent	Mold Temp	Flexural Strength	Modulus of Flexural
	^{o}C	psix10^3	psix10^5
V-PET	40	11.916	3.46875
0.5% Na_2CO_3	40	13.493	3.74158
0.5% $CaCO_3$	40	11.904	3.45459
0.5% Na_2CO_3	90	15.110	4.20197
0.5% $NaHCO_3$	90	14.123	4.15135
0.5% K_2CO_3	90	12.544	3.83708
0.5% $MgCO_3$	90	12.748	4.02373
0.5% $CaCO_3$	90	12.979	4.01821
0.5% $SrCO_3$	90	12.032	3.55982
0.5% $BaCO_3$	90	13.184	3.96669
0.5% $ZnCO_3$	90	12.428	3.65278
0.5% $CdCO_3$	90	13.312	4.08938
0.5% $PbCO_3$	90	12.480	3.73440

The rate of cross head is 0.05 in/min at room temperature.

Table 4.57 Percent Shrinkage of Nucleated R-PET when placed in a vacuum oven at temperature of 225 ^{o}F (107.2 ^{o}C).

Material R-PET	Comp wt%	Mold Temp ^{o}C	L_o cm	L_f cm	Shrinkage %	Duration hr/min
R-PET		40	12.80	12.10	5.47	44/22
$CaCO_3$	0.5	40	12.80	12.10	5.47	44/22
Na_2CO_3	0.5	40	12.78	12.55	1.80	44/22
Na_2CO_3	0.3	90	12.62	12.60	0.16	44/22
Na_2CO_3	0.5	90	12.63	12.60	0.24	48
Na_2CO_3	1.0	90	12.62	12.60	0.16	44/22
Na_2CO_3	0.5	90	12.62	12.60	0.24	48
$NaHCO_3$	0.5	90	12.63	12.60	0.24	48
K_2CO_3	0.5	90	12.72	12.40	2.52	48
$MgCO_3$	0.5	90	12.80	12.60	1.56	48
$CaCO_3$	0.5	90	12.70	12.55	1.18	48
$SrCO_3$	0.5	90	12.70	12.48	1.73	48
$BaCO_3$	0.5	90	12.68	12.30	3.00	48
$ZnCO_3$	0.5	90	12.67	12.35	2.53	48
$CdCO_3$	0.5	90	12.65	12.30	2.77	48
$PbCO_3$	0.5	90	12.70	12.28	3.31	48

Table 4.58 Percent Shrinkage of Nucleated G-PET when placed in a vacuum oven at temperature of 225 ^{o}F (107.2 ^{o}C).

Material	Comp wt%	Mold Temp ^{o}C	L_o cm	L_f cm	Shrinkage %	Duration hr/min
G-PET		40	12.80	12.16	5.0	44/22
$CaCO_3$	0.5	40	12.80	12.09	5.55	44/22
Na_2CO_3	0.5	40	12.77	12.55	1.72	44/22
Na_2CO_3	0.5	90	12.59	12.55	0.32	40
$NaHCO_3$	0.5	90	12.58	12.55	0.24	40
K_2CO_3	0.5	90	12.65	12.45	1.58	40
$MgCO_3$	0.5	90	12.70	12.60	0.79	40
$CaCO_3$	0.5	90	12.68	12.36	2.52	40
$SrCO_3$	0.5	90	12.55	12.18	2.95	40
$BaCO_3$	0.5	90	12.65	12.40	1.98	40
$ZnCO_3$	0.5	90	12.68	12.30	3.00	40
$CdCO_3$	0.5	90	12.60	12.18	3.33	40
$PbCO_3$	0.5	90	12.60	12.35	1.98	40

Table 4.59 Percent Shrinkage of Nucleated V-PET when placed in a vacuum oven at temperature of 225 ^{O}F (107.2 ^{O}C).

Material	Comp wt%	Mold Temp ^{O}C	L_o cm	L_f cm	Shrinkage %	Duration hr/min
V-PET		40	12.80	12.17	5.07	44/22
$CaCO_3$	0.5	40	12.82	12.19	4.91	44/22
Na_2CO_3	0.5	40	12.80	12.61	1.48	44/22
Na_2CO_3	0.5	90	12.60	12.55	0.4	49/30
$NaHCO_3$	0.5	90	12.60	12.55	0.40	49/30
K_2CO_3	0.5	90	12.67	12.40	2.13	49/30
$MgCO_3$	0.5	90	12.70	12.45	1.97	49/30
$CaCO_3$	0.5	90	12.60	12.42	1.43	49/30
$SrCO_3$	0.5	90	12.50	12.25	2.00	49/30
$BaCO_3$	0.5	90	12.60	12.30	2.38	49/30
$ZnCO_3$	0.5	90	12.65	12.45	1.58	49/30
$CdCO_3$	0.5	90	12.70	12.40	2.36	49/30
$PbCO_3$	0.5	90	12.65	12.55	0.79	49/30

Table 4.60 Apparent Crystallinity, Surface Appearance, and Thermal Stability of Molded R-PET with, and without Nucleating Agents.

R-PET with nucleating agents				
Nucleating Agent	Mold Temp	Apparent Crystallinity	Surface Appearance	Thermal Stability
	^{o}C			
R-PET	40	0	3	N
0.5% Na_2CO_3	40	3	5	N
0.5% $CaCO_3$	40	0	3	N
0.5% Na_2CO_3	90	5	5	Y
0.5% $NaHCO_3$	90	5	5	Y
0.5% K_2CO_3	90	2	2	N
0.5% $MgCO_3$	90	2	3	N
0.5% $CaCO_3$	90	1	4	N
0.5% $SrCO_3$	90	1	1	N
0.5% $BaCO_3$	90	1	2	N
0.5% $ZnCO_3$	90	1	1	N
0.5% $CdCO_3$	90	1	2	N
0.5% $PbCO_3$	90	1	1	N
0.3% Na_2CO_3	90	4	5	Y
0.5% Na_2CO_3	90	5	5	Y
1.0% Na_2CO_3	90	5	5	Y

Table 4.61 Apparent Crystallinity, Surface Appearance, and Thermal Stability of molded G-PET with, and without nucleating agents.

G-PET with nucleating agents				
Nucleating Agent	Mold Temp	Apparent Crystallinity	Surface Appearance	Thermal Stability
	°C			
R-PET	40	1	5	N
0.5% Na_2CO_3	40	3	5	N
0.5% $CaCO_3$	40	1	5	N
0.5% Na_2CO_3	90	5	5	Y
0.5% $NaHCO_3$	90	5	5	Y
0.5% K_2CO_3	90	2	1	N
0.5% $MgCO_3$	90	2	1	N
0.5% $CaCO_3$	90	2	1	N
0.5% $SrCO_3$	90	1	1	N
0.5% $BaCO_3$	90	1	1	N
0.5% $ZnCO_3$	90	1	3	N
0.5% $CdCO_3$	90	1	1	N
0.5% $PbCO_3$	90	1	1	N

Table 4.62 Apparent Crystallinity, Surface Appearance, and Thermal Stability of molded V-PET with, and without nucleating agents.

V-PET with nucleating agents				
Nucleating Agent	Mold Temp	Apparent Crystallinity	Surface Appearance	Thermal Stability
	^{o}C			
R-PET	40	1	5	N
0.5% Na_2CO_3	40	3	5	N
0.5% $CaCO_3$	40	1	5	N
0.5% Na_2CO_3	90	5	3	Y
0.5% $NaHCO_3$	90	5	3	Y
0.5% K_2CO_3	90	2	1	N
0.5% $MgCO_3$	90	2	1	N
0.5% $CaCO_3$	90	1	2	N
0.5% $SrCO_3$	90	1	1	N
0.5% $BaCO_3$	90	1	2	N
0.5% $ZnCO_3$	90	1	1	N
0.5% $CdCO_3$	90	1	4	N
0.5% $PbCO_3$	90	2	2	N

Table 4.63 Physical Properties of Gaflex and Hytrel.

	GAFLEX 547ZS	GAFLEX 555ZS	GAFLEX 572ZS	HYTREL 4056
Shore D Hardness	47	55	72	40
Specific Gravity	1.17	1.20	1.24	1.17
Melt Flow Rate 240 °C, g/10min	11-15	10-15	28-33	
Melting Point, °C	178	184	228	173
Heat Distortion Temperature, °C	55	74	81	54
Tensile Strength at 100% strain (10^3 psi)	1.6	2.0	2.7	N.A.
Flexural Modulus st 22 °C (10^3 psi)	16.8	25.0	90.8	7.0
Izod Impact, Notched at 40 °F (ft-lb/in)	No Break	No Break	3.0	N.A.

Data provided by GAF Corporation (GAFLEX), and Du Pont Company (Hytrel)

Table 4.64 Thermal and Mechanical Properties of Polyblends of R-PET and GAFLEX-547.

	R-PET	R-PET/GAFa 90:10	R-PET/GAFa 80:20
T_g (^oC)	81	80	79
T_{ch} (^oC)	138	122	120
T_{cc} (^oC)	181	189	190
T_m (^oC)	248	250	252
Tensile strength(10^3psi)			
10 ^oC mold	8.7		5.9
50 ^oC mold	8.6		6.3
Tensile modulus(10^3psi)			
10 ^oC mold	139.0		89.6
50 ^oC mold	136.0		96.0
Flexural strength(10^3psi)			
10 ^oC mold	13.3		8.9
50 ^oC mold	12.5		9.0
Flexural modulus(10^3psi)			
IO ^oC mold	405.0		262.8
50 ^oC mold	352.0		258.0
Shrinkage, %	5.6		0.3

GAFa represents GAFLEX547

Table 4.65 Thermal and Mechanical Properties of Polyblends of R-PET and GAFLEX-555.

	R-PET	R-PET/GAFb 90:10	R-PET/GAFb 80:20
T_g (^oC)	81	74	76
T_{ch} (^oC)	138	129	126
T_{cc} (^oC)	181	188	189
T_m (^oC)	248	253	250
Tensile strength(10^3psi)			
10 ^oC mold	8.7	6.7	5.6
40 ^oC mold	8.6	7.6	6.1
Tensile modulus(10^3psi)			
10 ^oC mold	139.0	120.0	96.0
40 ^oC mold	136.0	128.0	83.2
Flexural strength(10^3 psi)			
10 ^oC mold	13.3	9.8	9.0
40 ^oC mold	12.5	10.8	10.0
Flexural modulus(10^3psi)			
10 ^oC mold	405.0	286.7	255.4
40 ^oC mold	352.0	312.7	289.4
Shrinkage, %	5.6	1.2	0.832

GAFb represents GAFLEX555

Table 4.66 Thermal and Mechanical Properties of Polyblends of R-PET and GAFLEX-572.

	R-PET	R-PET/GAFc 90:10	R-PET/GAFc 80:20
T_g (^oC)	81	77	76
T_{ch} (^oC)	138	119	118
T_{cc} (^oC)	181	197	192
T_m (^oC)	248	248	250
Tensile strength(10^3psi)			
14 ^oC mold	8.7	8.0	7.5
40 ^oC mold	8.6	8.1	7.3
Tensile modulus(10^3psi)			
14 ^oC mold	139.0	125.2	113.7
40 ^oC mold	136.0	121.9	111.2
Flexural strength(10^3 psi)			
14 ^oC mold	13.3	12.0	10.7
40 ^oC mold	12.5		
Flexural modulus(10^3psi)			
14 ^oC mold	405.0	382.0	324.0
40 ^oC mold	352.0		
Shrinkage, %	5.6	1.2	0.832

GAFc represents GAFLEX572

Table 4.67 Thermal and Mechanical Properties of Polyblends of R-PET and HYTREL-4056.

	R-PET	R-PET/HTRL 90:10	R-PET/HTRl 80:20
T_g (^oC)	81	77	78
T_{ch} (^oC)	138	120	122
T_{cc} (^oC)	181	195	194
T_m (^oC)	248	248	252
Tensile strength(10^3psi)			
10 ^oC mold	8.7	7.2	6.3
40 ^oC mold	8.6	6.9	6.7
Tensile modulus(10^3psi)			
10 ^oC mold	139.0	104.0	107.5
40 ^oC mold	136.0	95.0	116.7
Flexural strength(10^3 psi)			
10 ^oC mold	13.3	9.7	9.2
40 ^oC mold	12.5	10.6	9.3
Flexural modulus(10^3psi)			
10 ^oC mold	405.0	304.0	275.9
40 ^oC mold	352.0	302.3	273.3
Shrinkage, %	5.6	1.9	0.734

HTRL represents HYTREL4056

Table 4.68 Tensile Properties of PET and PE Measured at Room Temperature.

Material	Tensile Strength	Tensile Modulus	Elongation	Toughness
	kpsi	kpsi	%	lb-ft
[a]R-PET-1	7.078	119.680		
[b]R-PET-2	8.0	137.14	173	69.84
[c]LDPE-1	1.48	13.94	190	26.11
[d]LDPE-2	1.73	8.32	145	23.76
[e]HDPE	3.04	74.46	122	33.80

"a": T_{mold}= 104 ^{o}F, T_{barrel}= 550 ^{o}F, with a cross-head speed of 0.2 in/min.
"b": T_{mold}= 104 ^{o}F, T_{barrel}= 540 ^{o}F, with a cross-head speed of 1 in/min.
"c": T_{mold}= 75 ^{o}F, T_{barrel}= 520 ^{o}F, with a cross-head speed of 1 in/min.
"d": T_{mold}= 75 ^{o}F, T_{barrel}= 520 ^{o}F, with a cross-head speed of 1 in/min.
"e": T_{mold}= 100 ^{o}F, T_{barrel}= 500 ^{o}F, with a cross-head speed of 1 in/min.

Table 4.69 Thermal Properties of PE and PET after Processing. The DSC scan rate is 20 °C/min.

Material	PE		PET		
	T_{cc}	T_m	T_{ch}	T_{cc}	T_m
	^{o}C	^{o}C	^{o}C	^{o}C	^{o}C
R-PET-1			138	181	248
R-PET-2			132	213	255
LDPE-1	93.5	114			
LDPE-2	90	109			
HDPE	110	129.5			

Table 4.70 Typical Properties of Ionomers.

AClyn low molecular weight ionomers, (Data supplied by Allied-Signal Co.)					
AClyn Grade	Cation Type	Acid No.	Melt Point	Tensile Strength	Tensile Elong.
		mg KOH/g	^{o}C	kpsi	%
262A	Na^{+}	40	102	1.550	10
272A	Na^{+}	20	105	1.200	6
276A	Na^{+}		98	1.200	6
285A	Na^{+}	20	82	1.350	3
Surlyn ionomers (Data supplied by Dupont Company)					
Surlyn Grade	Cation Type	Acid No.	Melt Point	Tensile Strength	Tensile Elong.
			^{o}C	kpsi	%
S8527	Na	medium	79	4.2	450
S8920	Na	high	80	5.4	350

Table 4.71 Tensile Properties of LDPE-1 at Mold Temperature of 75 °F, and 800 psi Pressure for Different Barrel Temperatures. The strain rate is 1 in/min.

LDPE-1				
Barrel Temp.	Tensile Strength	Tensile Modulus	Elongation	Toughness
°F	kpsi	kpsi	%	lb-ft
360	1.73	20.92	135	21.17
440	1.54	17.58	172	24.21
520	1.48	13.94	190	26.11

Table 4.72 Thermal Properties of LDPE-1 Molded at 75 °F with Different Barrel Temperatures. The DSC scan rate is 20 °C/min.

LDPE-1		
Barrel Temp.	T_{cc}	T_m
°F	°C	°C
360	94.5	114
400	94	114
440	94	114
480	93	114
520	93.5	114

Table 4.73 Tensile Properties for Polyblends of 10% R-PET-1 (fine particles) and 90% LDPE-1 at mold temperature of 75 °F and pressure of 800 psi at different barrel temperatures (strain rate = 1 in/min).

90% LDPE-1/10% R-PET-1				
Barrel Temp.	Tensile Strength	Tensile Modulus	Elongation	Appearance PET particles
°F	kpsi	kpsi	%	
360	1.41	14.78	68	unmelted
380	1.35	15.06	69	unmelted
400	1.48	14.56	95	partly melted
420	1.60	14.98	130	tiny
440	1.60	16.48	183	not observed
460	1.58	18.35	182	not observed

Table 4.74 Thermal Properties for a Polyblends of 90% LDPE-1 and 10% R-PET-1 (fine particles) Molded at Different Barrel Temperatures. The DSC scan rate is 20 °C/min.

90% LDPE-1/10% R-PET-1					
Barrel Temp.	LDPE		PET		
	T_{cc}	T_m	T_{ch}	T_{cc}	T_m
°F	°C	°C	°C	°C	°C
360	94.5	112	-	-	-
380	95	112.5	-	-	-
400	95	112.5	-	-	246
420	95	112.5	-	182	248
440	95	112.5	-	182	248
460	95	112.5	-	182	248

90% LDPE-1/10% R-PET-1					
Barrel Temp.	W_m(PE)	W_m(PET)	W_{cc}(PE)	W_{cc}(PET)	W_{ch}(PET)
°F	%	%	%	%	%
360	1	-	1	-	-
380	1	-	1	-	-
400	1	-	1	-	-
420	0.975	0.025	1	-	-
440	0.958	0.042	1	-	-
460	0.949	0.051	1	-	-

Table 4.75 Tensile Properties of LDPE-1/R-PET-1 Blends Measured at Room Temperature with a cross-head speed of 1 in/min. Injection molding conditions: barrel temperature 460 °F and, mold temperature 75 °F.

LDPE-1/R-PET-1				
PE/PET Comp.	Tensile Strength	Tensile Modulus	Elongation	Toughness
	kpsi	kpsi	%	lb-ft
100/0	1.57	15.24	180	27.04
80/20	1.78	24.21	155	26.95
60/40	2.72	42.13	250	50.35
50/50	3.31	49.07	115	24.83
40/60	3.87	57.92	35	7.33
20/80	5.01	80.11	30	7.86

Table 4.76 Tensile Properties of LDPE-1 and R-PET-2 Blends Measured at Room Temperature with a coss-head speed of 1 in/min. Injection molding conditions: barrel temperature 460 °F and mold temperature 75 °F.

LDPE-1/R-PET-2				
PE/PET Comp.	Tensile Strength	Tensile Modulus	Elongation	Toughness
	kpsi	kpsi	%	lb-ft
100/0	1.57	15.24	180	27.04
90/10	1.81	22.43	163	27.24
80/20	2.06	30.73	133	24.18
70/30	2.35	34.96	275	52.01
60/40	3.02	45.56	180	46.75
50/50	3.55	52.17	80	15.56
40/60	4.34	64.64	60	11.48
30/70	4.94	75.28	16	6.15
20/80	5.38	85.99	17	6.16
10/90	7.07	101.3	17	8.99
0/100	8.0	137.1	173	69.84

Table 4.77 Thermal Properties of LDPE-1/R-PET-1 Blends Mixed at 460 °F. The DSC scan rate is 20 °C/min.

LDPE-1/R-PET-1						
LDPE/PET	LDPE		PET			
Comp.	T_{cc}	T_m	T_{ch}	T_{cc}	T_m	Run
%	°C	°C	°C	°C	°C	
100/0	93.5	114	-	-	-	
90/10	95	112.5	-	182	248	
80/20	94 -	113.5 113	130 137	180 -	248 -	1 2
60/40	94 -	113 113	129 136	182 -	248 248	1 2
50/50	94 -	113 113	130 136	181 -	248 248	1 2
40/60	94 94	113 112	130 136	183.5 183	249 249	1 2
20/80	95 -	112 112	128 135	188 -	250 249	1 2
0/100	-	-	138	181	248	

Table 4.77 Continued.

LDPE-1/R-PET-1					
LDPE/PET	W_m(PE)	W_m(PET)	W_{cc}(PE)	W_{cc}(PET)	W_{ch}(PET)
Comp.	%	%	%	%	%
80/20	0.911	0.089	0.970	0.030	0.388
60/40	0.788 0.779	0.212 0.221	0.823 -	0.177 -	0.372 0.475
50/50	0.736 0.734	0.264 0.266	0.721 -	0.279 -	0.270 0.470
40/60	0.674 0.671	0.326 0.329	0.626 0.618	0.374 0.382	0.311 0.394
20/80	0.429 0.414	0.571 0.586	0.326 -	0.674 -	0.344 0.256

Table 4.78 Thermal Properties of LDPE-1/R-PET-2 Blends, Mixed at 460 °F. The DSC scan rate is 20 c/min.

LDPE-1/R-PET-2						
LDPE/PET	LDPE		PET			
Comp.	T_{cc}	T_m	T_{ch}	T_{cc}	T_m	Run
%	°C	°C	°C	°C	°C	
100/0	93.5	114	-	-	-	1
90/10	- 96	113 113	- -	- 204	256 254	1 2
80/20	- 95	113 113	128 -	- 207	256 256	1 2
70/30	- 95	113 113	128 -	- 207	256 256	1 2
60/40	- 95	113 113	129 -	- 208	257 256	1 2
50/50	- 95	113 113	129 -	- 210	257 257	1 2
40/60	- 95	112 112	128 -	- 209	257 256	1 2
30/70	- 95	112 111.5	127 -	- 210	256 256	1 2
20/80	- 95	112 112	125 -	- 215	256 257	1 2
10/90	 95	112 111.5	124 -	- 214	257 257	1 2
0/100	-	-	132 -	- 213	260 255	1 2

Table 4.78 Continued.

LDPE-1/R-PET-2					
LDPE/PET	W_m(PE)	W_m(PET)	W_{cc}(PE)	W_{cc}(PET)	W_{ch}(PET)
Comp.	%	%	%	%	%
90/10	0.953 0.961	0.047 0.039	- 0.977	- 0.023	- -
80/20	0.901 0.878	0.099 0.122	- 0.909	- 0.091	0.280 0
70/30	0.839 0.878	0.161 0.122	- 0.855	- 0.145	0.2 0
60/40	0.799 0.807	0.201 0.193	- 0.774	- 0.226	0.313 0
50/50	0.765 0.751	0.235 0.249	- 0.719	- 0.281	0.304 0
40/60	0.619 0.600	0.381 0.400	- 0.541	- 0.459	0.391 0
30/70	0.539 0.516	0.461 0.484	- 0.451	- 0.549	0.366 0
20/80	0.475 0.424	0.525 0.576	- 0.349	- 0.651	0.438 0
10/90	0.380 0.221	0.620 0.779	- 0.199	- 0.801	0.405 0

Table 4.79 Tensile Properties of LDPE/R-PET Blends with AClyn Ionomers, measured at room temperature with a cross-head speed of 1 in/min. Injection molding conditions: barrel temperature 460 °F, and mold temperature 75 °F.

90% LDPE-2/10% R-PET-2				
AClyn Ionomers	Tensile Strength	Tensile Modulus	Elongation	Toughness
	kpsi	kpsi	%	lb-ft
None	1.80	12.8	105	21.30
2% 262A	1.71	12.8	139	20.89
2% 272A	1.68	12.8	150	21.66
2% 276A	1.79	12.16	145	19.09
2% 285A	1.95	14.40	138	22.82

20% LDPE-1/80% R-PET-2				
AClyn Ionomers	Tensile Strength	Tensile Modulus	Elongation	Toughness
	kpsi	kpsi	%	lb-ft
None	5.38	85.99	17	6.16
2% 285A	6.03	93.33	22	10.80
6% 285A	5.96	94.44	14	5.90

Table 4.80 Thermal Properties of LDPE/PET Blends with AClyn Ionomers Mixed at 460 °F. The DSC scan rate is 20 °C/min.

90% LDPE-2/10% R-PET-2 with AClyn ionomers					
Ionomer	LDPE		PET		
Comp.	T_{cc}	T_m	T_{ch}	T_{cc}	T_m
%	°C	°C	°C	°C	°C
Plain	90	109.5	-	209	256
2% 262A	90	109	-	202	242
2% 272A	91	109.5	-	212	246
2% 276A	90	109	-	225	253
2% 285A	91	109	-	222	254

90% LDPE-2/10% R-PET-2 with AClyn ionomers					
Ionomer	W_m(PE)	W_m(PET)	W_{cc}(PE)	W_{cc}(PET)	W_{ch}(PET)
%.	%	%	%	%	%
Plain	0.954	0.046	0.957	0.043	0
2% 262A	0.961	0.039	0.954	0.046	0
2% 272A	0.957	0.043	0.962	0.038	0
2% 276A	0.941	0.059	0.934	0.066	0
2% 285A	0.959	0.041	0.947	0.053	0

Table 4.81 Tensile Properties of PE/R-PET Blends with Surlyn Ionomers, measured at room temperature with a cross-head speed of 1 in/min. Injection molding conditions: barrel temperature 480 °F and, mold temperature 75 °F.

90% LDPE-2/10% R-PET-1				
Surlyn Ionomers	Tensile Strength	Tensile Modulus	Elongation	Toughness
	kpsi	kpsi	%	lb-ft
2% S8527	1.8	12.96	130	20.22
2% S8920	1.7	12.32	120	16.98

50% LDPE-2/50% R-PET-1				
Surlyn Ionomers	Tensile Strength	Tensile Modulus	Elongation	Toughness
	kpsi	kpsi	%	lb-ft
None	2.96	43.2	75	24.80
2% S8920	3.04	45.12	115	42.10

20% LDPE-1/80% R-PET-2				
Surlyn Ionomers	Tensile Strength	Tensile Modulus	Elongation	Toughness
	kpsi	kpsi	%	lb-ft
None	5.38	85.99	17	6.16
2% S8527	6.06	82.08	39	20.49
6% S8527	6.24	68.24	40	28.03

Table 6.81 Continued.

20% HDPE/80% R-PET-2, T_{barrel}=500 °F				
Surlyn Ionomers	Tensile Strength	Tensile Modulus	Elongation	Toughness
	kpsi	kpsi	%	lb-ft
None	5.43	88	10.9	4.10
2% S8527	6.00	91.68	12.0	4.77

Table 4.82 Thermal Properties of PE/PET Blends with Surlyn Ionomers Mixed at 460 °F. The DSC scan rate is 20 °C/min.

90% LDPE-2/10% R-PET-1 with Surlyn ionomers						
Ionomer	LDPE		PET			
Comp.	T_{cc}	T_m	T_{ch}	T_{cc}	T_m	Run
%	°C	°C	°C	°C	°C	
2% S8527	- 91	110 110	- -	- 196	244 246	1 2
2% S8920	- 91	110 110	- -	- 196	245 245	1 2
90% LDPE-2/10% R-PET-1 with Surlyn ionomers						
Ionomer	W_m(PE)	W_m(PET)	W_{cc}(PE)	W_{cc}(PET)	W_{ch}(PET)	
Comp.	%	%	%	%	%	
2% S8527	0.965 0.976	0.035 0.021	- 0.972	- 0.028	0 0	
2% S8920	0.960 0.982	0.040 0.018	- 0.969	- 0.031	0 0	

Table 4.82 Continued.

50% LDPE-2/50% R-PET-1 with ionomers mixed at 480 °F						
Ionomer	LDPE		PET			
Comp.	T_{cc}	T_m	T_{ch}	T_{cc}	T_m	Run
%	°C	°C	°C	°C	°C	
Plain	- 92	109 109	130 137	- 188	248 248	1 2
2% S8920	- 92	109 110	126 -	- 199	248 248	1 2

50% LDPE-2/50% R-PET-1 with ionomers mixed at 480 °F					
Ionomer	W_m(PE)	W_m(PET)	W_{cc}(PE)	W_{cc}(PET)	W_{ch}(PET)
Comp.	%	%	%	%	%
Plain	0.763 0.726	0.237 0.274	- 0.683	- 0.317	0.262 0.511
2% S8920	0.754 0.737	0.246 0.263	- 0.683	- 0.317	0.341 0

Table 4.82 Continued

20% LDPE-1/80% R-PET-2 with ionomers mixed at 480 °F						
Ionomer	LDPE		PET			
Comp.	T_{cc}	T_m	T_{ch}	T_{cc}	T_m	Run
%	°C	°C	°C	°C	°C	
2% S8527	- 94.5	116 111	130 -	- 217	- 255	1 2
6% S8527	94.5 94.5	112.5 111	121 -	220 221	259 253	1 2

20% LDPE-1/80% R-PET-2 with ionomers mixed at 480 °F					
Ionomer	W_m(PE)	W_m(PET)	W_{cc}(PE)	W_{cc}(PET)	W_{ch}(PET)
Comp.	%	%	%	%	%
2% S8527	0.418	0.582	0.317	0.683	0
6% S8527	0.439 0.418	0.561 0.582	0.333 0.324	0.667 0.676	0.386 0

20% HDPE/80% R-PET-2 with ionomers mixed at 480 °F						
Ionomer	LDPE		PET			
Comp.	T_{cc}	T_m	T_{ch}	T_{cc}	T_m	Run
%	°C	°C	°C	°C	°C	
None	- 110.5	129 127	133 -	- 212	- 254	1 2
2% S8527	111	128	-	218	256	1

20% HDPE-1/80% R-PET-2 with ionomers mixed at 480 °F					
Ionomer	W_m(PE)	W_m(PET)	W_{cc}(PE)	W_{cc}(PET)	W_{ch}(PET)
Comp.	%	%	%	%	%
Plain	0.537	0.463	0.483	0.517	0
2% S8527	0.537	0.463	0.481	0.519	0

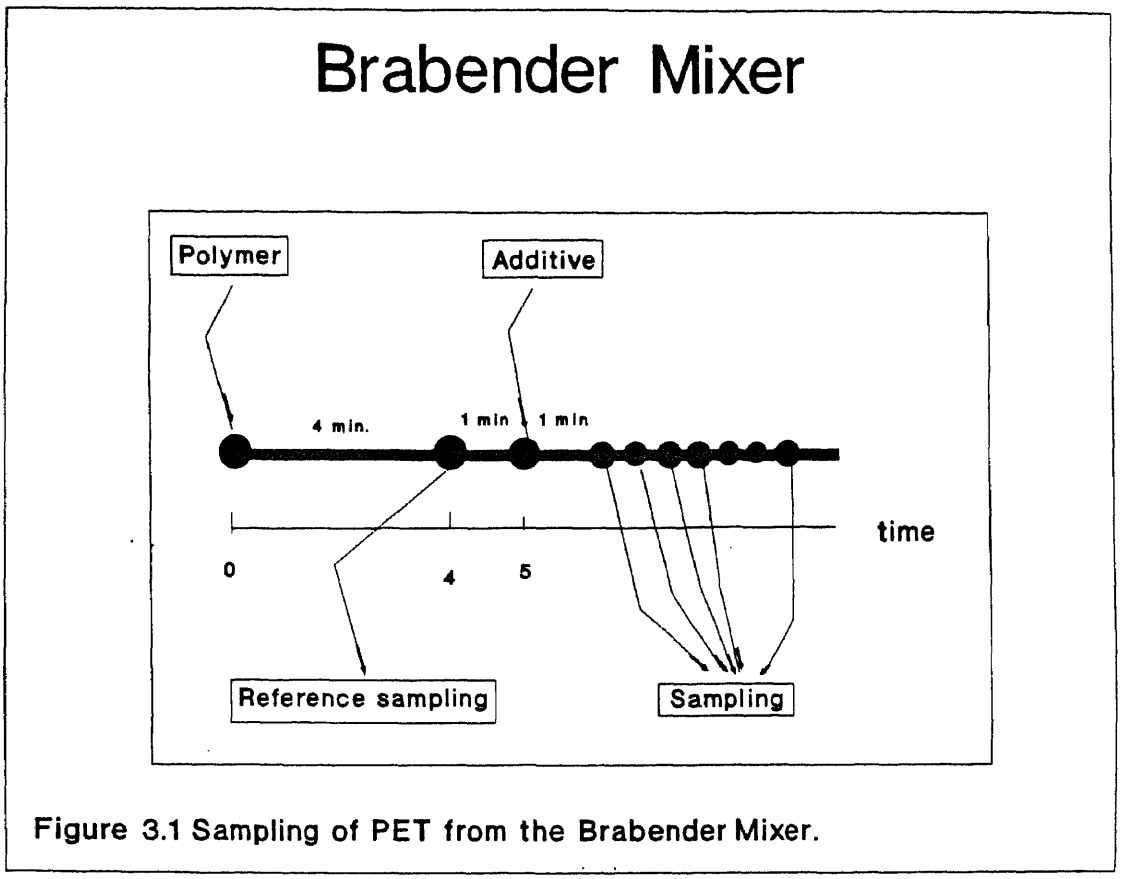

Figure 3.1 Sampling of PET from the Brabender Mixer.

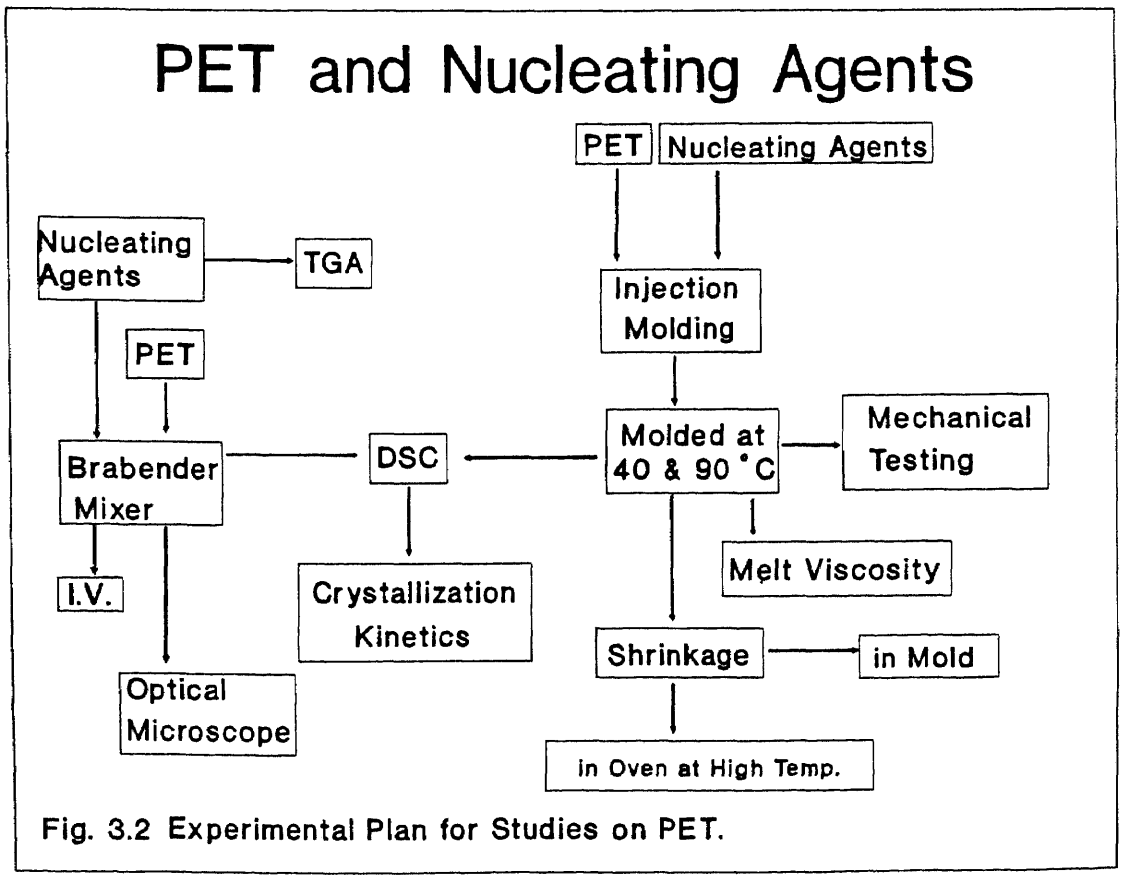

Fig. 3.2 Experimental Plan for Studies on PET.

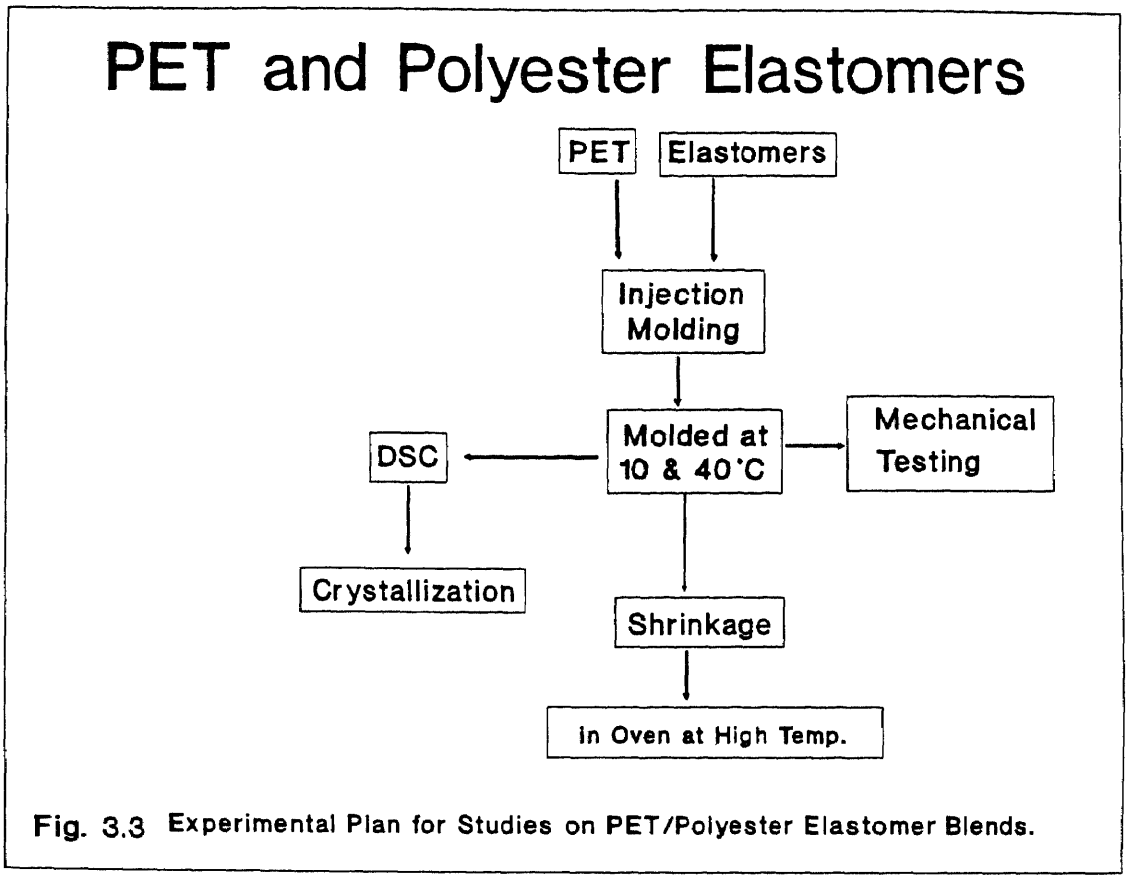

Fig. 3.3 Experimental Plan for Studies on PET/Polyester Elastomer Blends.

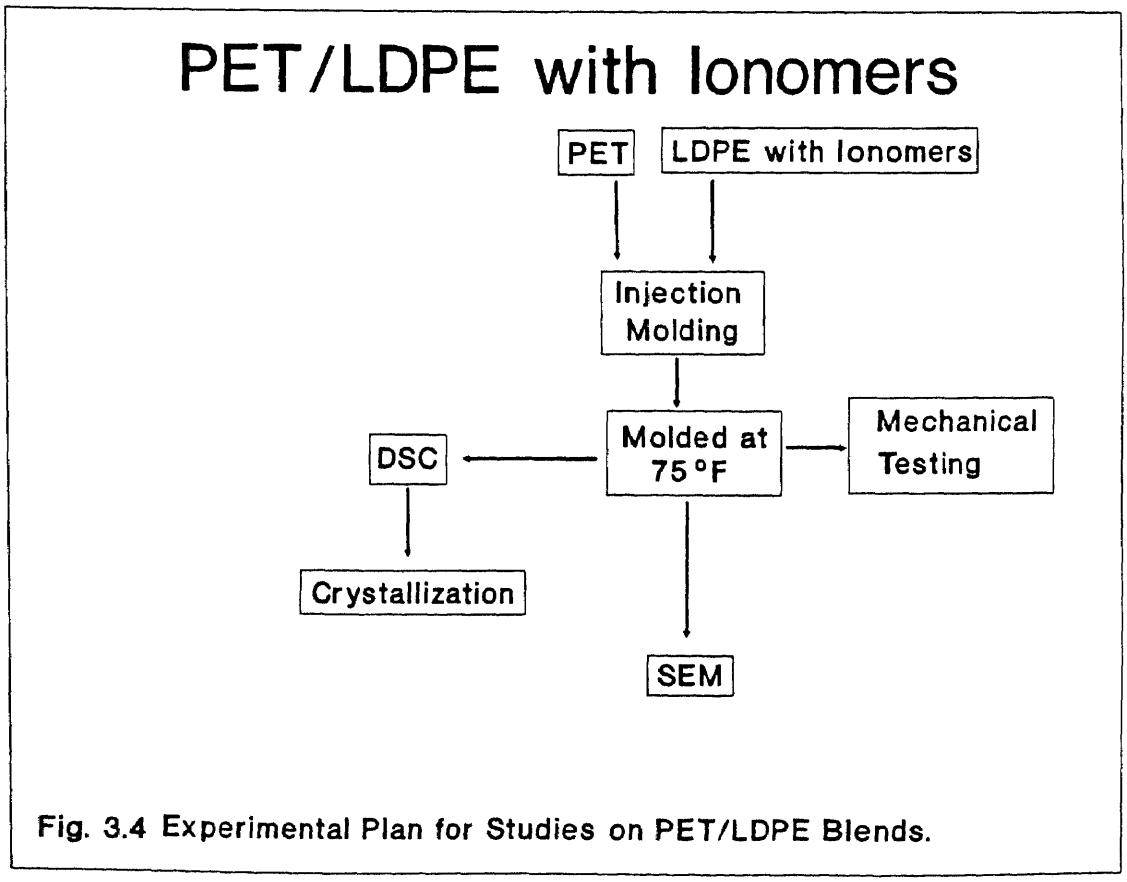

Fig. 3.4 Experimental Plan for Studies on PET/LDPE Blends.

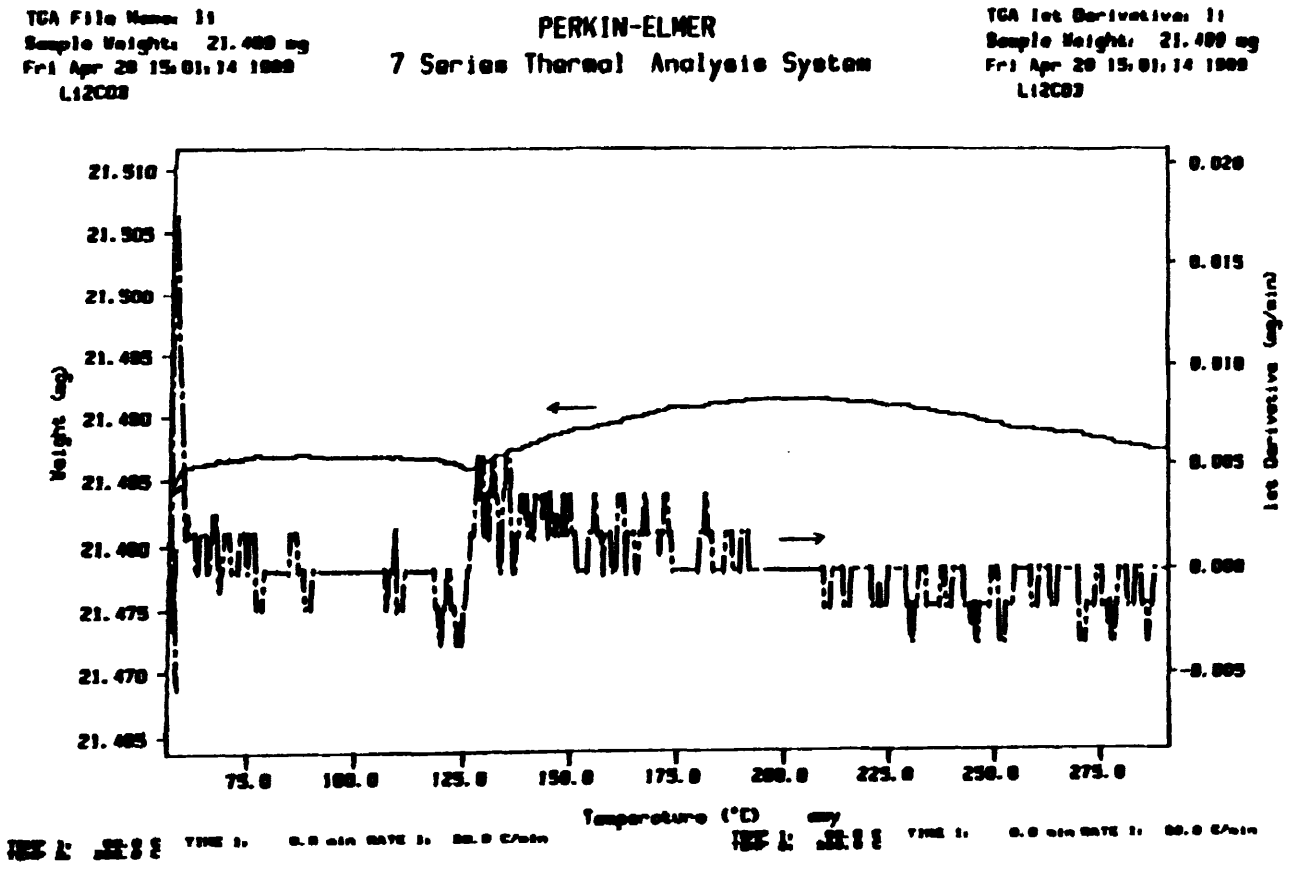

Figure 4.1 TGA Scans for Lithium Carbonate (Li_2CO_3) at scan rate of 20 ^{o}C/min

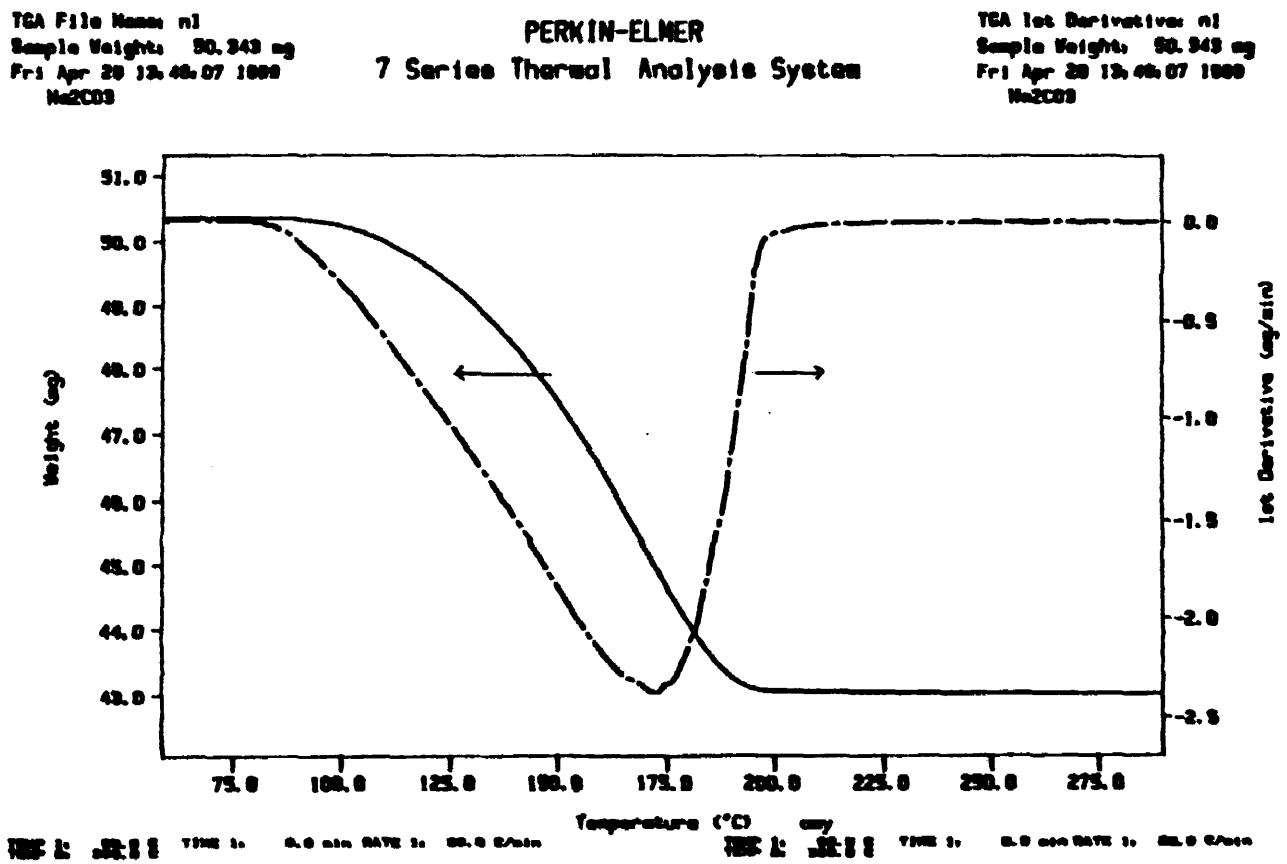

Figure 4.2 TGA Scans for Sodium Carbonate (Na_2CO_3) at scan rate of 20 ^{o}C/min

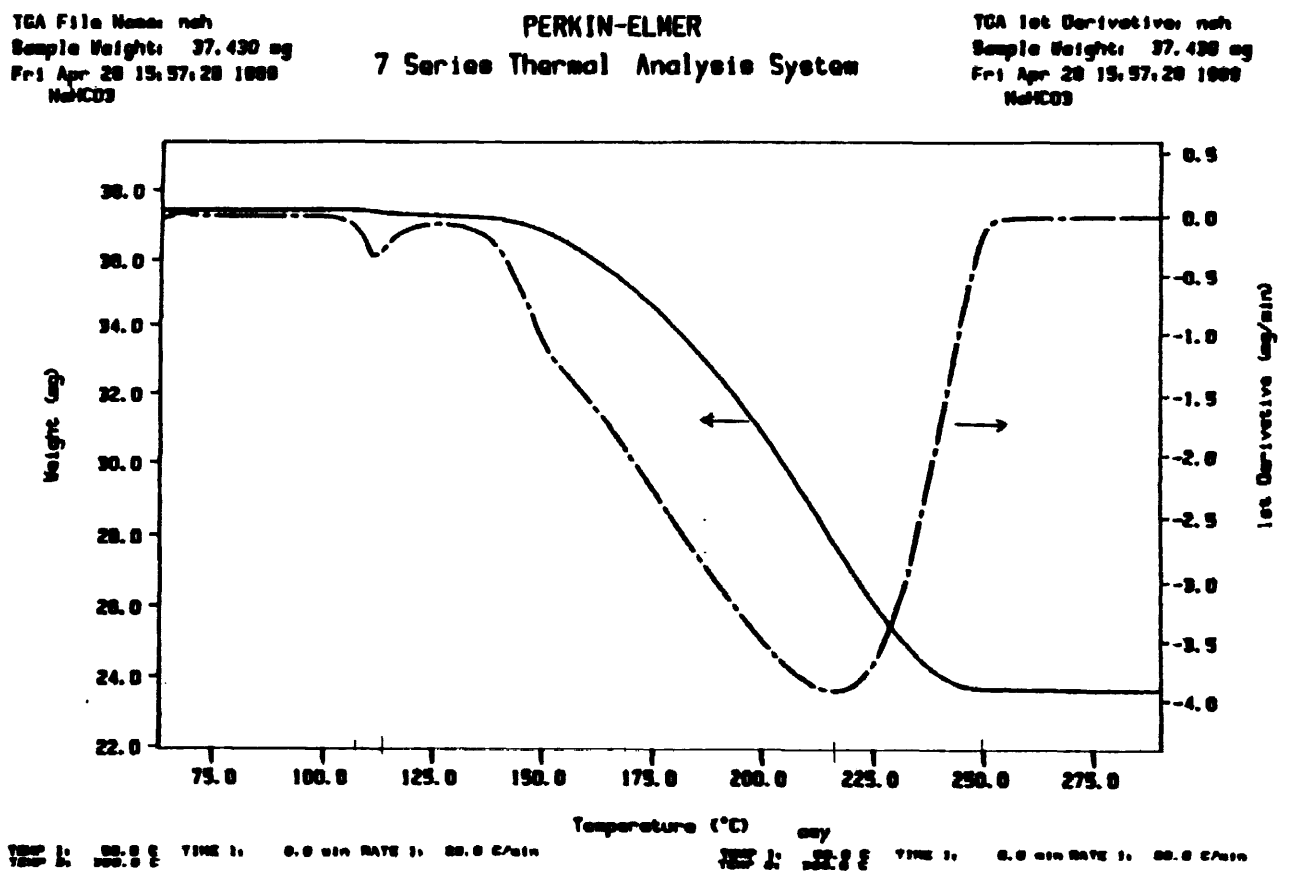

Figure 4.3 TGA Scans for Sodium Bicarbonate ($NaHCO_3$) at scan rate of 20 ^{o}C/min

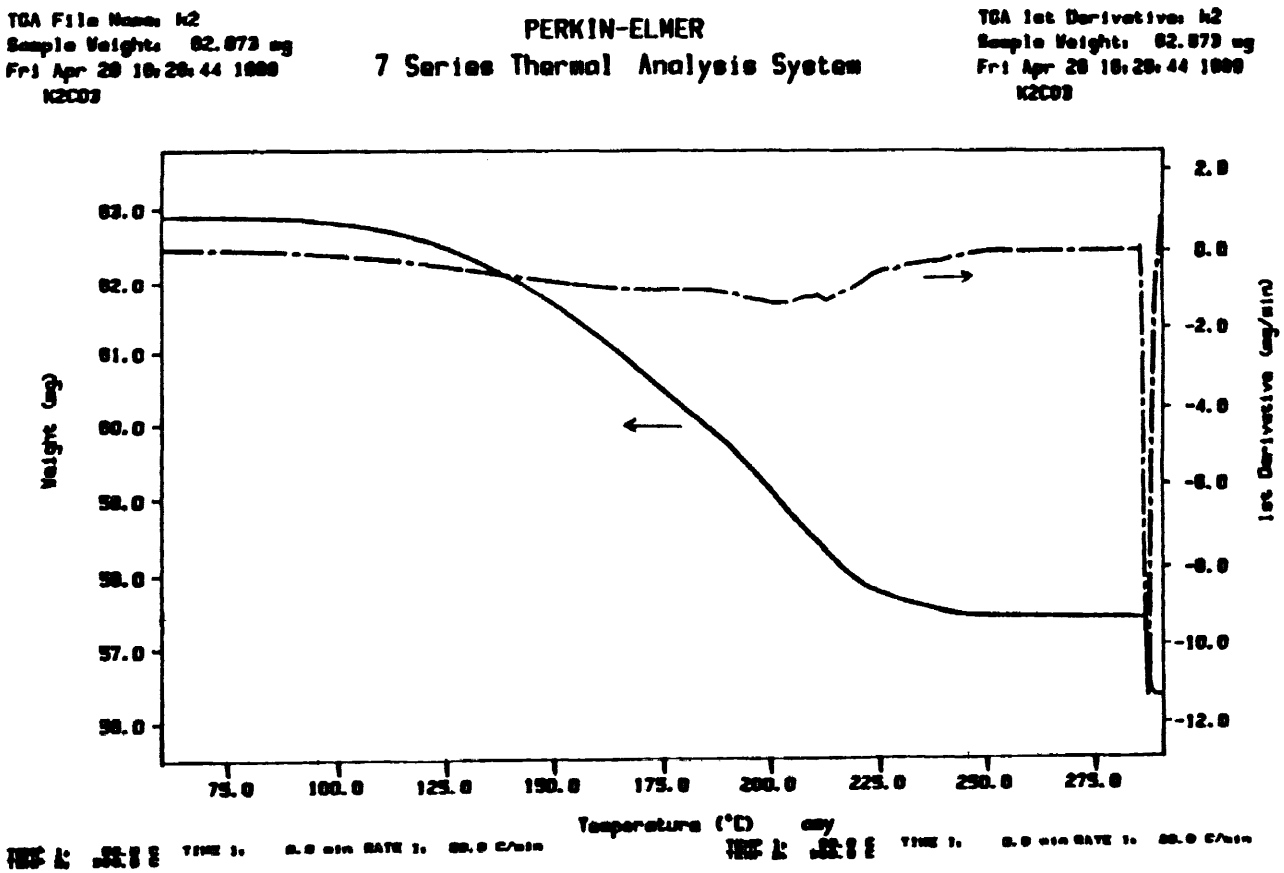

Figure 4.4 TGA Scans for Potassium Carbonate (K_2CO_3) at scan rate of 20 ^{o}C/min

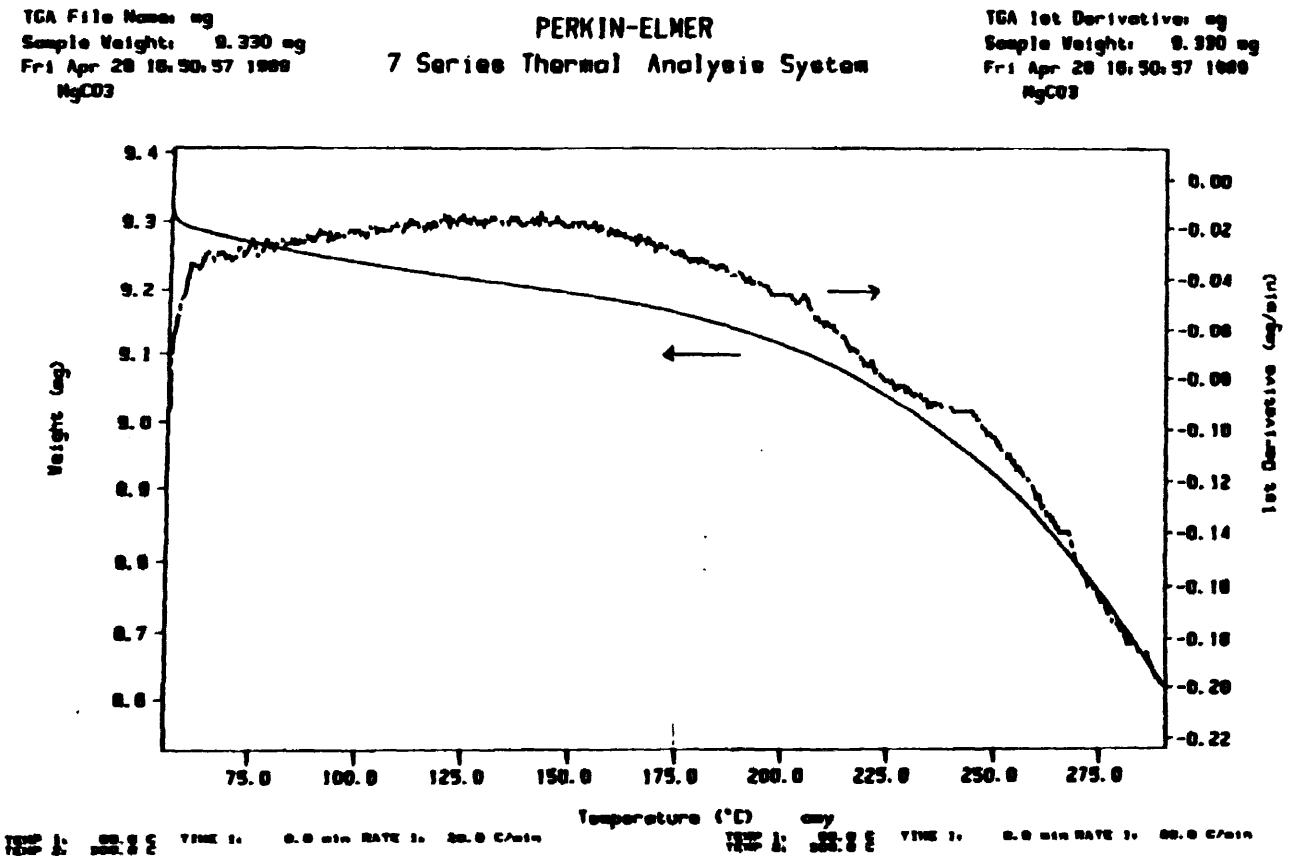

Figure 4.5 TGA Scans for Magnesium Carbonate ($MgCO_3$) at scan rate of 20 ^{o}C/min

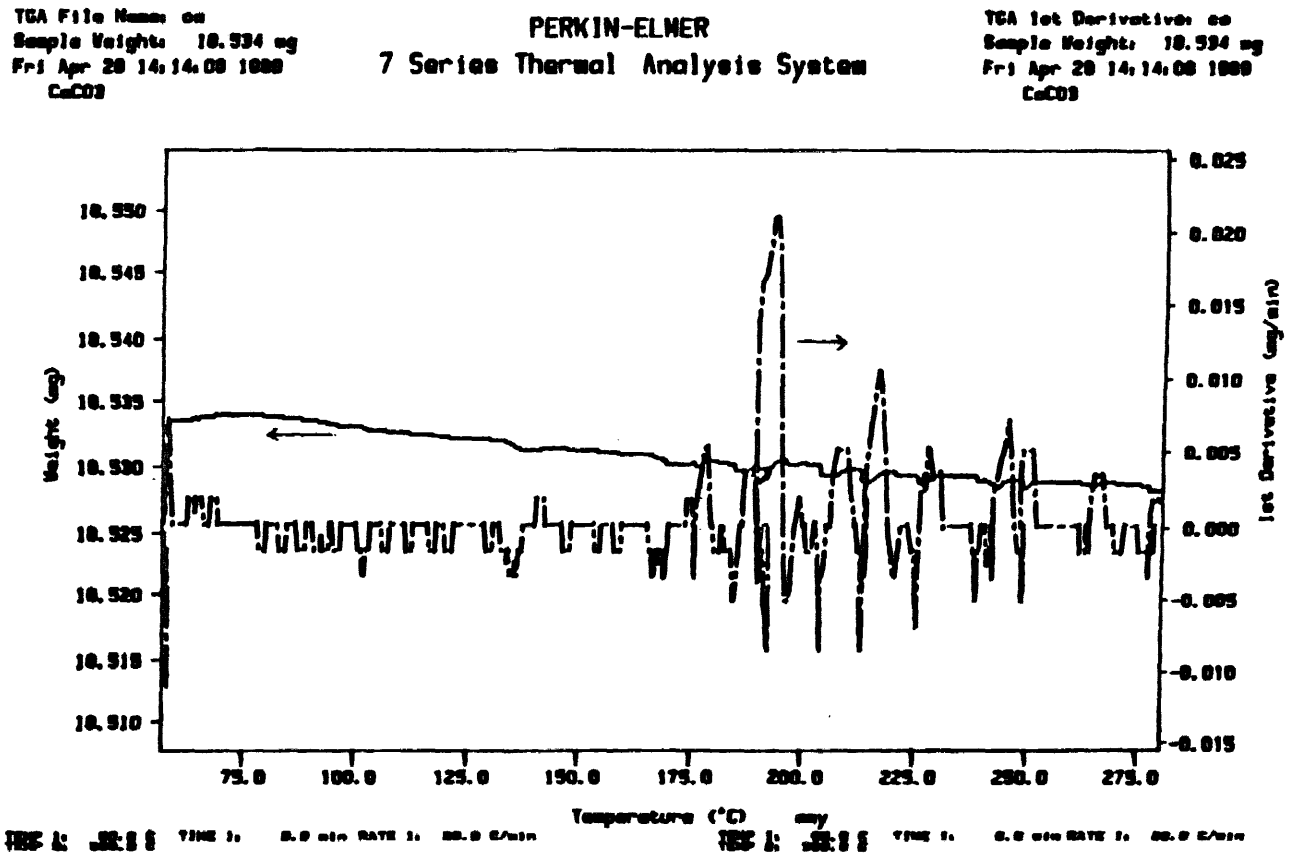

Figure 4.6 TGA Scans for Calcium Carbonate ($CaCO_3$) at scan rate of 20 ^{o}C/min

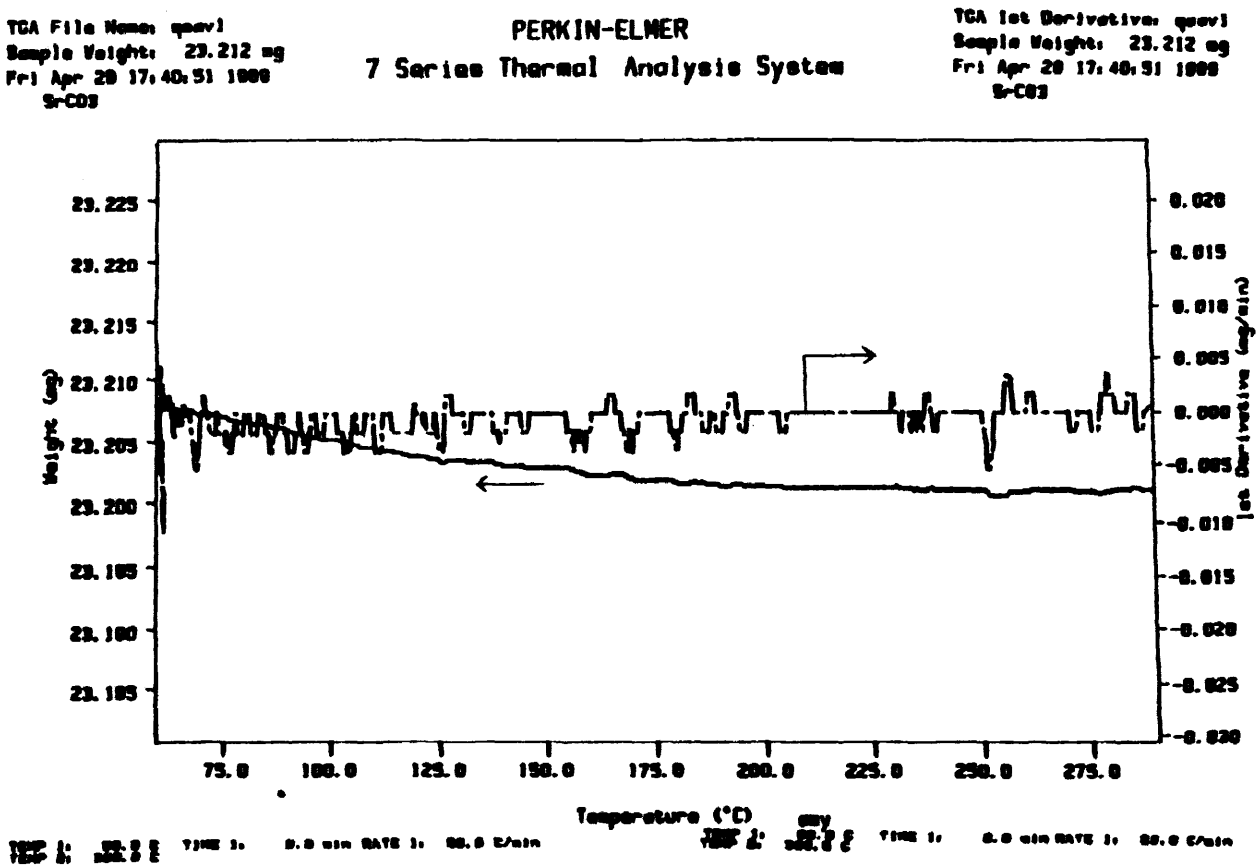

Figure 4.7 TGA Scans for Strontium Carbonate ($SrCO_3$) at scan rate of 20 ^{o}C/min

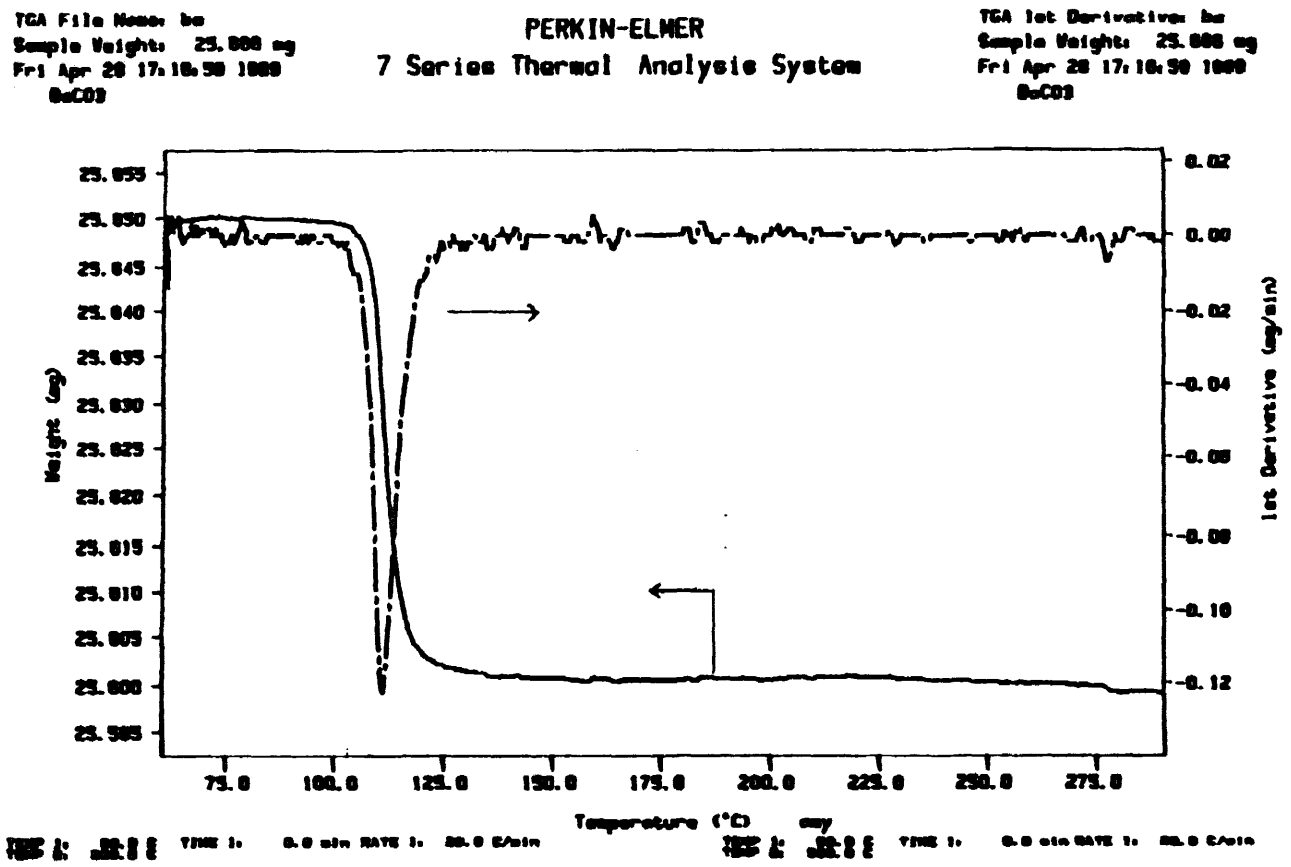

Figure 4.8 TGA Scans for Barium Carbonate ($BaCO_3$) at scan rate of 20 ^{o}C/min

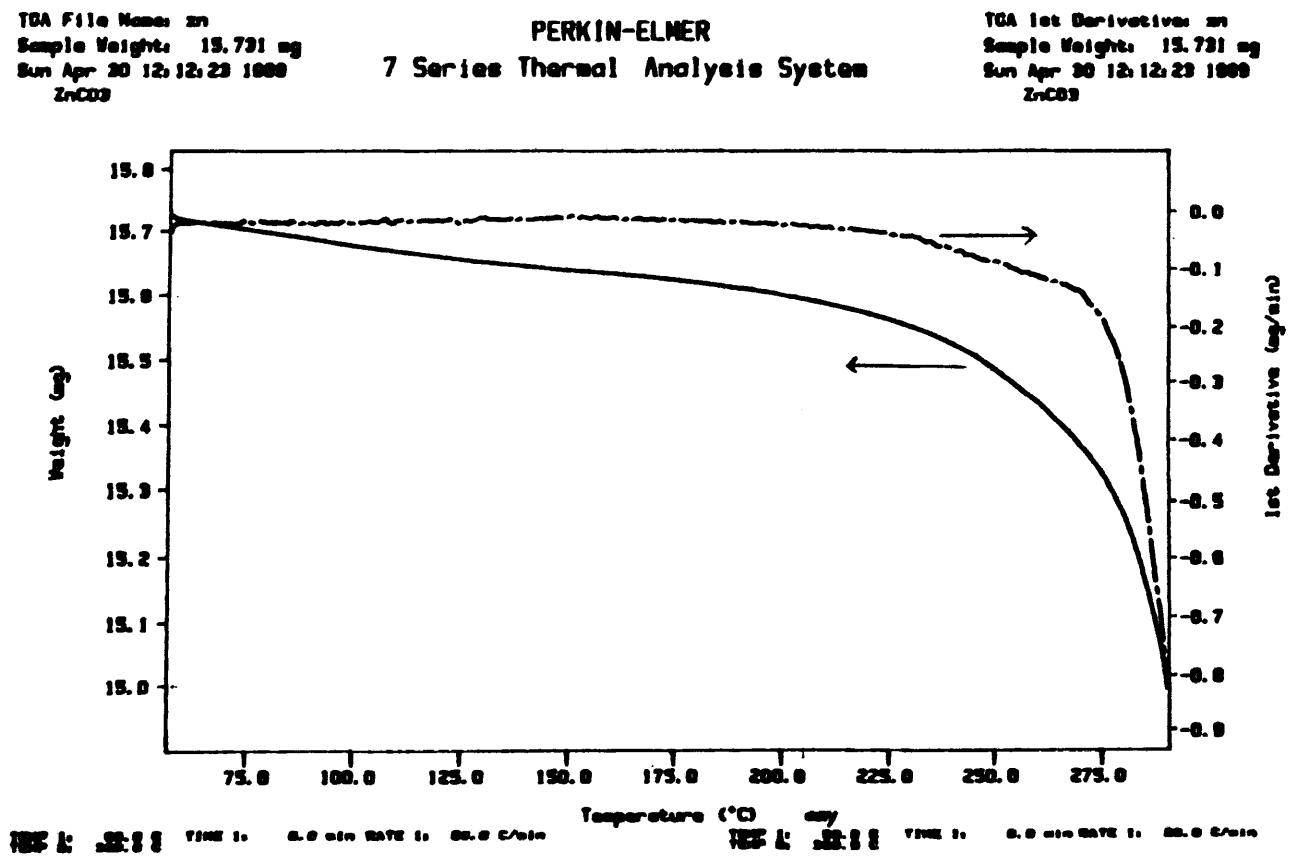

Figure 4.9 TGA Scans for Zinc Carbonate ($ZnCO_3$) at scan rate of 20 ^{o}C/min

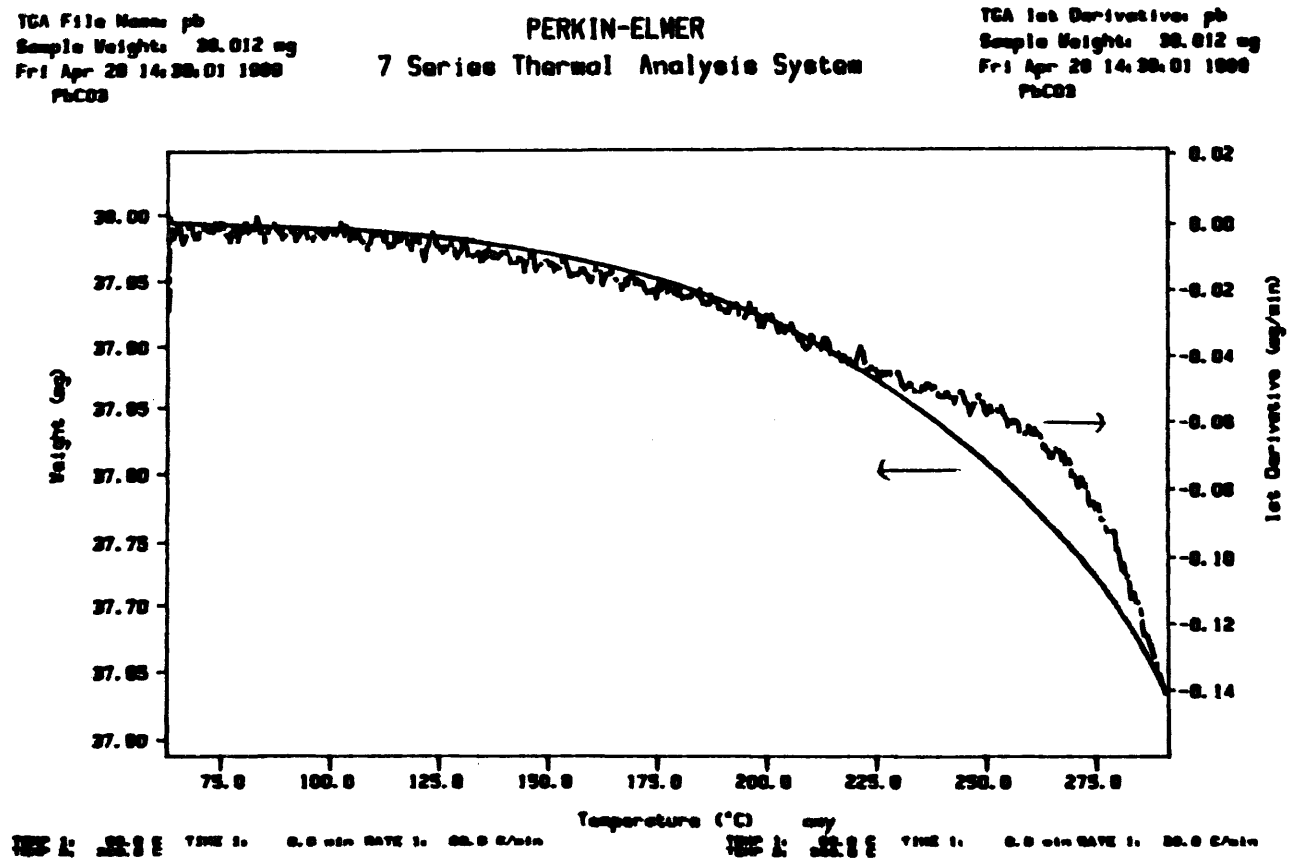

Figure 4.10 TGA Scans for Lead Carbonate ($PbCO_3$) at scan rate of 20 ^{o}C/min

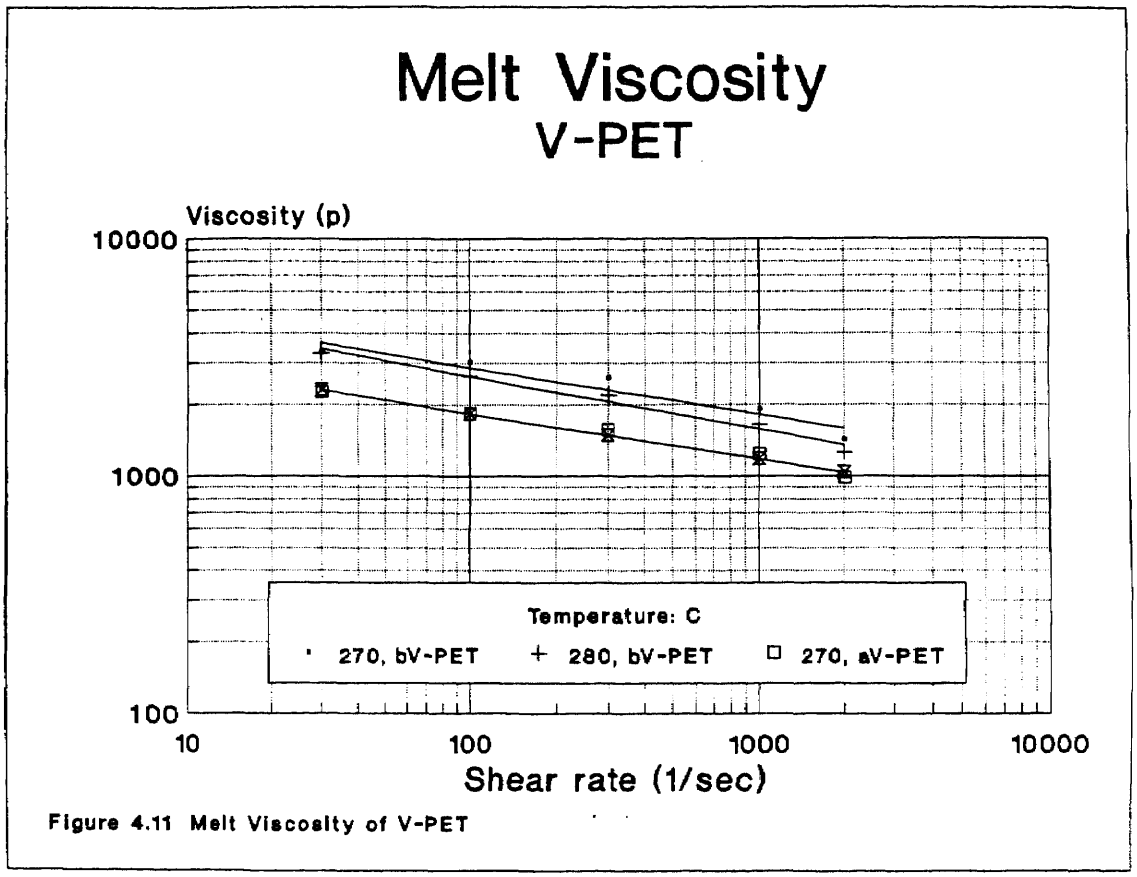

Figure 4.11 Melt Viscosity of V-PET

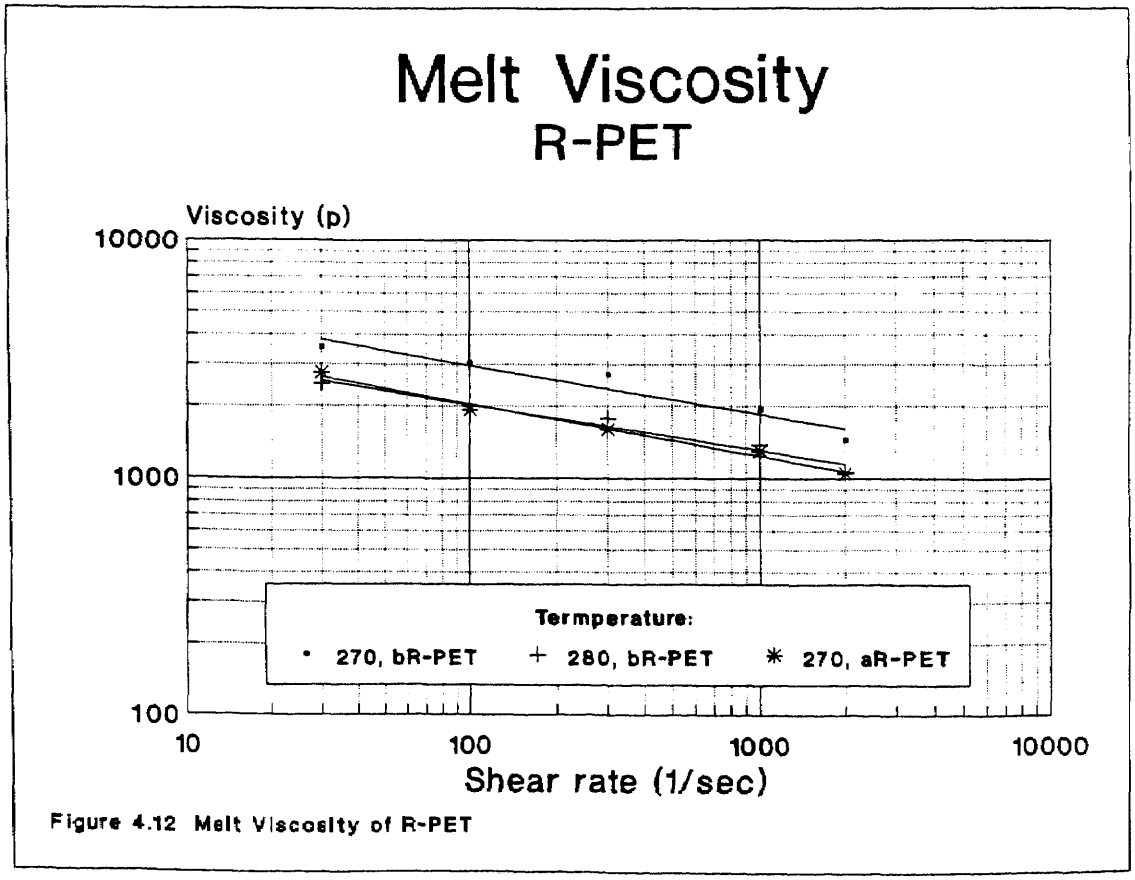

Figure 4.12 Melt Viscosity of R-PET

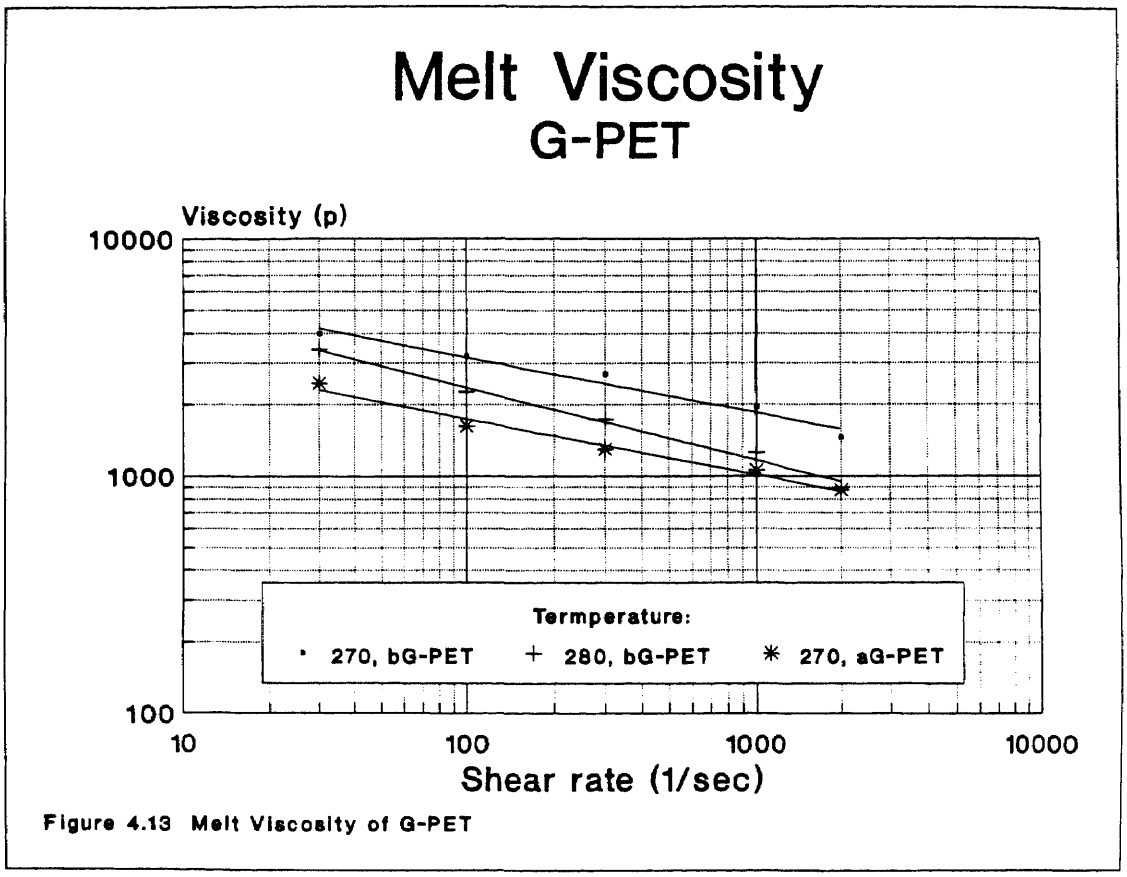

Figure 4.13 Melt Viscosity of G-PET

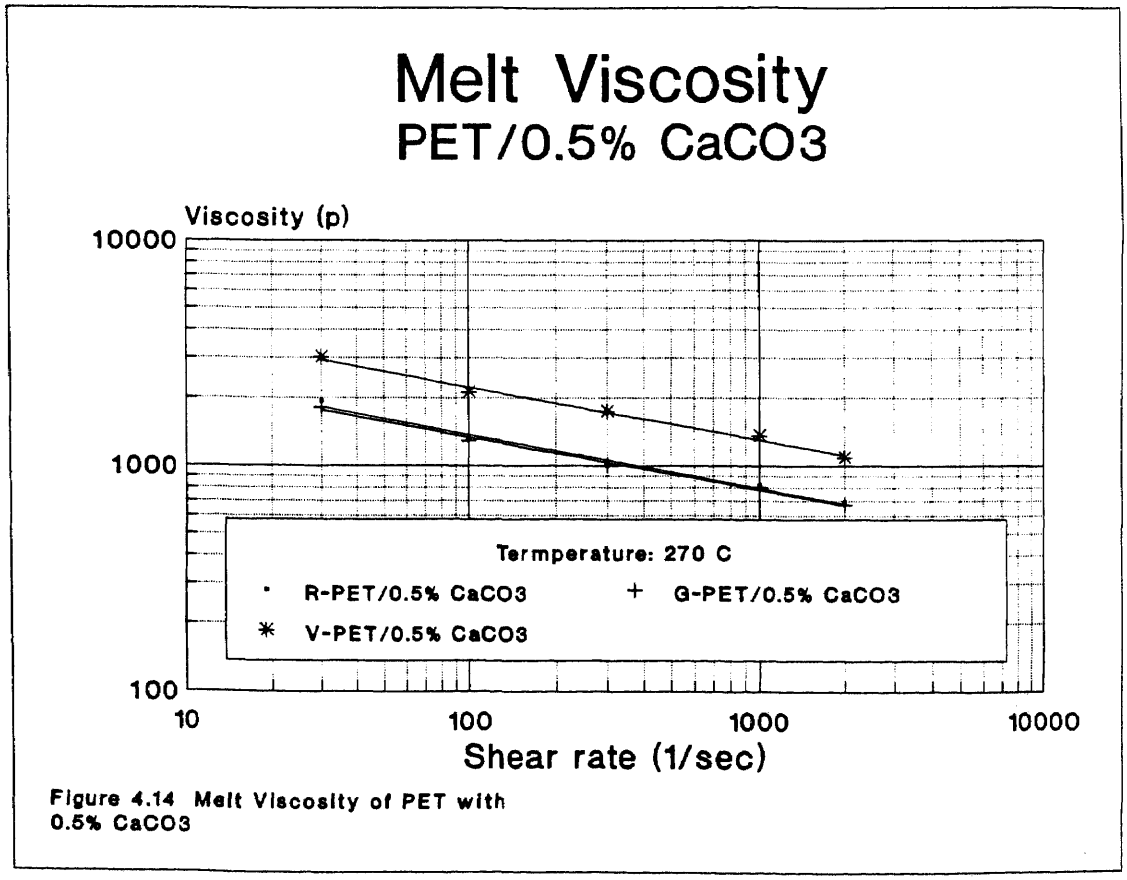

Figure 4.14 Melt Viscosity of PET with 0.5% CaCO3

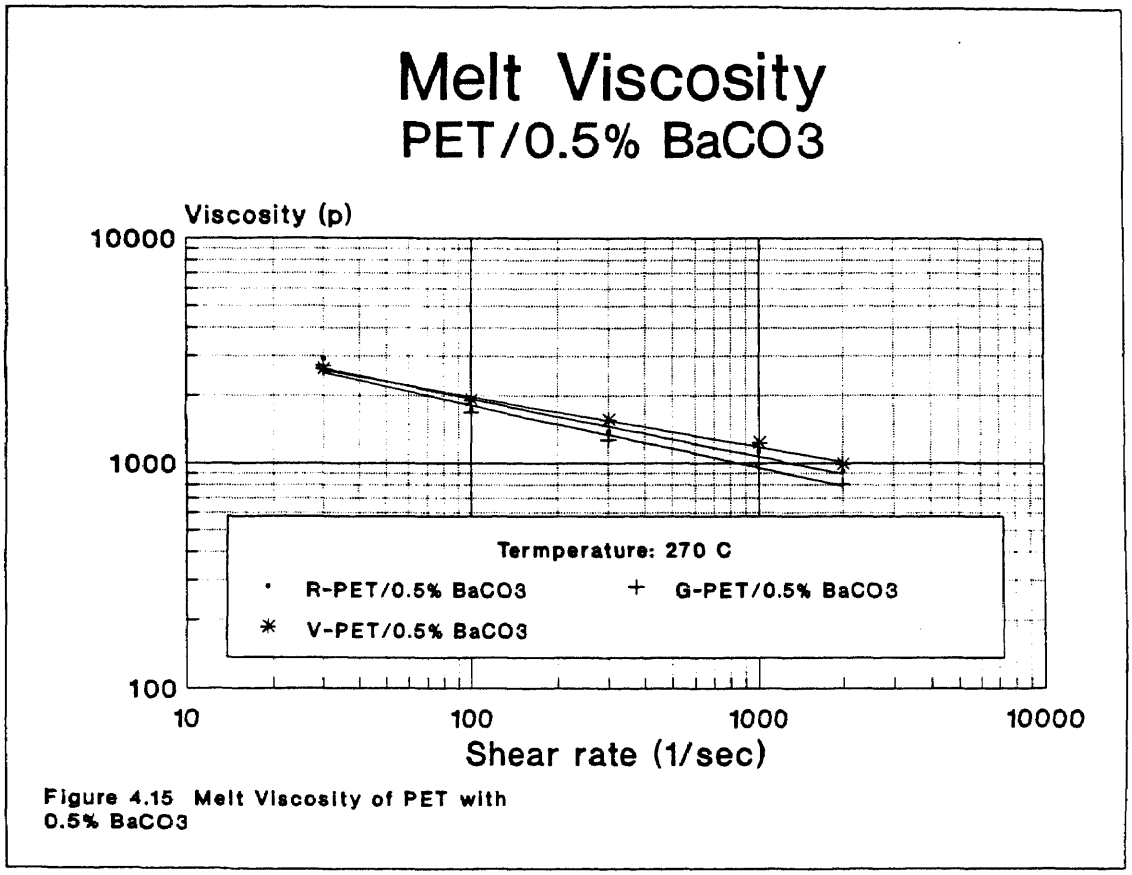

Figure 4.15 Melt Viscosity of PET with 0.5% $BaCO_3$

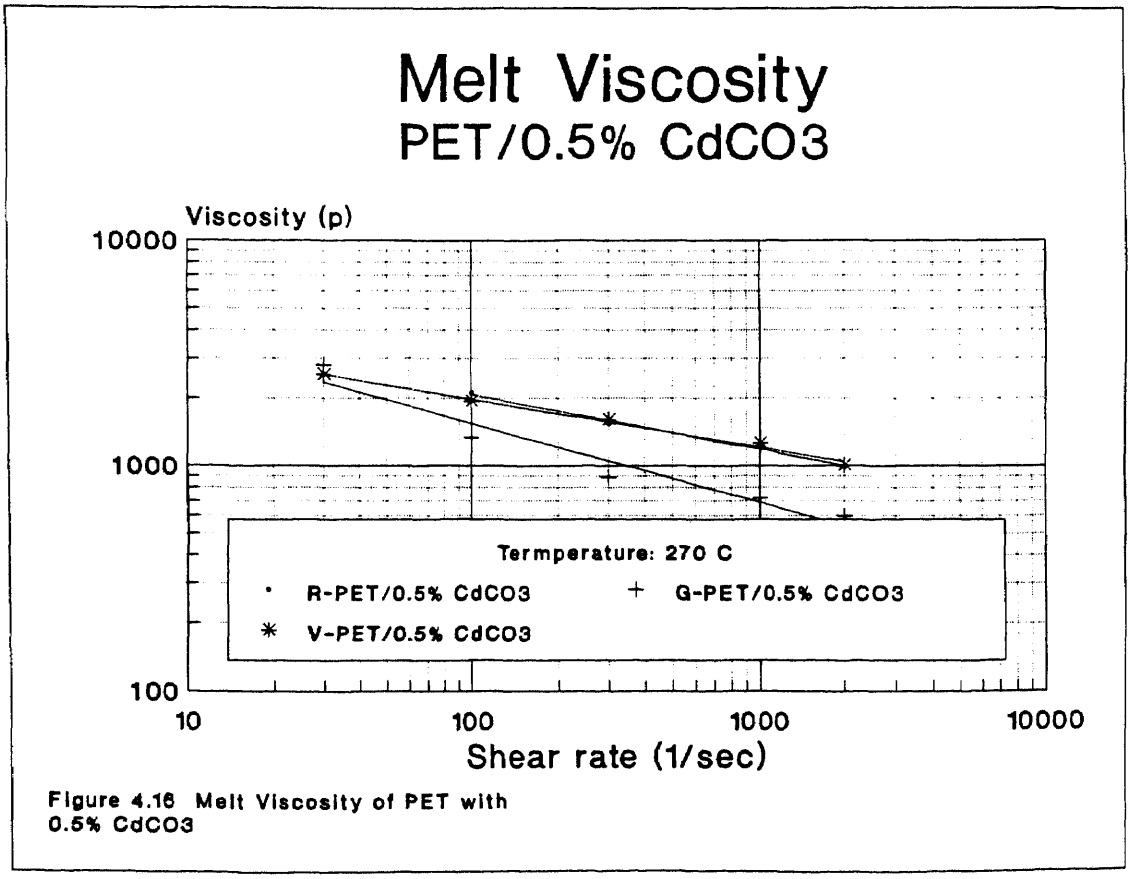

Figure 4.16 Melt Viscosity of PET with 0.5% $CdCO_3$

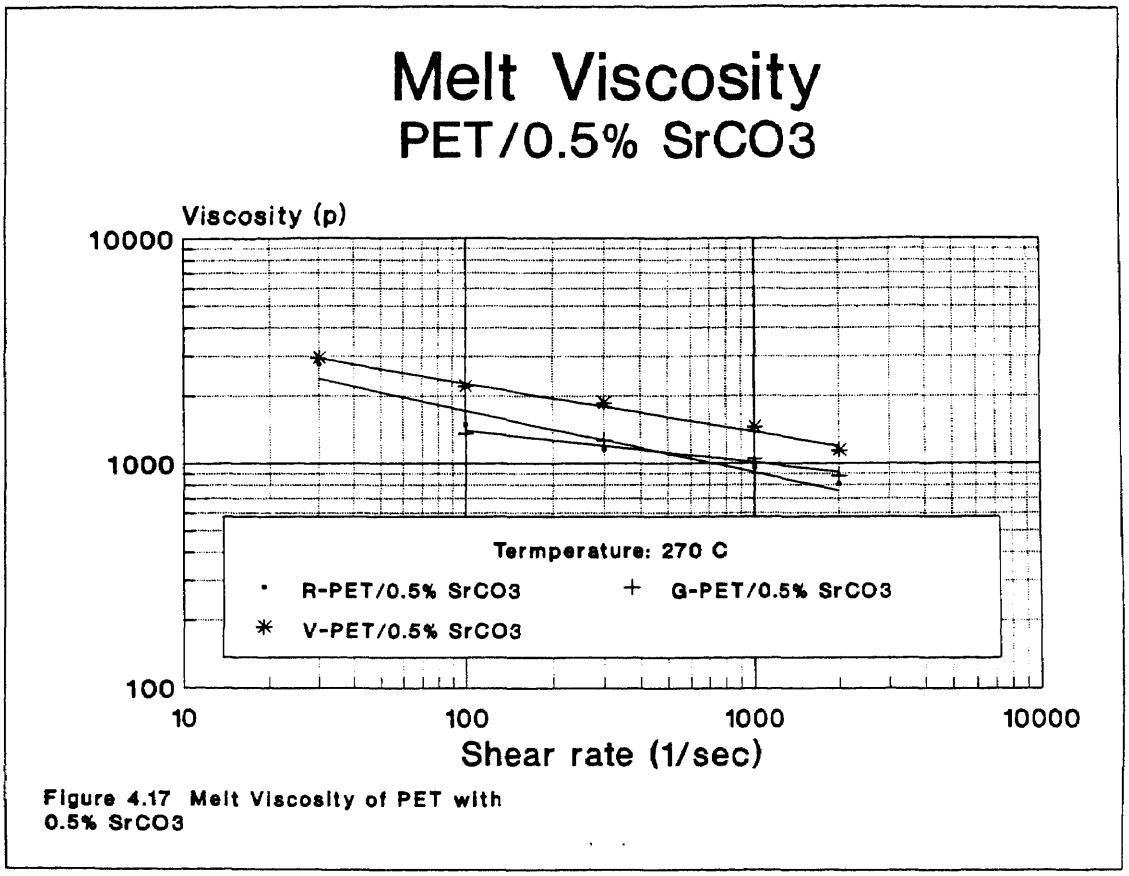

Figure 4.17 Melt Viscosity of PET with 0.5% SrCO3

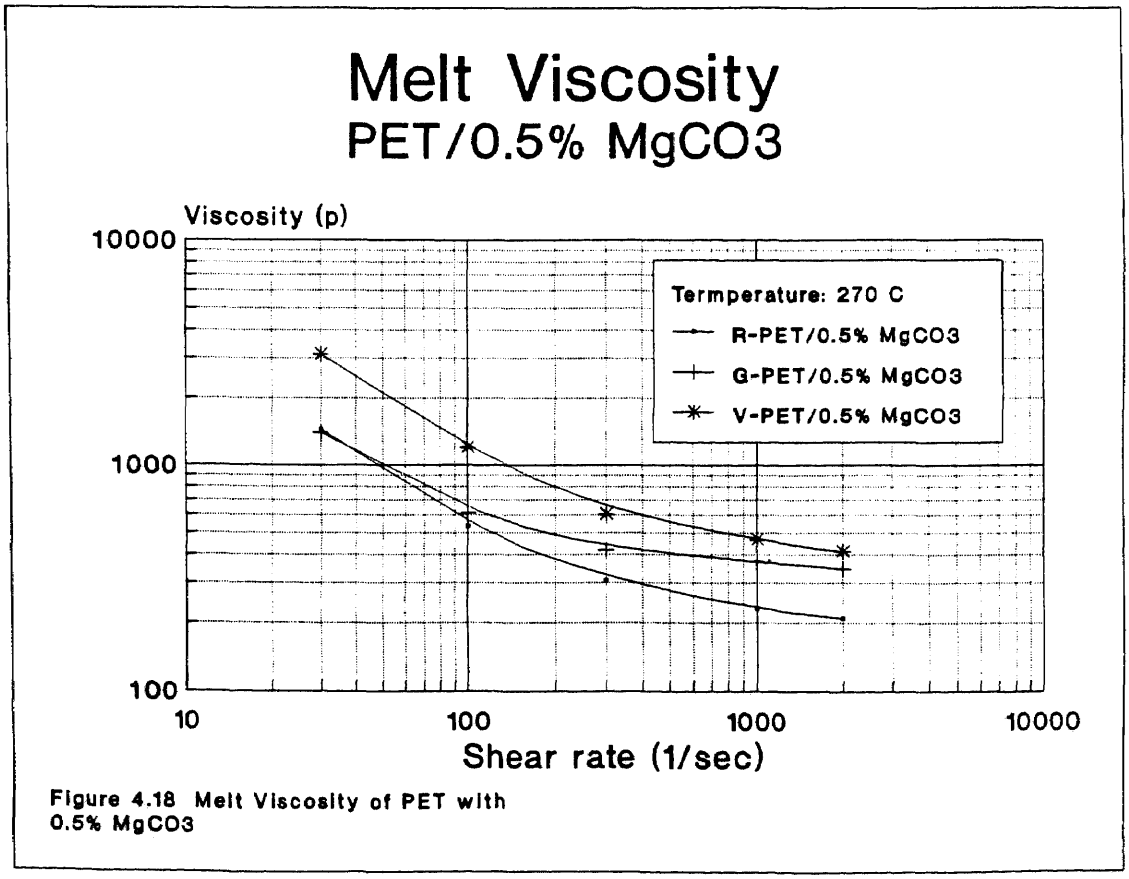

Figure 4.18 Melt Viscosity of PET with 0.5% MgCO3

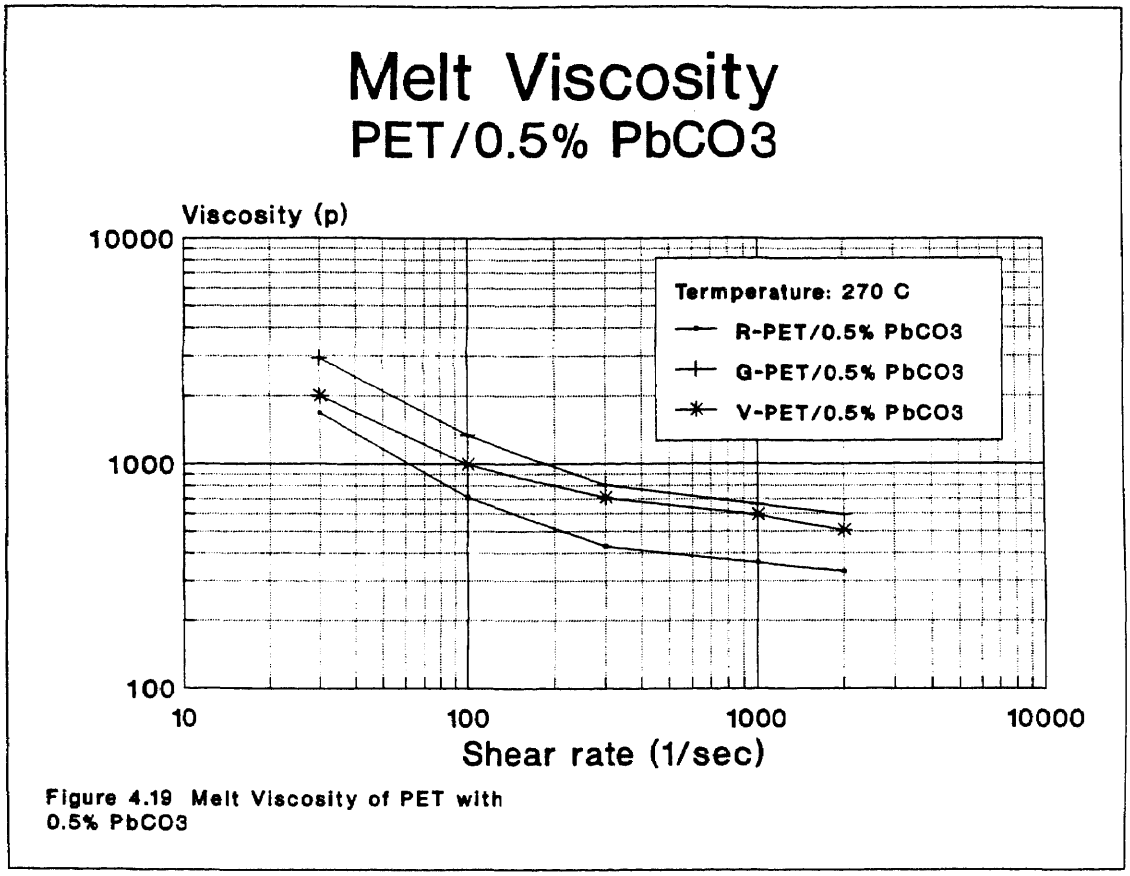

Figure 4.19 Melt Viscosity of PET with 0.5% PbCO3

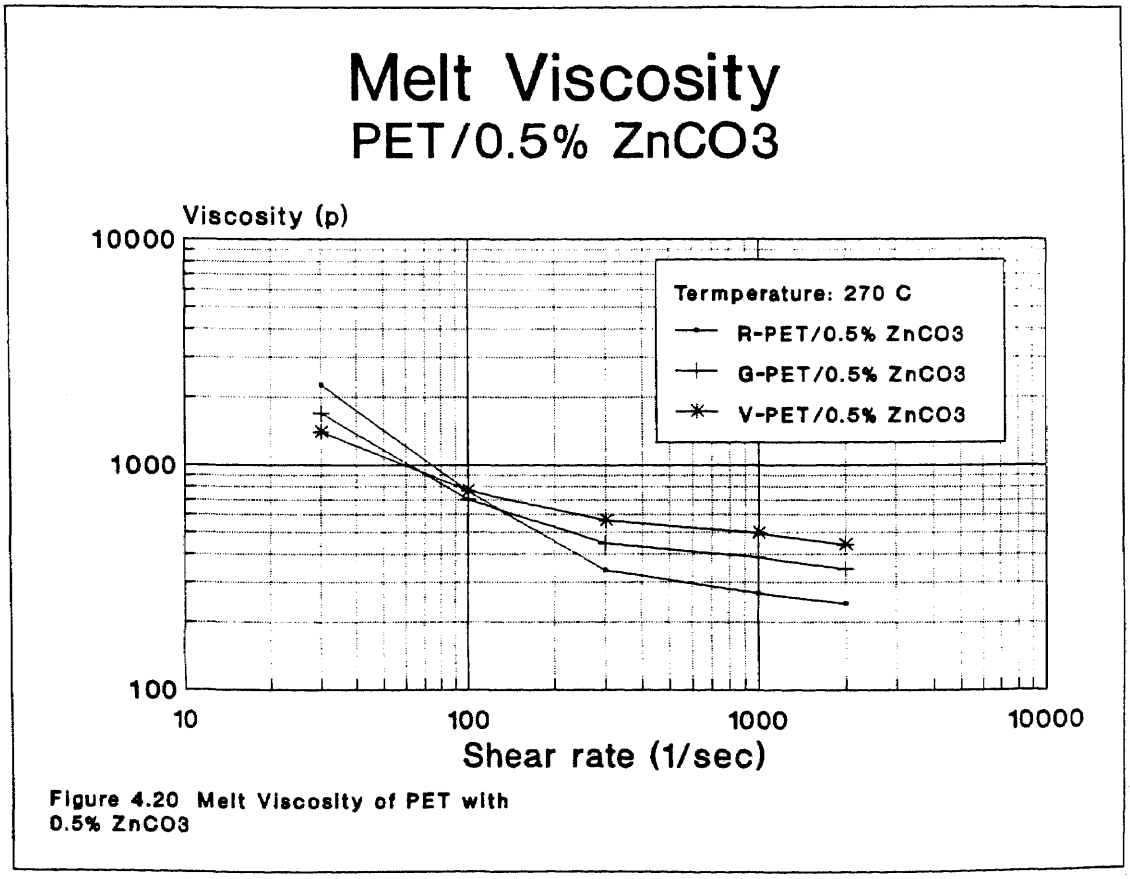

Figure 4.20 Melt Viscosity of PET with 0.5% ZnCO3

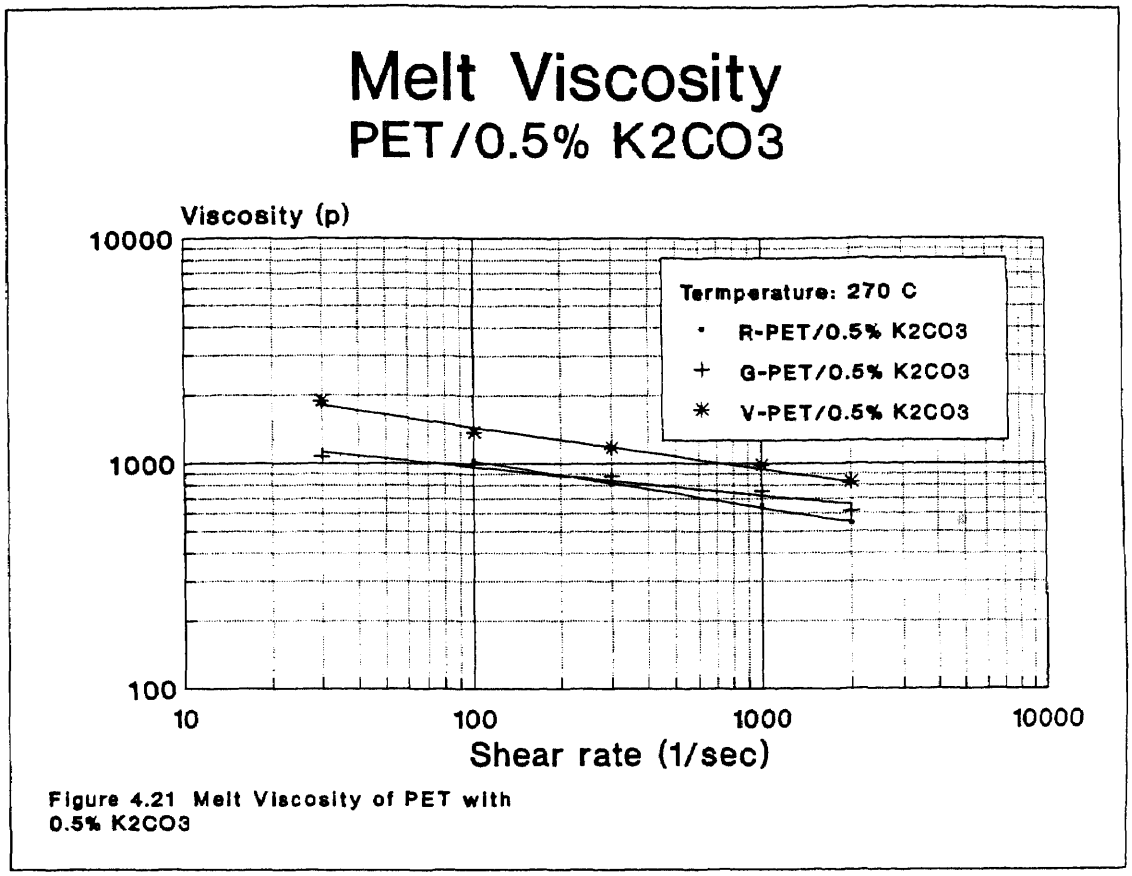

Figure 4.21 Melt Viscosity of PET with 0.5% K2CO3

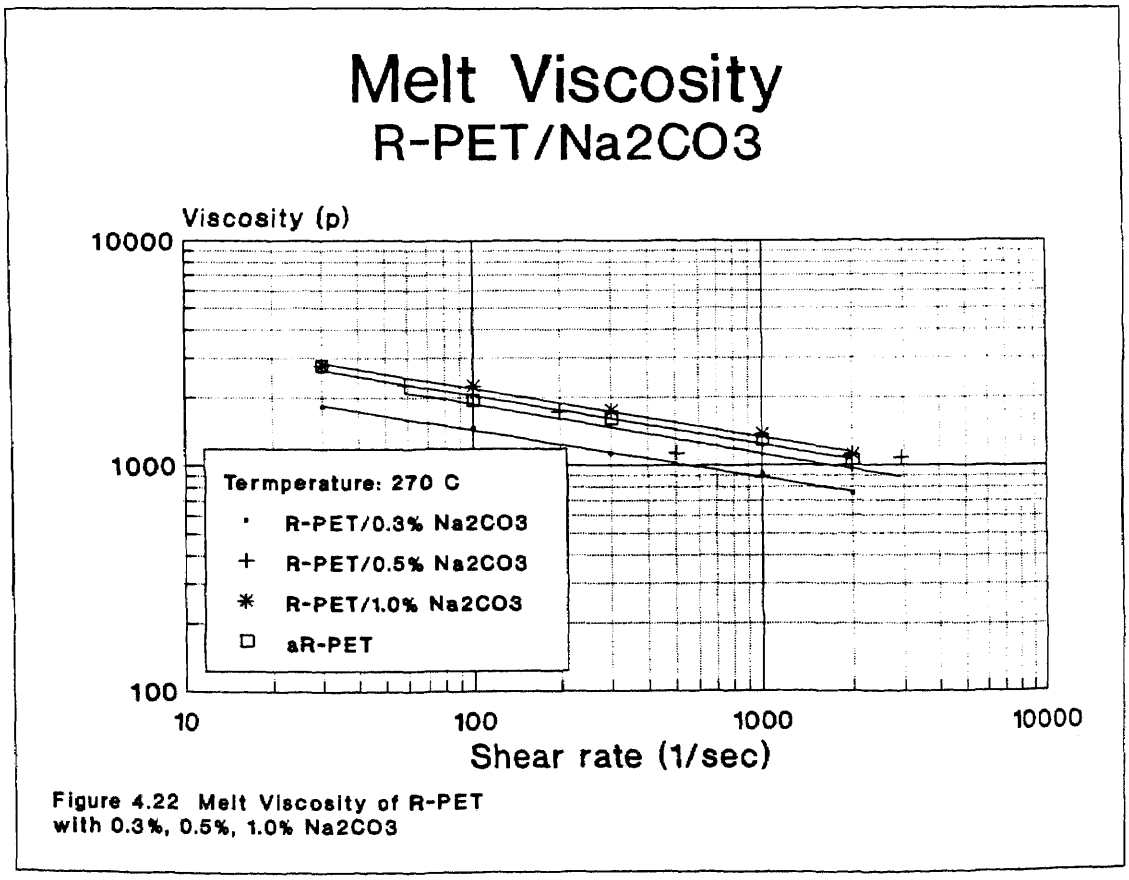

Figure 4.22 Melt Viscosity of R-PET with 0.3%, 0.5%, 1.0% Na2CO3

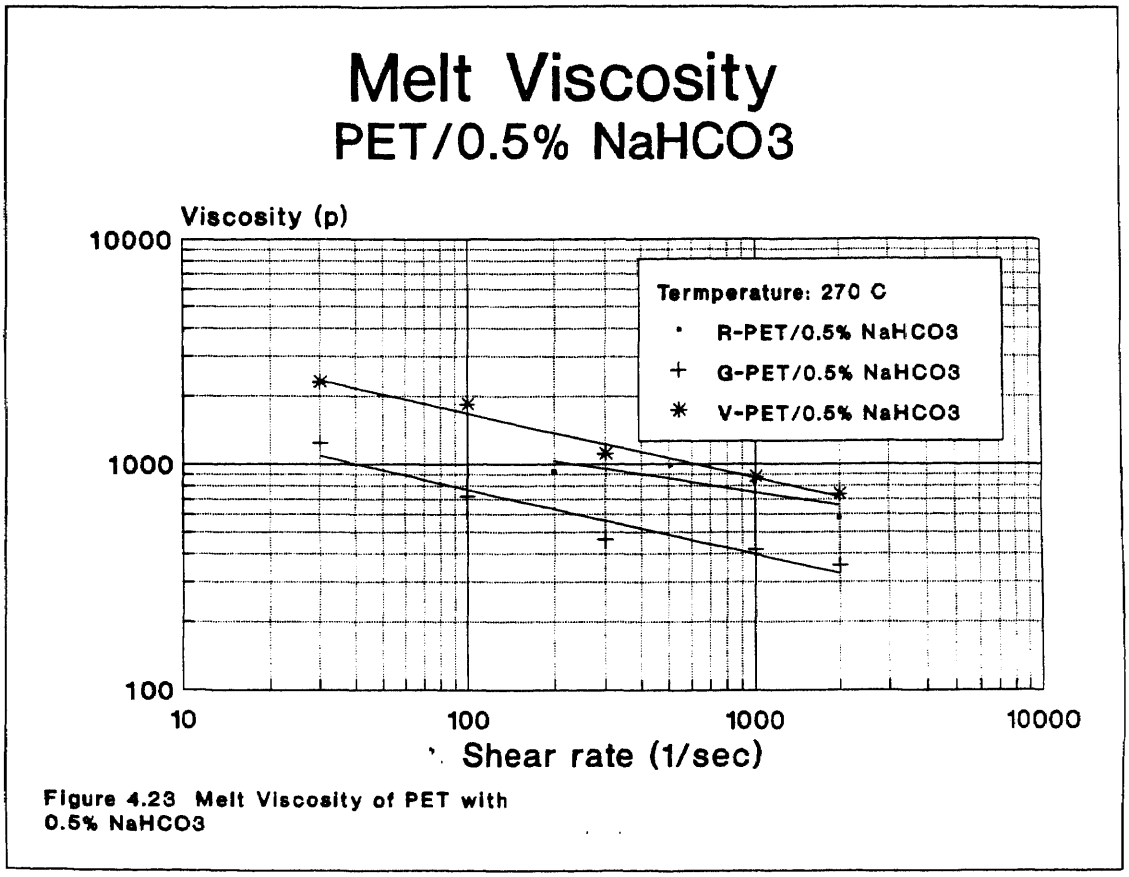

Figure 4.23 Melt Viscosity of PET with 0.5% NaHCO3

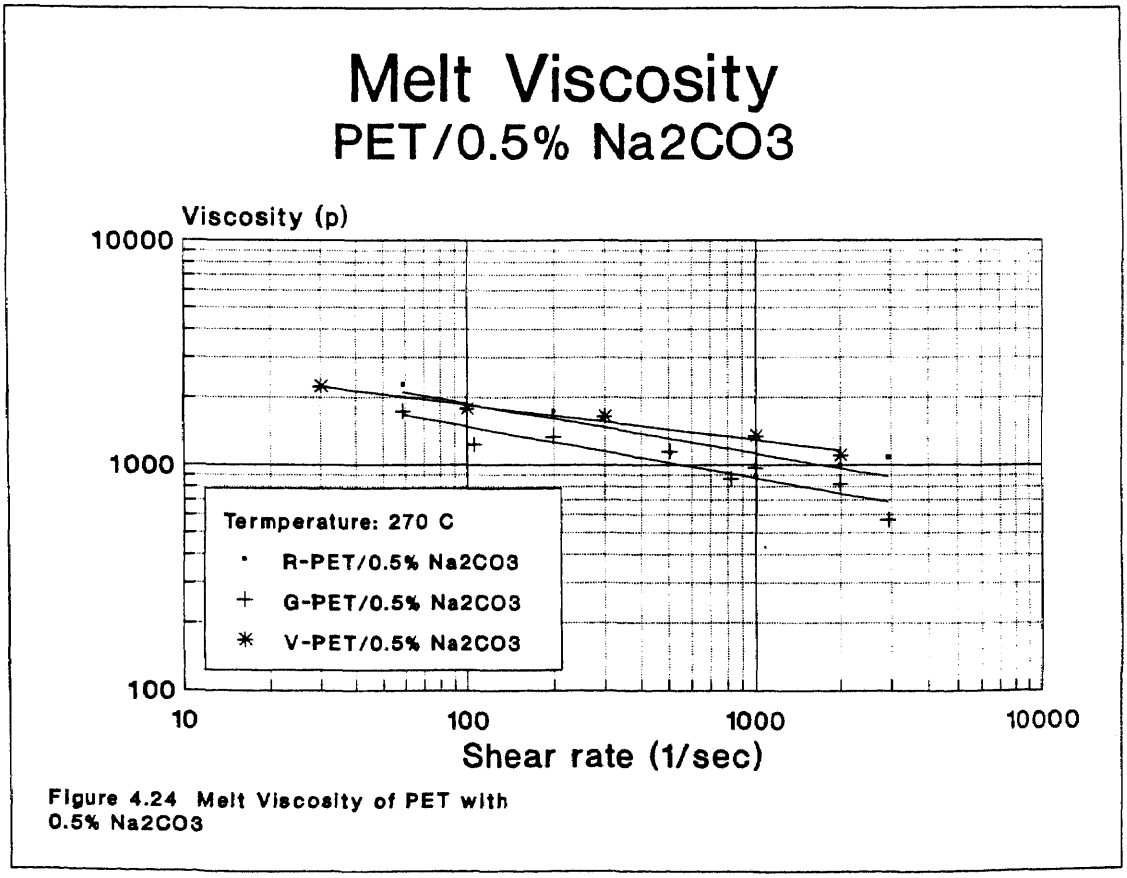

Figure 4.24 Melt Viscosity of PET with 0.5% Na2CO3

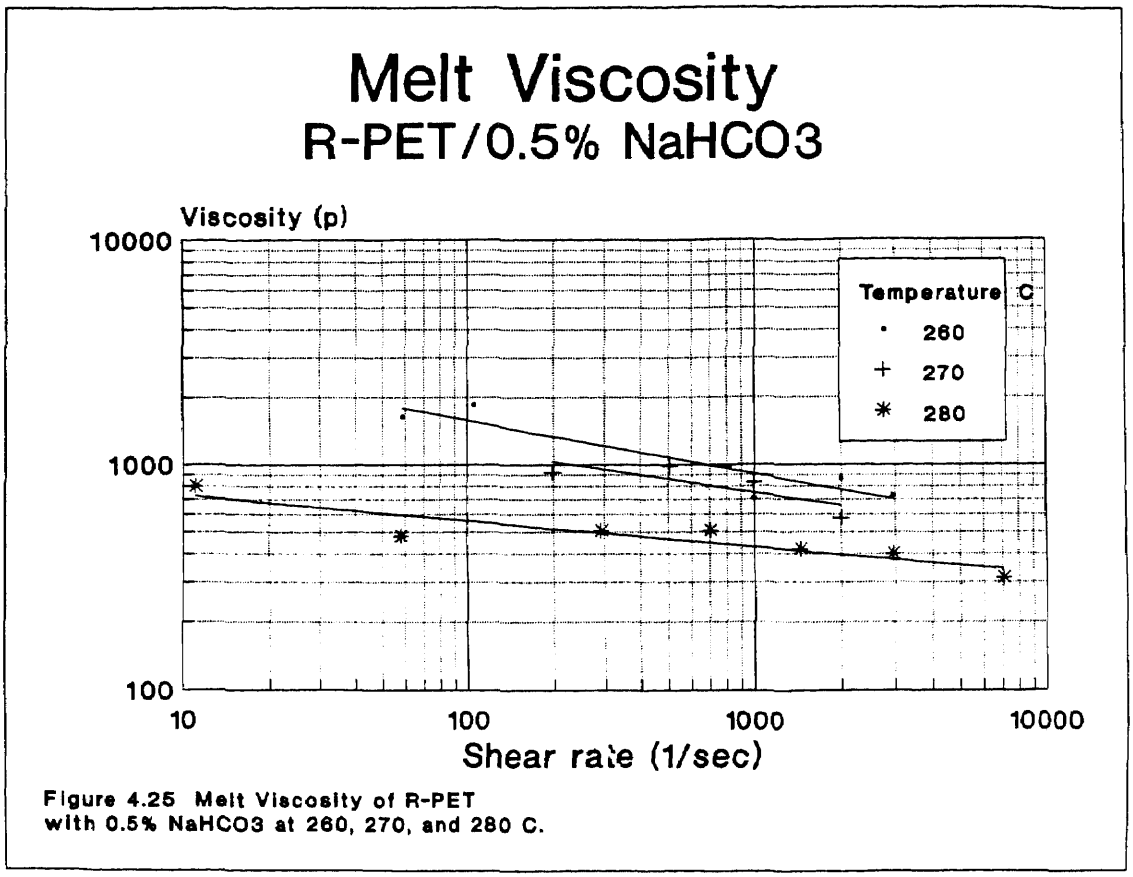

Figure 4.25 Melt Viscosity of R-PET with 0.5% NaHCO3 at 260, 270, and 280 C.

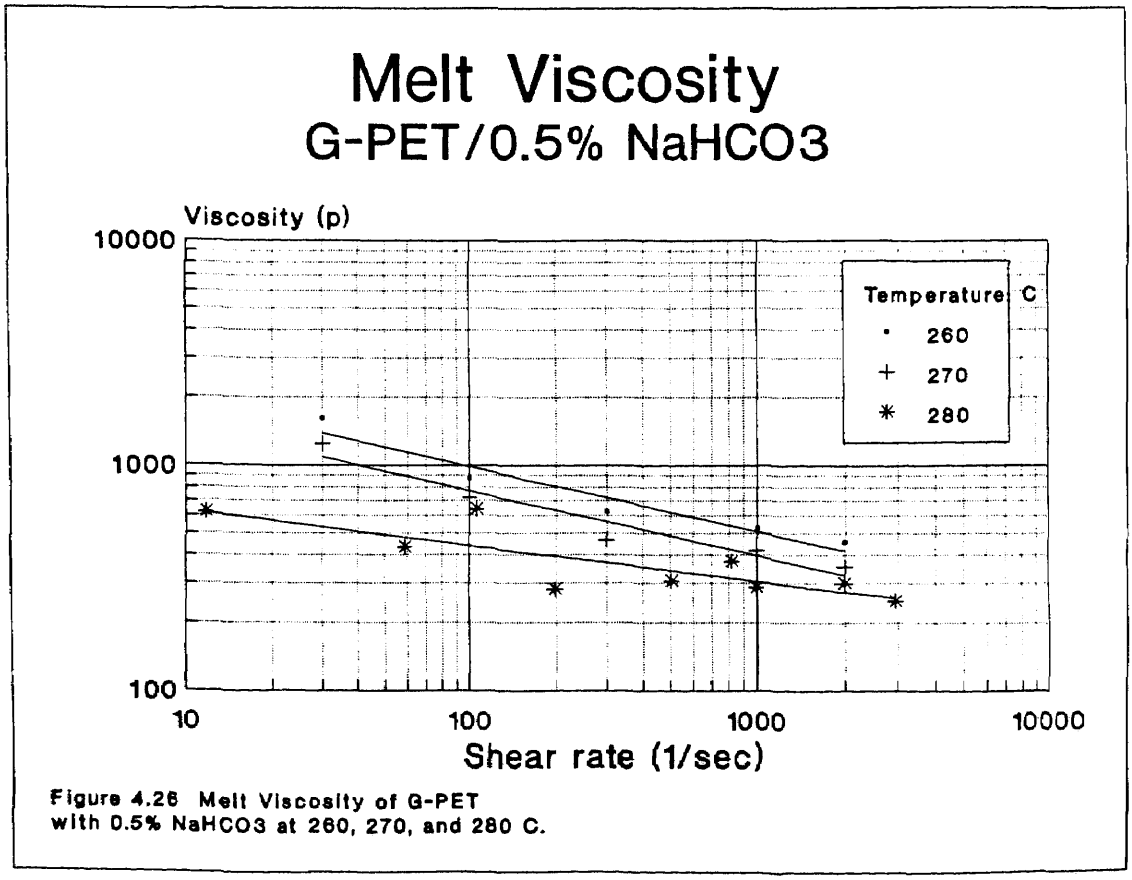

Figure 4.26 Melt Viscosity of G-PET with 0.5% NaHCO3 at 260, 270, and 280 C.

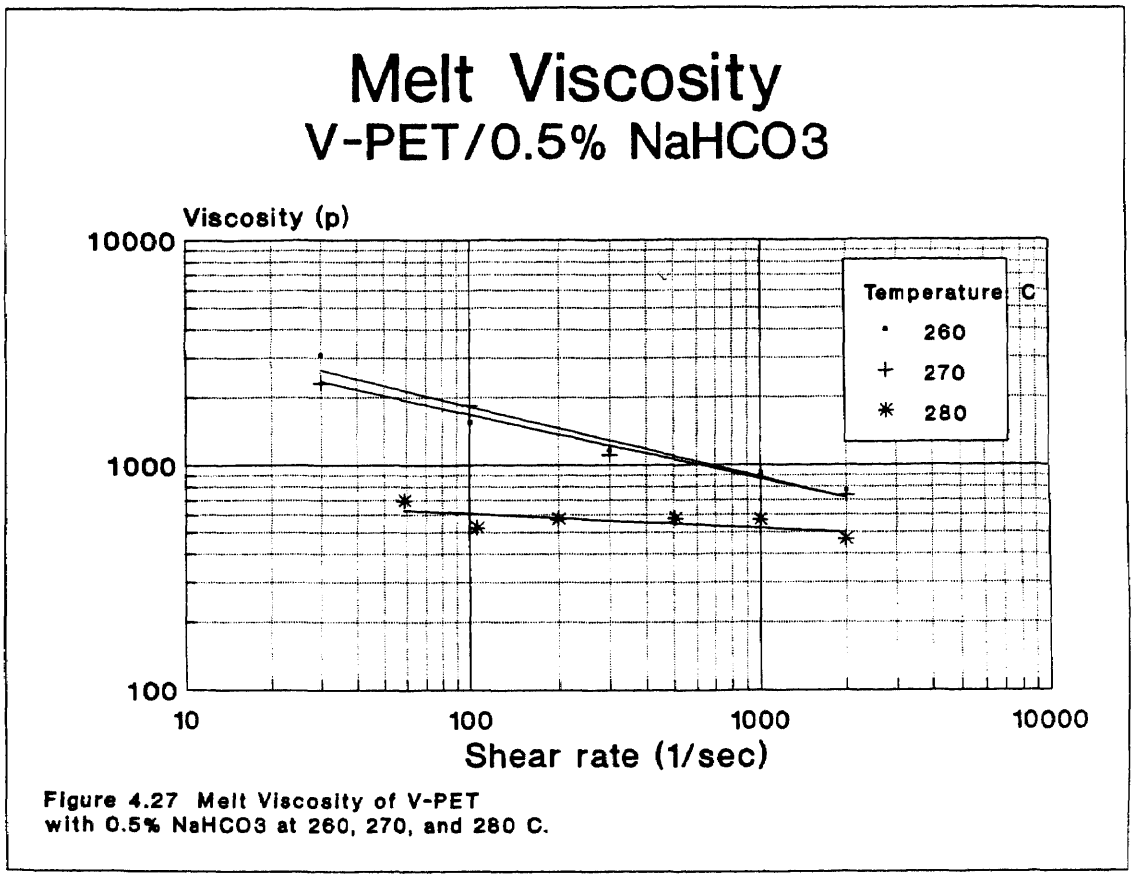

Figure 4.27 Melt Viscosity of V-PET with 0.5% NaHCO3 at 260, 270, and 280 C.

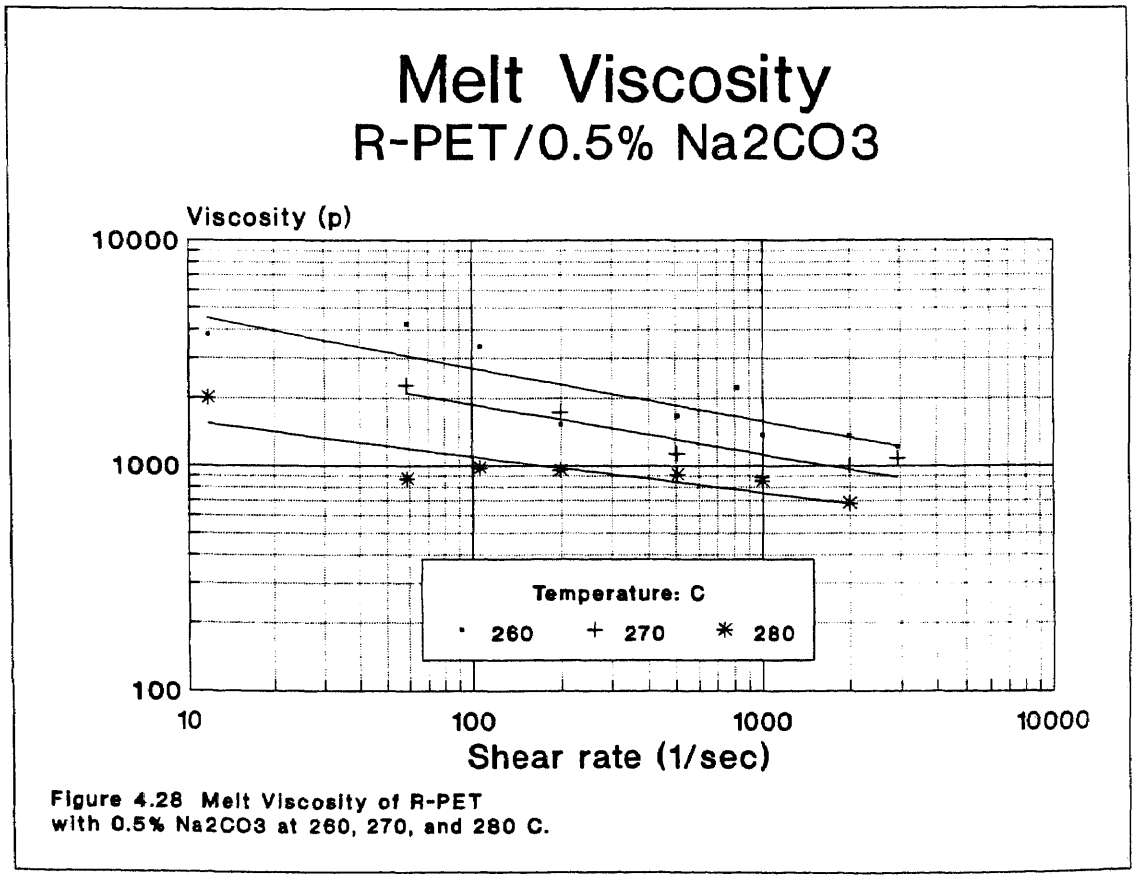

Figure 4.28 Melt Viscosity of R-PET with 0.5% Na2CO3 at 260, 270, and 280 C.

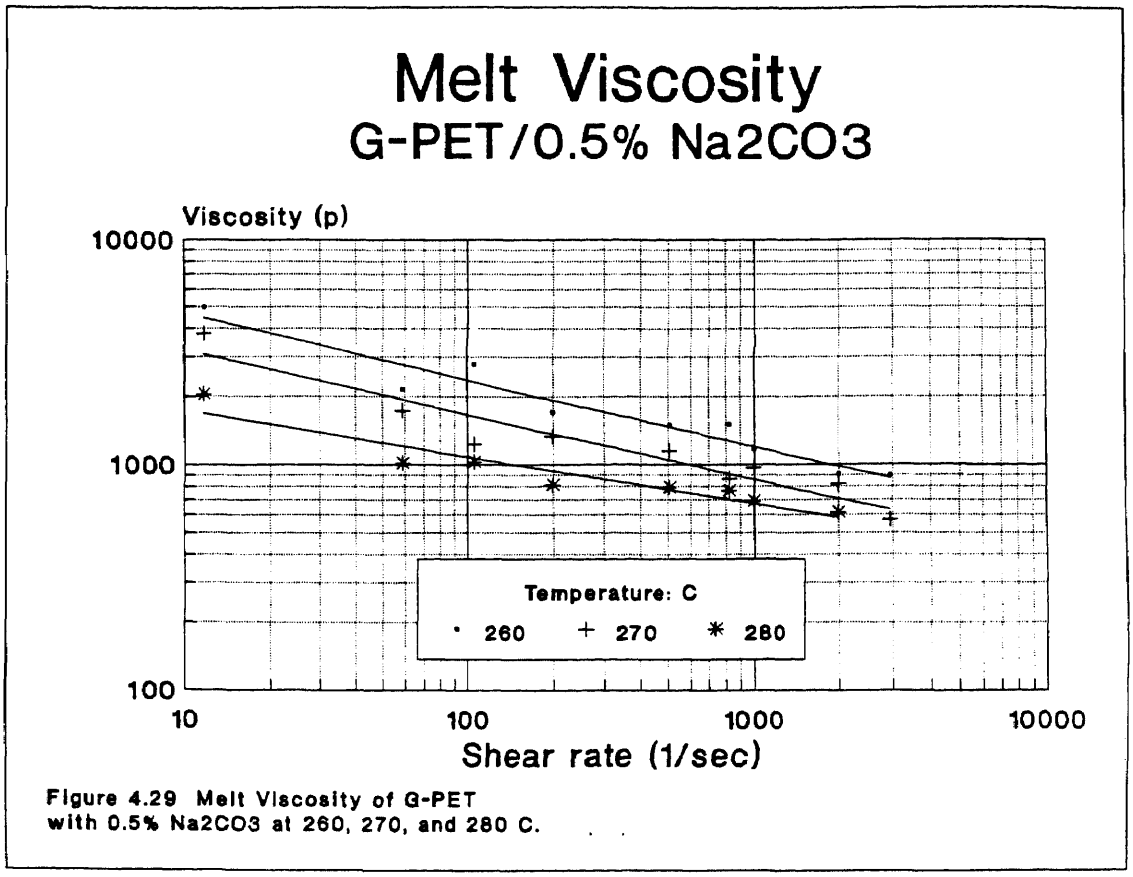

Figure 4.29 Melt Viscosity of G-PET with 0.5% Na2CO3 at 260, 270, and 280 C.

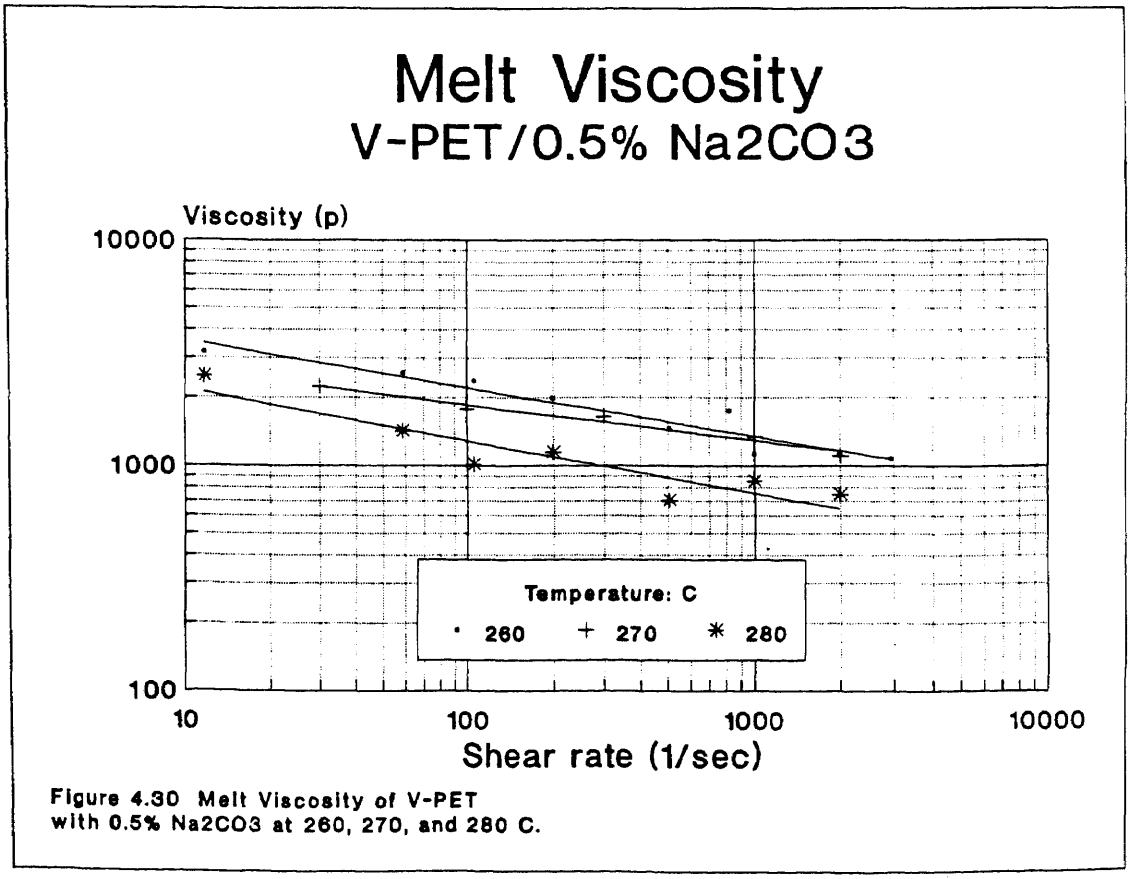

Figure 4.30 Melt Viscosity of V-PET with 0.5% Na2CO3 at 260, 270, and 280 C.

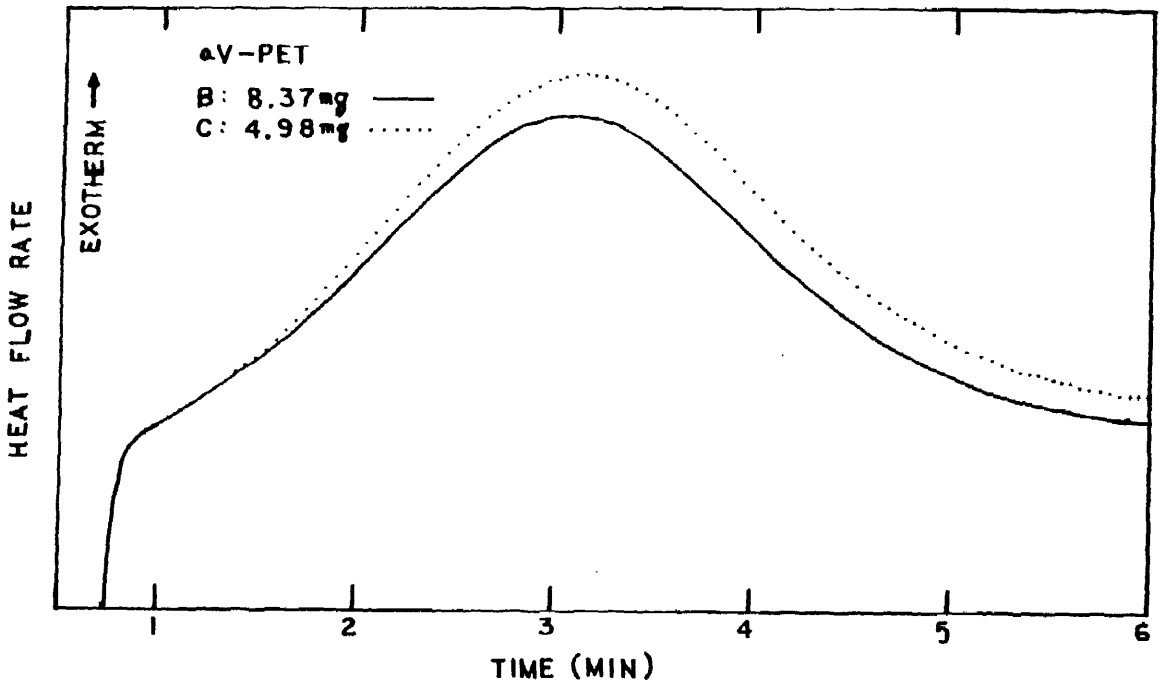

Figure 4.31 DSC Curves of aV-PET Samples for Isothermal Crystallization at 200 ^{o}C.
Curve B: 8.37 mg of aV-PET;
Curve C: 4.98 mg of aV-PET

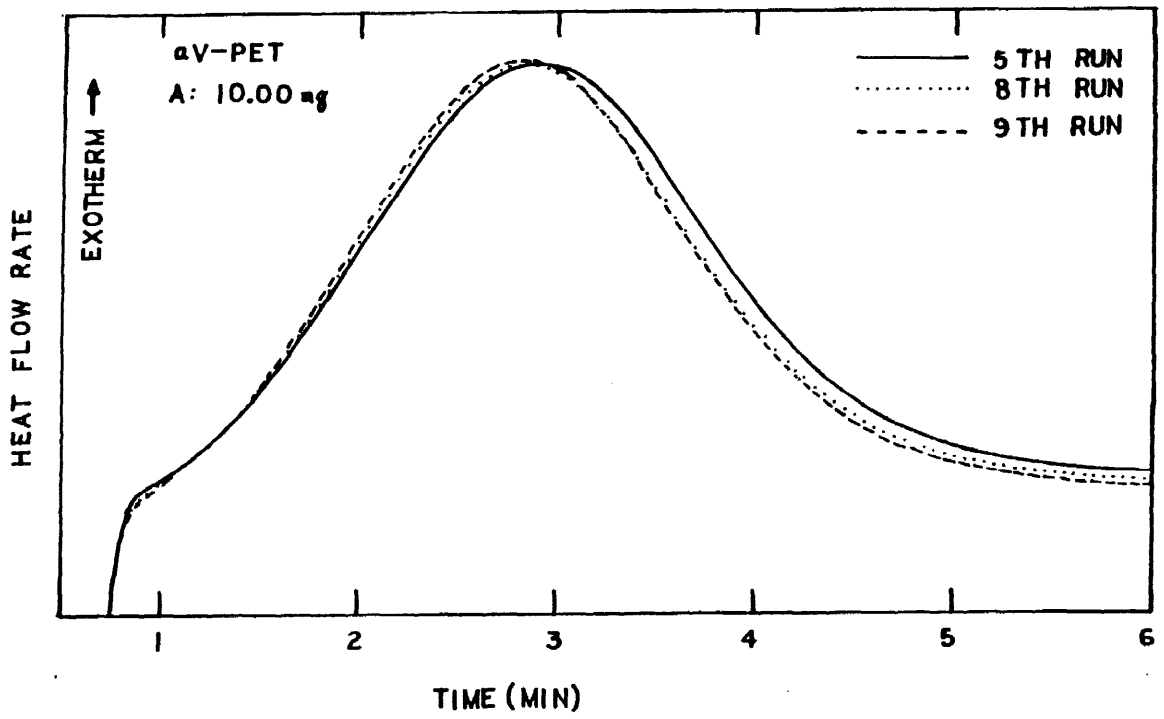

Figure 4.32 DSC Curves of aV-PET for Isothermal Crystallization at 200 ^{o}C. (same sample, different runs)

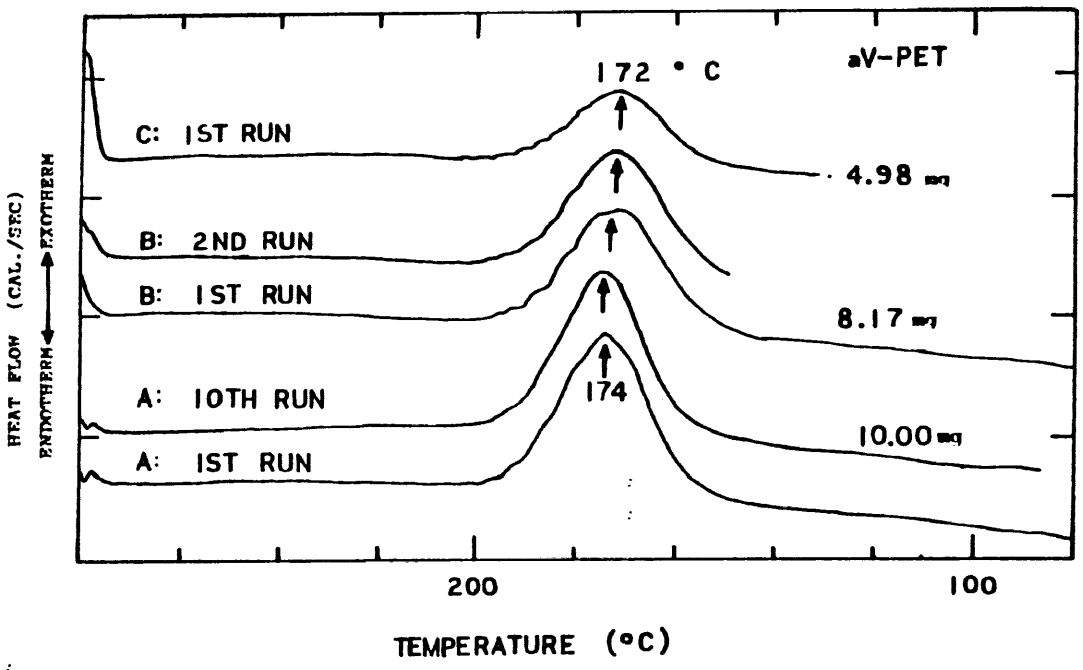

Figure 4.33 DSC Curves of Various aV-PET Samples at scan cooling rate of 20 ^{o}C/min

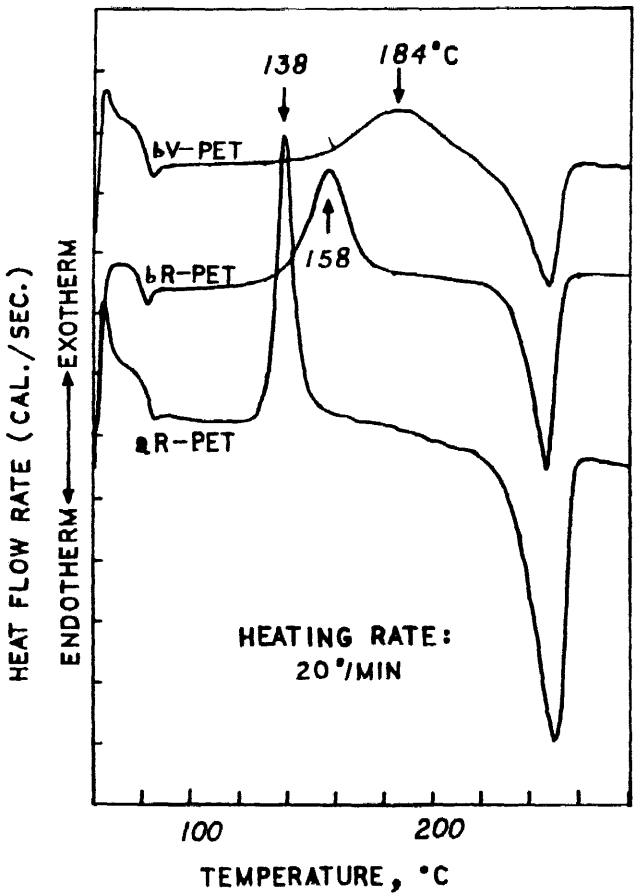

Figure 4.34 DSC Curves for Various PET types at scan heating rate of 20 ^{o}C/min

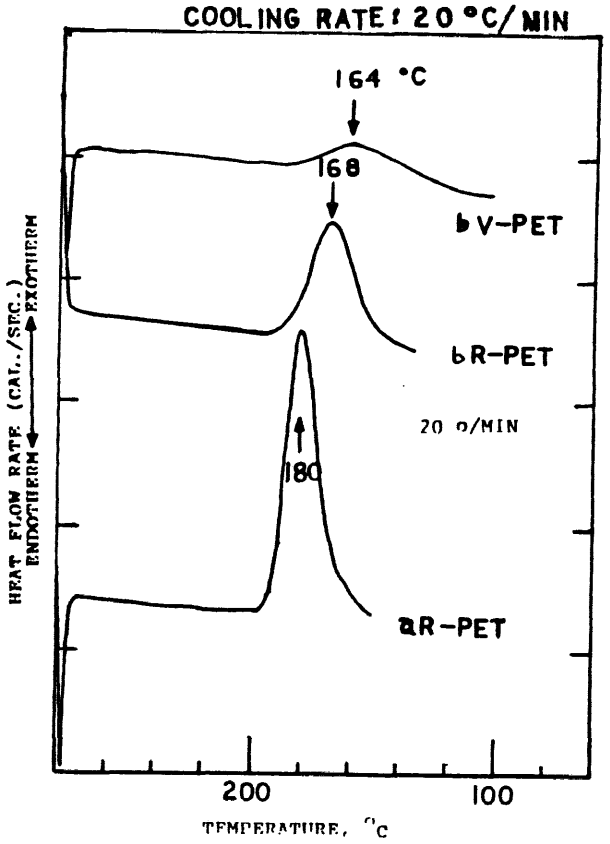

Figure 4.35 DSC Curves for Various PET types at scan cooling rate of 20 ^{o}C/min

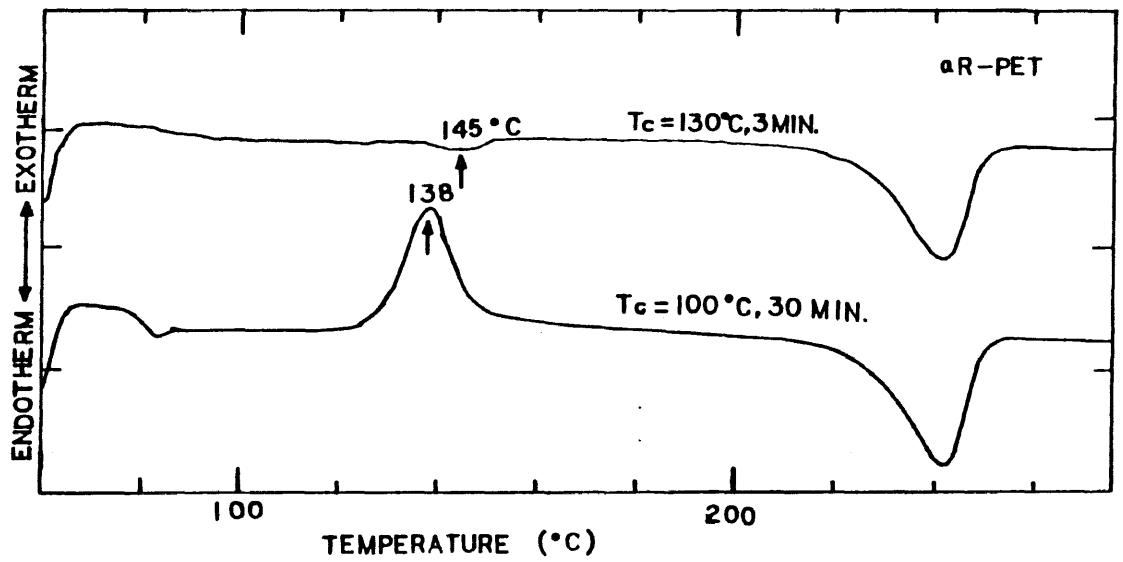

Figure 4.36 DSC Heating Scans for aR-PET Annealed at 100 and 130 ^{o}C (scan rate: 20 ^{o}C/min)

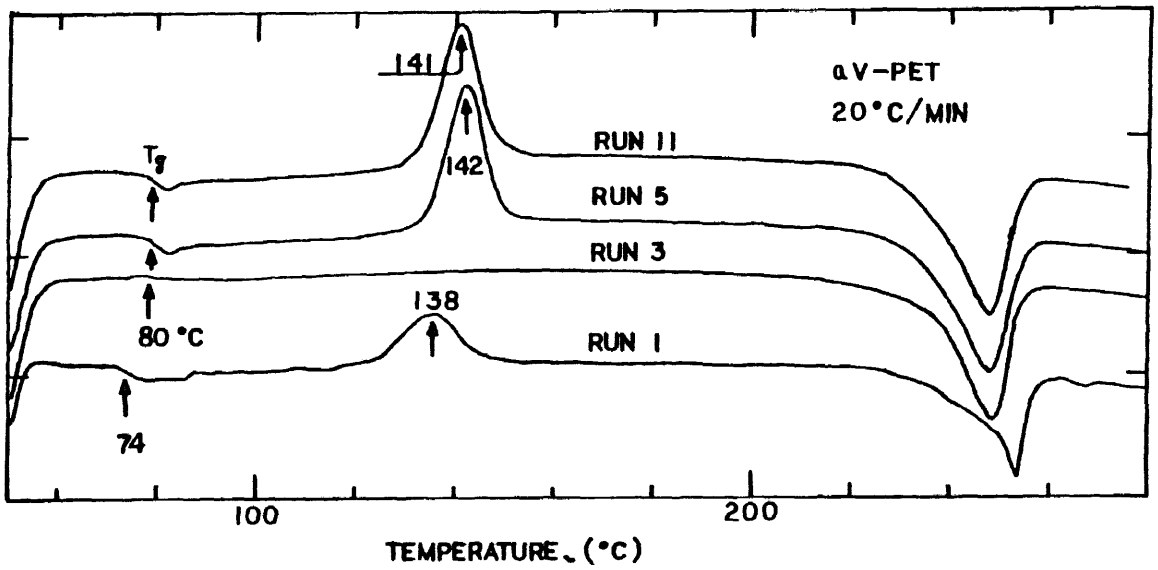

Figure 4.37 DSC Heating Scans for aV-PET (scan rate: 20 ^{o}C/min)

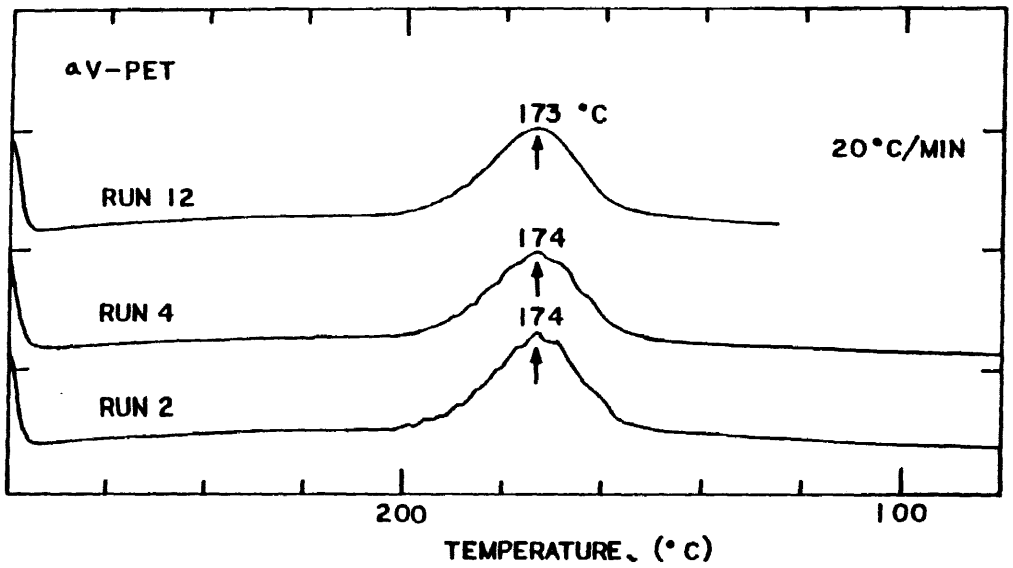

Figure 4.38 DSC Cooling Scans for aV-PET (scan rate: 20 ^{o}C/min)

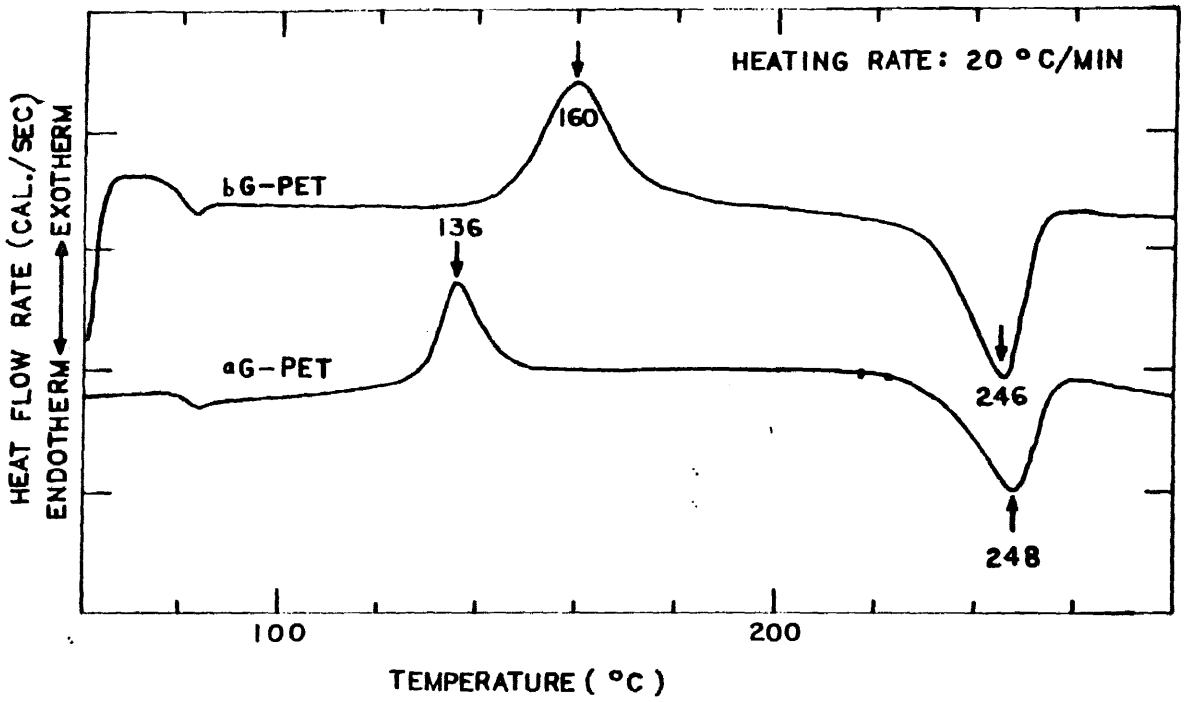

Figure 4.39 DSC Heating Thermograms for bG-PET and aG-PET at scan heating rate of 20 °C/min

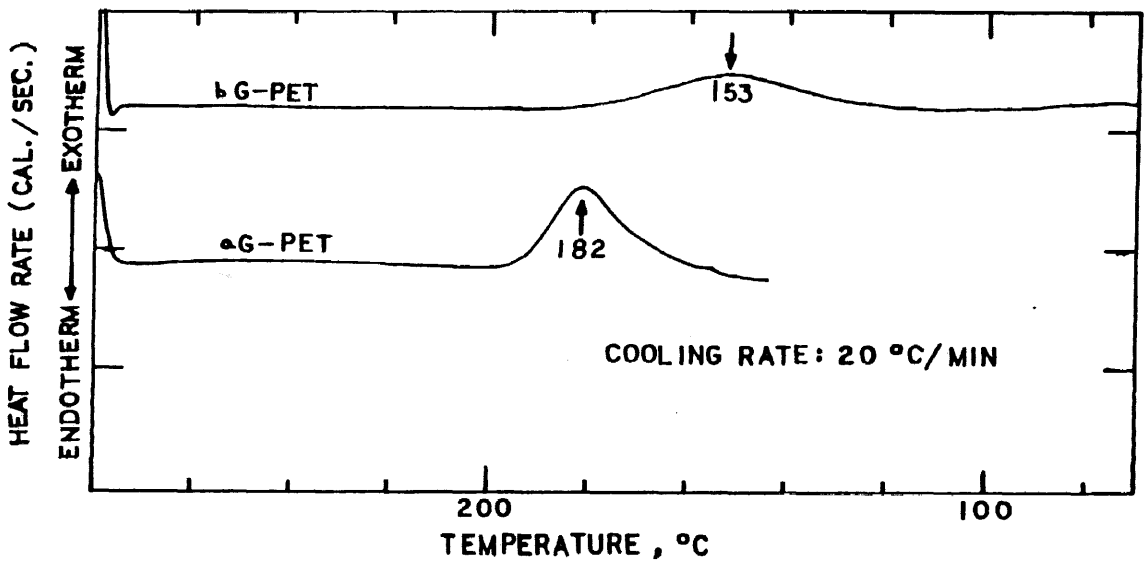

Figure 4.40 DSC Cooling Thermograms for bG-PET and aG-PET. (scan rate: 20 ^{o}C/min)

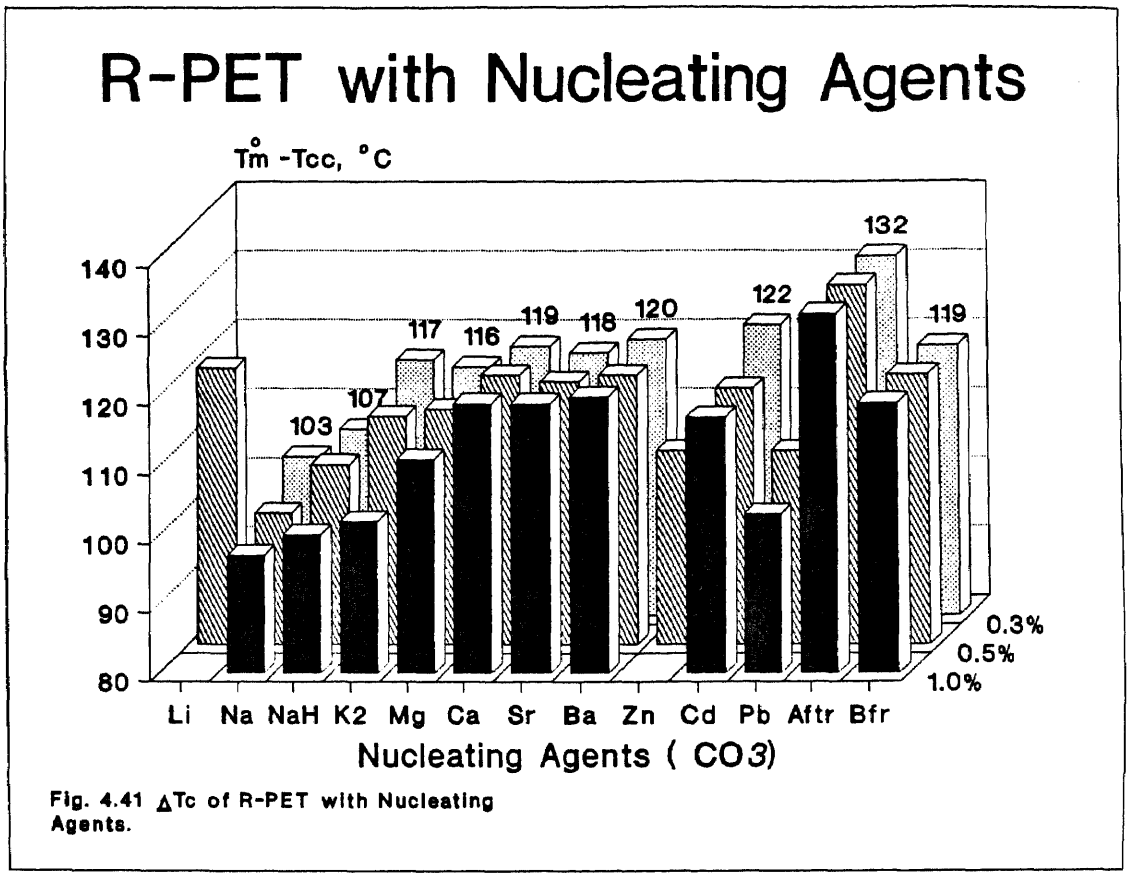

Fig. 4.41 ΔTc of R-PET with Nucleating Agents.

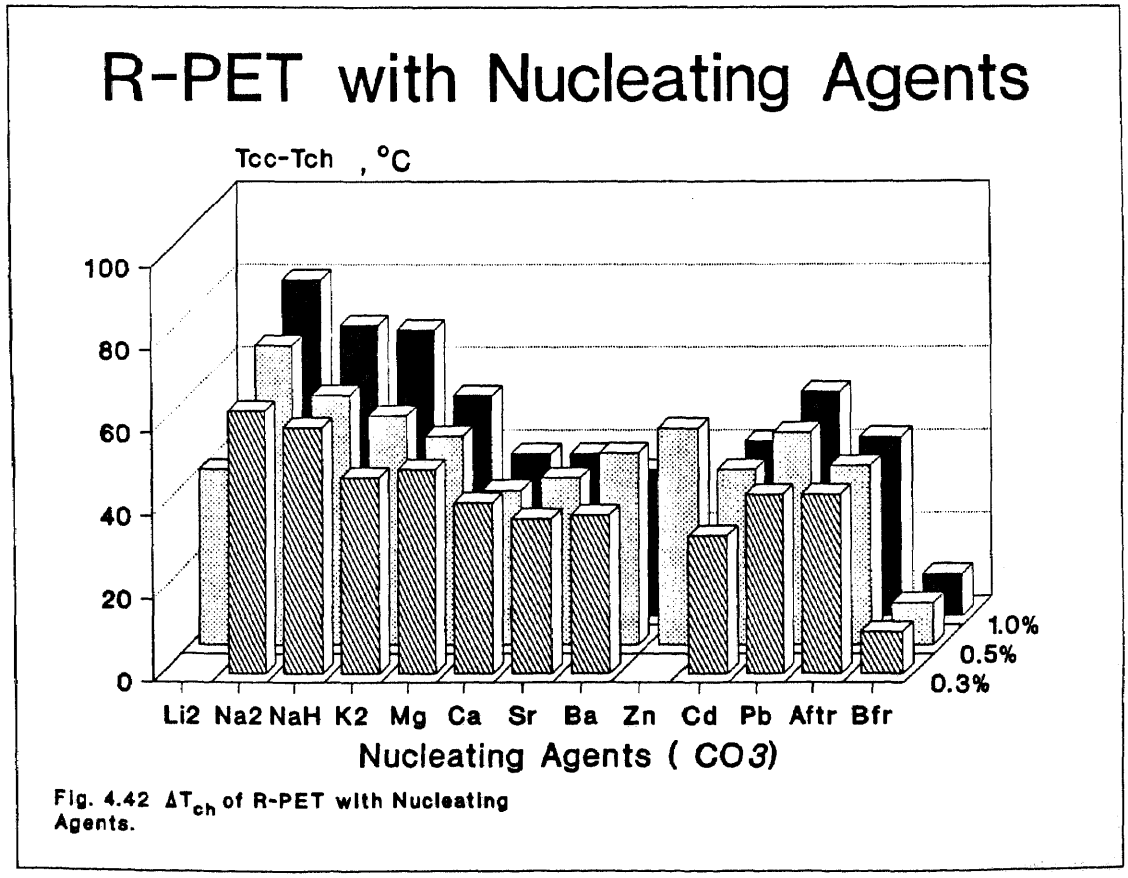

Fig. 4.42 ΔT_{ch} of R-PET with Nucleating Agents.

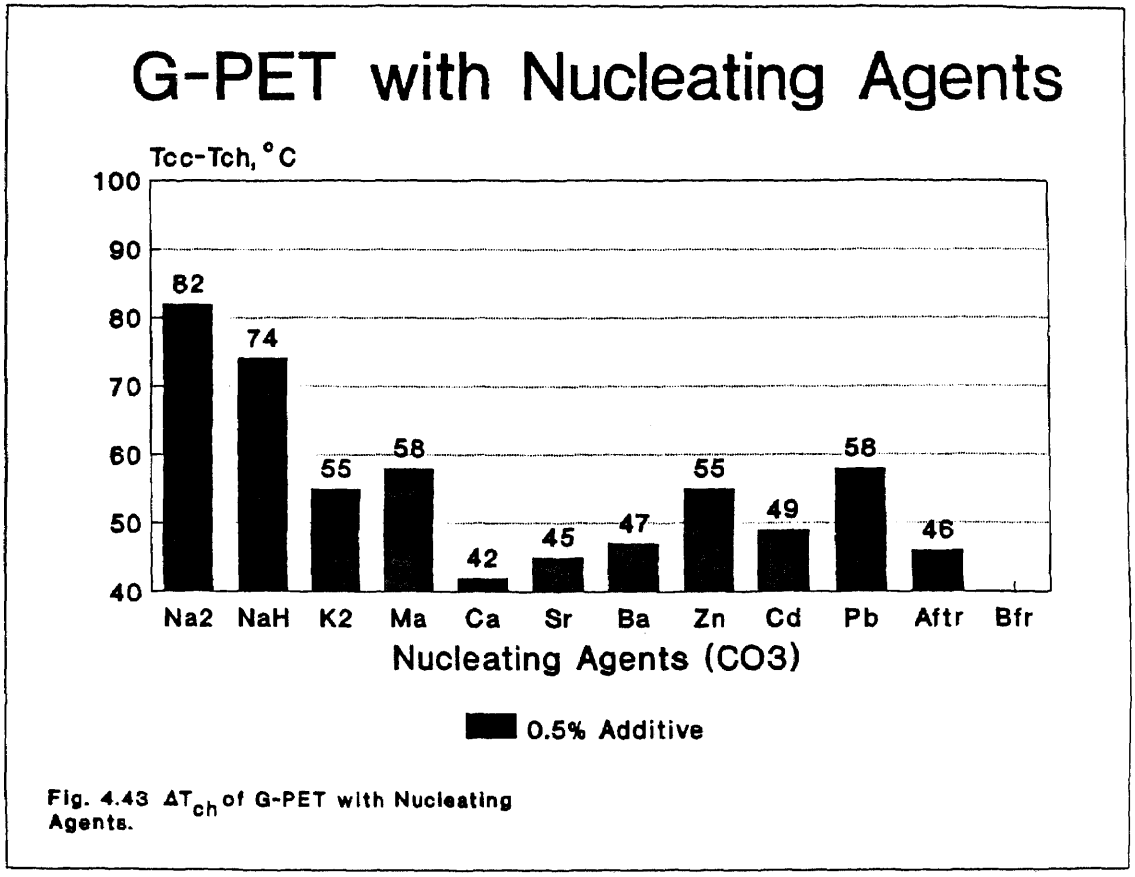

Fig. 4.43 ΔT_{ch} of G-PET with Nucleating Agents.

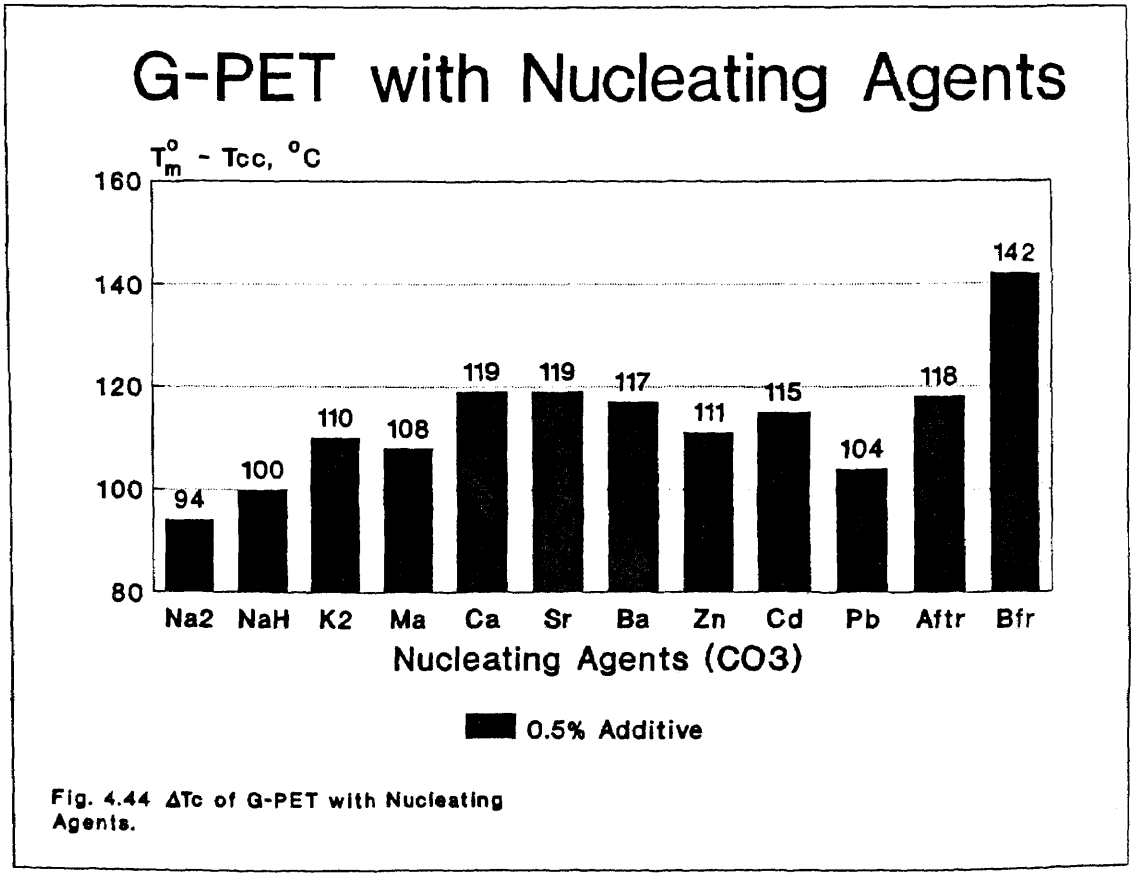

Fig. 4.44 ΔTc of G-PET with Nucleating Agents.

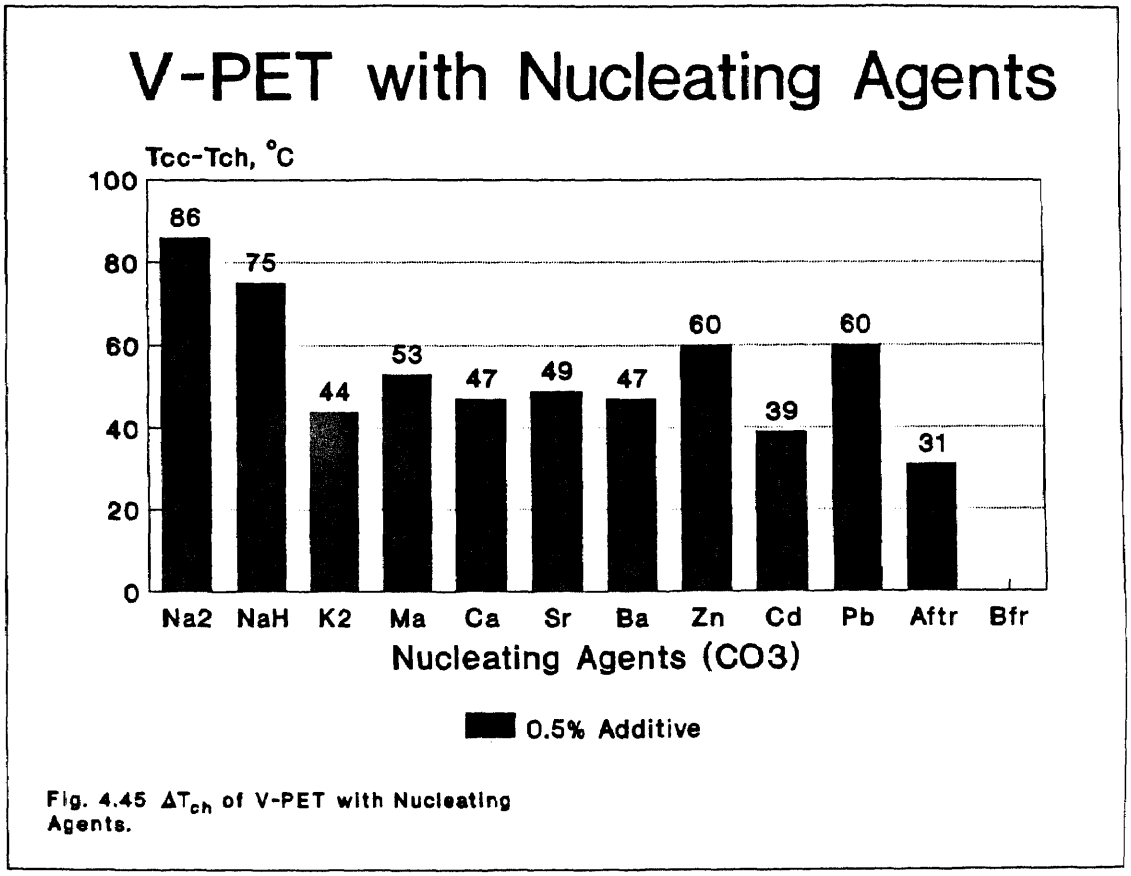

Fig. 4.45 ΔT_{ch} of V-PET with Nucleating Agents.

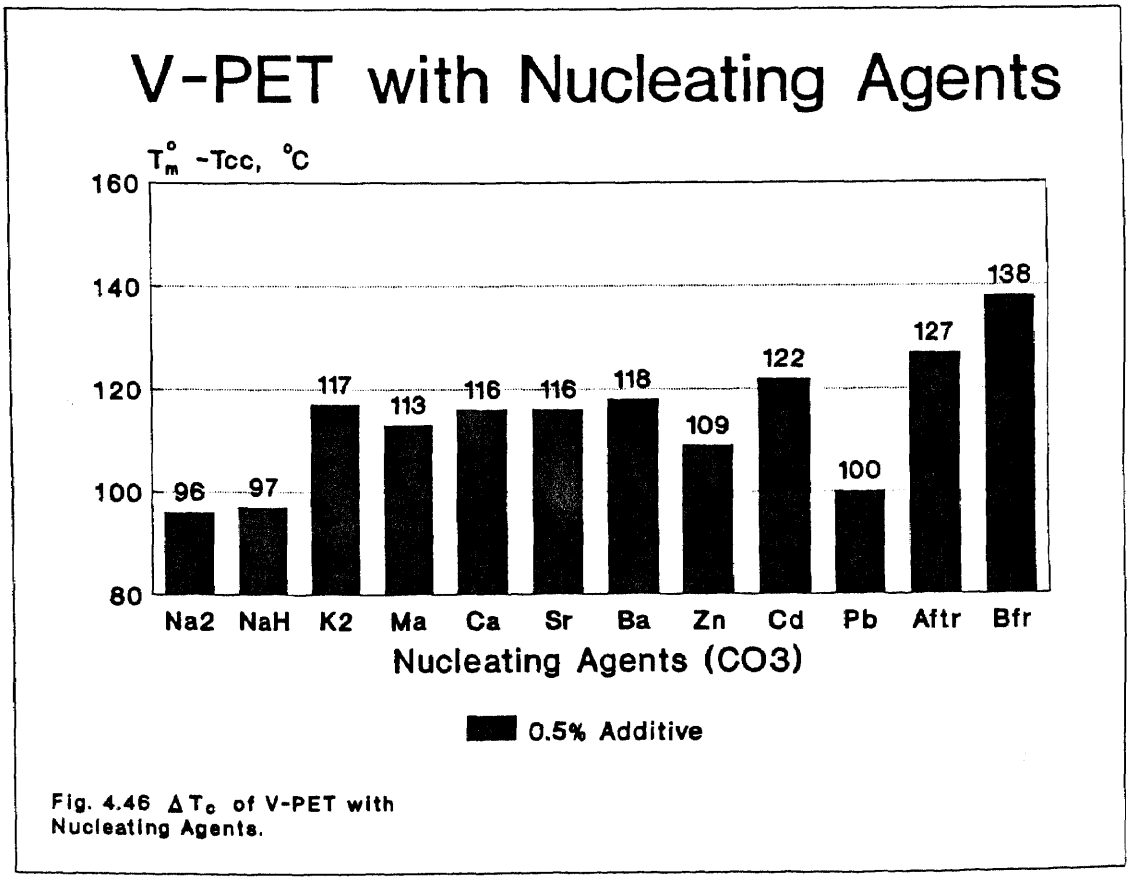

Fig. 4.46 ΔT_c of V-PET with Nucleating Agents.

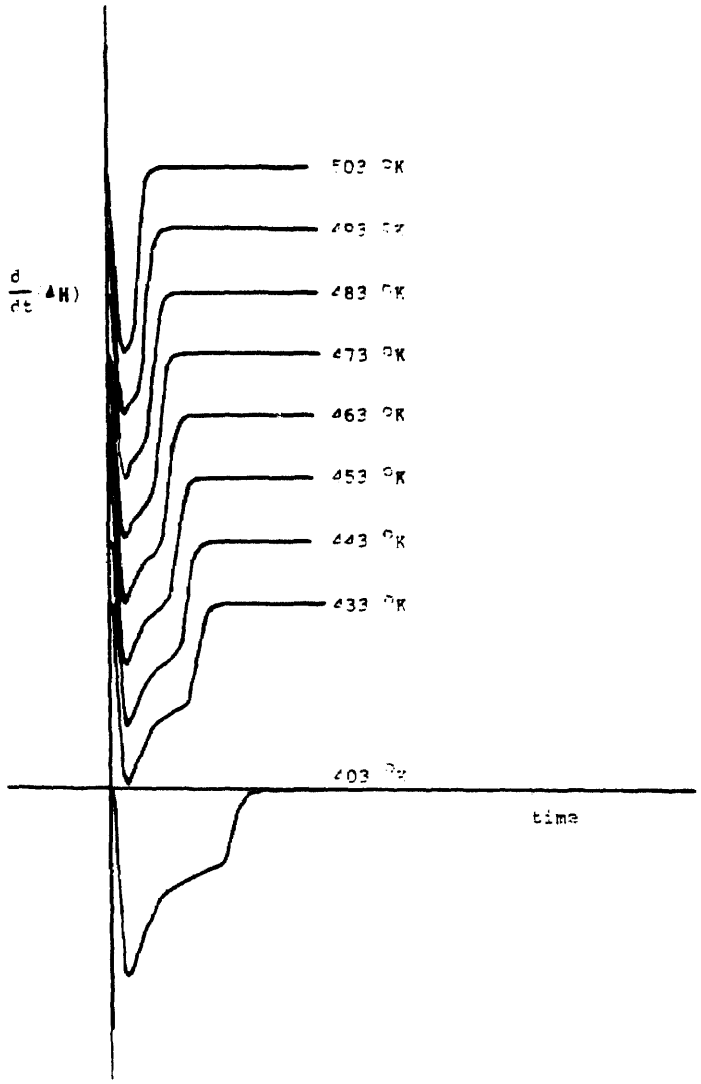

Figure 8 DSC Thermograms from an Empty Sample Pan at Different Isothermal Temperatures.

DSC curve at empty pan

Temperature at 170 °C from 300 °C.

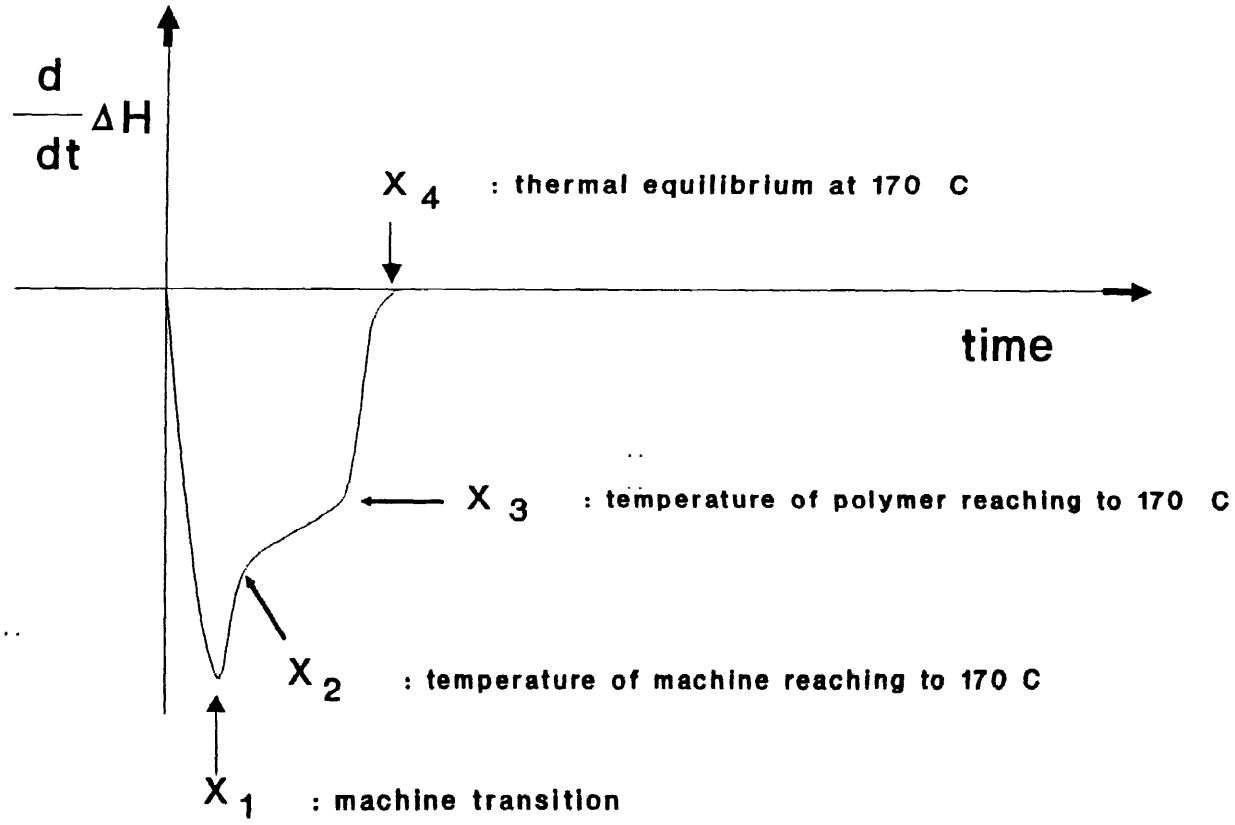

Fig. 4.48 Typical DSC Curve from an Empty Sample Pan.

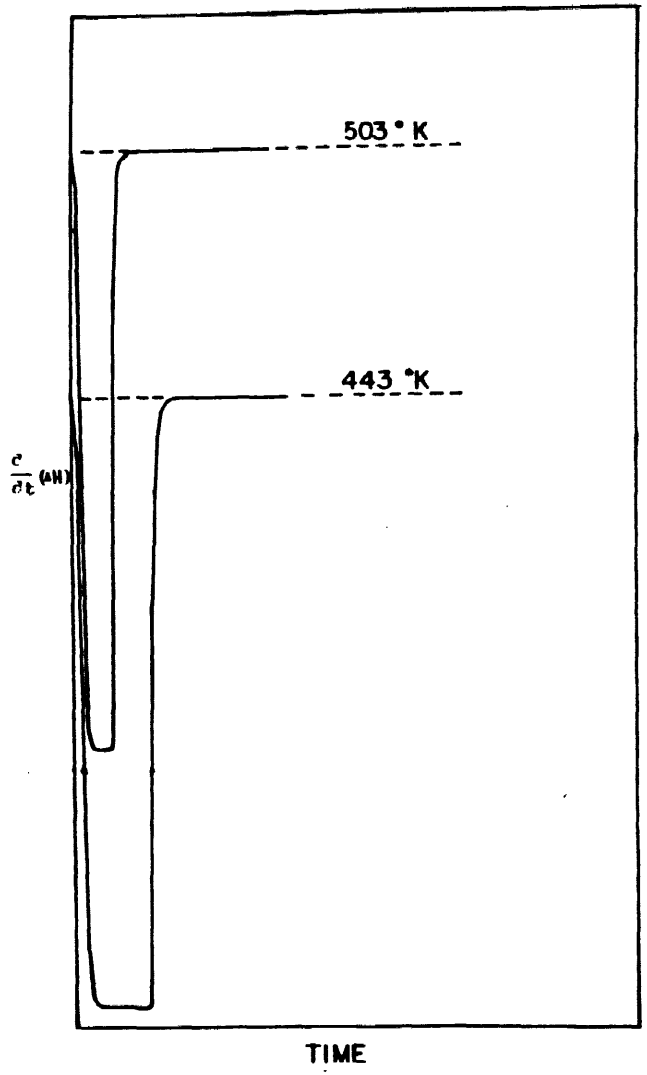

Figure 4.49 DSC Thermograms at Different Isothermal Temperatures, when the DSC Cell Contains the Reference Pan Only

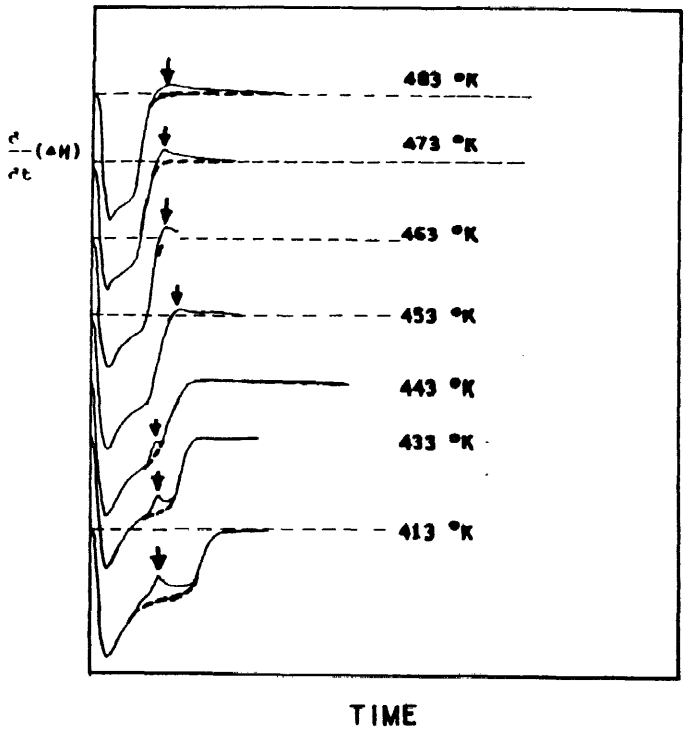

Figure 4.50 DSC Thermograms of PET at Different Isothermal Temperatures

DSC curve

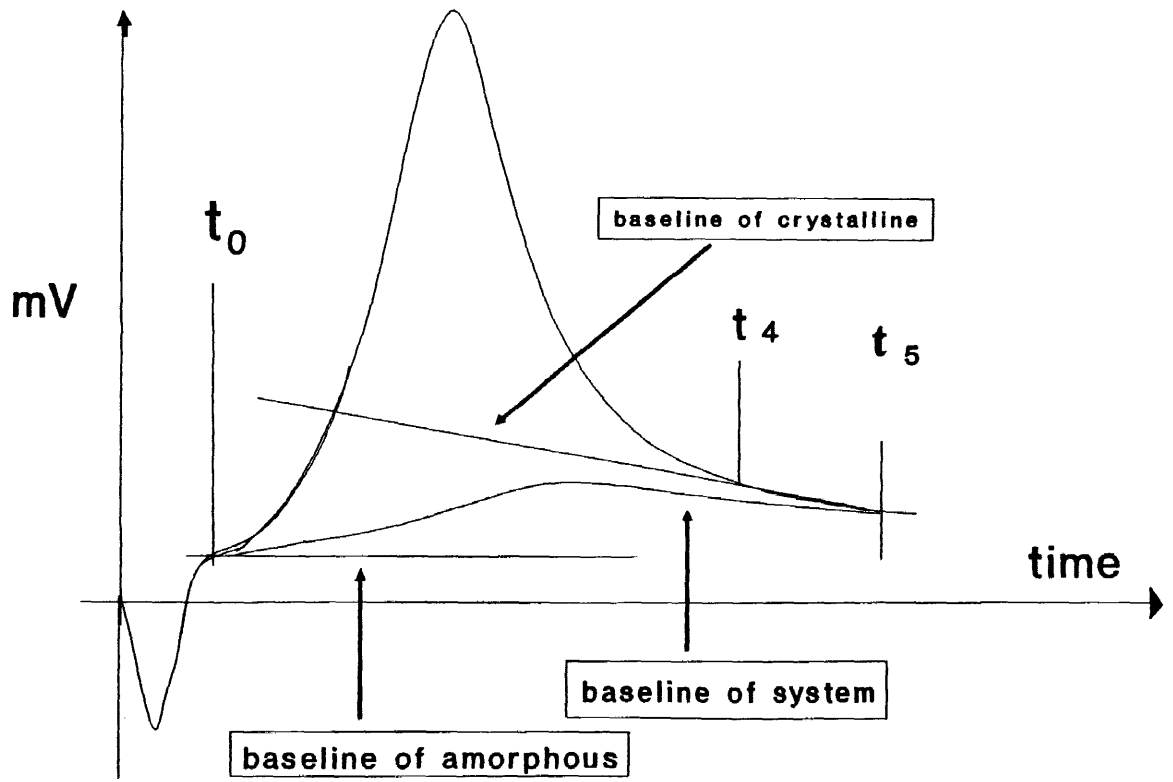

Figure 4.51 Baseline for Isothermal Crystallizatiion.

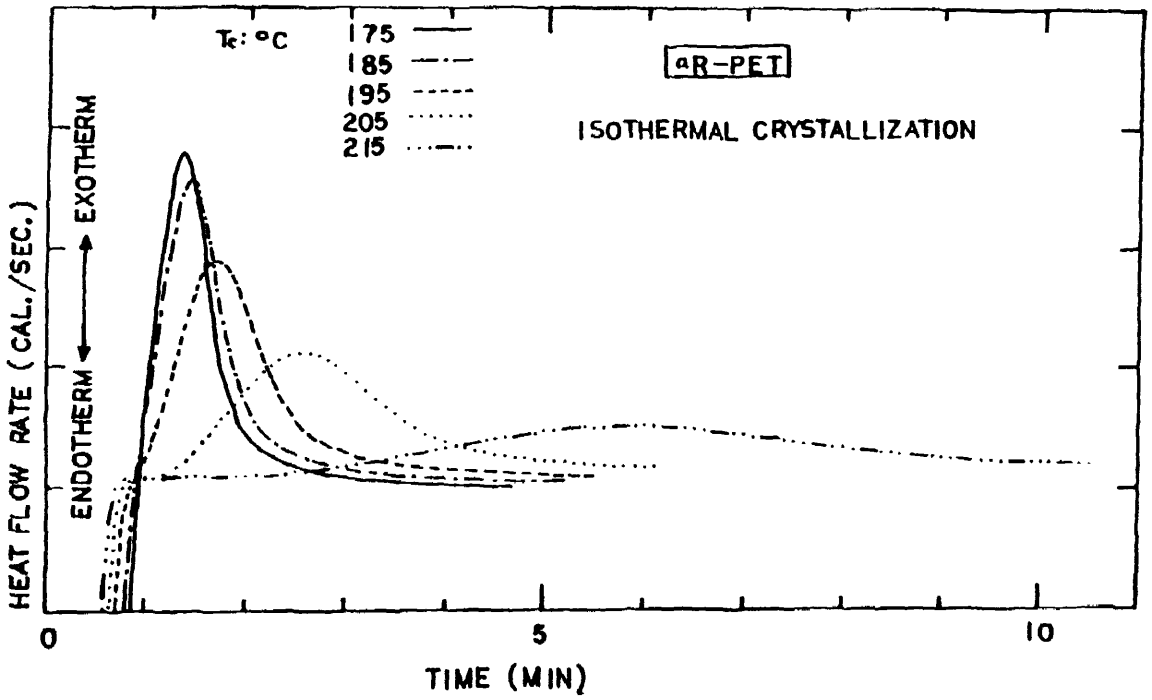

Figure 4.52 DSC Thermograms of aR-PET at Different Isothermal Temperatures

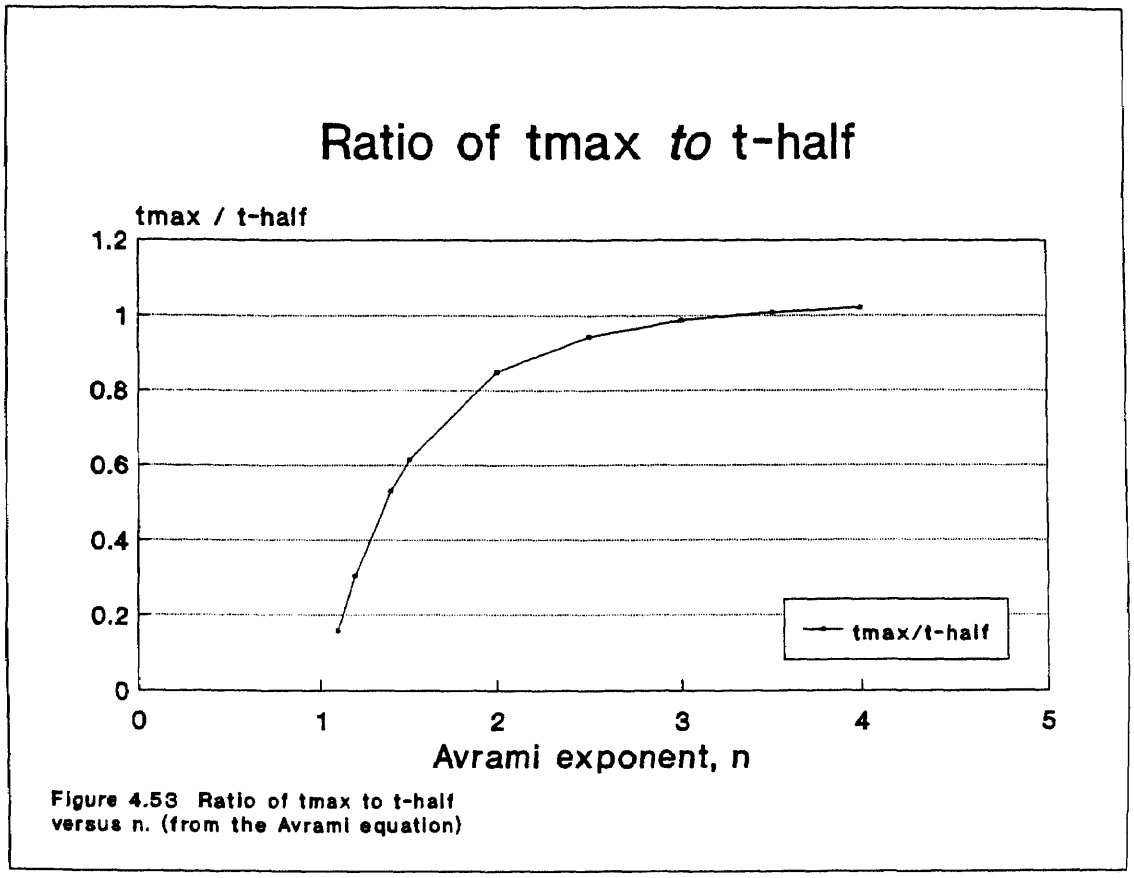

Figure 4.53 Ratio of tmax to t-half versus n. (from the Avrami equation)

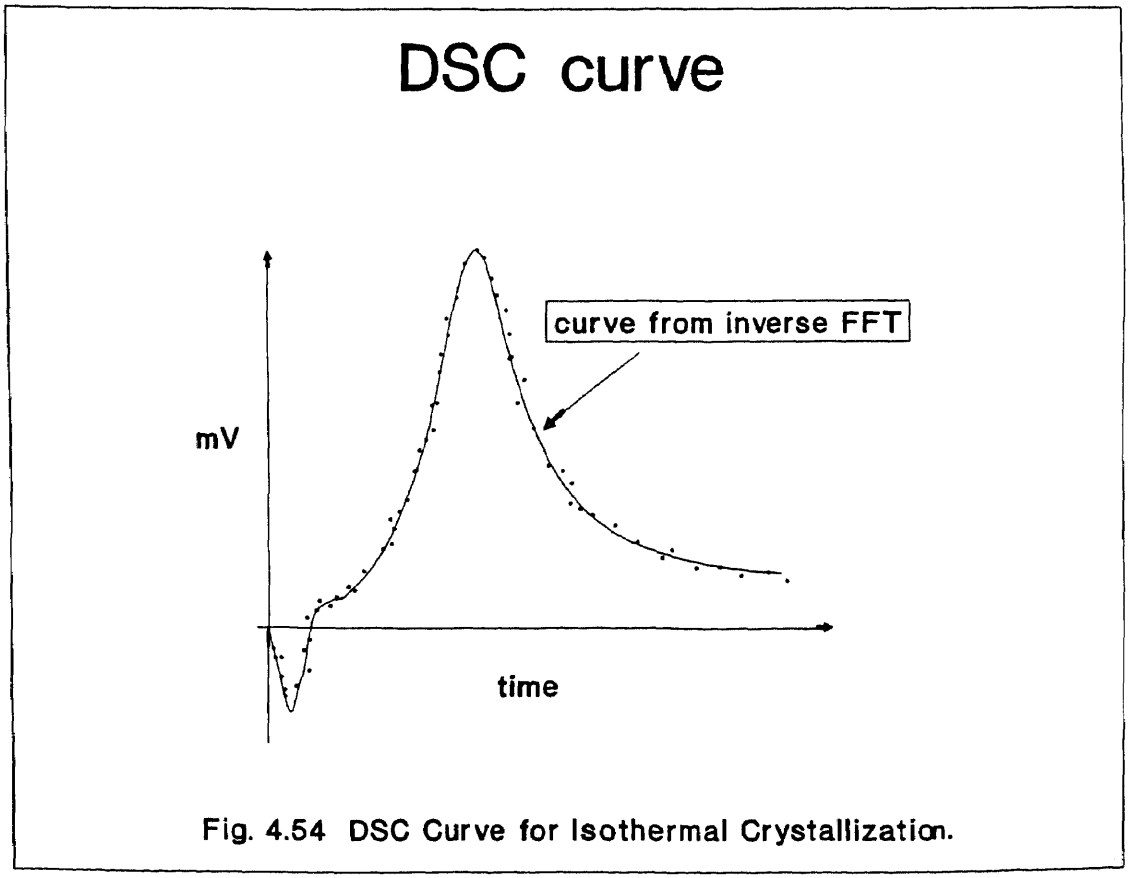

Fig. 4.54 DSC Curve for Isothermal Crystallization.

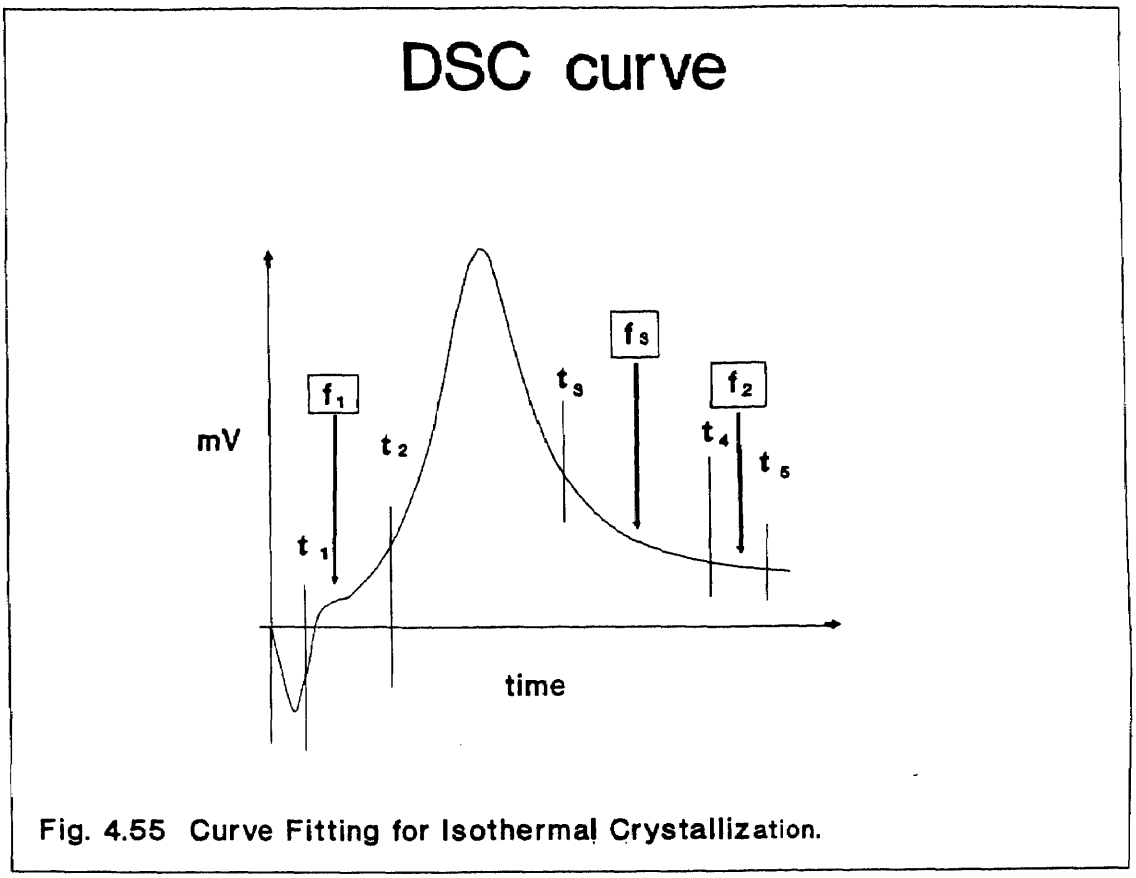

Fig. 4.55 Curve Fitting for Isothermal Crystallization.

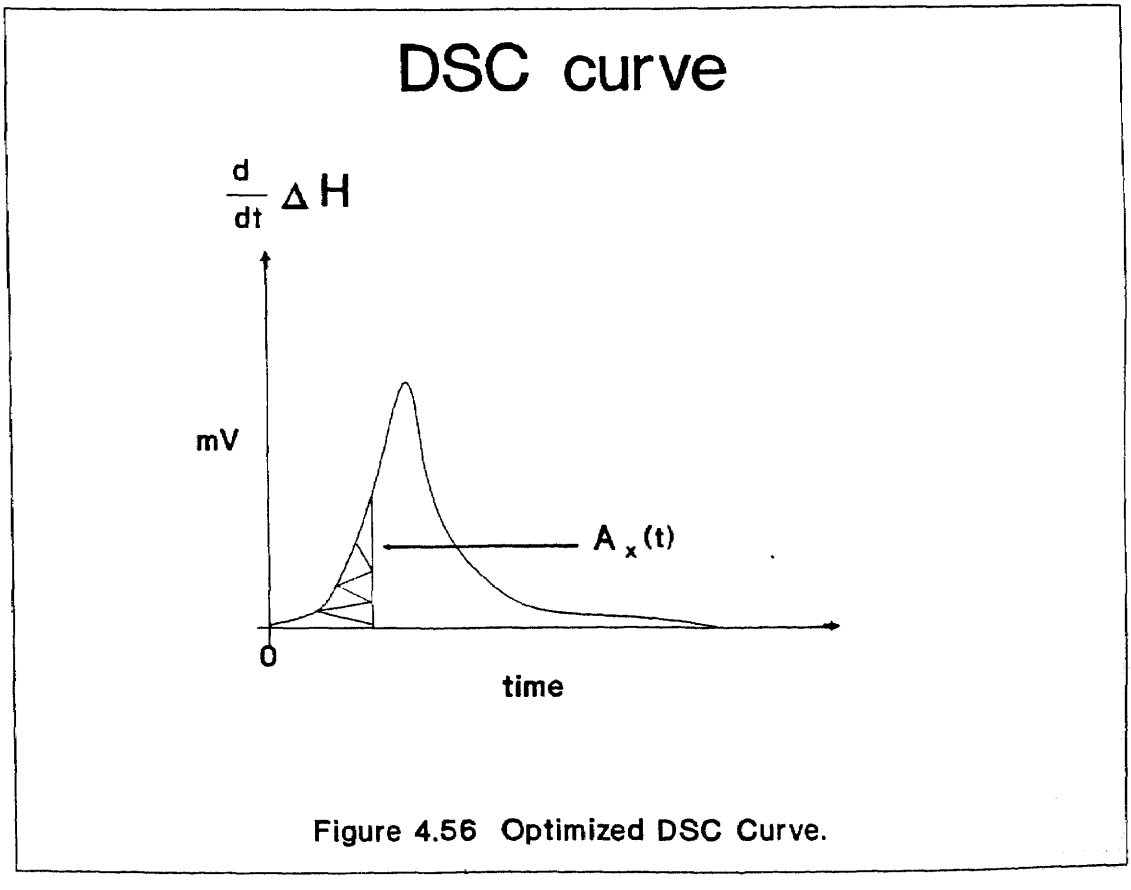

Figure 4.56 Optimized DSC Curve.

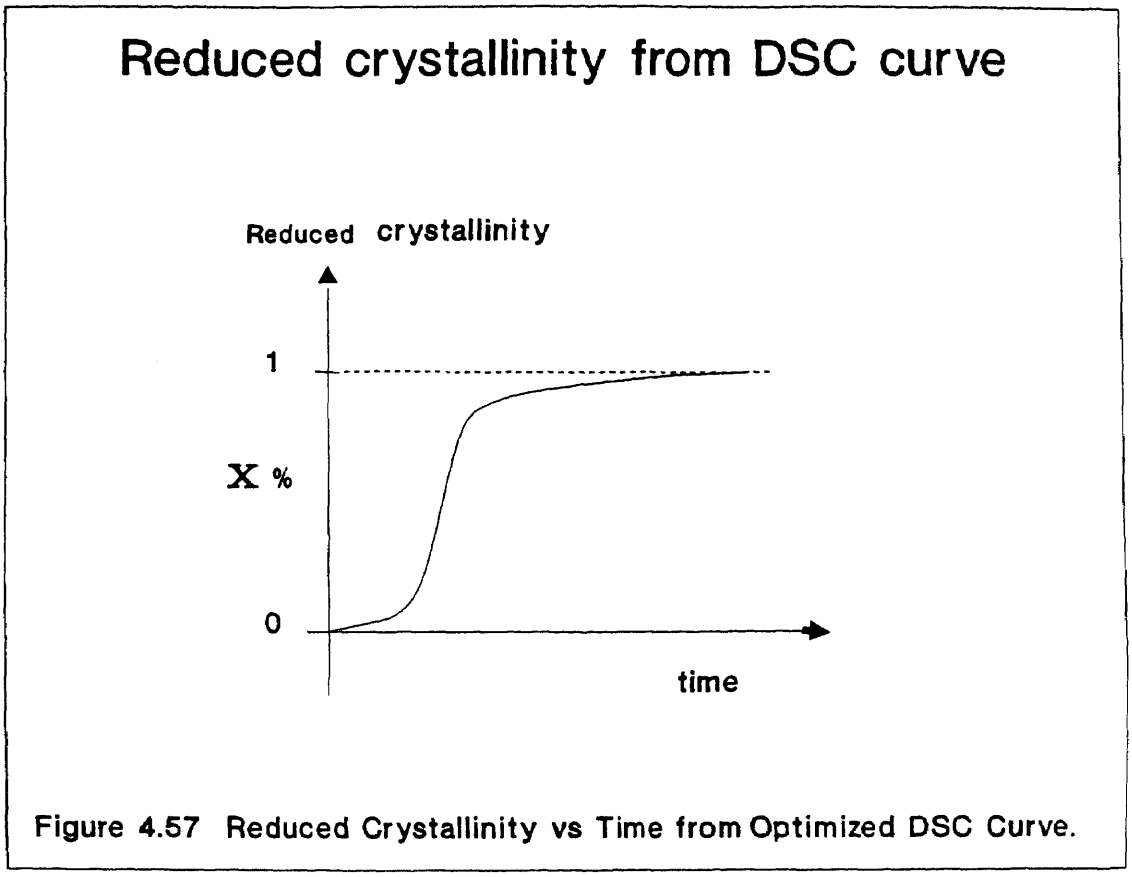

Figure 4.57 Reduced Crystallinity vs Time from Optimized DSC Curve.

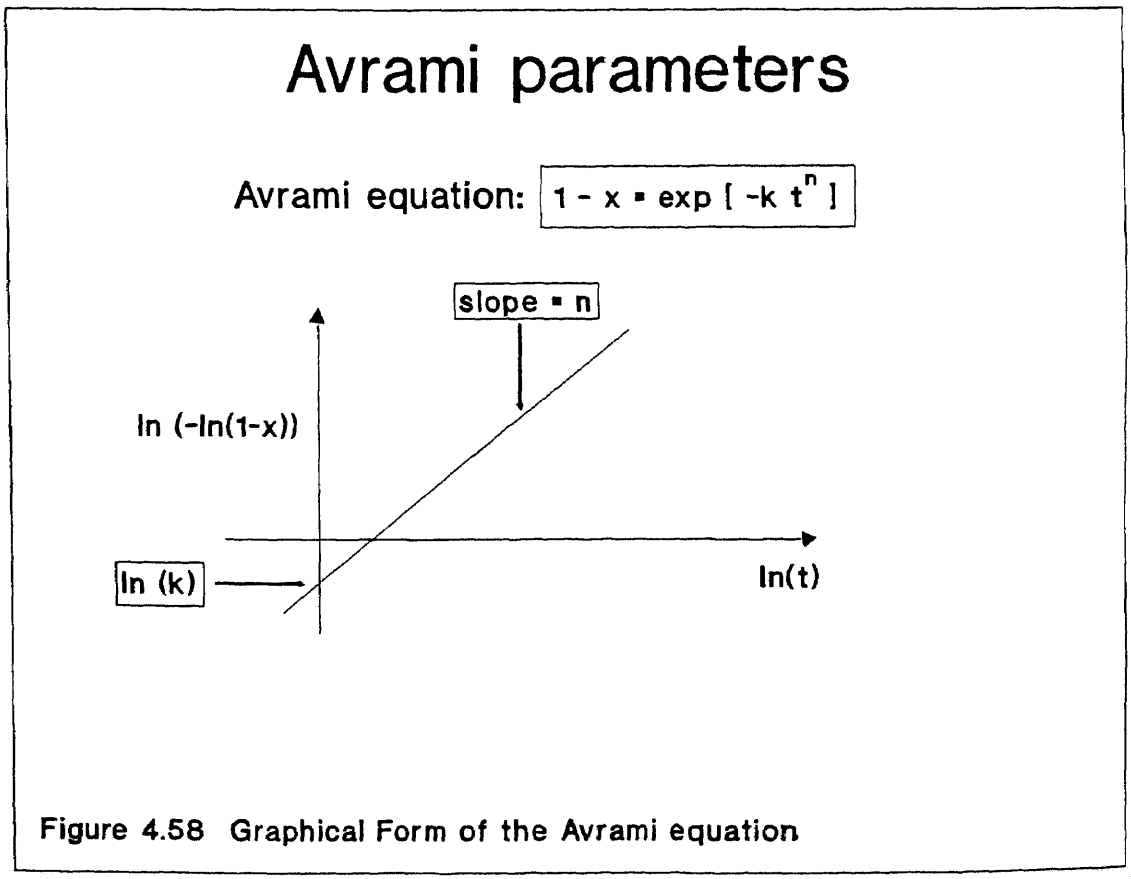

Figure 4.58 Graphical Form of the Avrami equation

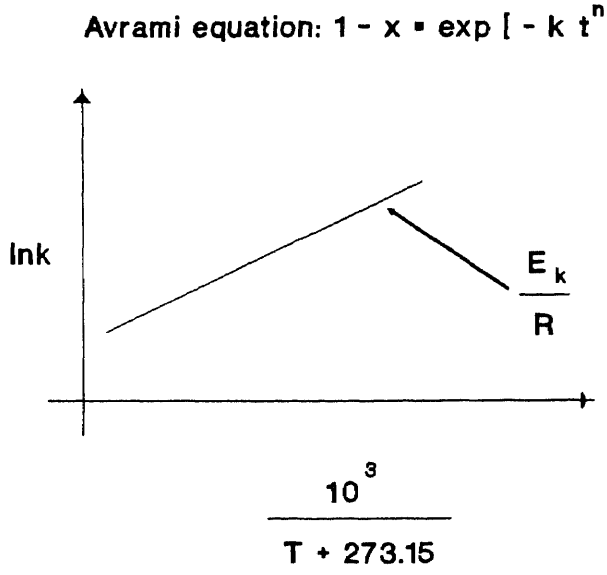

Figure 4.59 "Activation" (E_k) Energy from k.

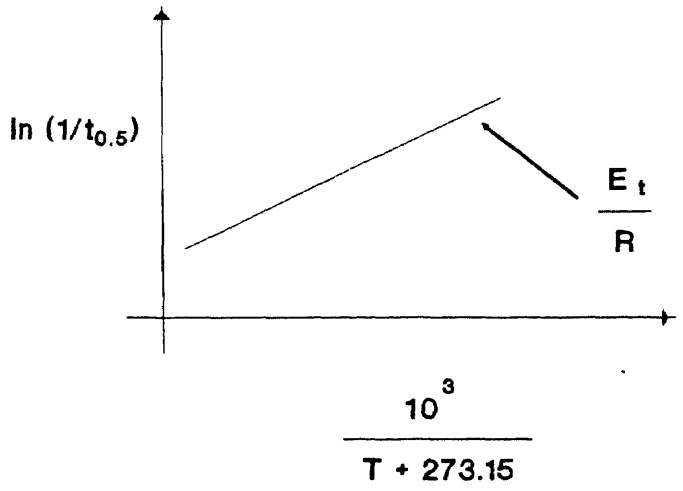

Fig. 4.60 "Activation" (E_t) Energy from ($1/t_{0.5}$).

Modified Avrami equation : $1 - x = \exp [- (k_n t)^n]$

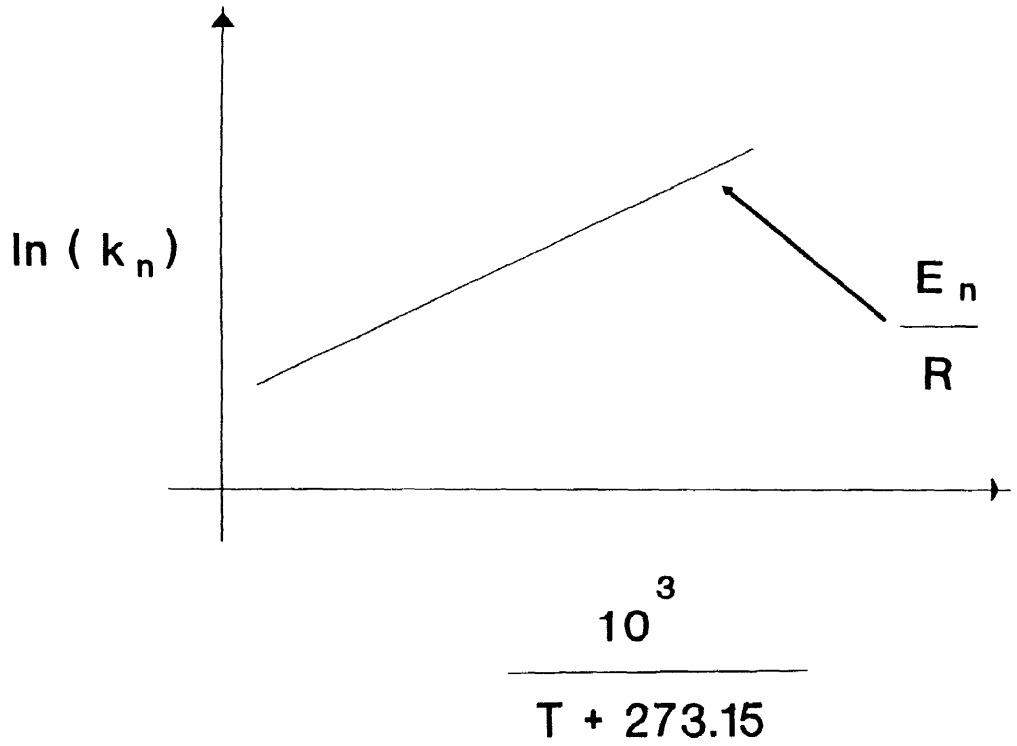

Figure 4.61 "Activation" (E_n) Energy from kn.

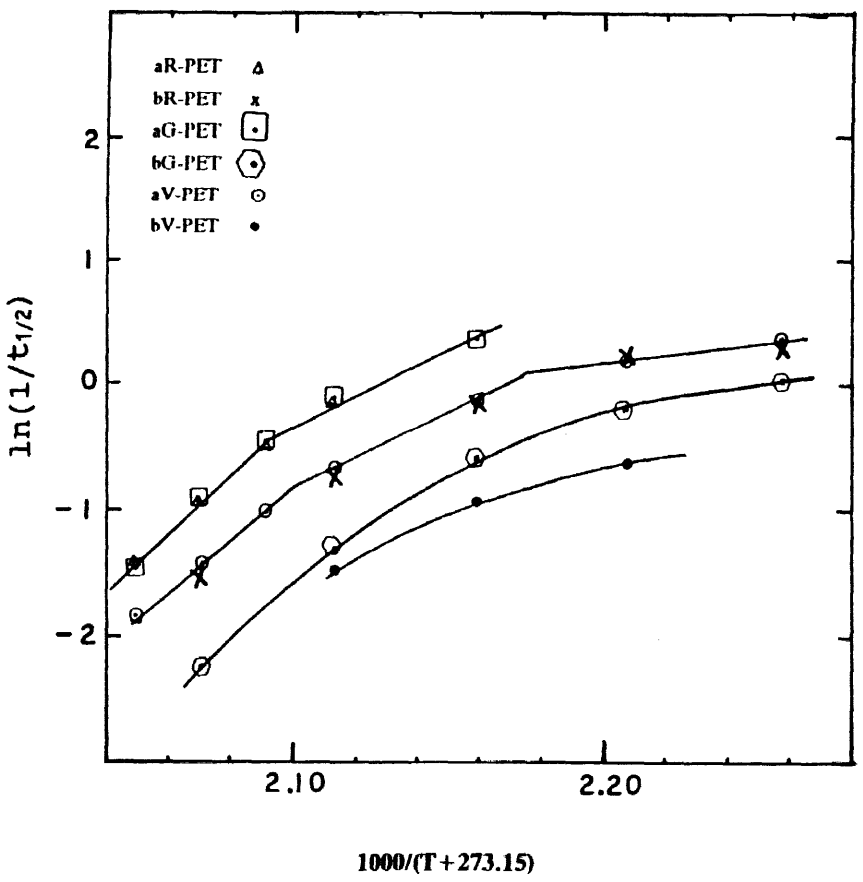

Figure 4.62 Dependence of Crystallization Rate Constant ($\ln(1/t_{1/2})$) on Temperature (1/T) for Different Types of PET

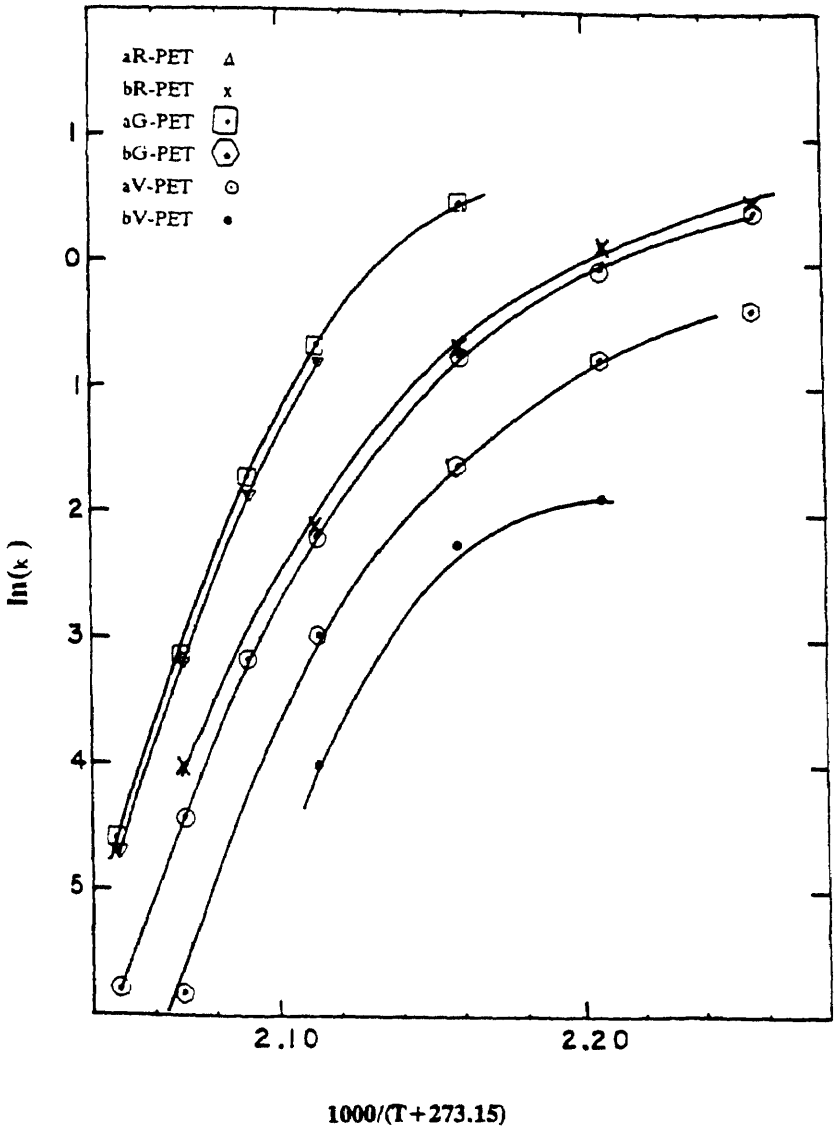

Figure 4.63 Dependence of Crystallization Rate Constant (lnk) on Temperature (1/T) for Different Types of PET

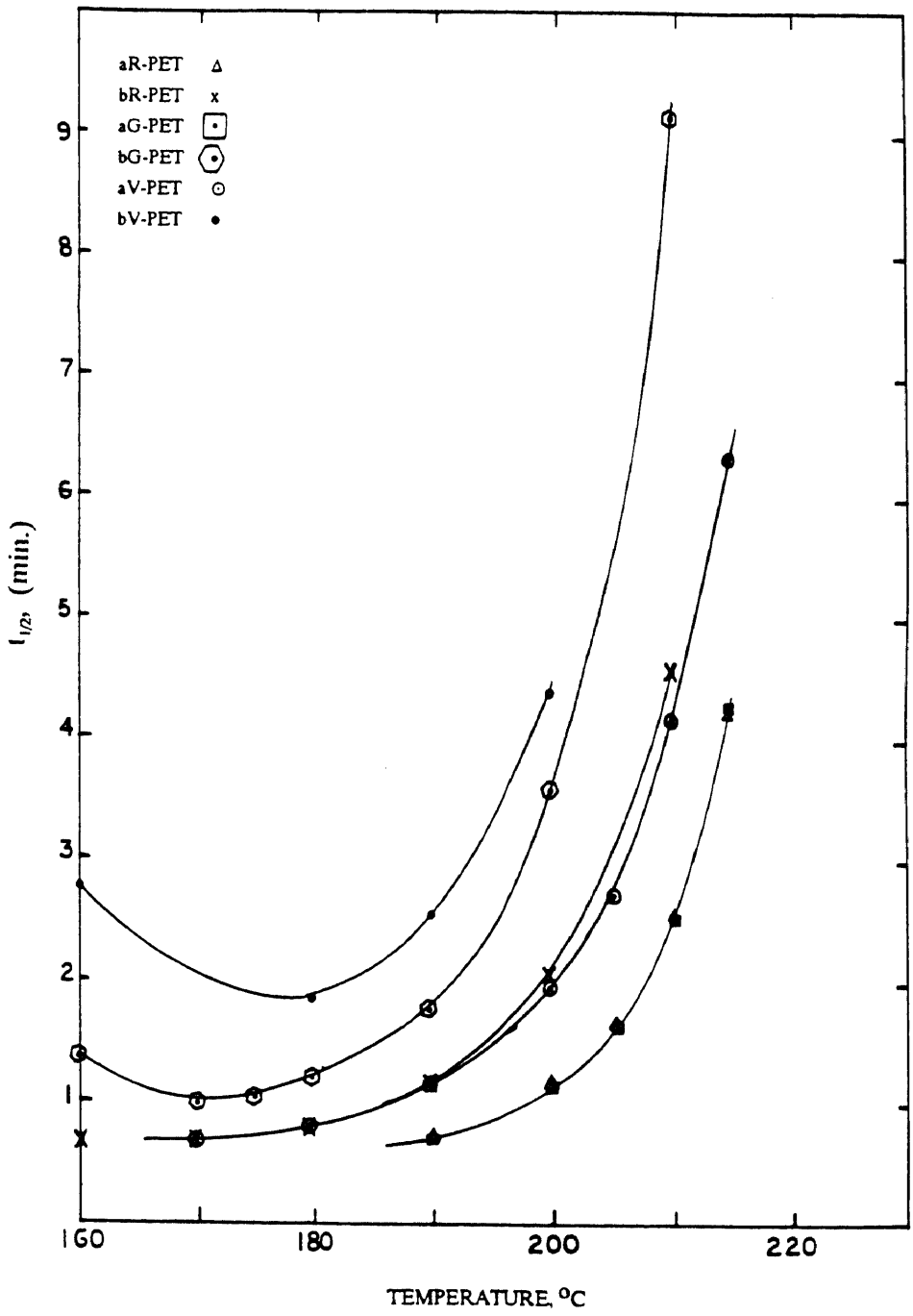

Figure 4.64 Crystallization Half-time ($t_{1/2}$) vs. Temperature for Different Types of PET

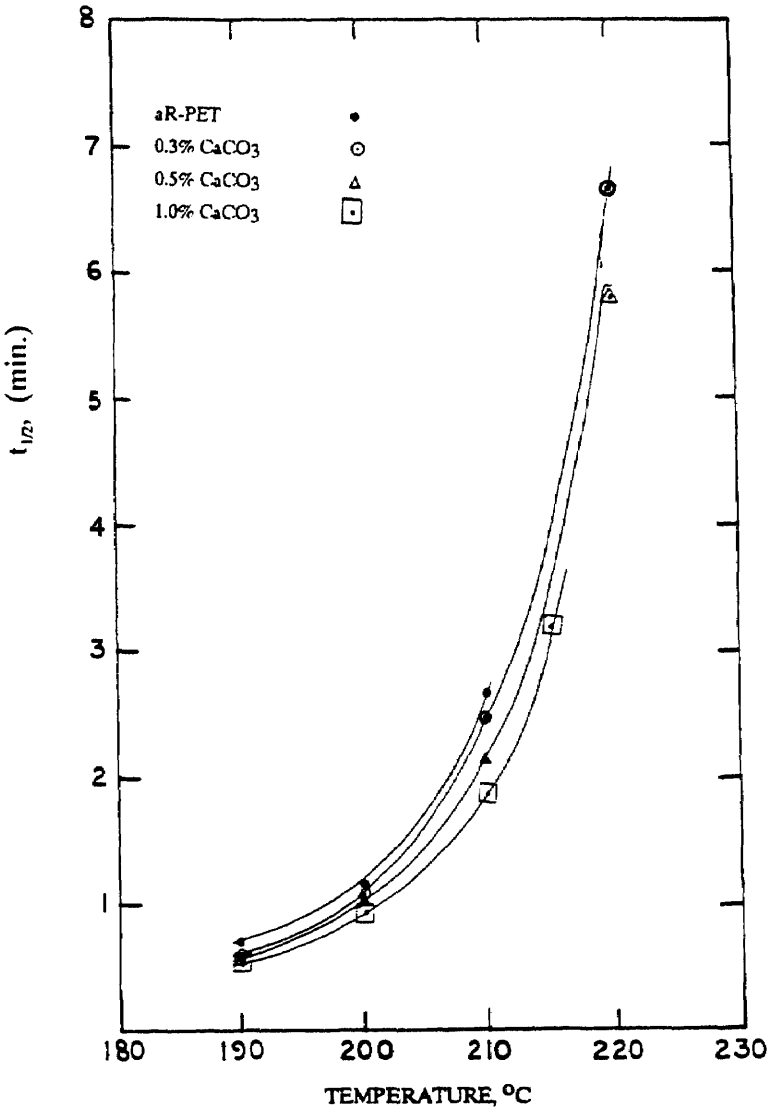

Figure 4.65 Crystallization Half-time ($t_{1/2}$) vs. Temperature for R-PET with Different concentrations of $CaCO_3$

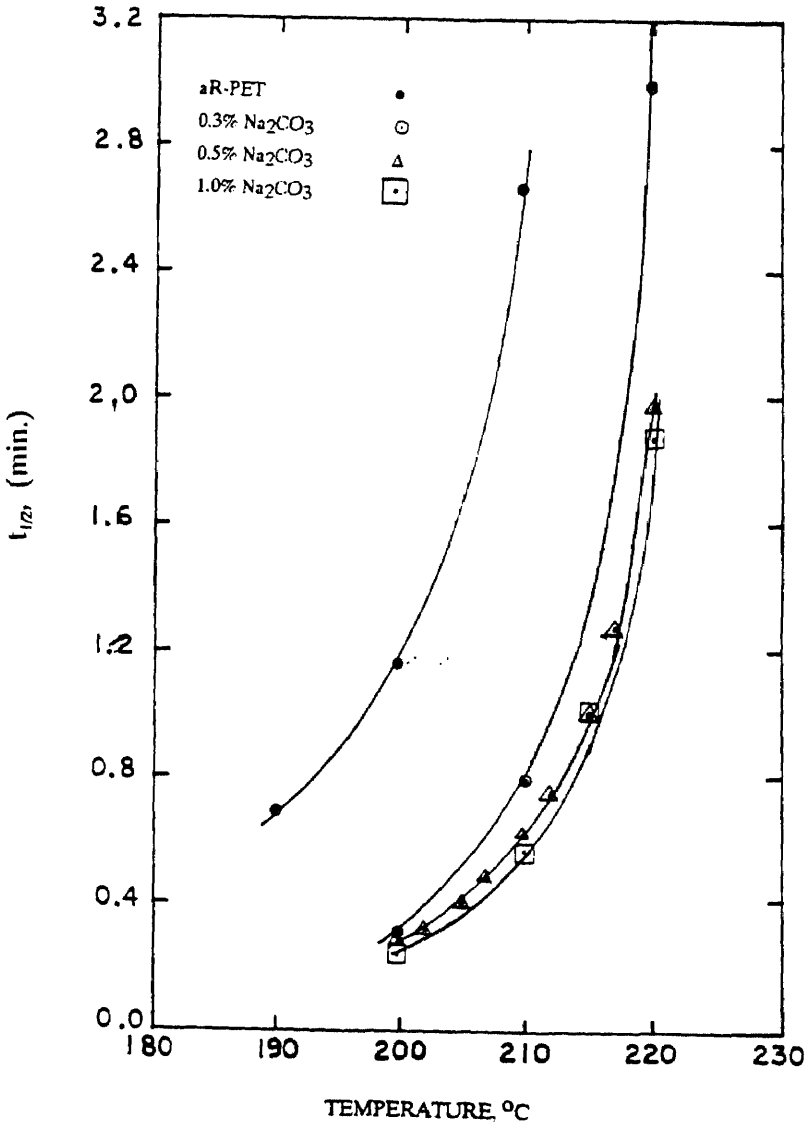

Figure 4.66 Crystallization Half-time ($t_{1/2}$) vs. Temperature for Different Cconcentrations of R-PET with Na_2CO_3

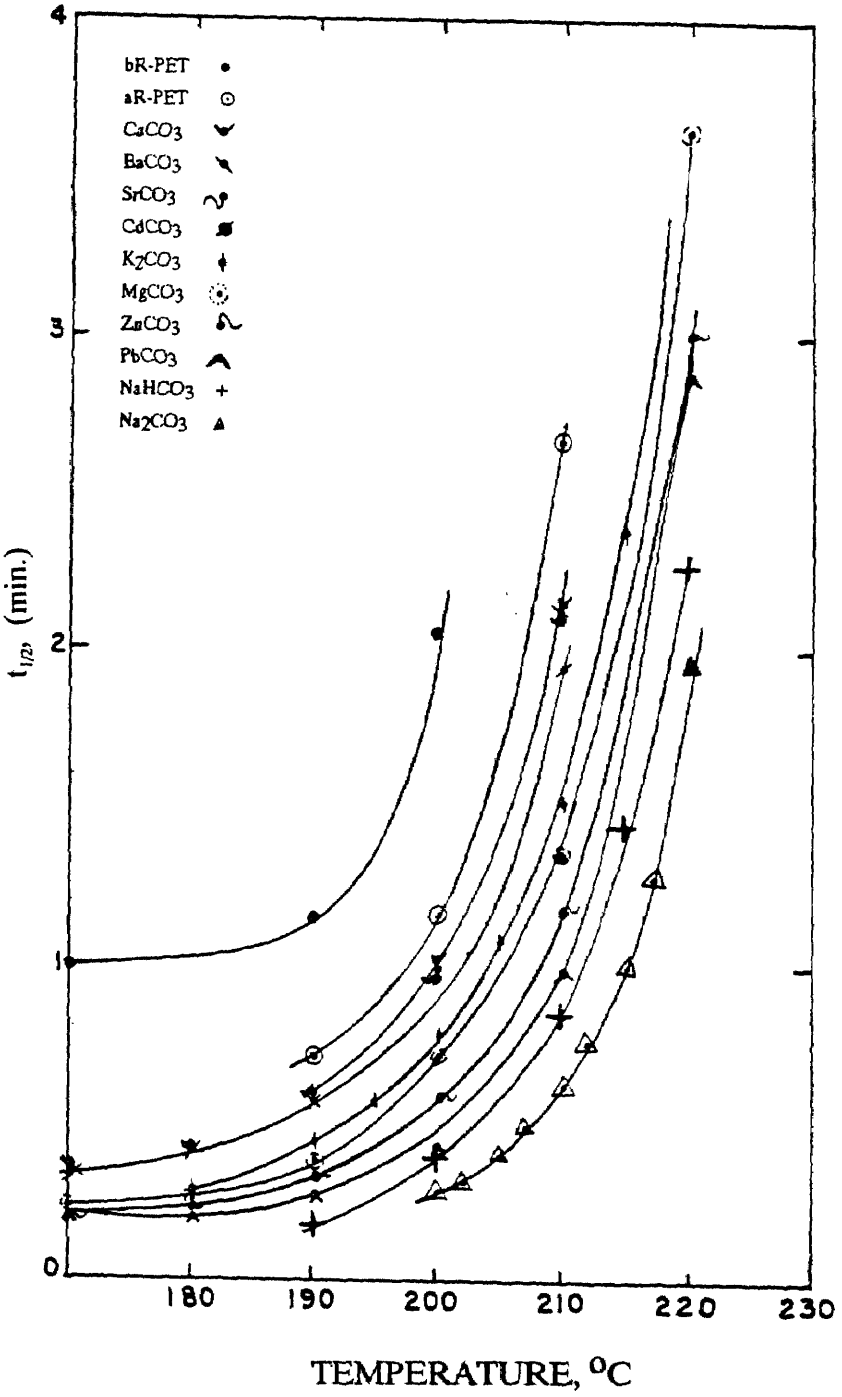

Figure 4.67 Crystallization Half-time ($t_{1/2}$) vs. Temperature for R-PET Containing Nucleating Agents at 0.5%

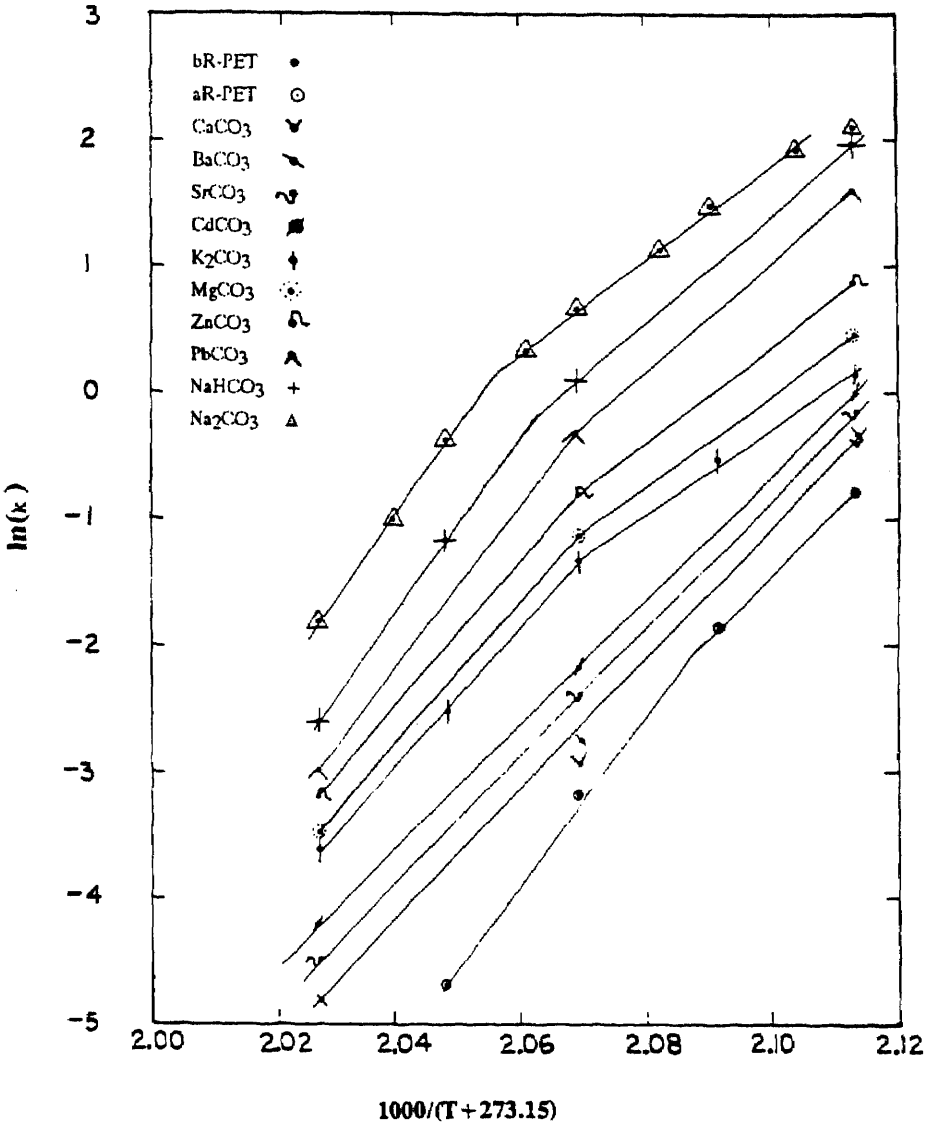

Figure 4.68 Dependence of Crystallization Rate Constant (lnk) on Temperature (1/T) for R-PET Containing Nucleating Agents at 0.5%

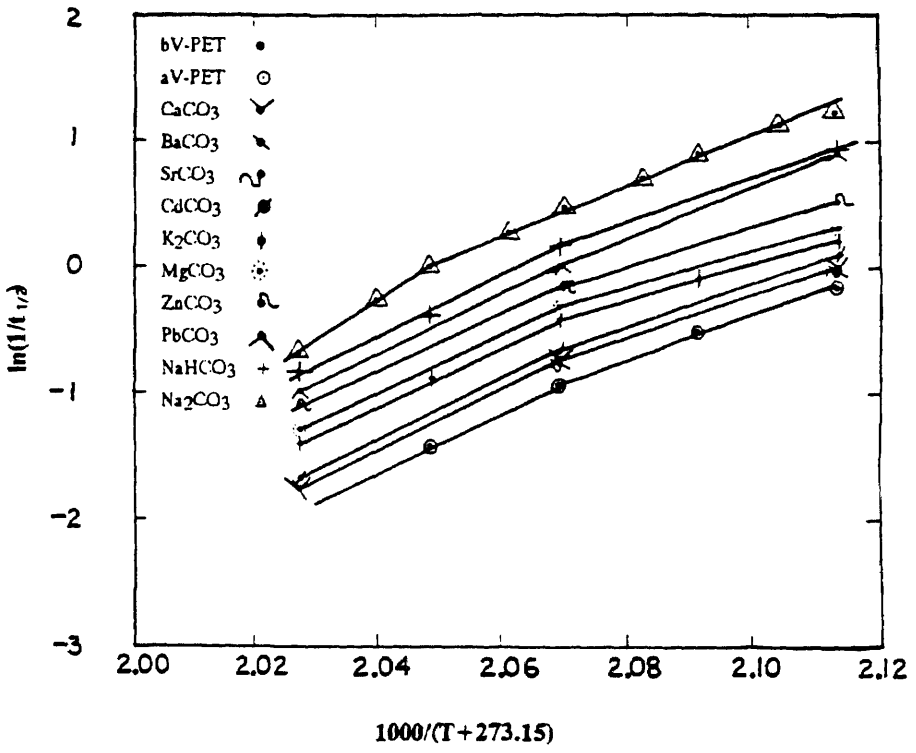

Figure 4.69 Dependence of Crystallization Rate Constant ($\ln(1/t_{1/2})$) on Temperature (1/T) for R-PET Containing Nucleating Agents at 0.5%

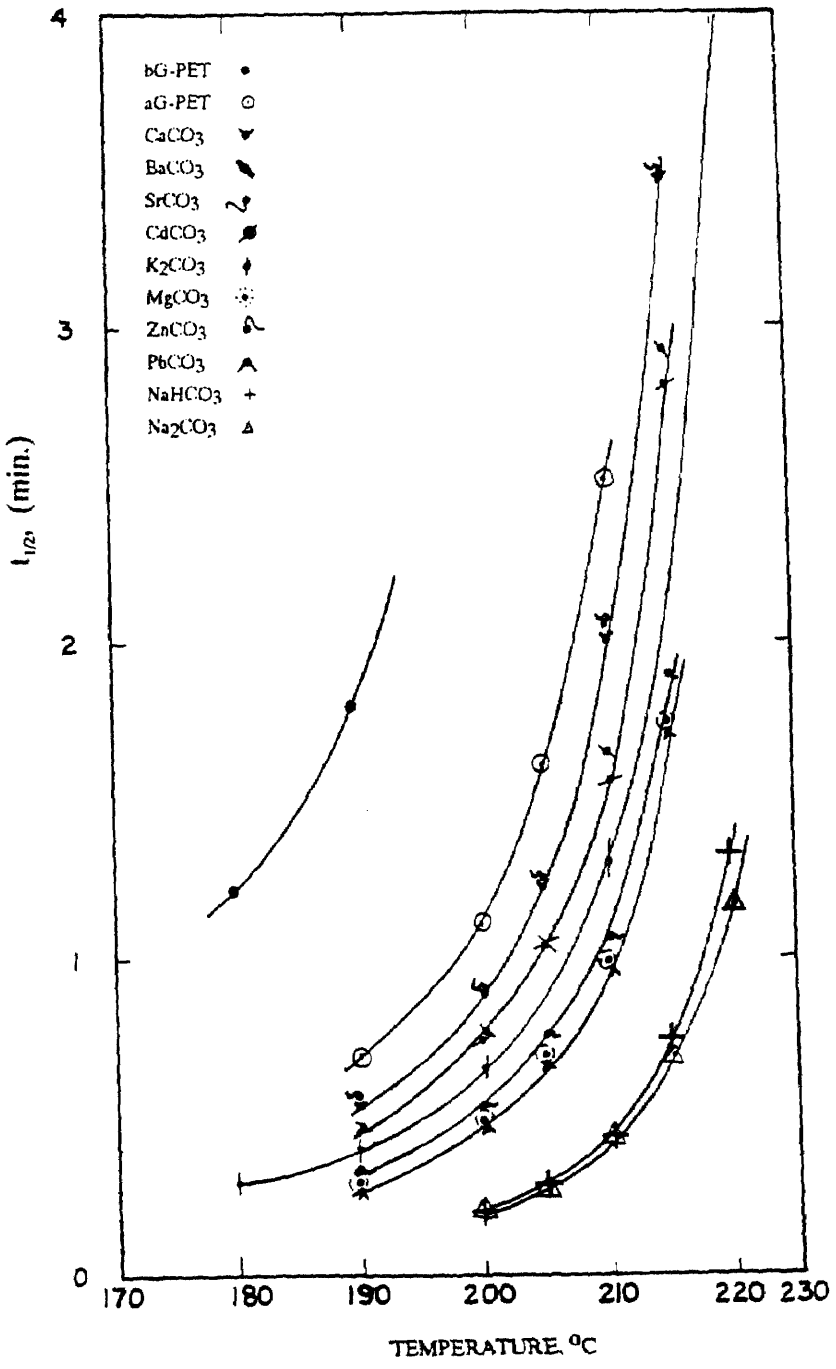

Figure 4.70 Crystallization Half-time ($t_{1/2}$) vs. Temperature for G-PET Containing Nucleating Agents at 0.5%

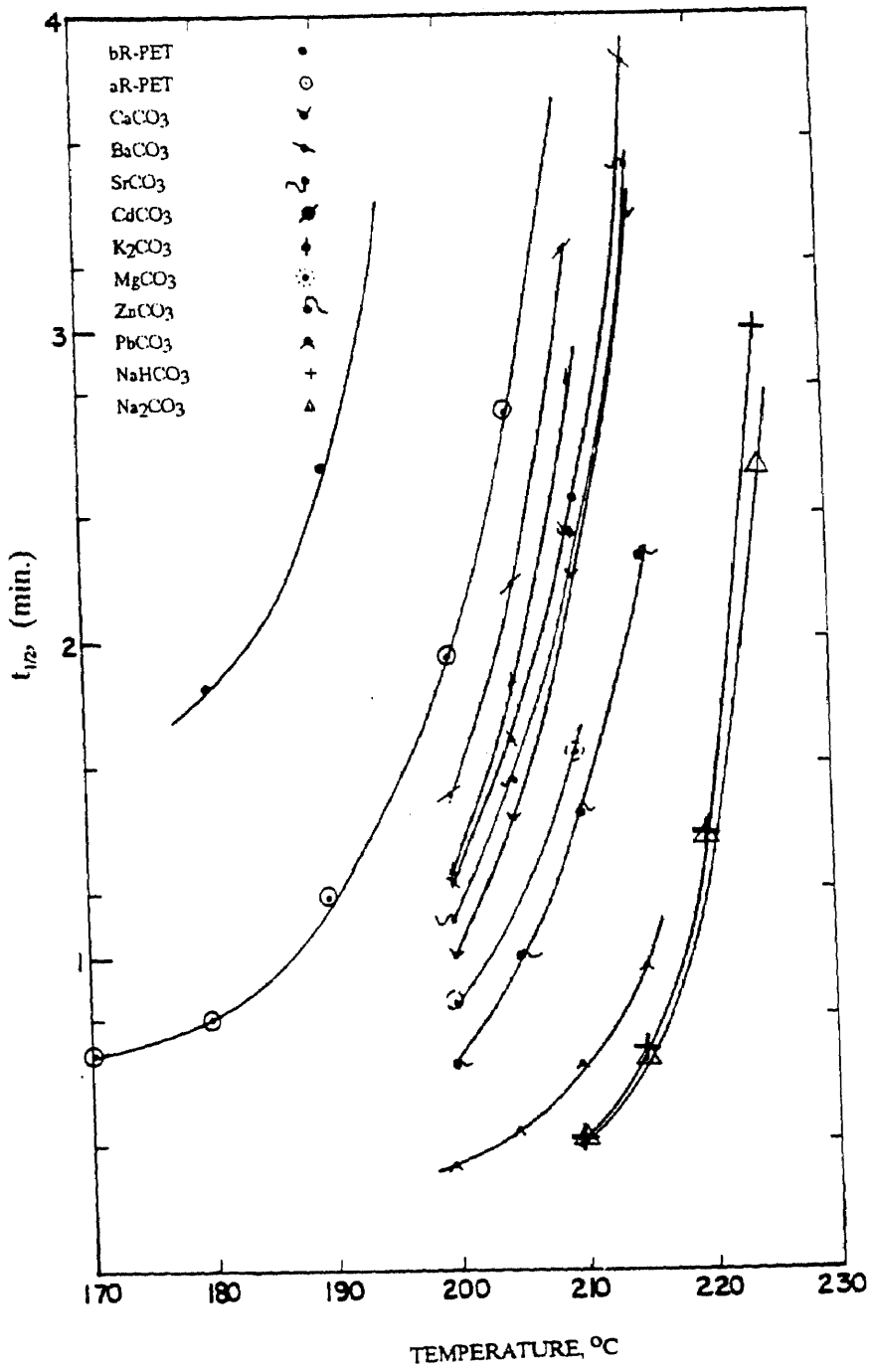

Figure 4.71 Crystallization Half-time ($t_{1/2}$) vs. Temperature for V-PET Containing Nucleating Agents at 0.5%

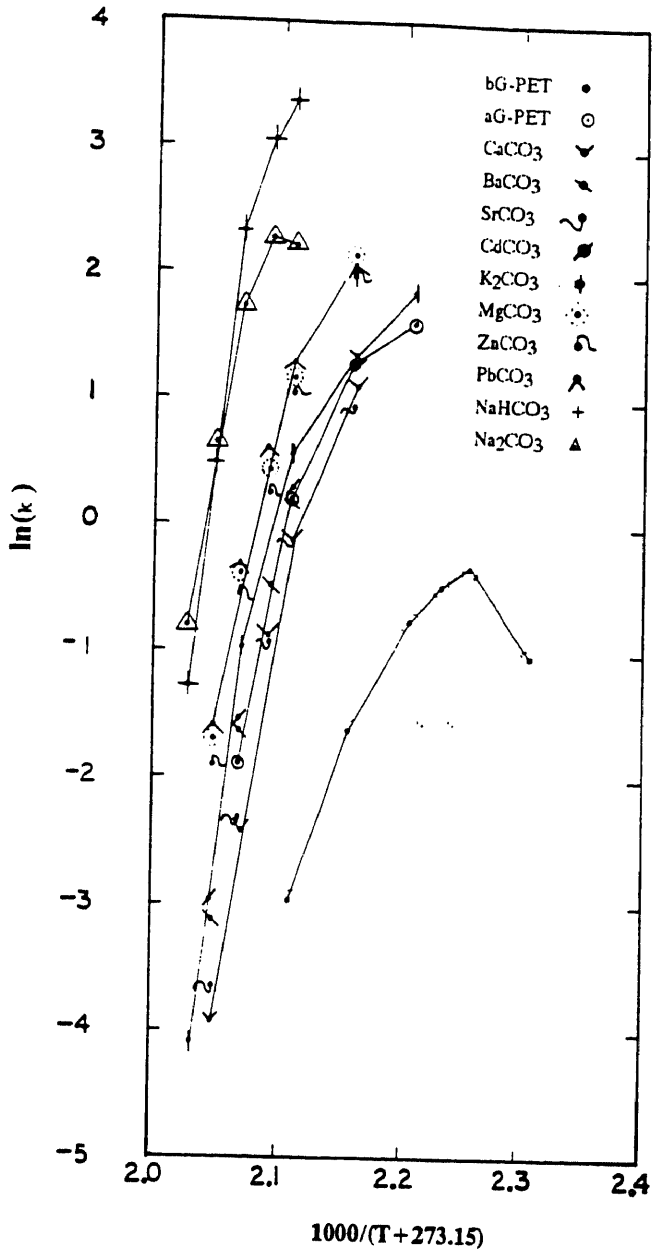

Figure 4.72 Dependence of Crystallization Rate Constant (lnk) on Temperature (1/T) for G-PET Containing Nucleating Agents at 0.5%

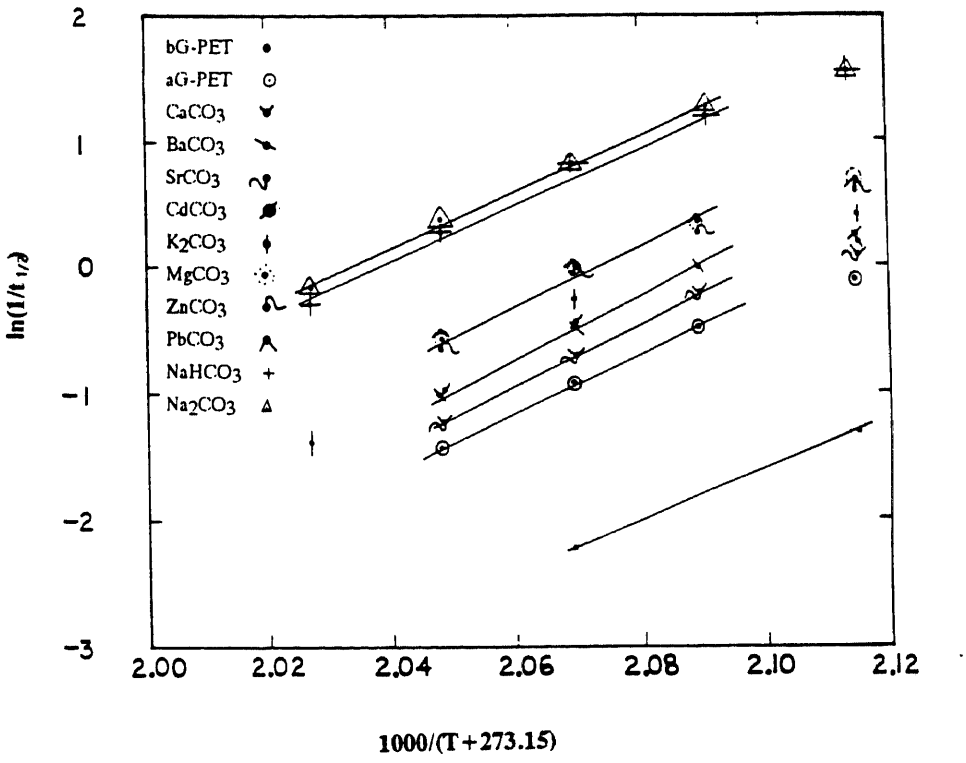

Figure 4.73 Dependence of Crystallization Rate Constant ($\ln(1/t_{1/2})$) on Temperature (1/T) for G-PET Containing Nucleating Agents at 0.5%

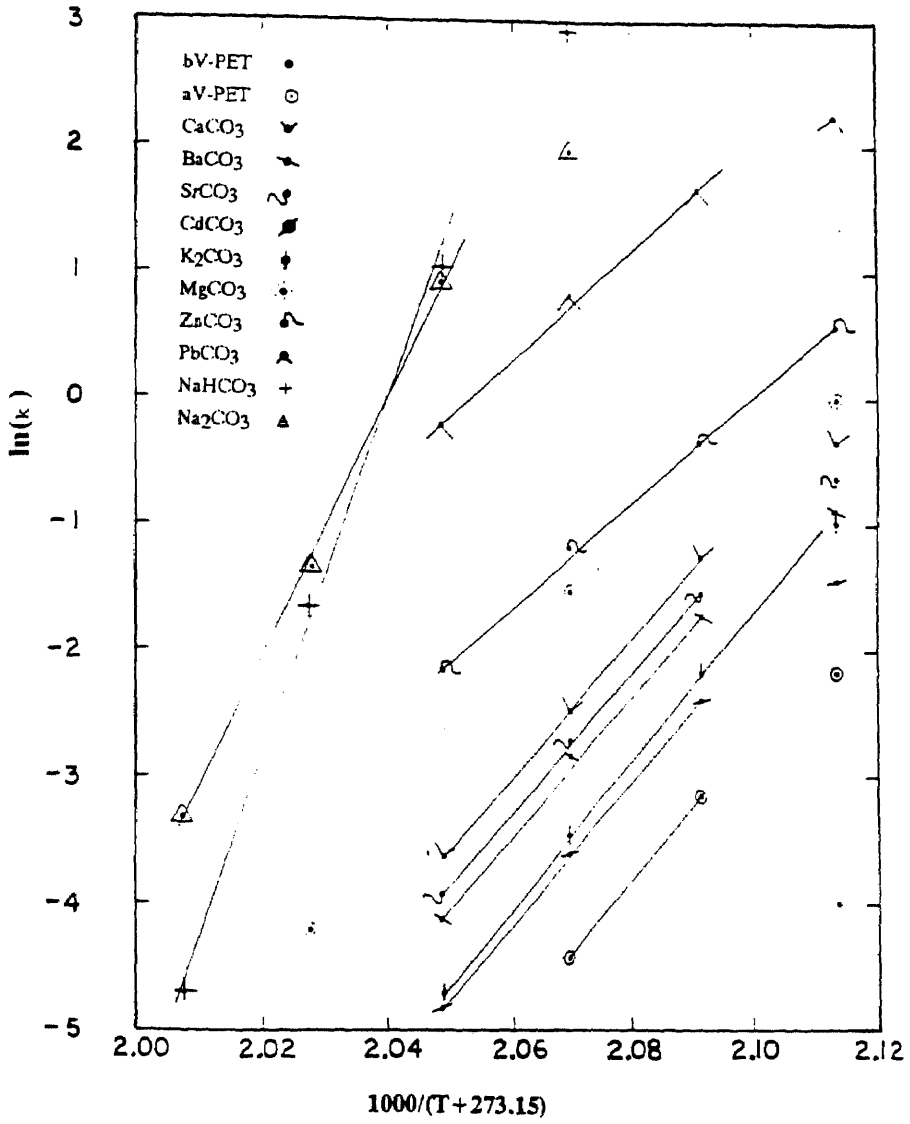

Figure 4.74 Dependence of Crystallization Rate Constant (lnk) on Temperature (1/T) for V-PET Containing Nucleating Agents at 0.5%

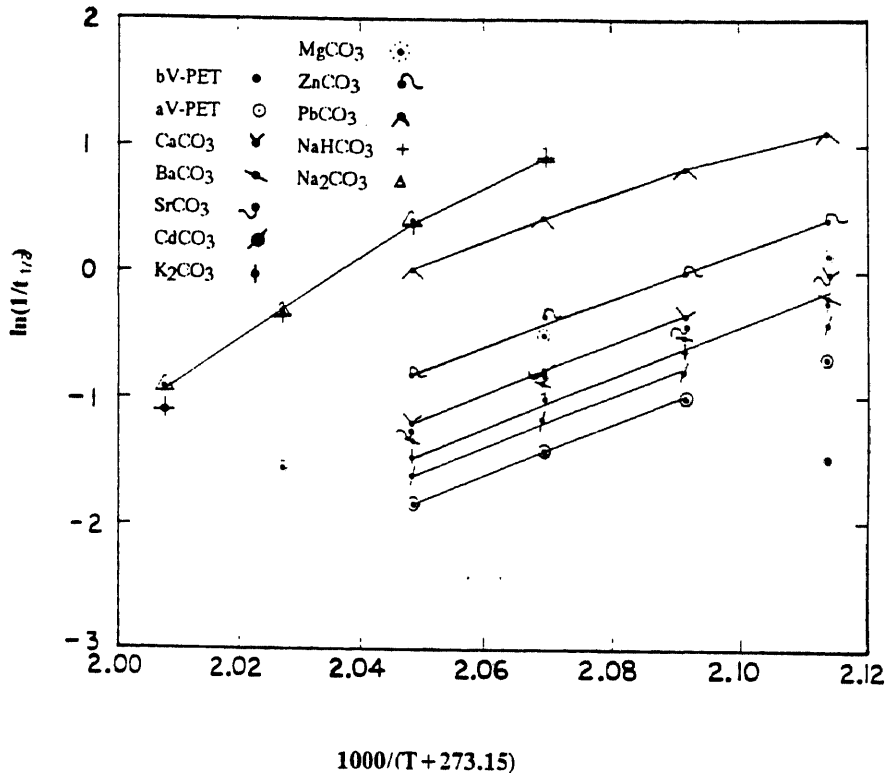

Figure 4.75 Dependence of Crystallization Rate Constant ($\ln(1/t_{1/2})$) on Temperature (1/T) for V-PET Containing Nucleating Agents at 0.5%

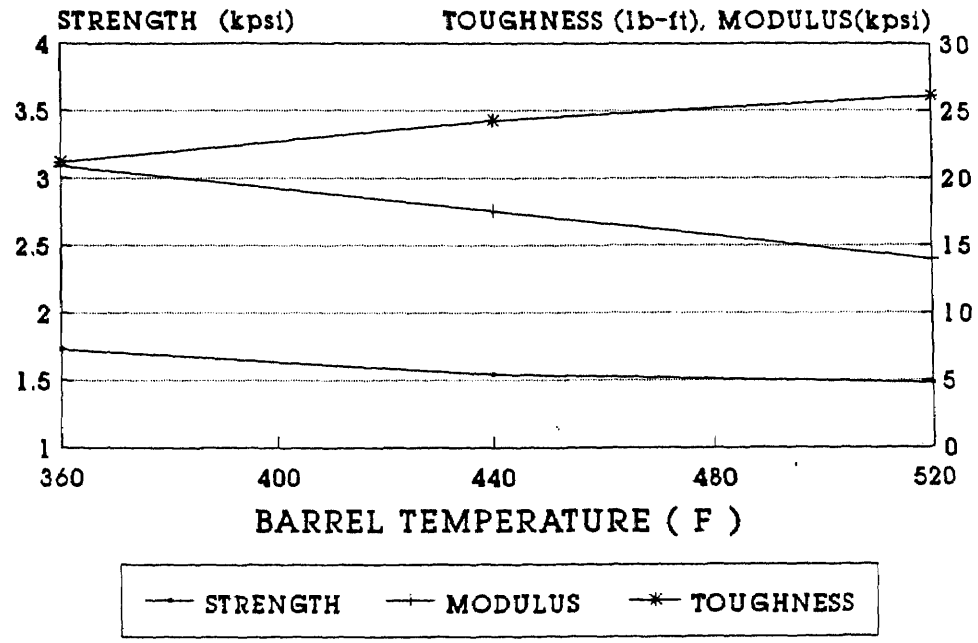

Fig. 4.76 Mechanical Properties of LDPE-1 at Different Barrel Temperatures.

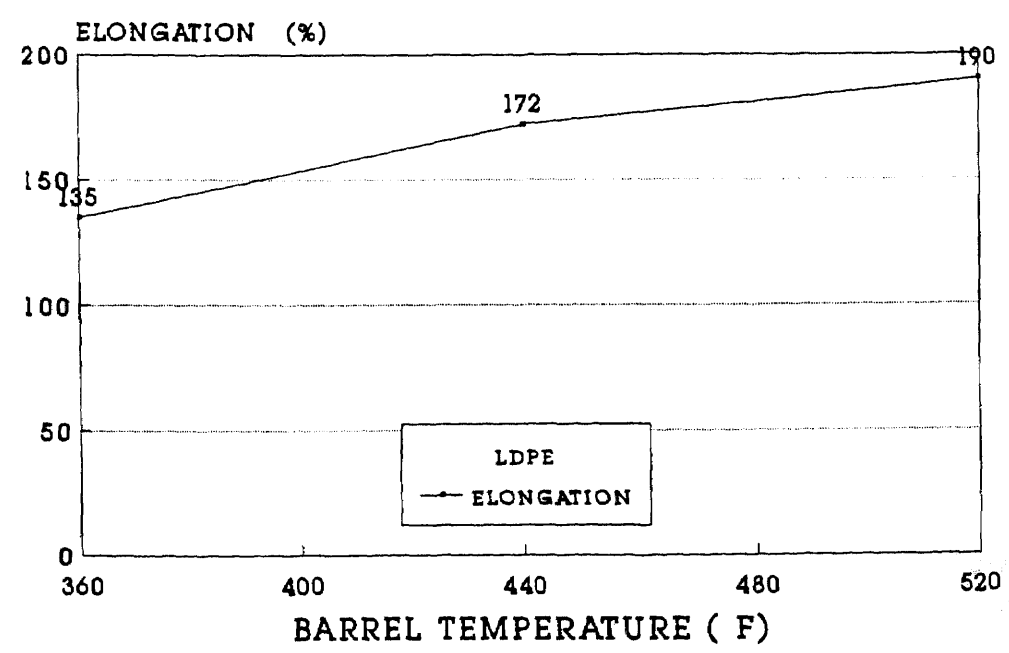

Fig. 4.77 Elongation of LDPE-1 at Different Barrel Temperatures.

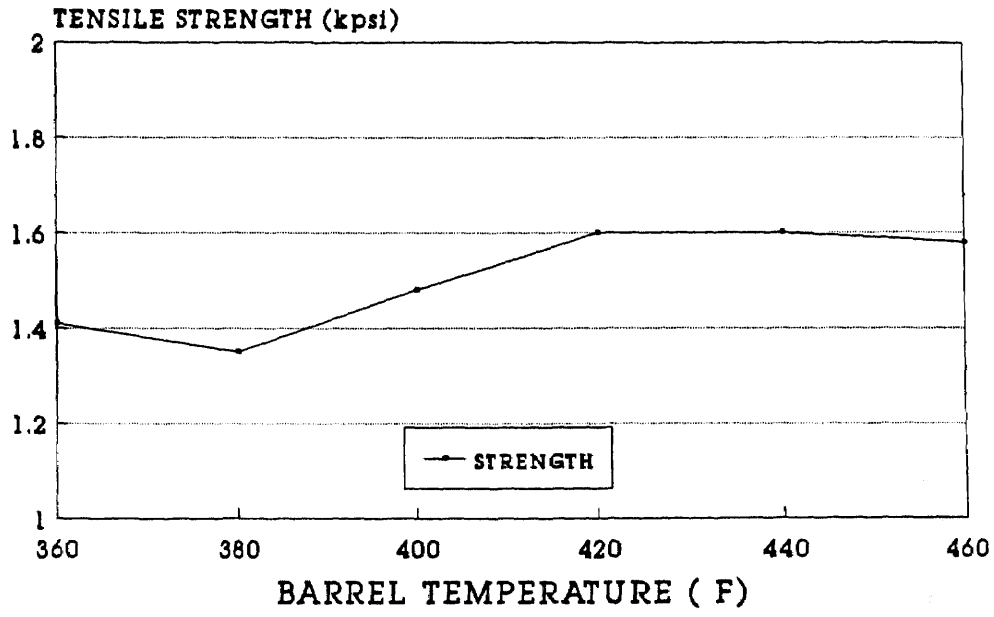

Figure 4.78 Tensile Strength of 90% LDPE-1/10% PET-1 Blend as a Function of Barrel Temperature.

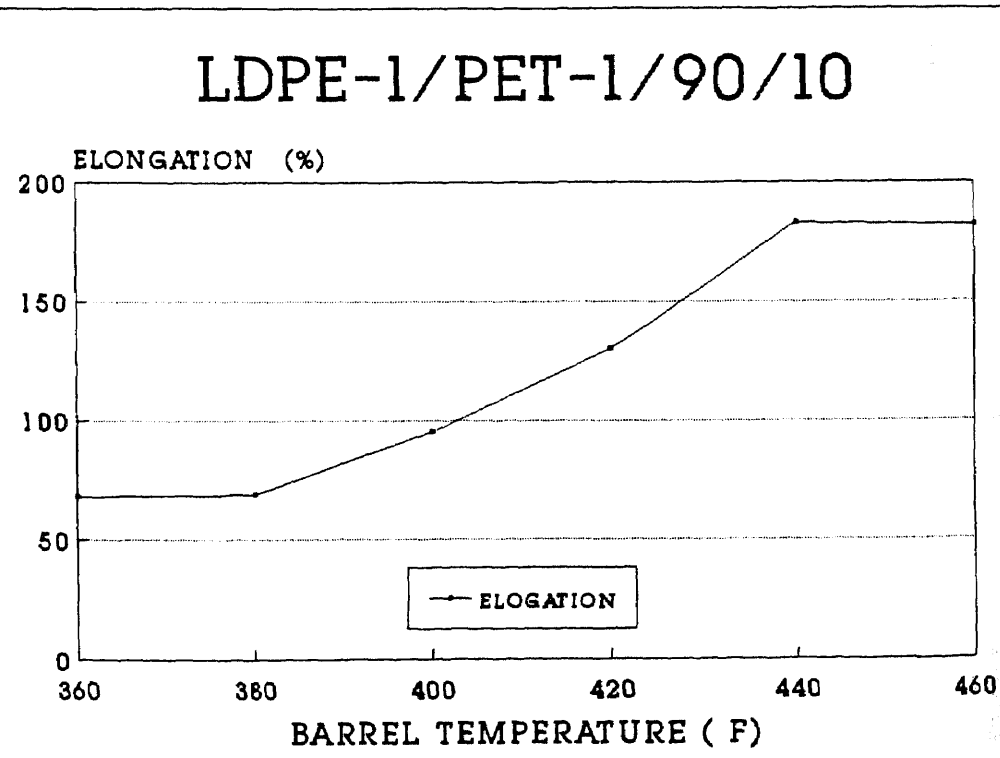

Fig. 4.79 Elongation of a 90% LDPE-1/ 10% R-PET-1 Blend as a Function of Barrel Temperature.

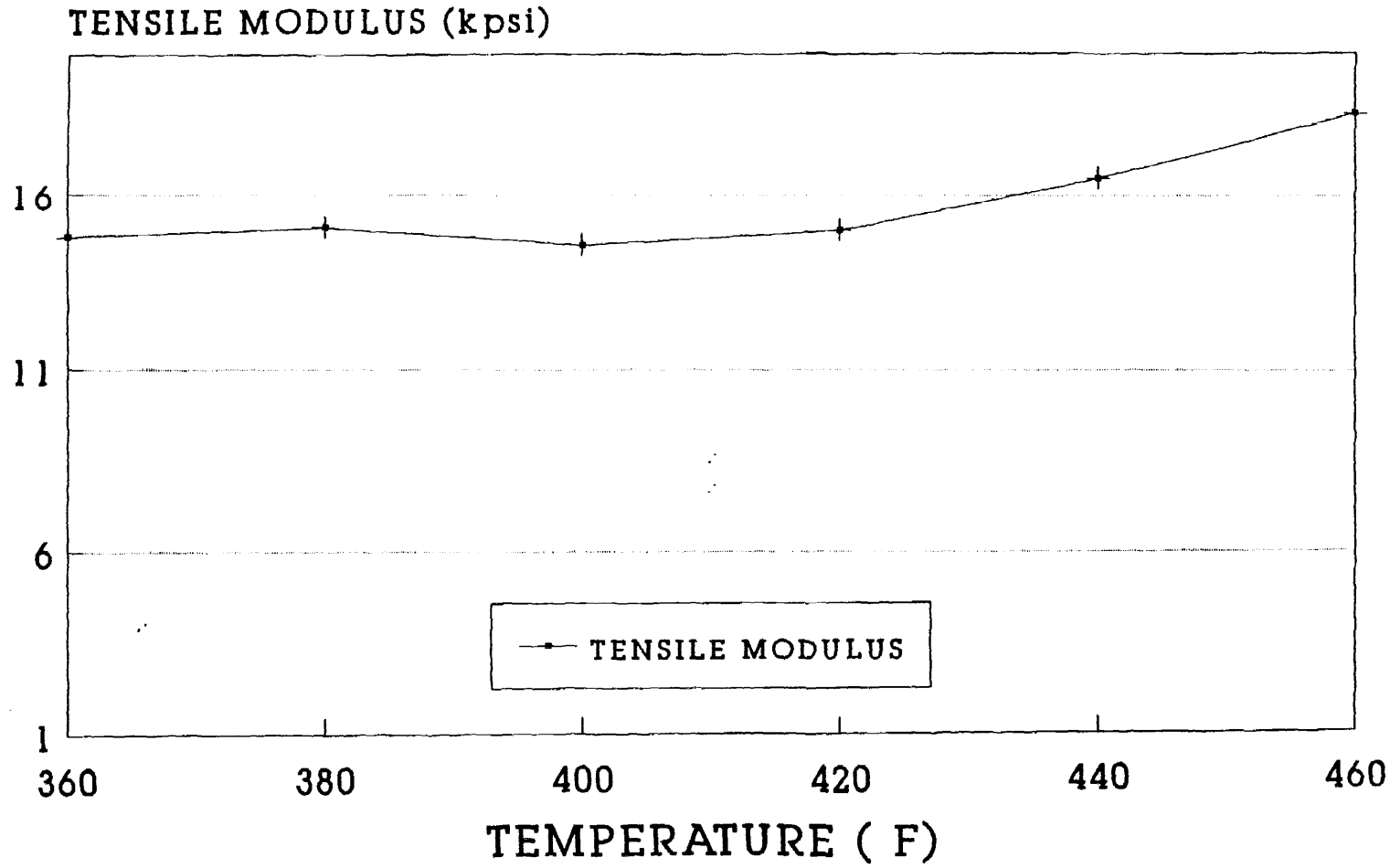

Figure 4.80 Tensile Modulus of a 90% LDPE-1/10% R-PET-1 Blend as a Function of Barrel Temperature.

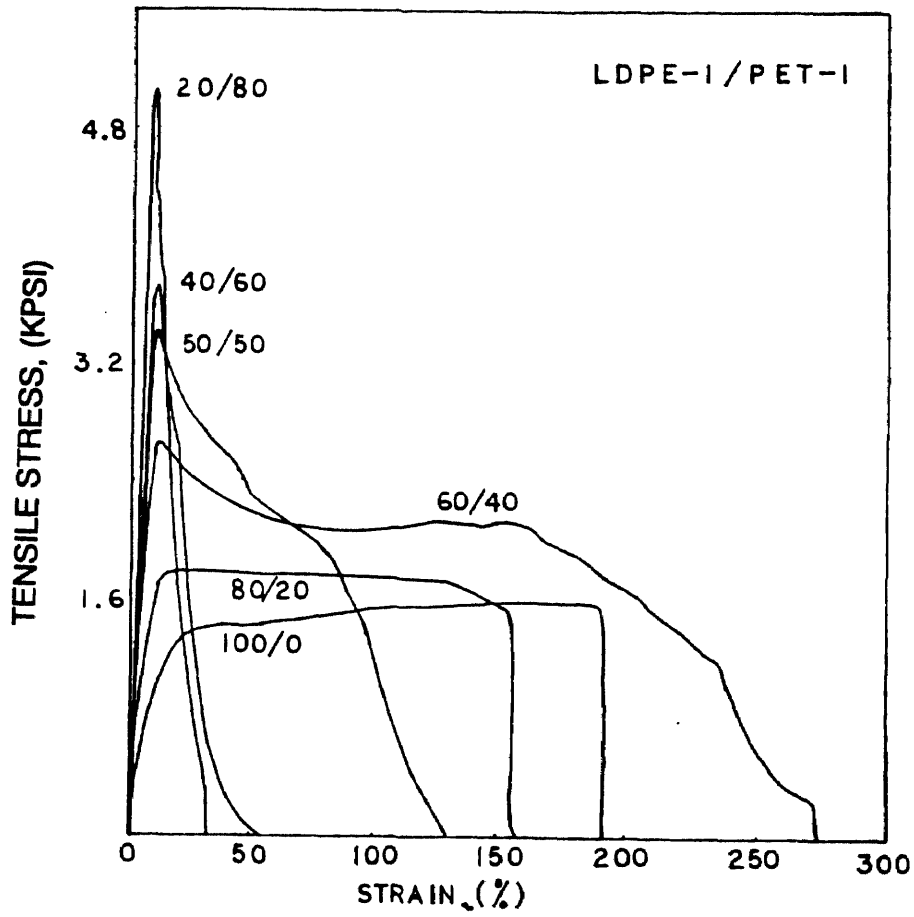

Figure 4.81 Stress-Strain Curves by Tensile Testing for LDPE-1/R-PET-1 Blends (stain rate: 1 in/min)

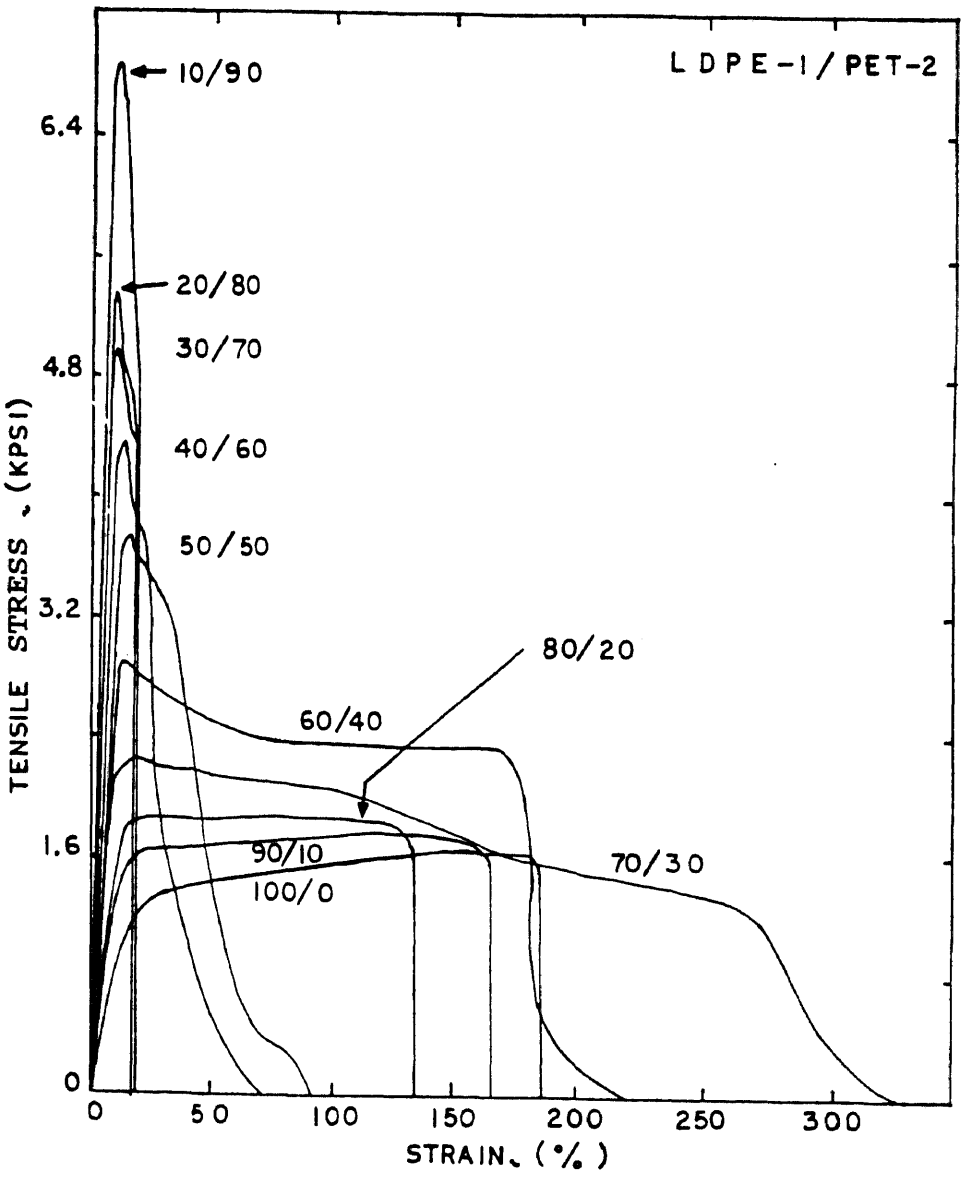

Figure 4.82 Stress-Strain Curves by Tensile Testing for LDPE-1/R-PET-2 Blends (stain rate: 1 in/min)

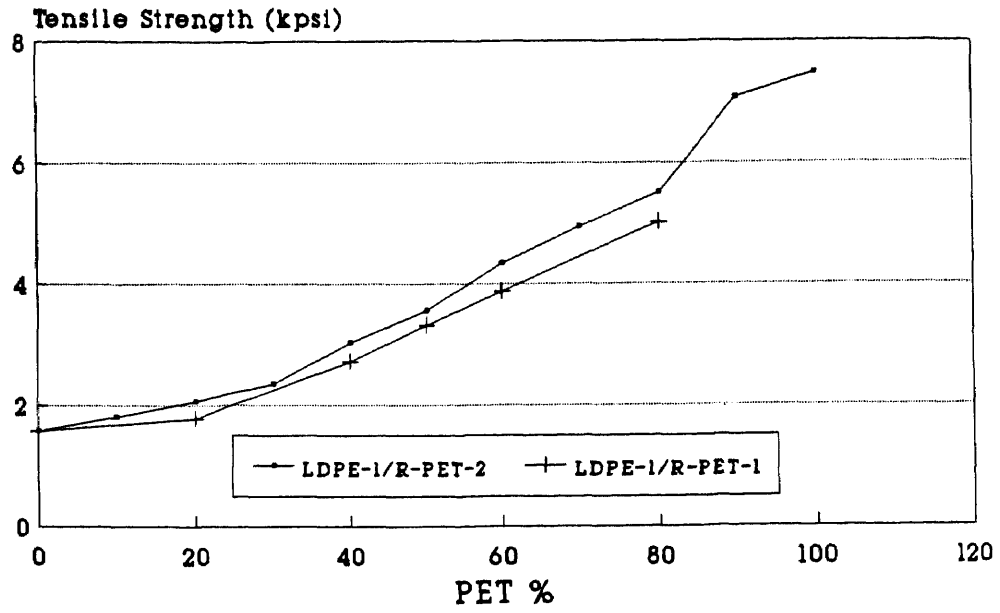

Fig. 4.83 Tensile Strength of LDPE-1/ R-PET Blends as a Function of R-PET Percentage in the Blend.

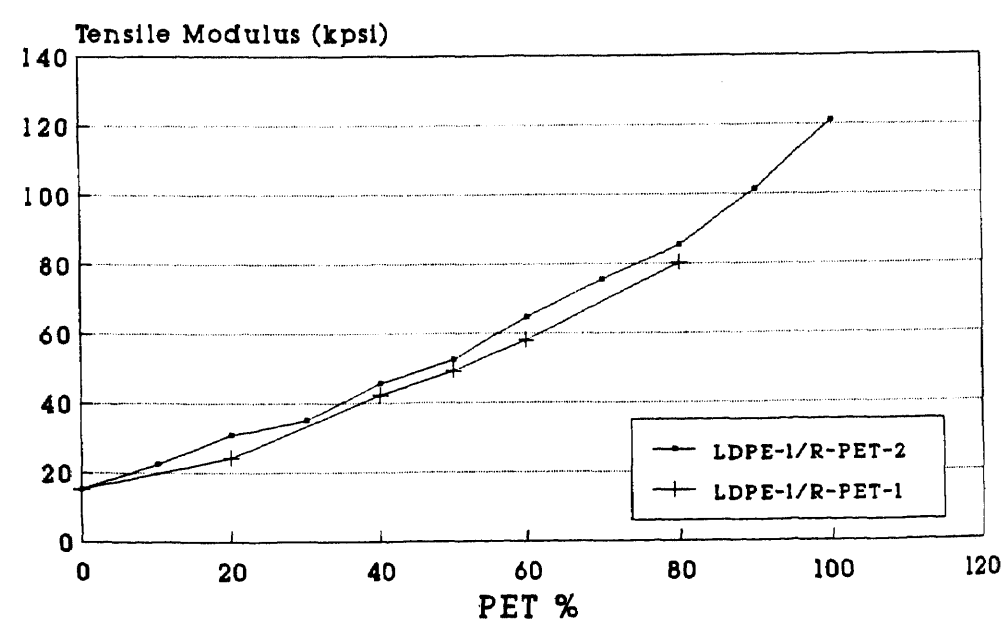

Fig. 4.84 Tensile Modulus of LDPE-1/ R-PET Blends as a Function of R-PET Percentage in the Blend.

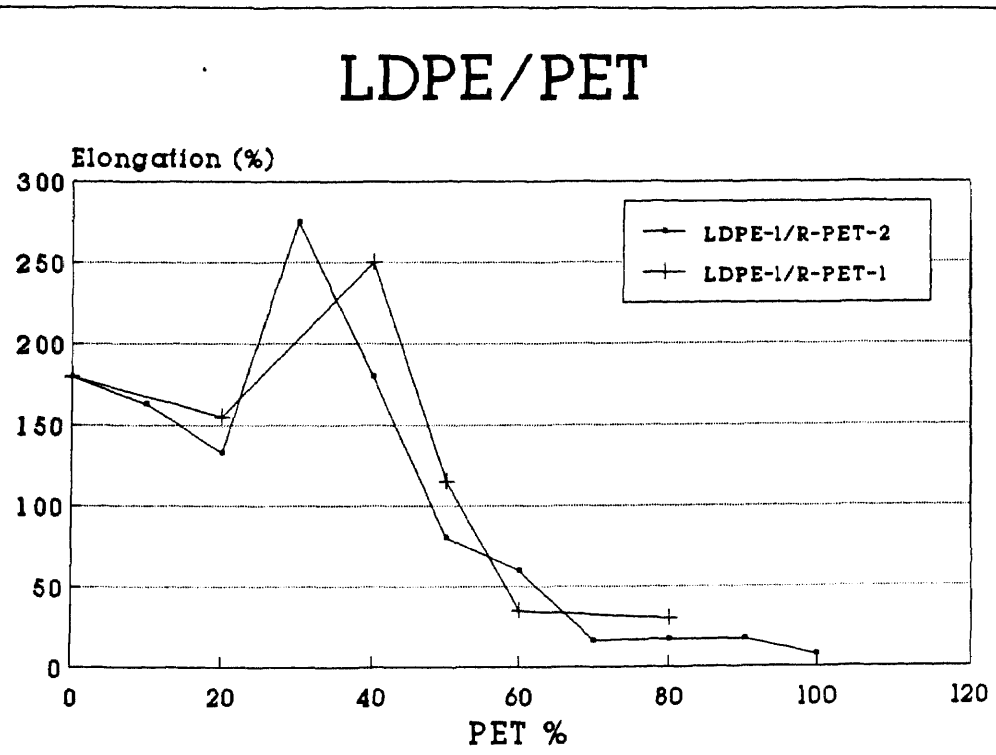

Fig. 4.85 Elongation of LDPE-1/R-PET Blends as a Function of R-PET Percentage in the Blend.

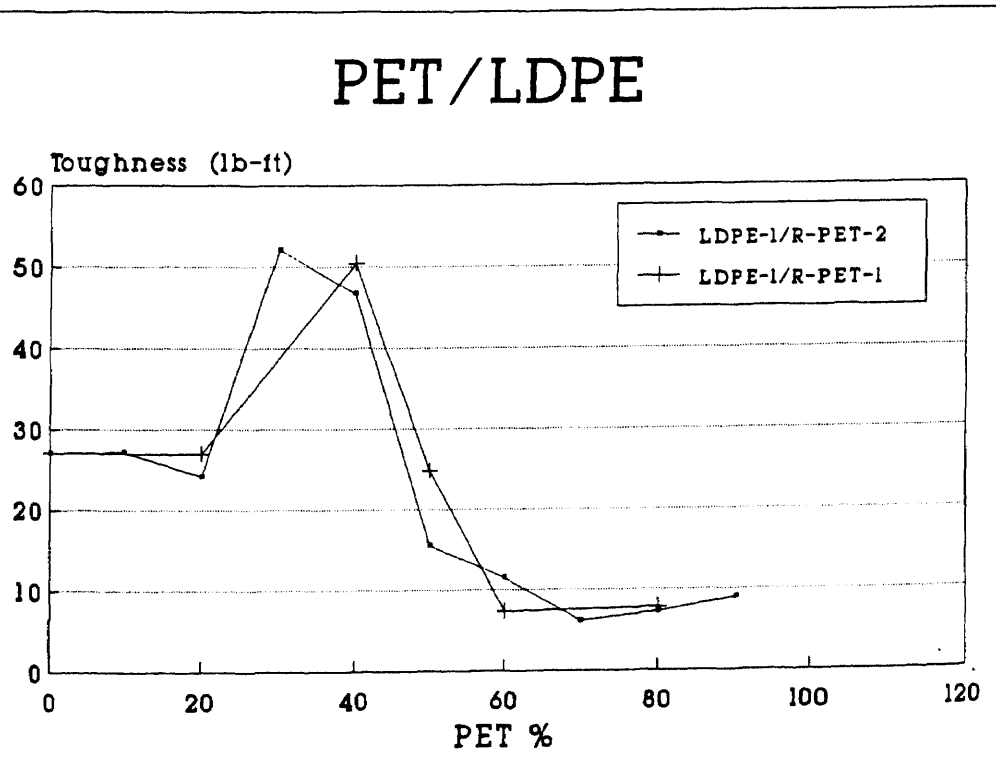

Fig. 4.86 Toughness of LDPE-1/R-PET Blends as a Function of R-PET Percentage in the Blend.

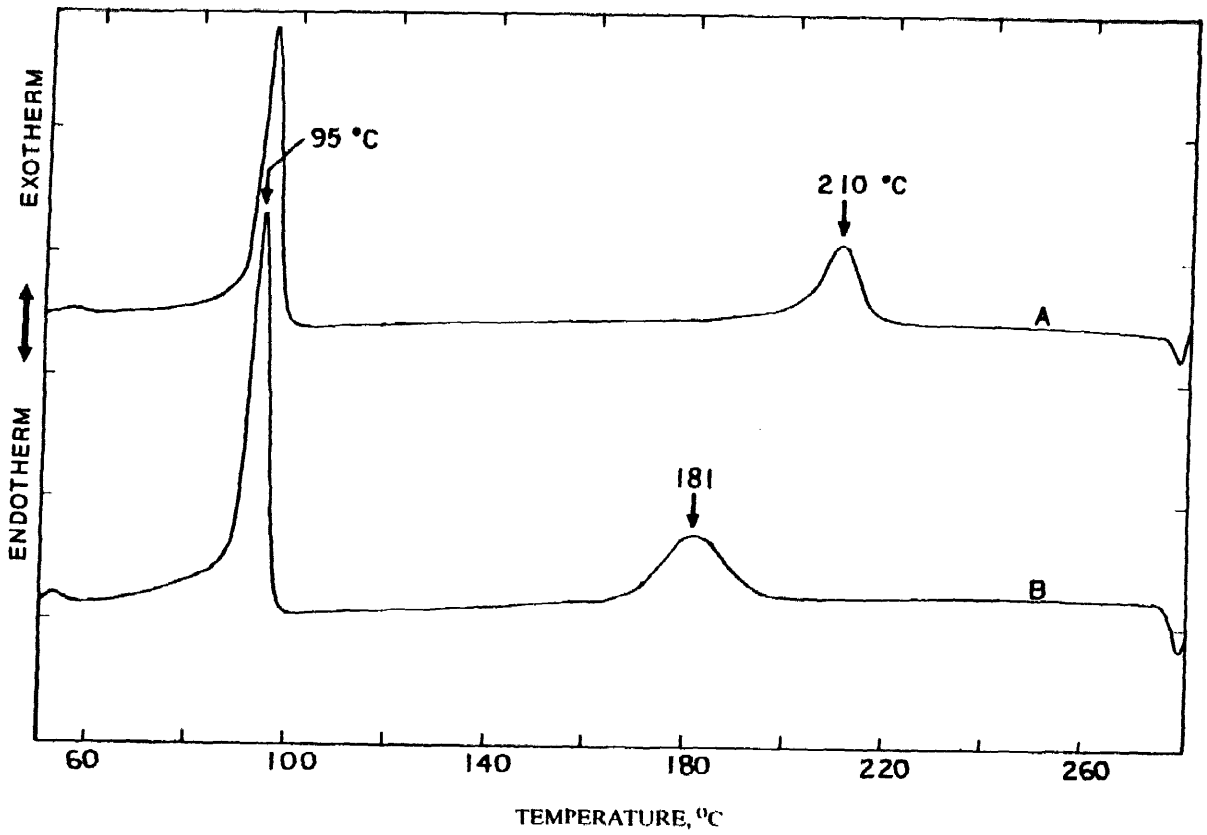

Figure 4.87 DSC Cooling Scans for LDPE/R-PET Blends.
(scan rate: 20 °C/min).
A: 50% LDPE-1/50% R-PET-2;
B: 50% LDPE-1/50% R-PET-1

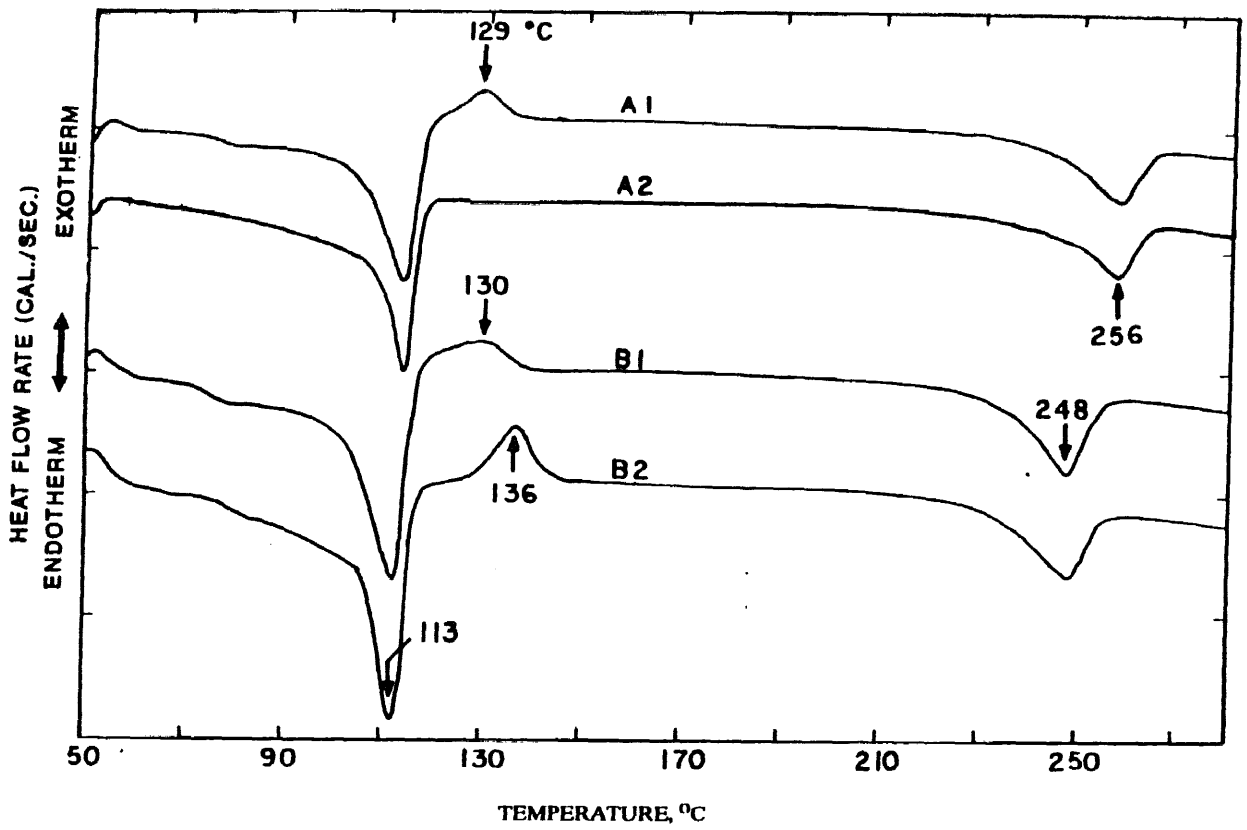

Figure 4.88 DSC Heating Scans for 50% LDPE-1/50% R-PET Blends (scan rate: 20 °C/min).
Curve A1: R-PET-2, original sample.
Curve A2: R-PET-2, sample quenched from 280 to 50 °C;
Curve B1: R-PET-1, original sample.
Curve B2: R-PET-1, sample quenched from 280 to 50 °C

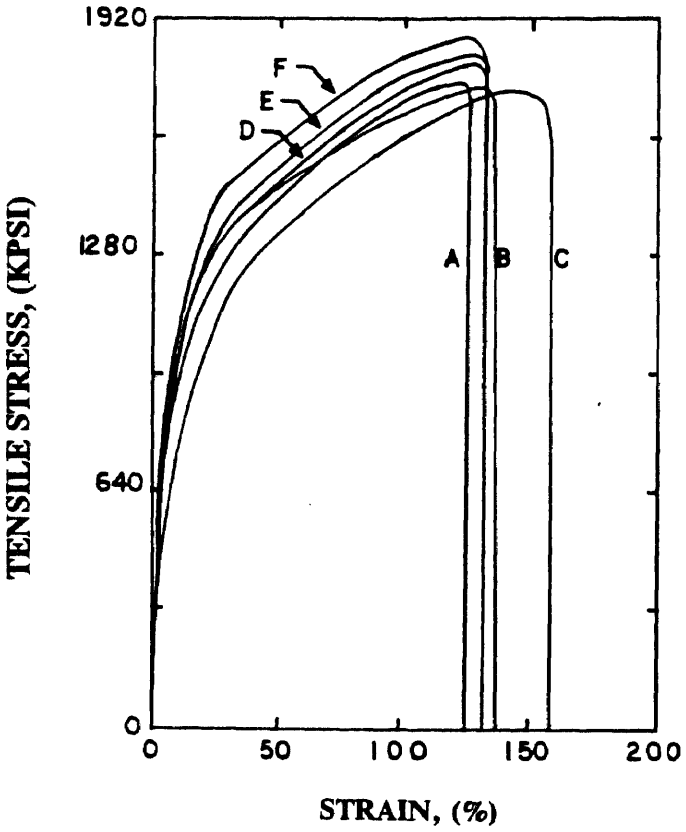

Figure 4.89 Stress-Strain Curves by Tensile Testing for:
Pure LDPE-2 (curve C);
90% LDPE-2/10% R-PET-2 (curve E);
blend as in curve E with 2% AClyn resin
(276A: curve A; 262A: curve B;
272A: curve D; 285A: curve F)

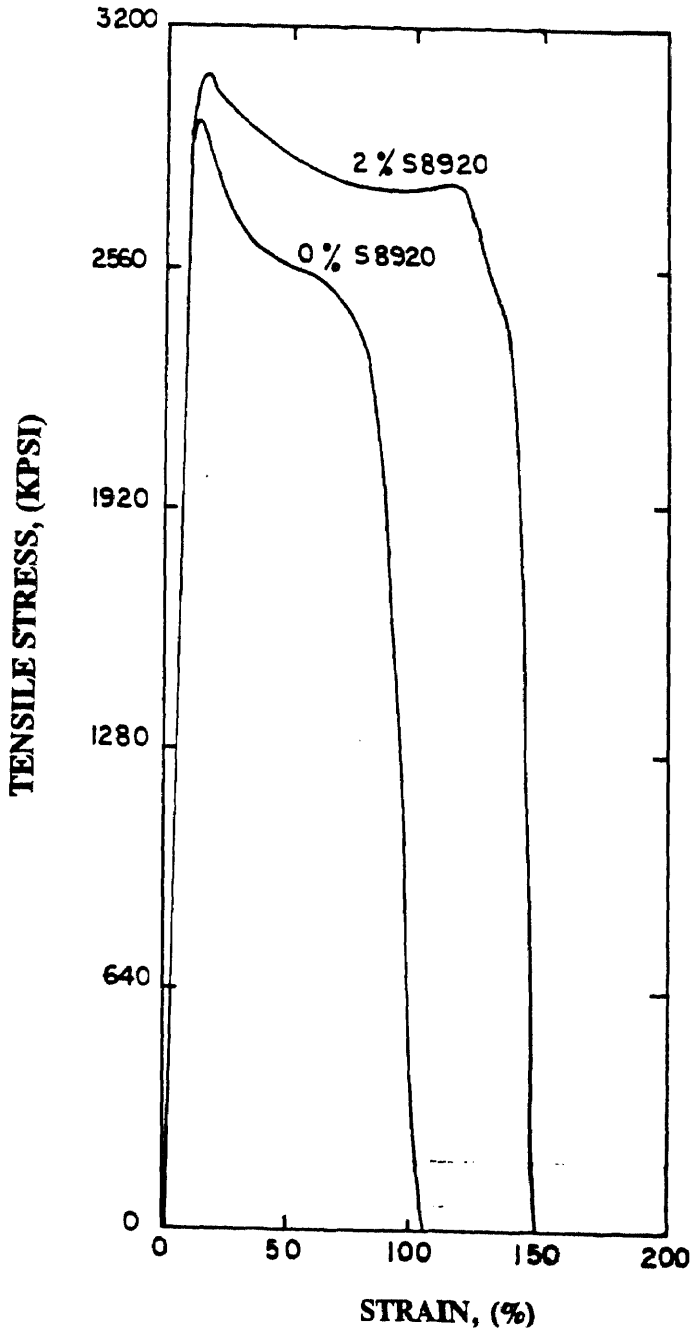

Figure 4.90 Stress-Strain Curves by Tensile Testing for 50% LDPE-2/50% R-PET-1 Blends with Surlyn S8920 Ionomer (Stain rate: 1 in/min)

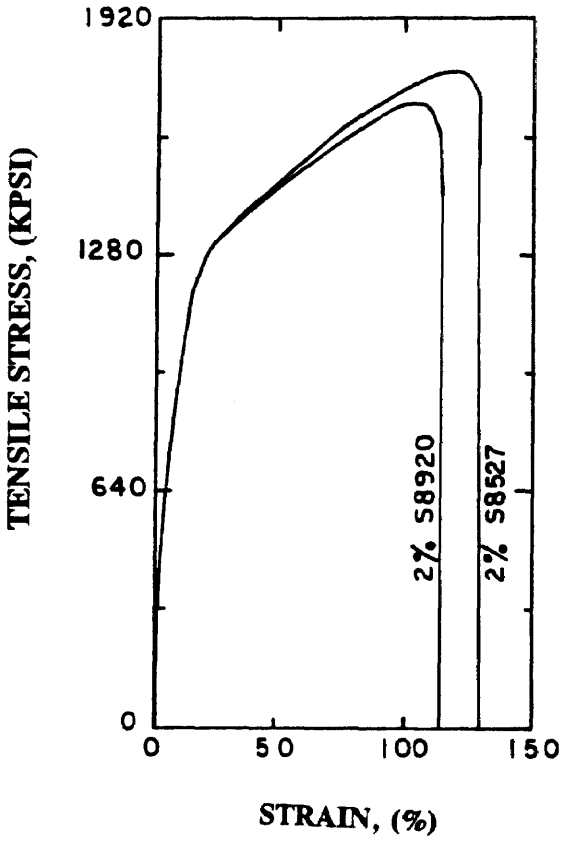

Figure 4.91 Stress-Strain Curves by Tensile Testing for 90% LDPE-2/10% R-PET-1 Blends with 2% Surlyn Ionomers (Stain rate: 1 in/min)

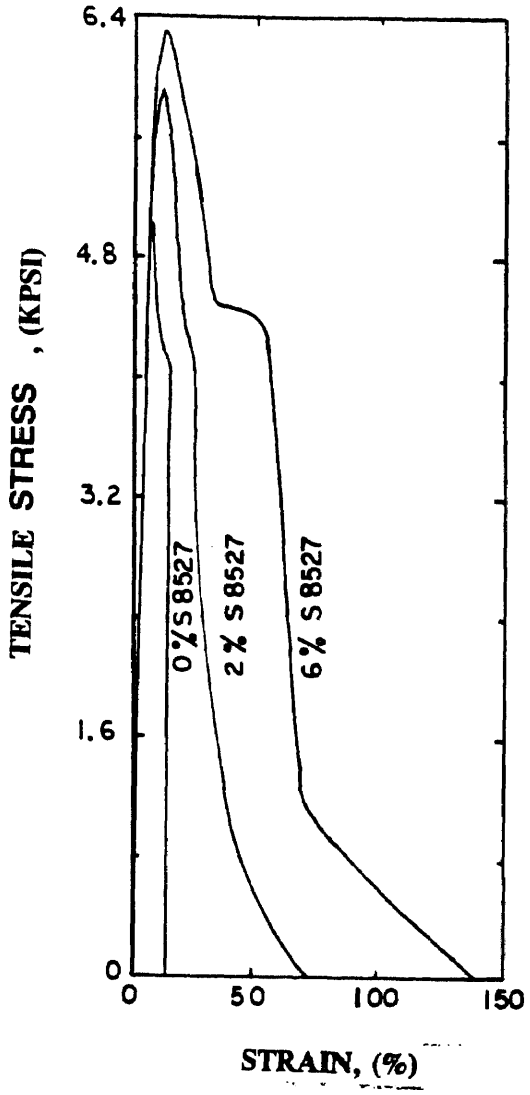

Figure 4.92 Stress-Strain Curves by Tensile Testing for 20% LDPE-1/80% R-PET-2 with Different Contents of S8527 Ionomer (Stain rate: 1 in/min)

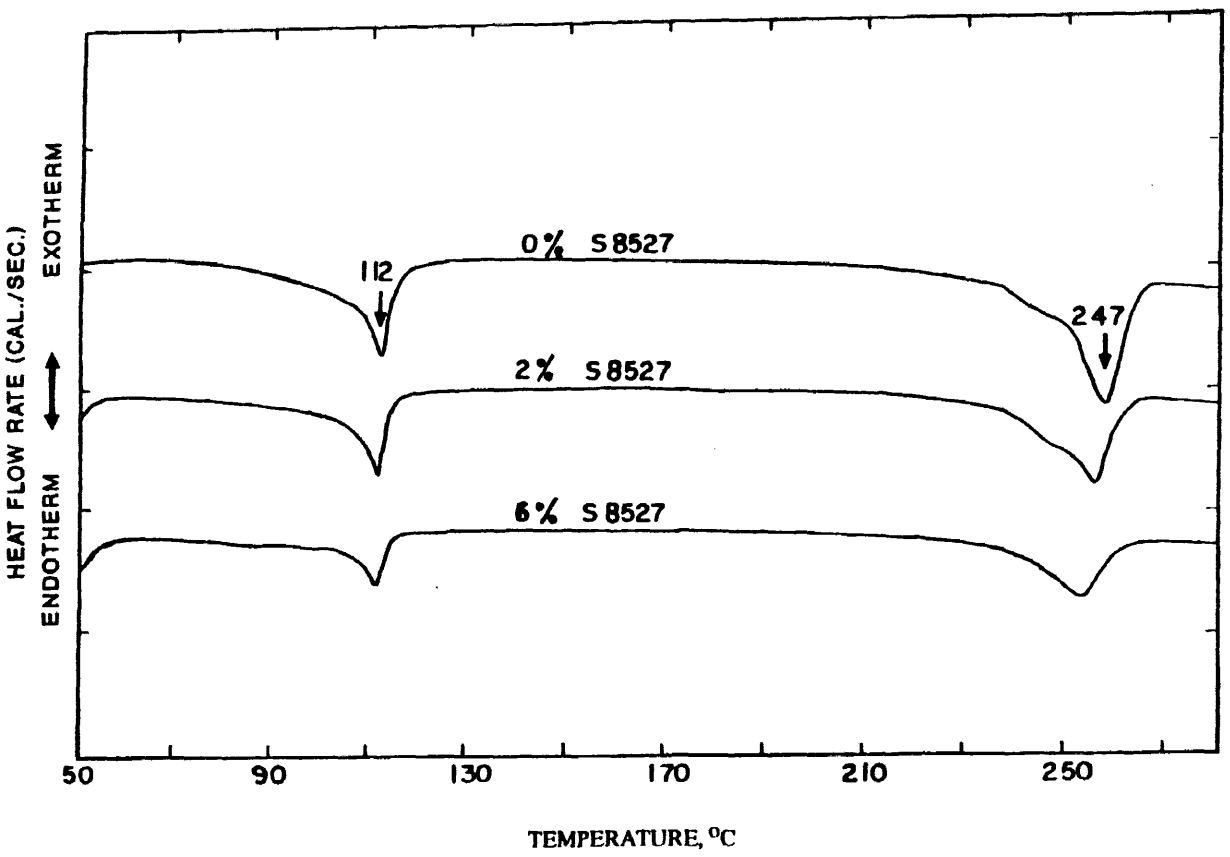

Figure 4.93 DSC Heating Scans for 20% LDPE-1/80% R-PET-2 Blends with Different Contents of S8527 Ionomer (scan rate: 20 °C/min)

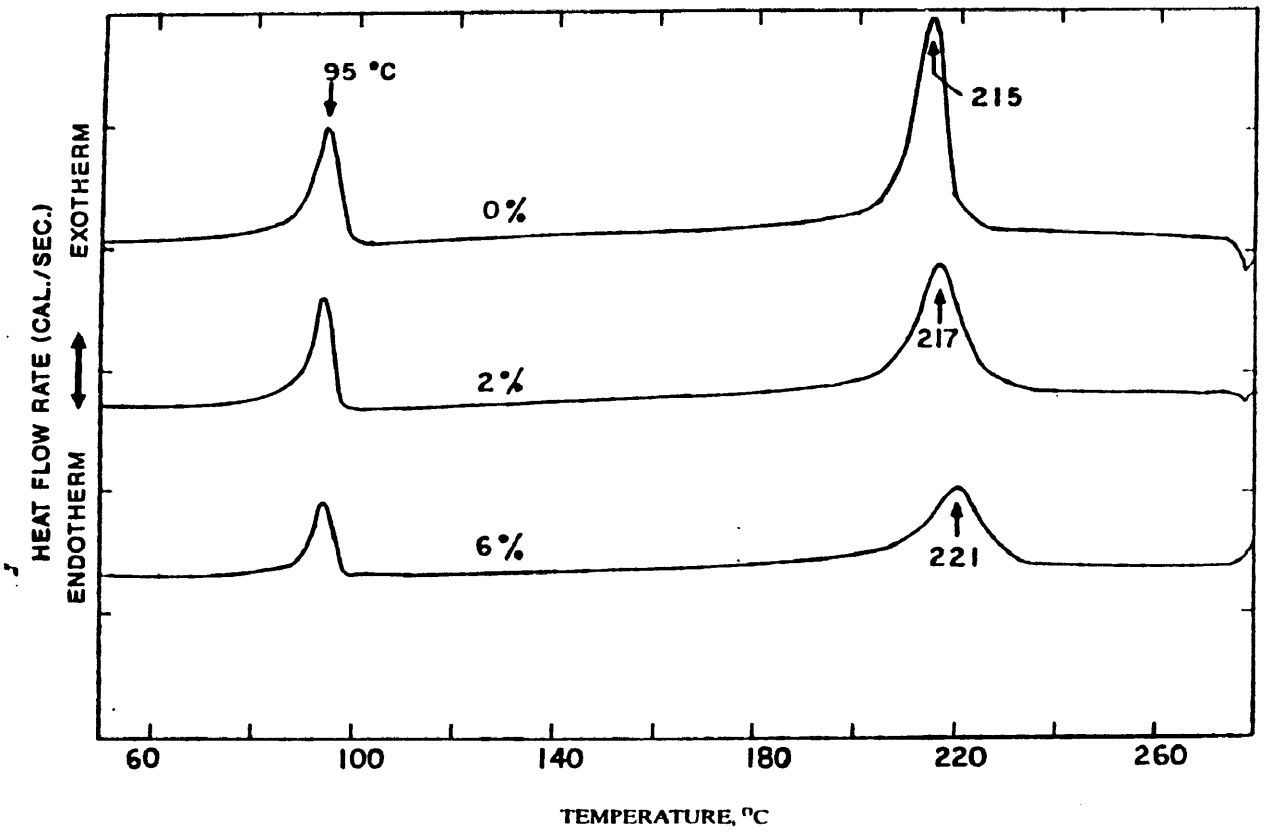

Figure 4.94 DSC Cooling Scans for 20% LDPE-1/80% R-PET-2 Blends with Different Contents of S8527 Ionomer (scan rate: 20 °C/min)

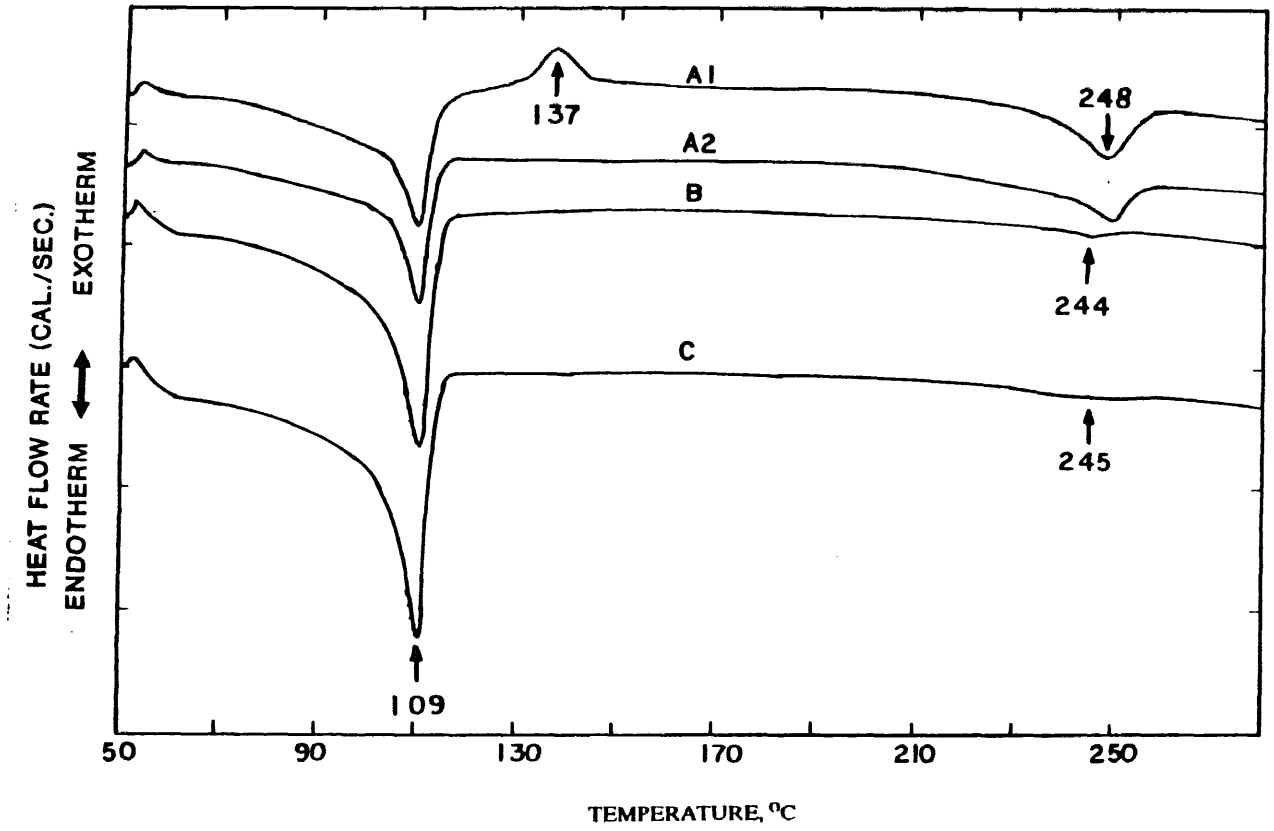

Figure 4.95 DSC Heating Scans for LDPE-2/R-PET-1 Blends with Surlyn Ionomers (scan rate: 20 °C/min)
A1: 50/50/0
A2: 50/50/2% S8920
B: 90/10/2% S8920
C: 90/10/2% S8527

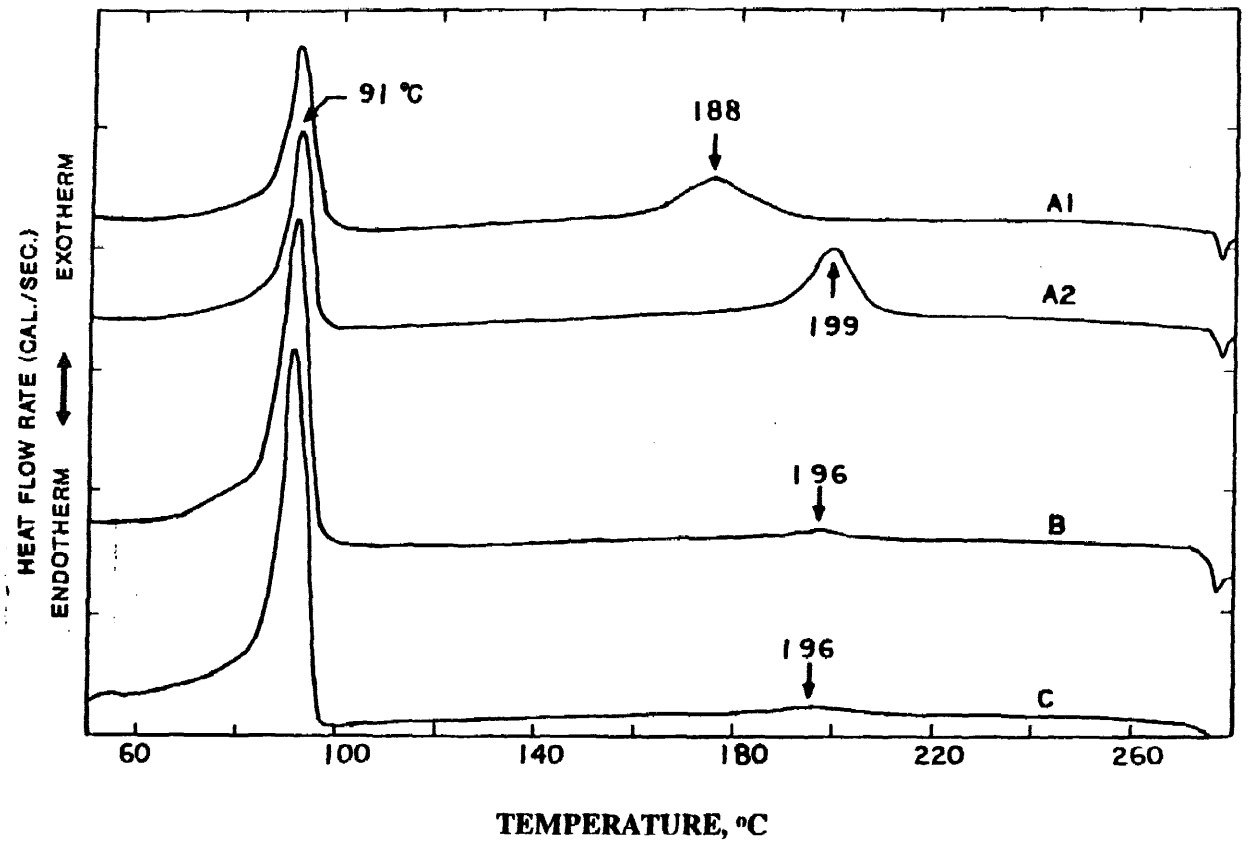

Figure 4.96 DSC Cooling Scans for LDPE-2/R-PET-1 Blends with Surlyn Ionomers (scan rate: 20 ^{o}C/min)

A1: 50/50/0
A2: 50/50/2% S8920
B: 90/10/2% S8920
C: 90/10/2% S8527

Pictures 4.1 - 4.14

Spherulites of PET observed by optical microscopy between crossed polarizers. Nonisothermal crystallization (slow cooling) form melt.

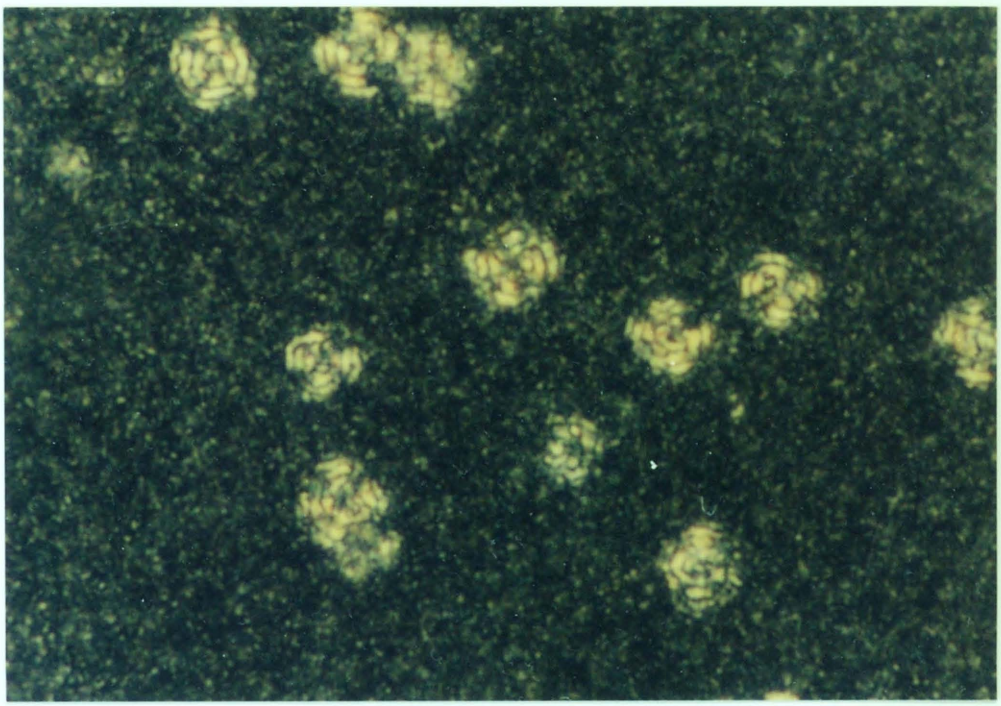

Picture 4.1 bR-PET (x200)

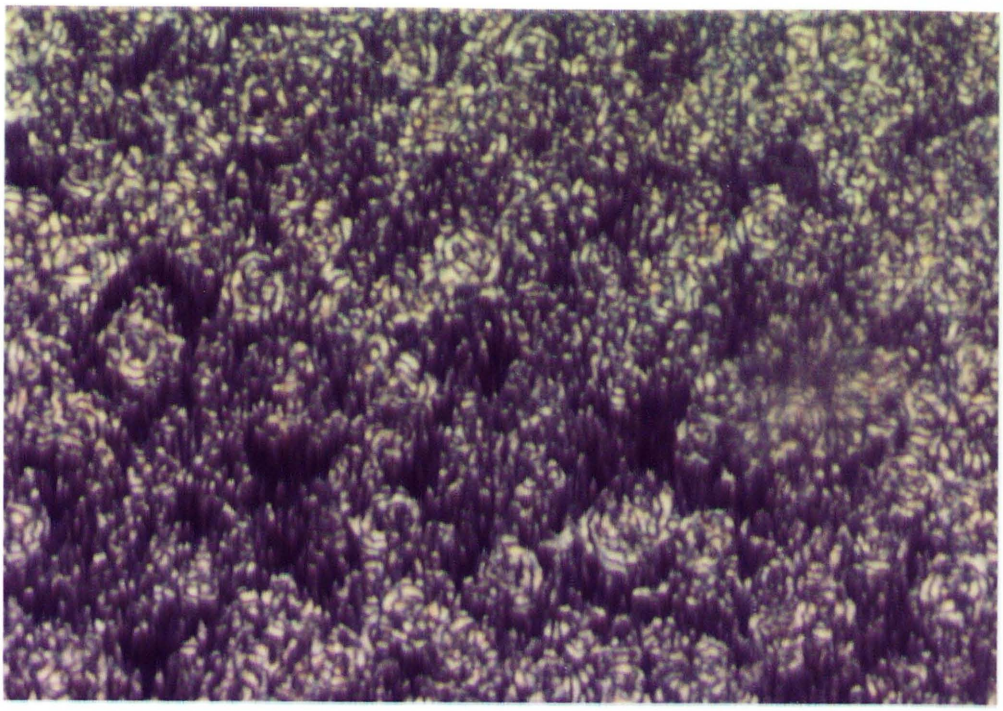

Picture 4.2 aR-PET (x200)

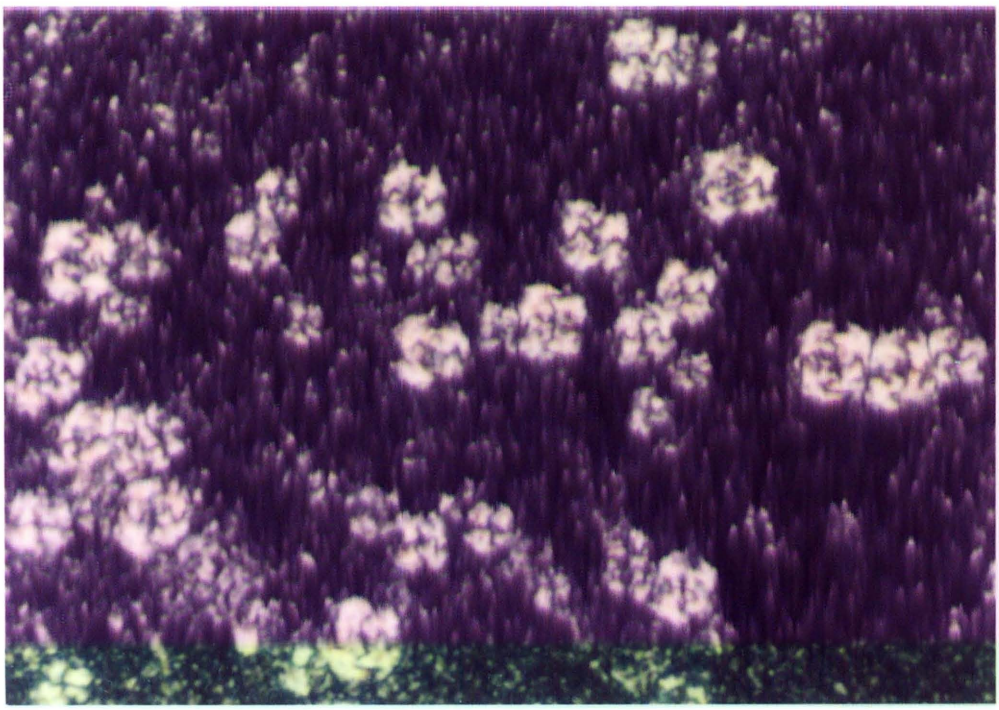

Picture 4.3 bG-PET (x200)

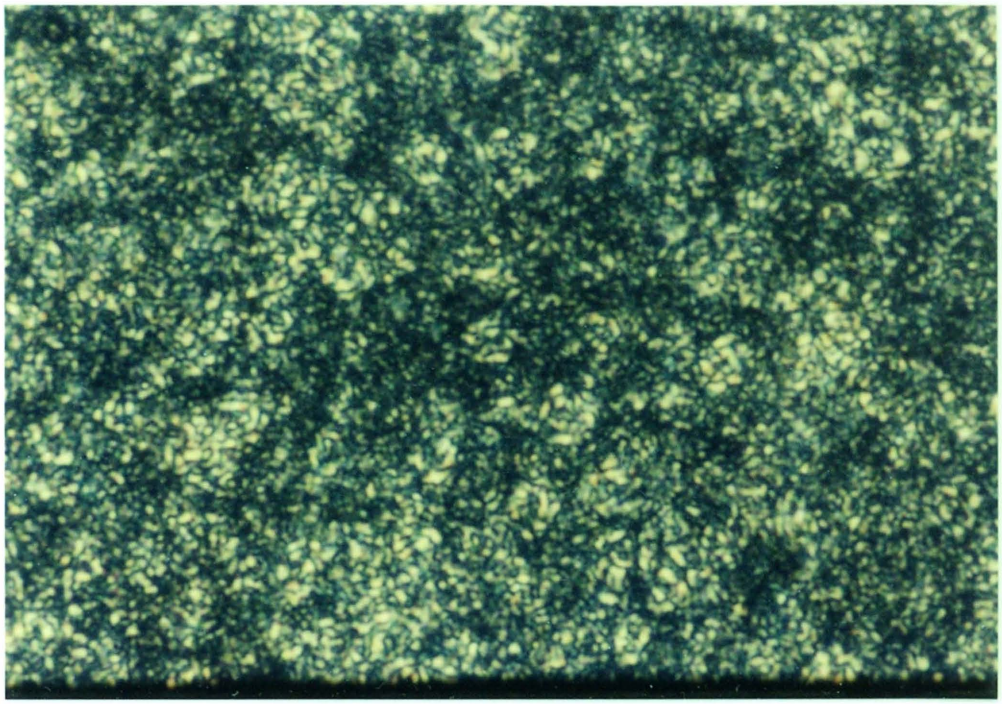

Picture 4.4 aG-PET (x200)

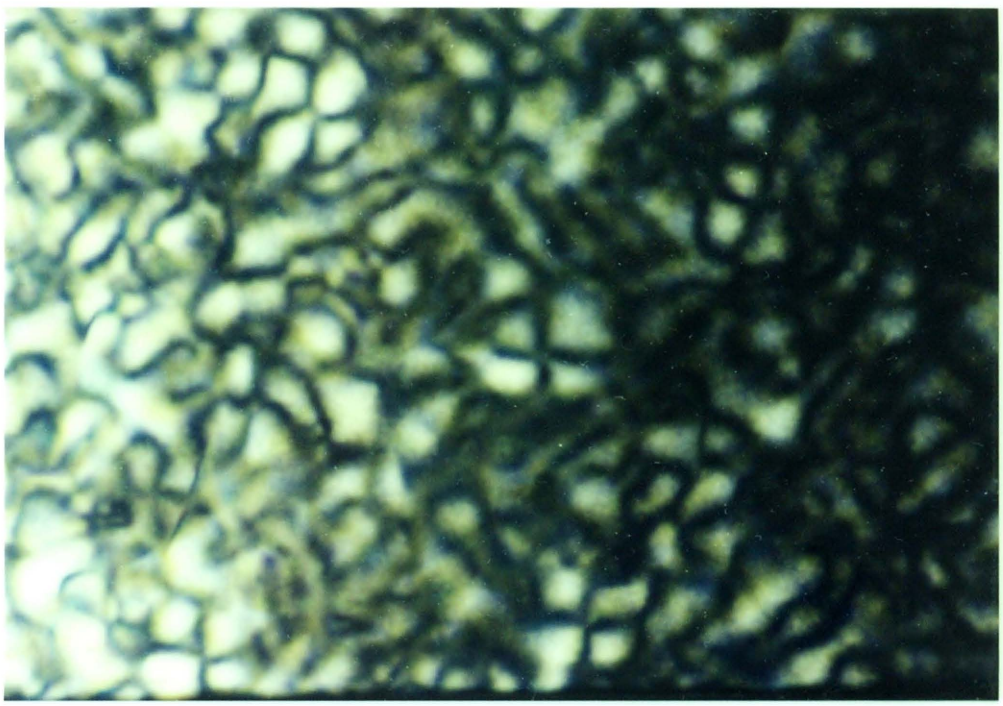

Picture 4.5 bV-PET (x200)

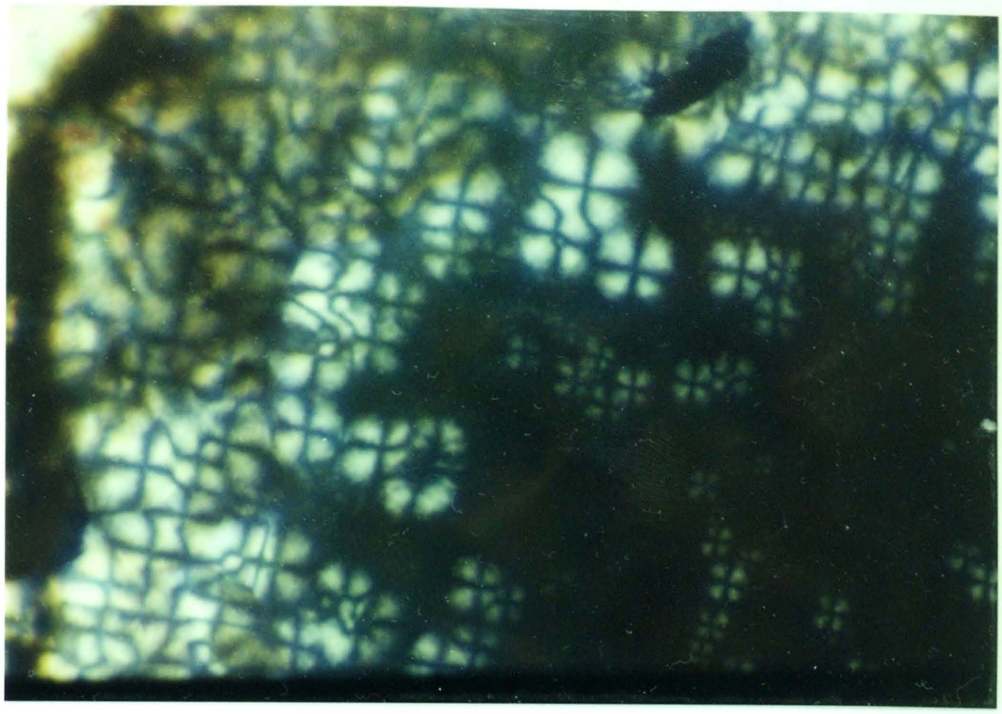

Picture 4.6 bV-PET (x200)

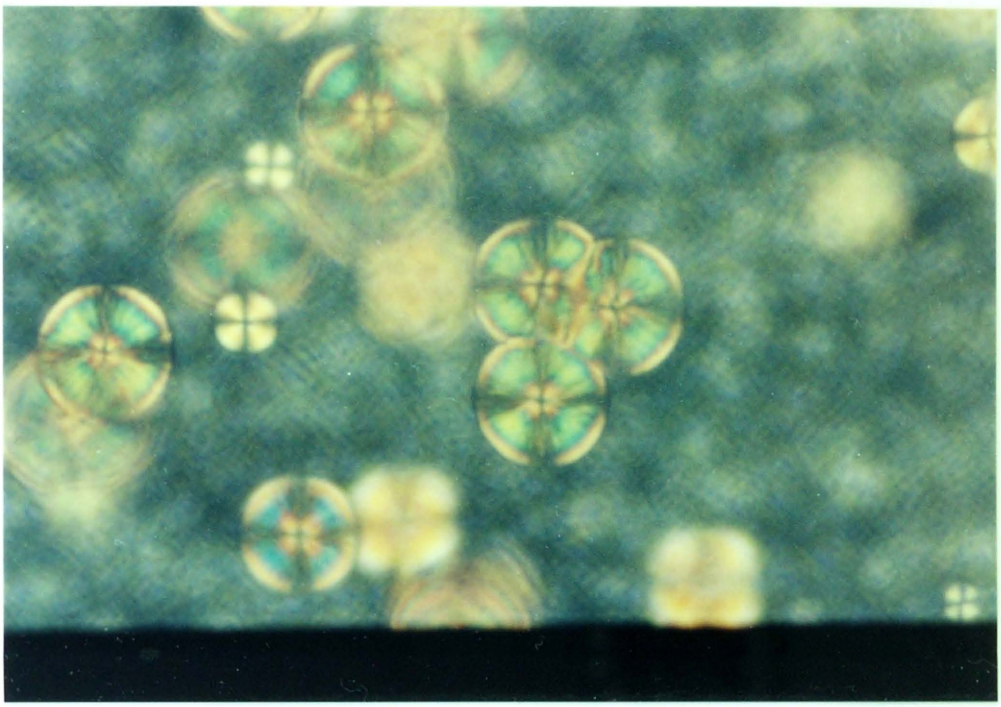

Picture 4.7 bV-PET (x200)

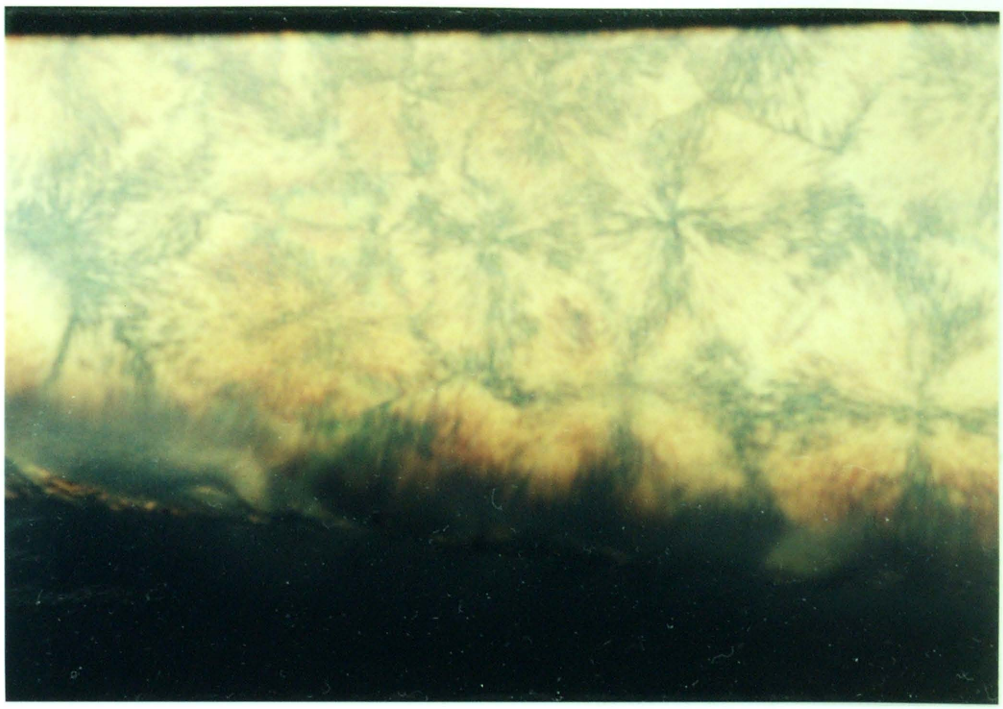

Picture 4.8 bV-PET (x200)

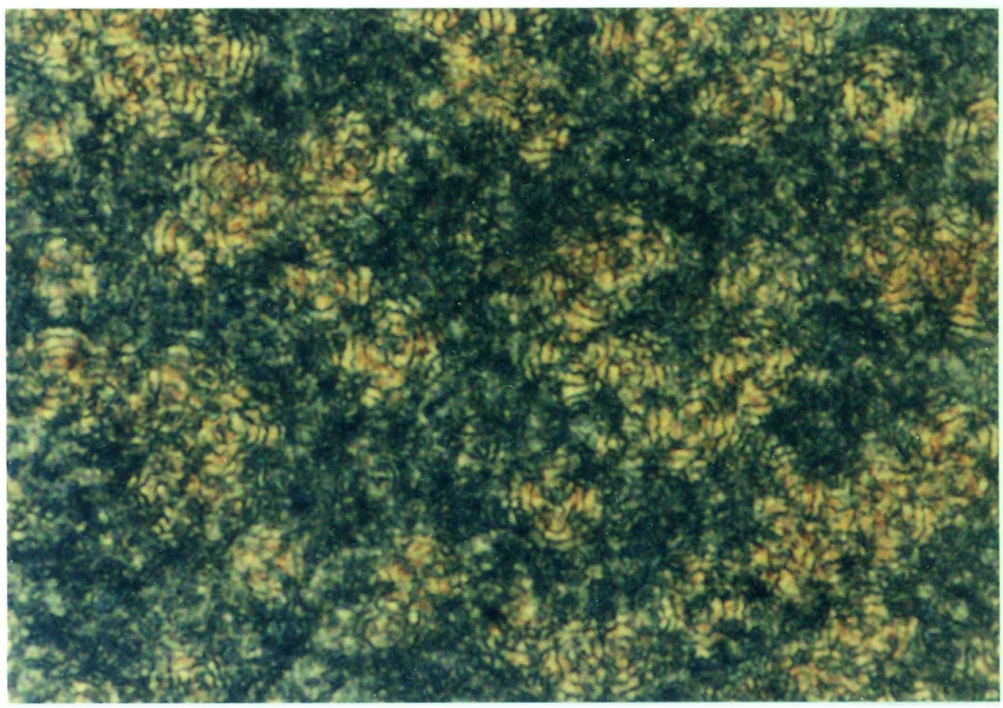

Picture 4.9 aV-PET (x200)

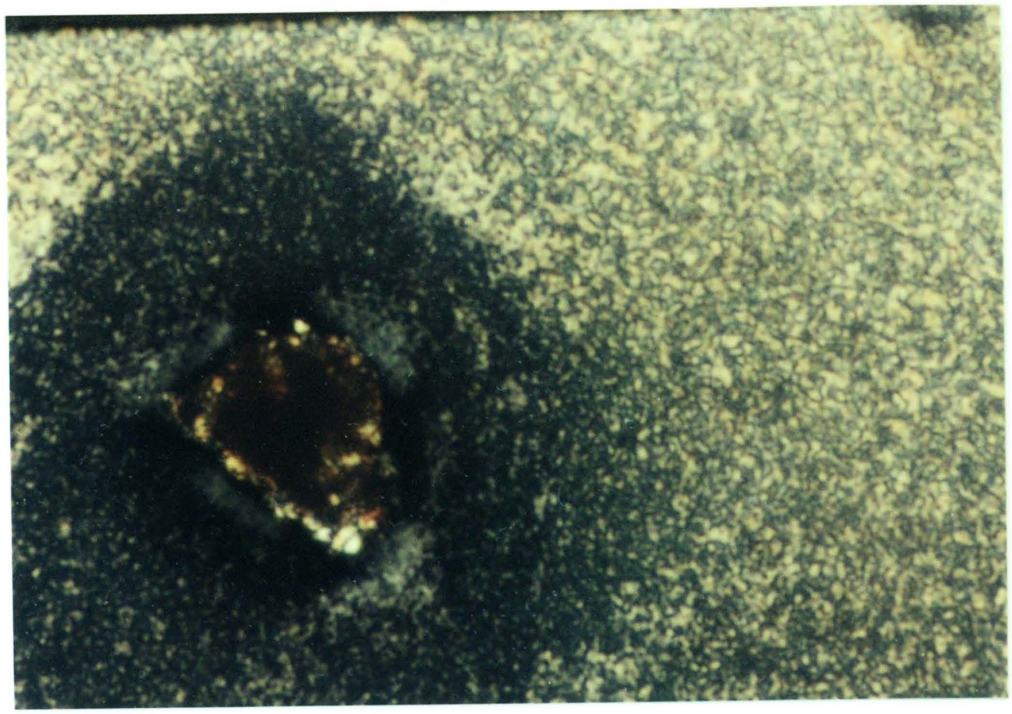

Picture 4.10 R-PET with 0.063% Na_2CO_3 (x200)

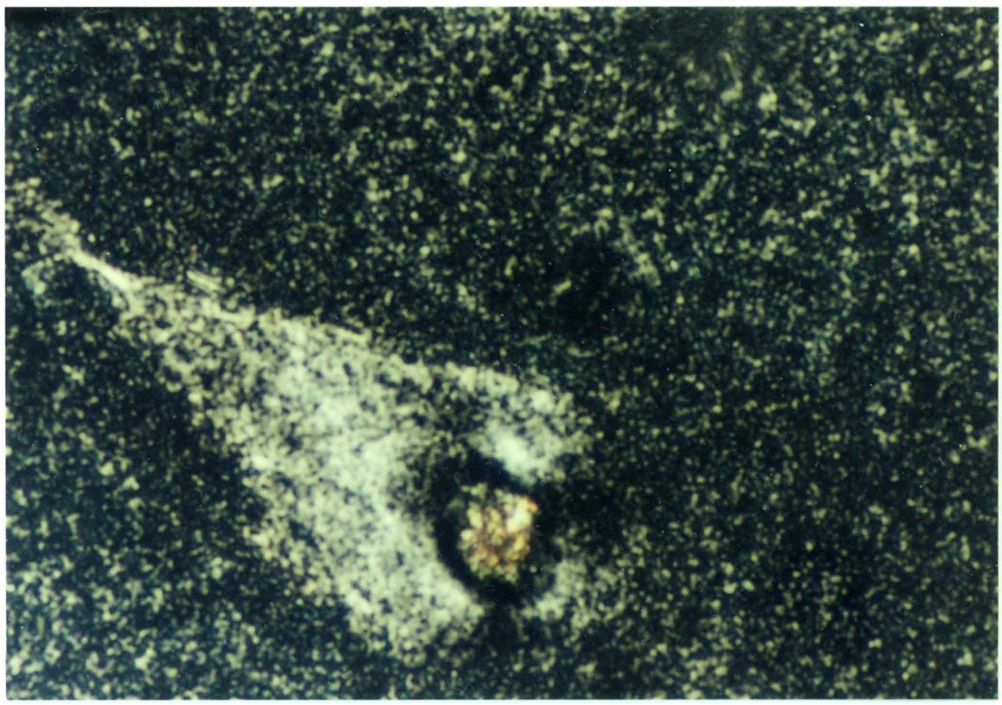

Picture 4.11 R-PET with 0.3% Na_2CO_3 (x200)

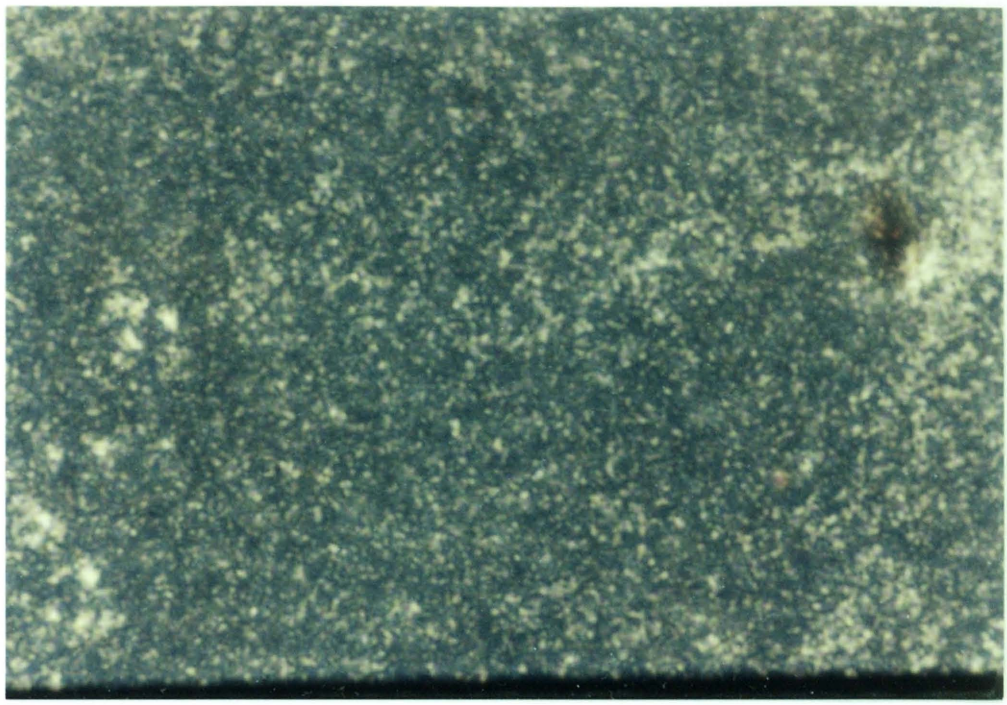

Picture 4.12 R-PET with 0.5% Na_2CO_3 (x200)

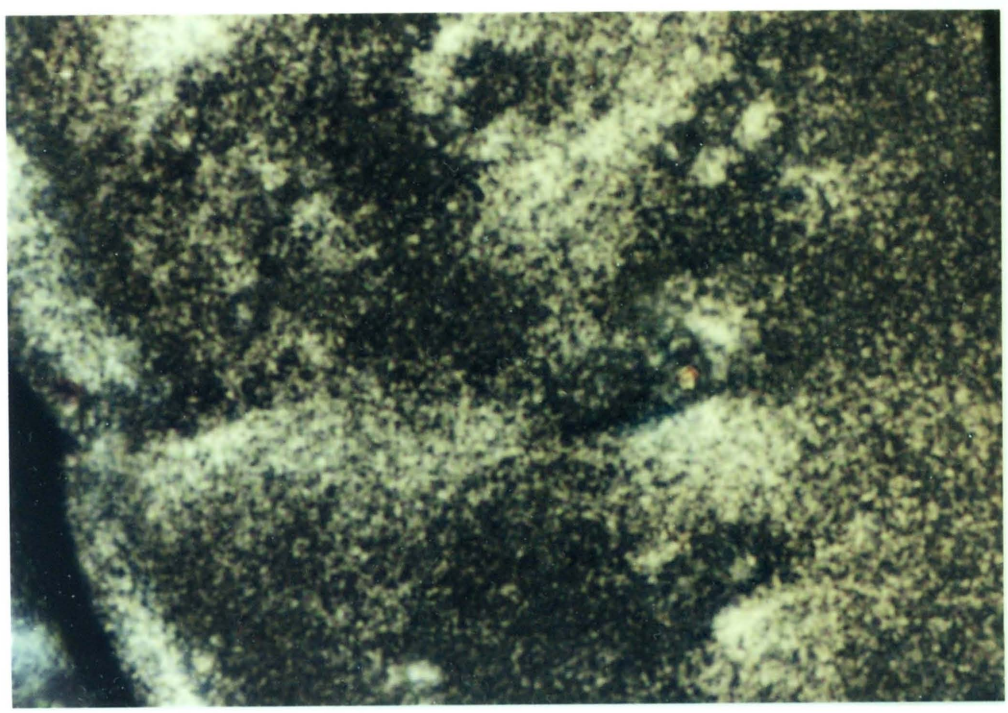

Picture 4.13 R-PET with 1.0% Na_2CO_3 (x200)

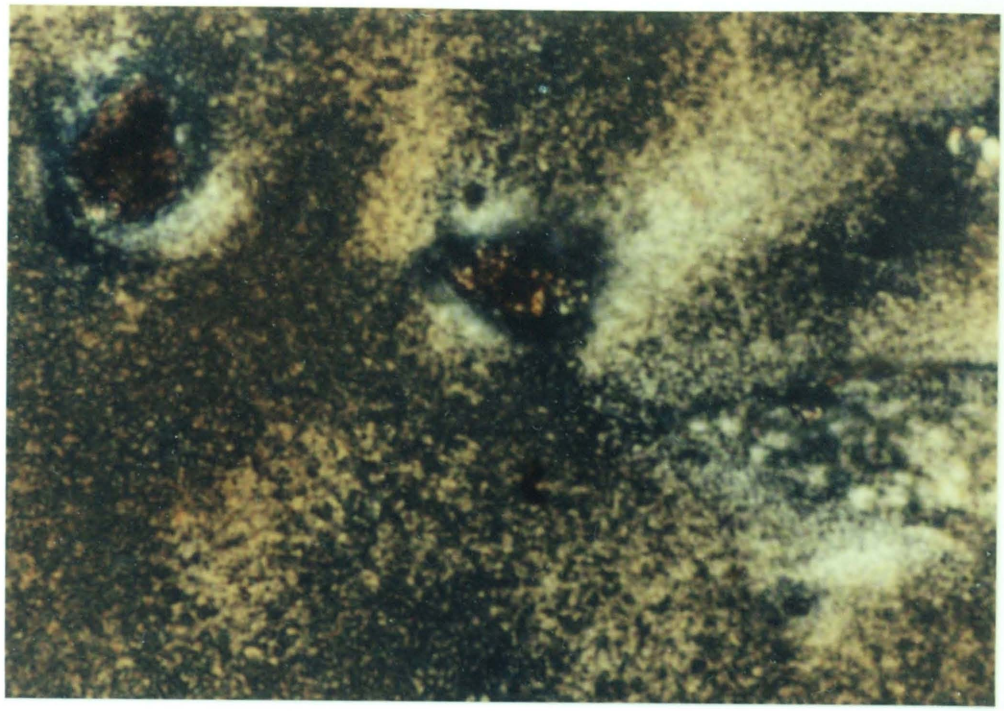

Picture 4.14 G-PET with 0.5% Na_2CO_3 (x200) [see also Picture 4.15]

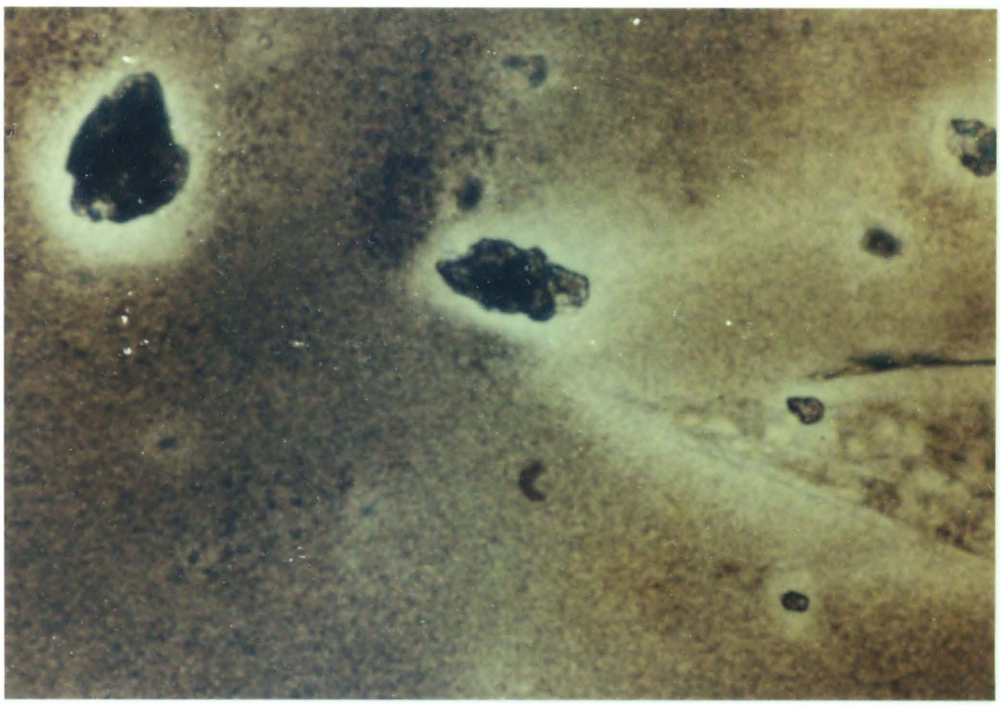

Picture 4.15 Spherulites of G-PET crystallized in the presence of 0.5% Na_2CO_3. Observation by optical microscopy without analyzer (x200). Nonisothermal crystallization (slow cooling) from melt. Location same as the one shown in Picture 4.14

Pictures 4.16 - 4.31

Spherulites of PET observed by optical microscopy between crossed polarizers. Isothermal crystallization from melt.

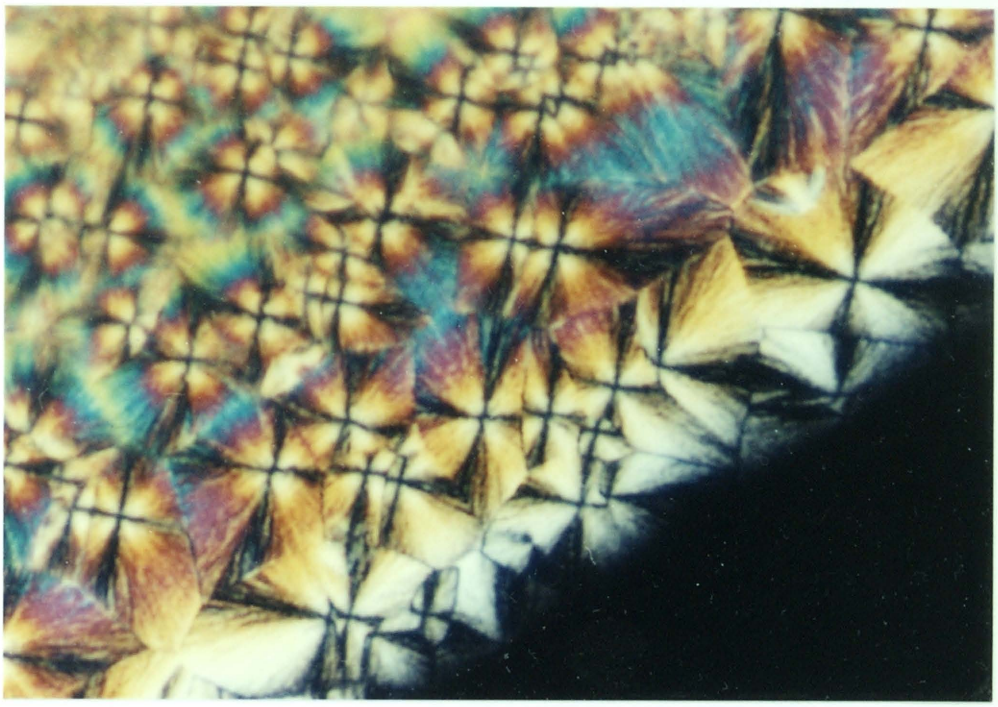

Picture 4.16 bV-PET crystallized at 240 °C (x200)

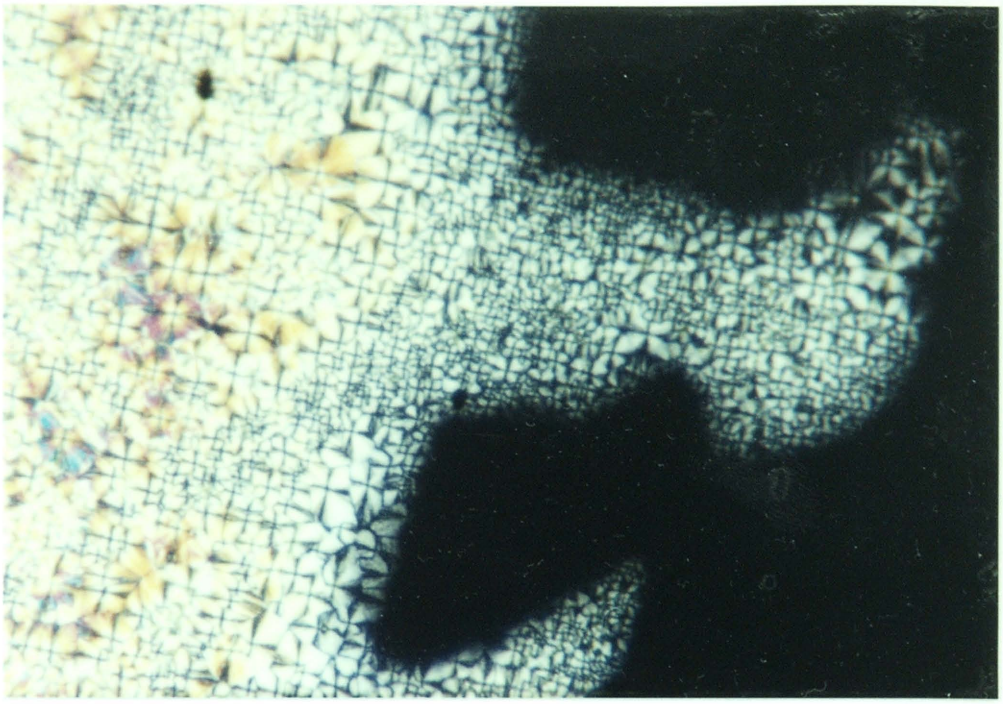

Picture 4.17 aV-PET crystallized at 240 °C (x100)

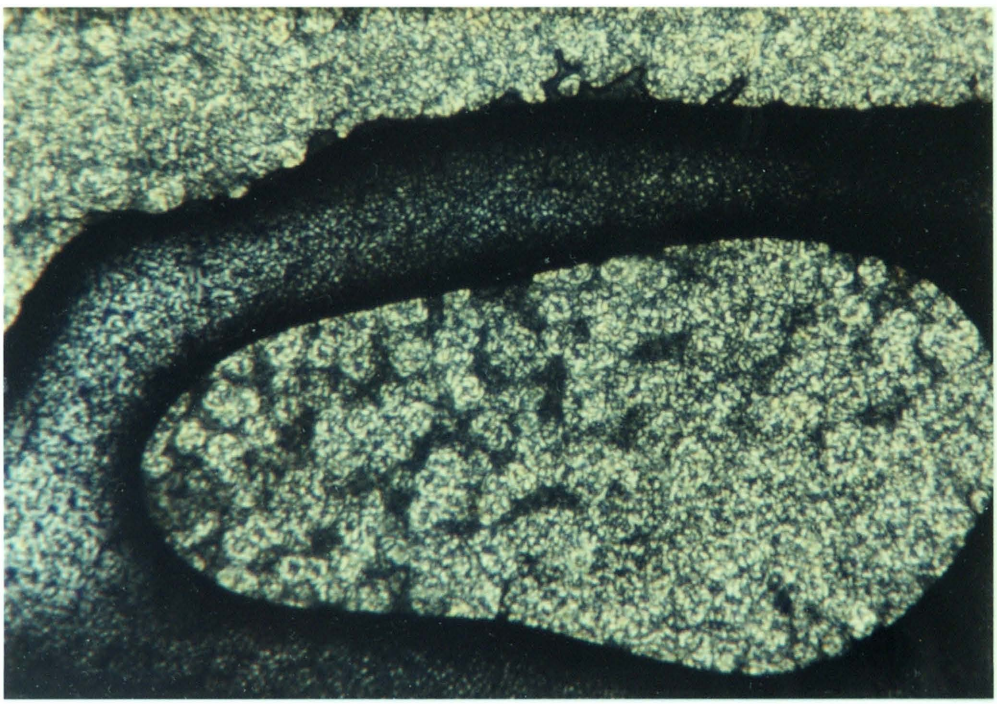

Picture 4.18 aV-PET crystallized at 240 °C (x100). Location different from the one shown in Picture 4.17

Picture 4.19 bR-PET crystallized at 240 °C (x200)

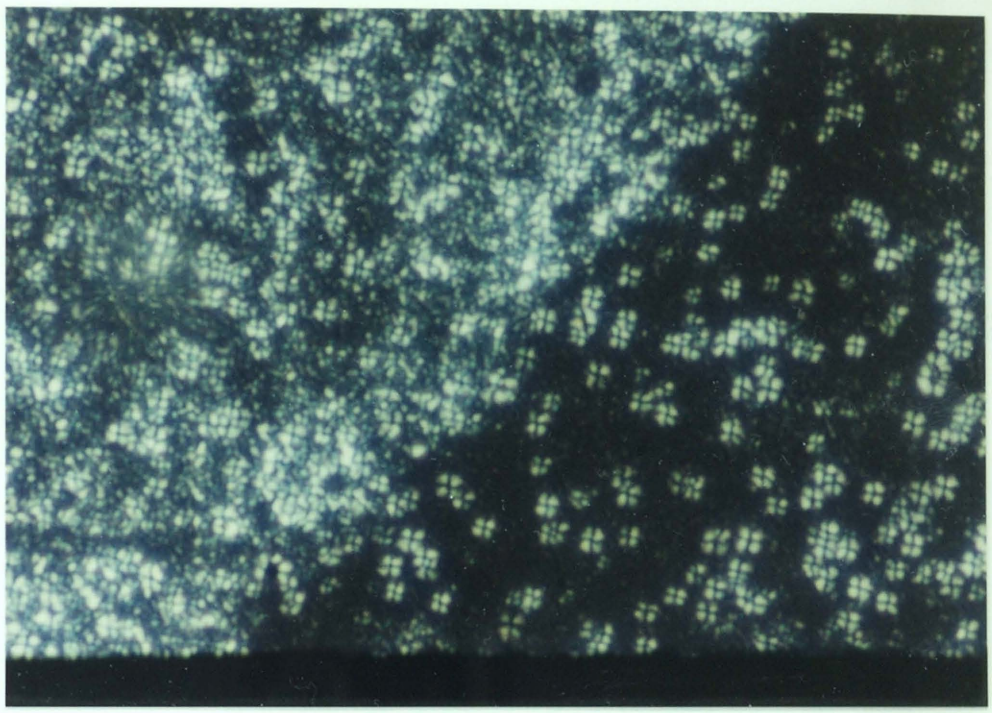

Picture 4.20 aR-PET crystallized at 240 °C (x200)

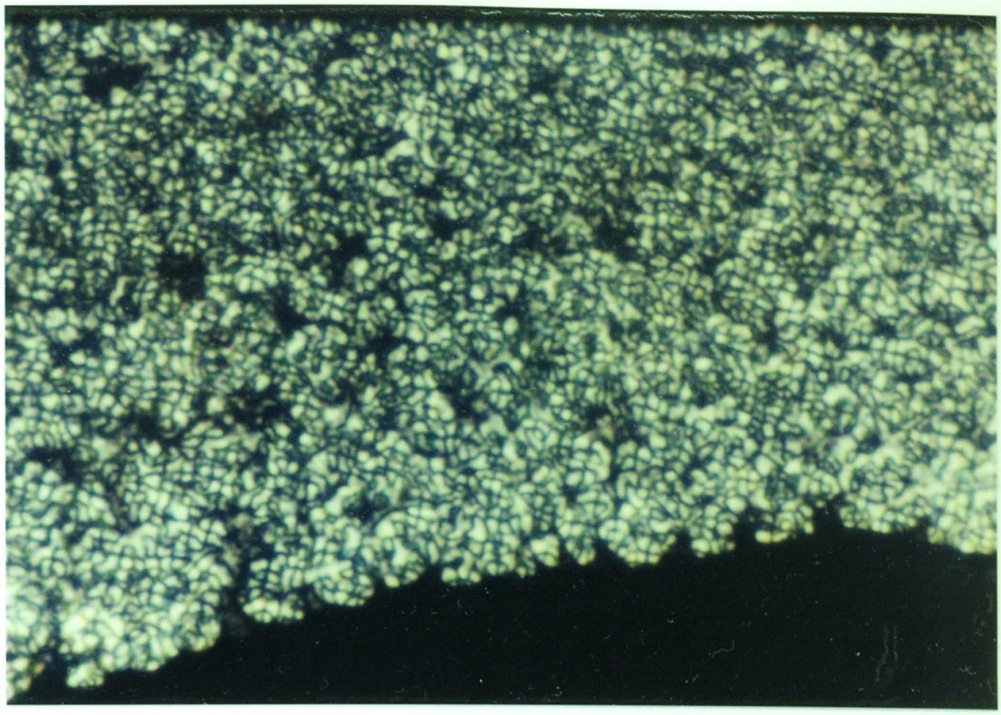

Picture 4.21 aR-PET crystallized at 240 °C (x200). Location different from the one shown in Picture 4.20

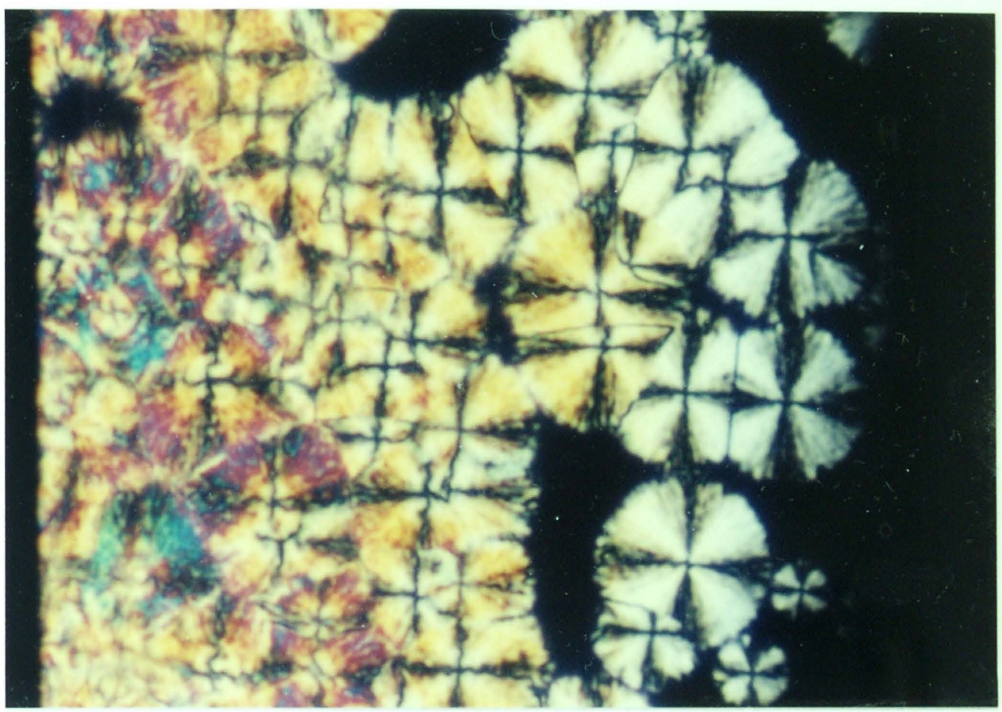

Picture 4.22 bG-PET crystallized at 230 °C (x200)

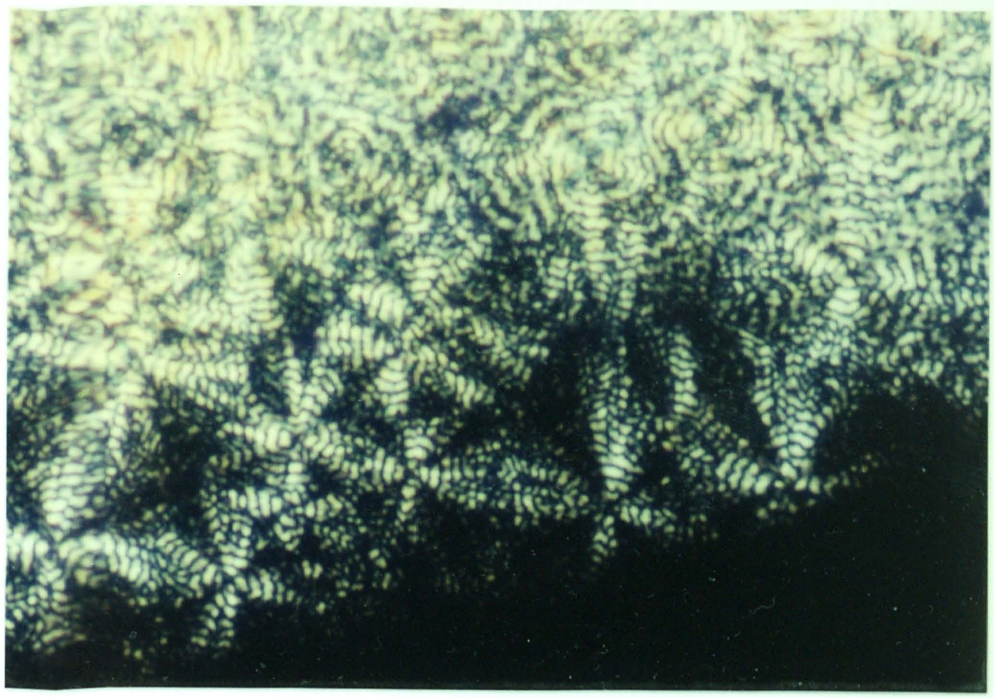

Picture 4.23 bG-PET crystallized at 230 °C (x200). Location different from the one shown in Picture 4.22

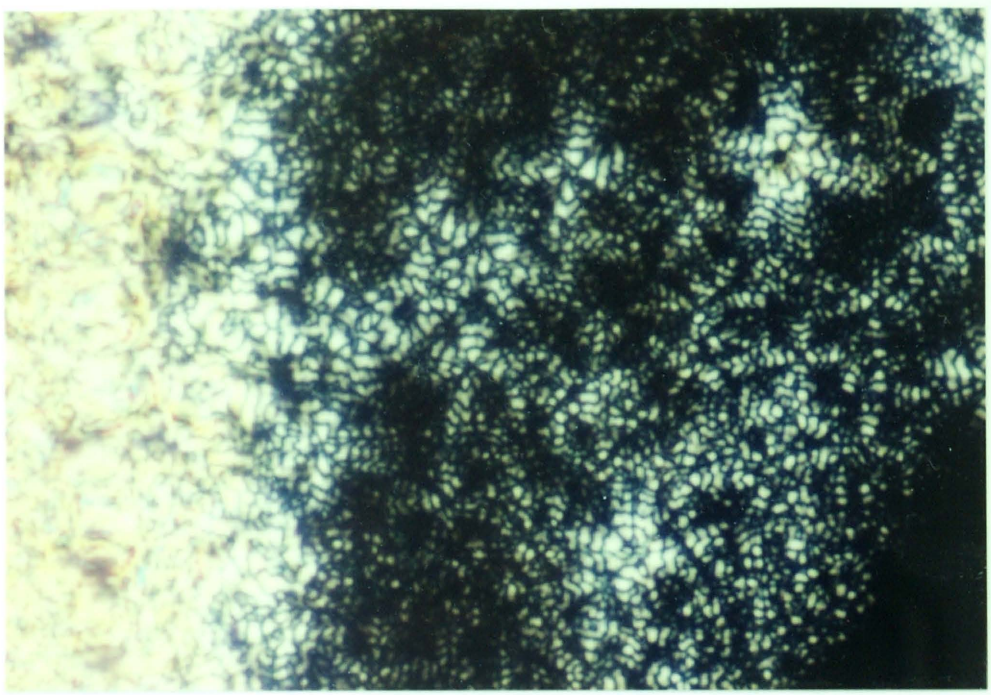

Picture 4.24 aG-PET crystallized at 240 °C (x200)

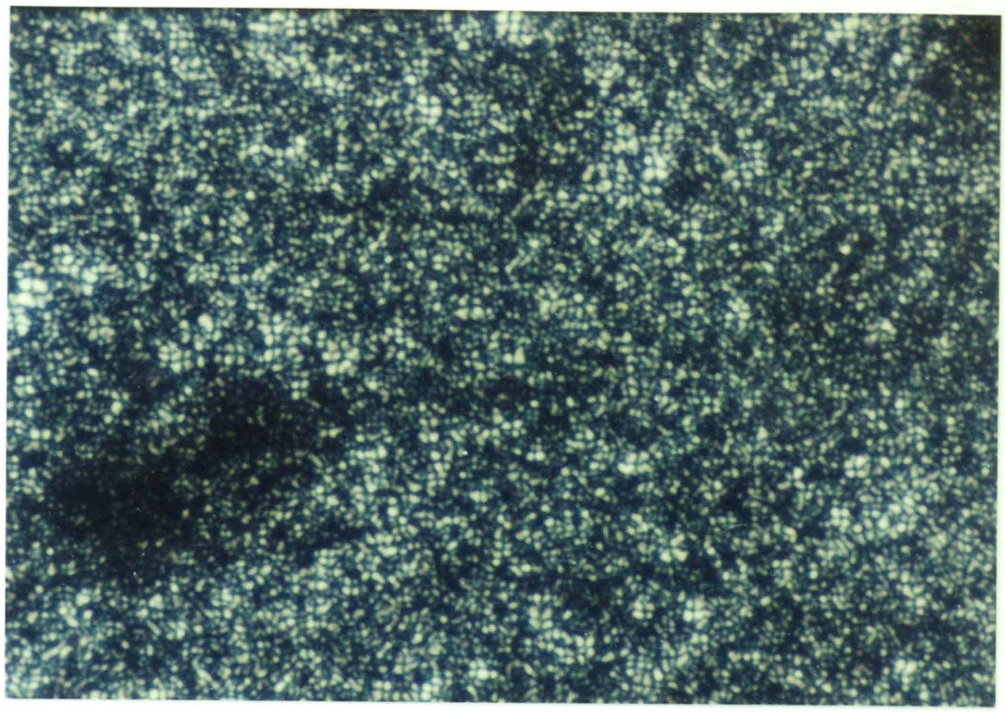

Picture 4.25 R-PET with 0.063% Na_2CO_3. Crystallization at 230 °C (x200)

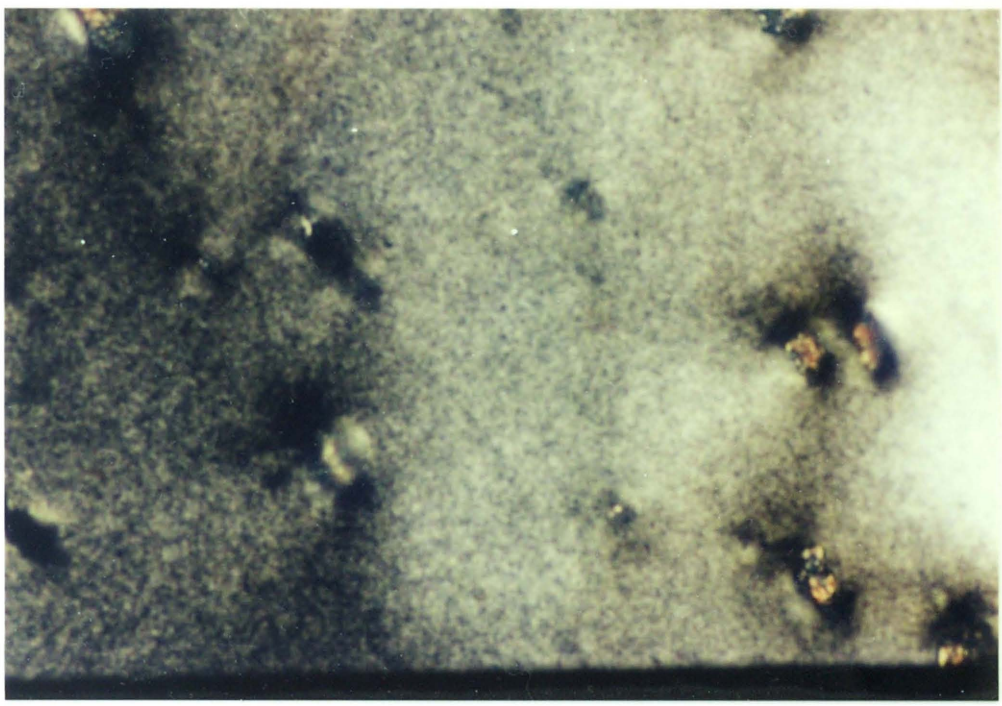

Picture 4.26 R-PET with 1.0% Na_2CO_3. Crystallization at 230 °C (x200)

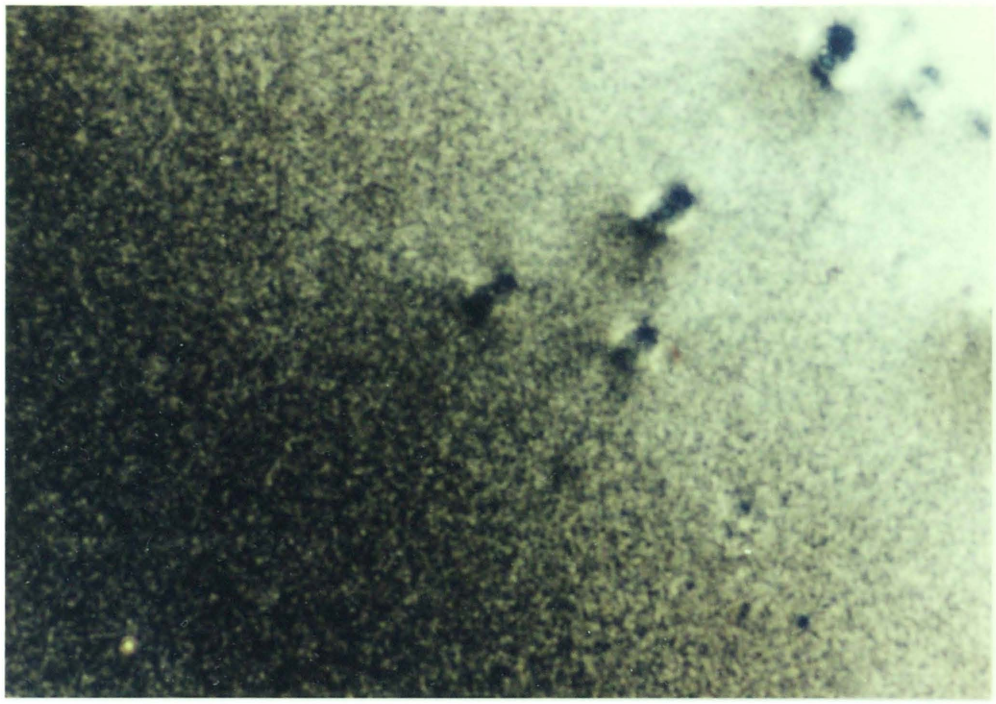

Picture 4.27 G-PET with 0.5% Na_2CO_3. Crystallization at 225 °C (x200)

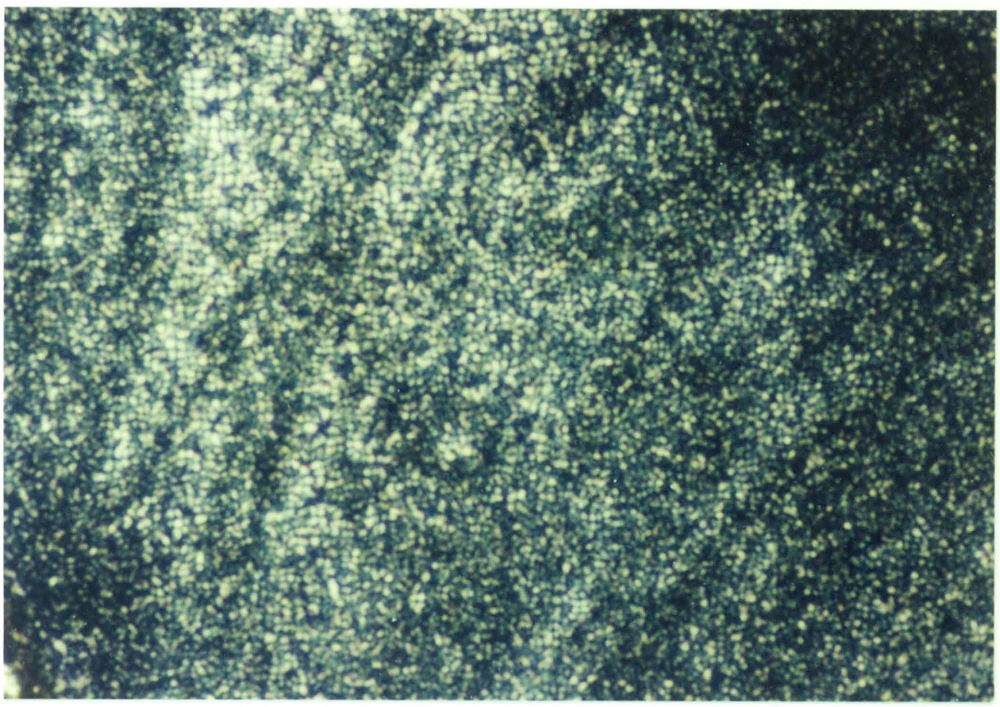

Picture 4.28 V-PET with 0.5% Na_2CO_3. Crystallization at 230 °C (x200)

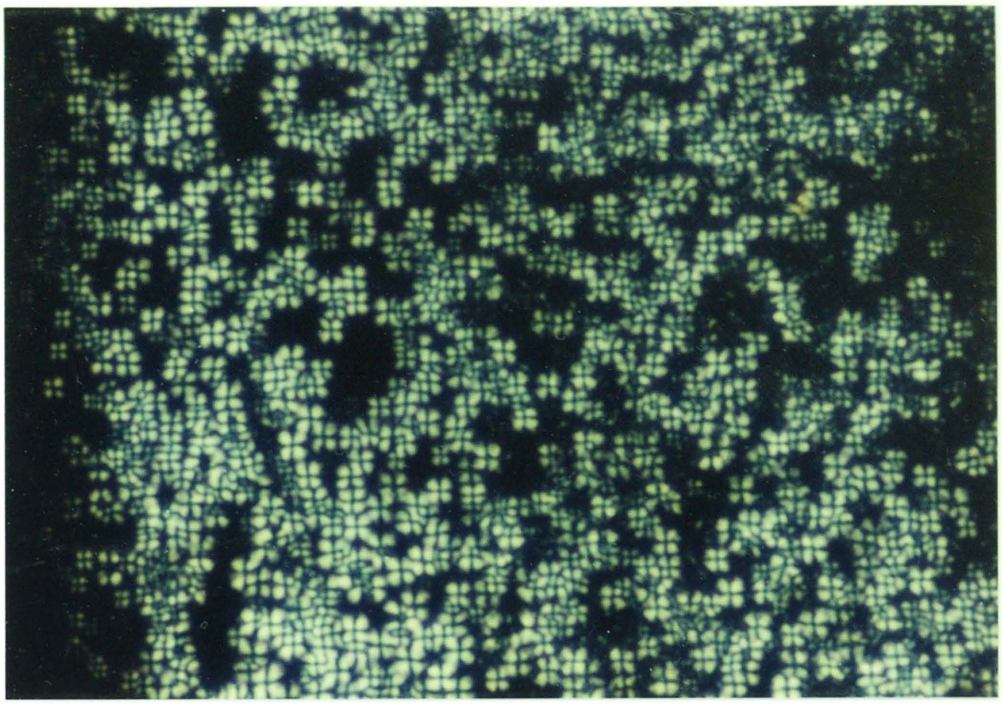

Picture 4.29 R-PET with 0.5% $CaCO_3$. Crystallization at 240 °C (x200)

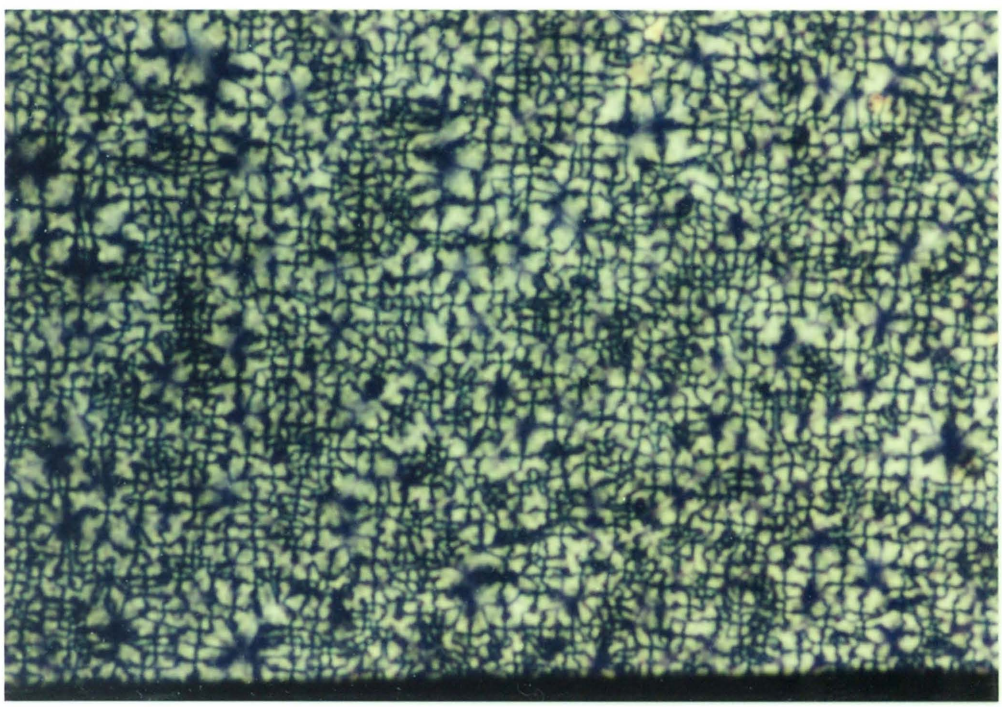

Picture 4.30 G-PET with 0.5% $CaCO_3$. Crystallization at 240 °C (x200)

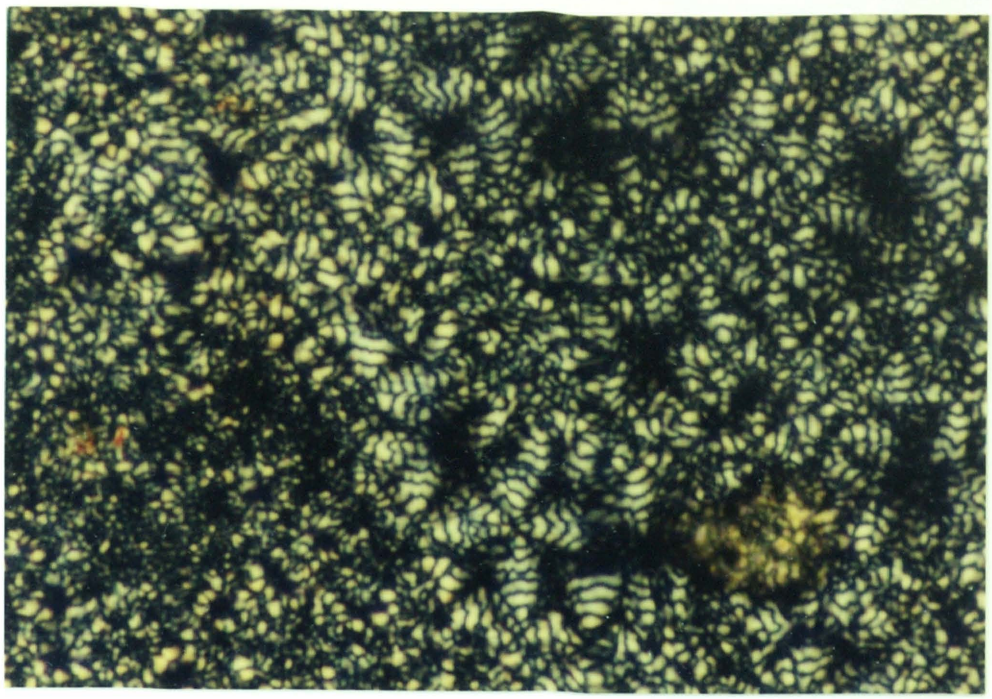

Picture 4.31 V-PET with 1.0% $CaCO_3$. Crystallization at 230 °C (x200)

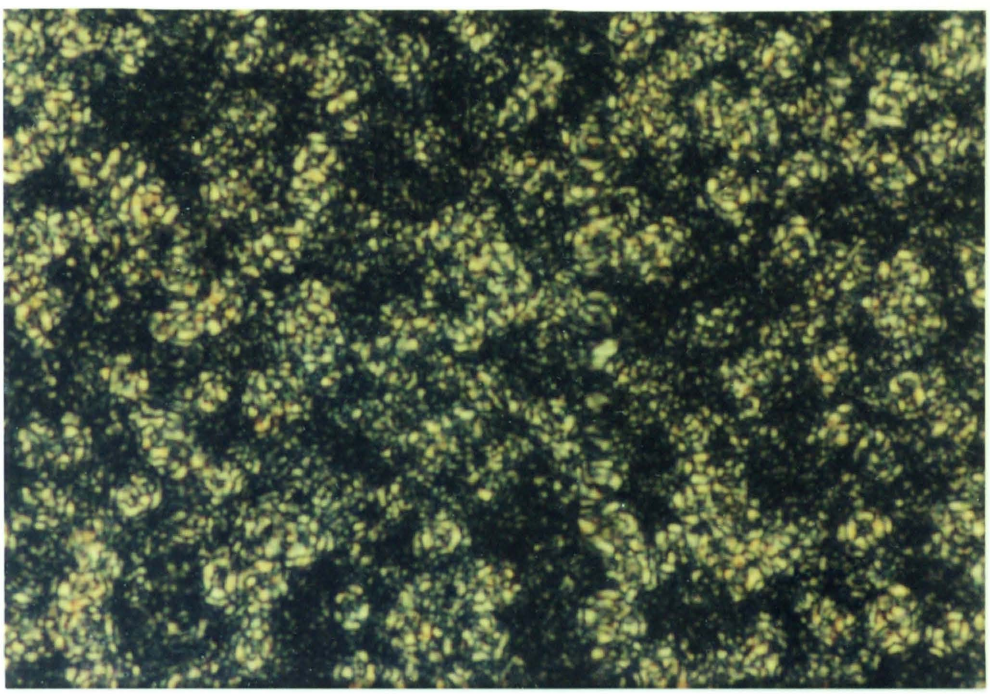

Picture 4.32 Spherulites of R-PET containing 0.5% $PbCO_3$, observed by optical microscopy between crossed polarizers (x200). Nonisothermal crystallization (slow cooling) from melt

Pictures 4.33 - 4.38

Scanning electron micrographs (SEM) of fractured surfaces from tensile fractured specimens of 90% LDPE-1/10% R-PET-1 blends at different barrel temperatures

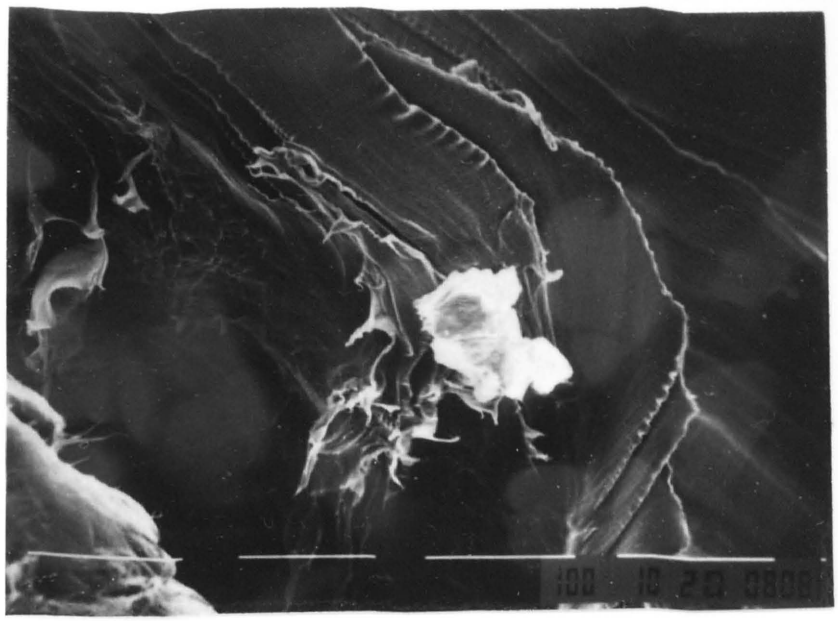

Picture 4.33 360 ^{O}F

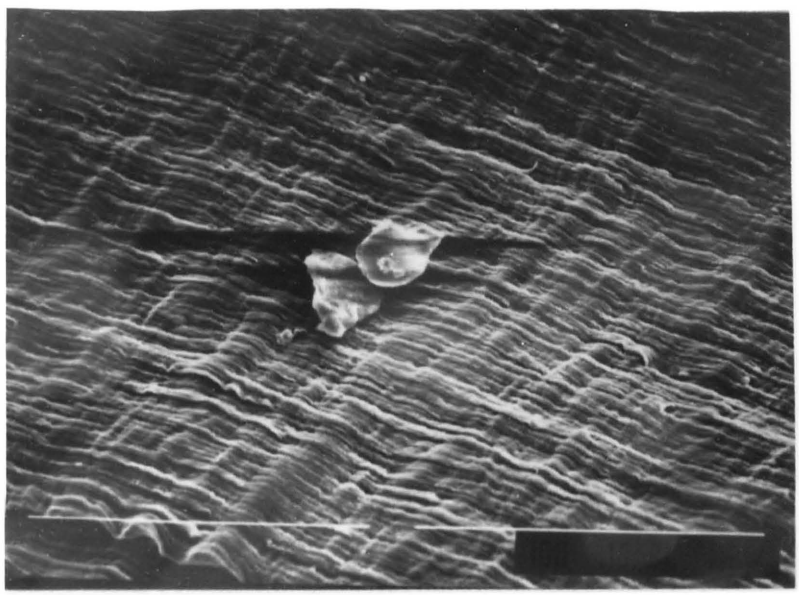

Picture 4.34 380 ^{O}F

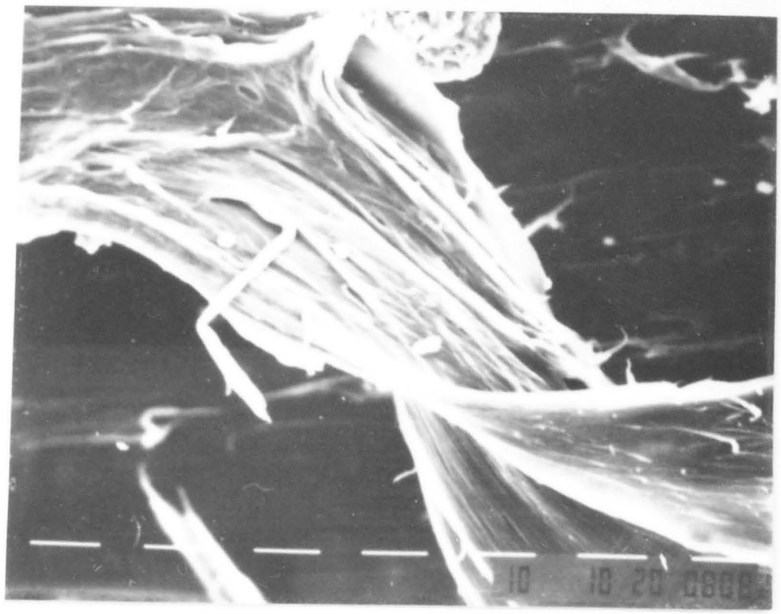

Picture 4.35 400 ^{O}F

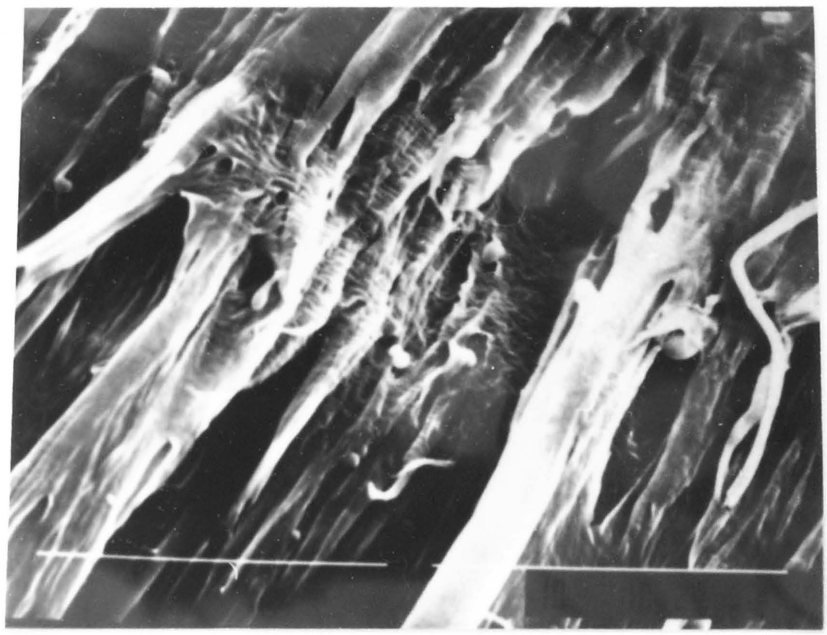

Picture 4.36 420 ^{O}F

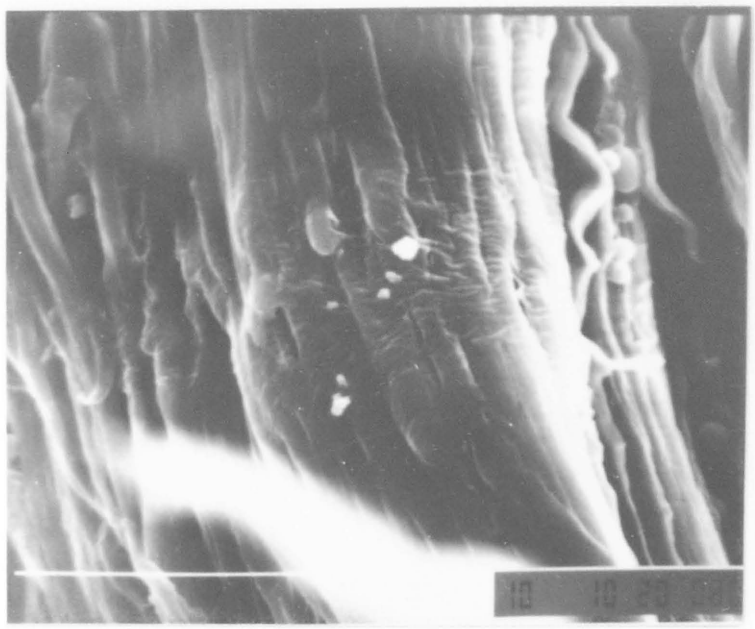

Picture 4.37 440 ^{O}F

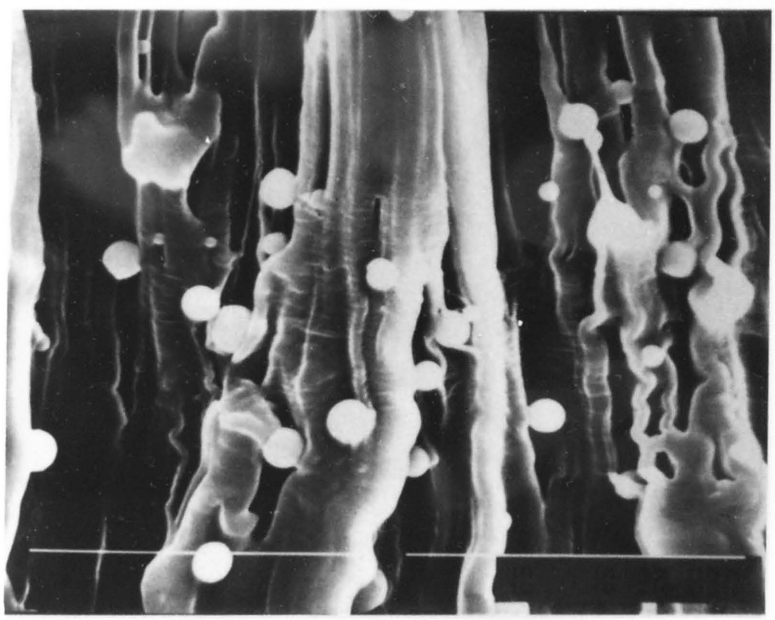

Picture 4.38 460 ^{O}F

Pictures 4.39 - 4.42

Scanning electron micrographs (SEM) of fractured surfaces from tensile fractured specimens of LDPE-1/R-PET-2 blends processed at 480 ^{O}F barrel temperature (injection molding).

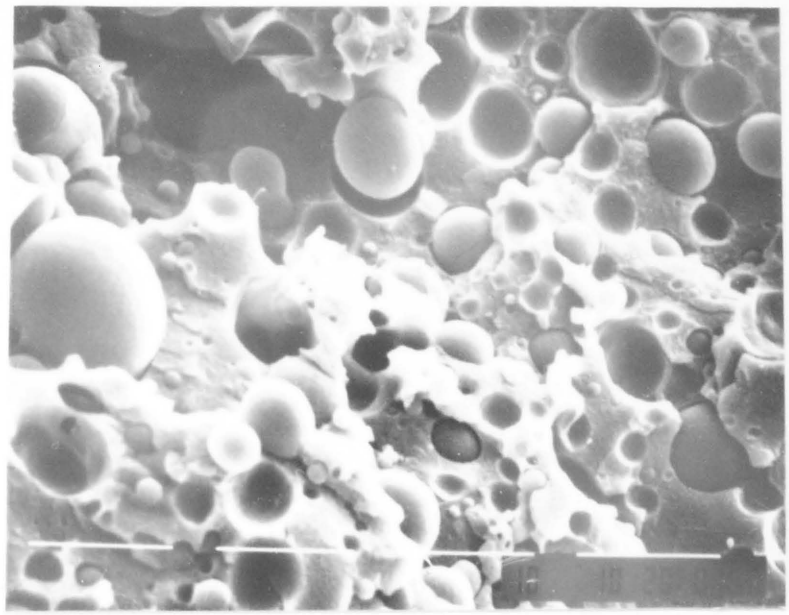

Picture 4.39 20% LDPE-1/80% R-PET-2 (core)

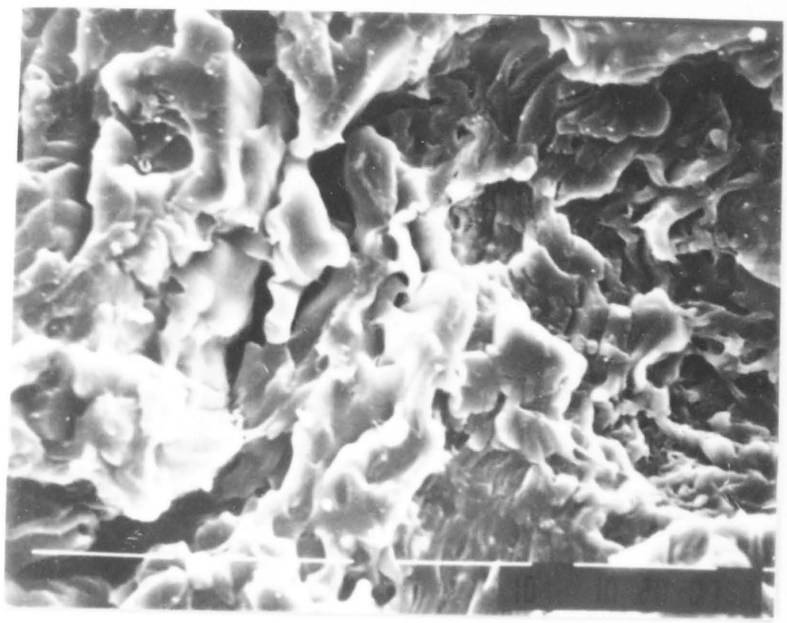

Picture 4.40 20% LDPE-1/80% R-PET-2 (edge)

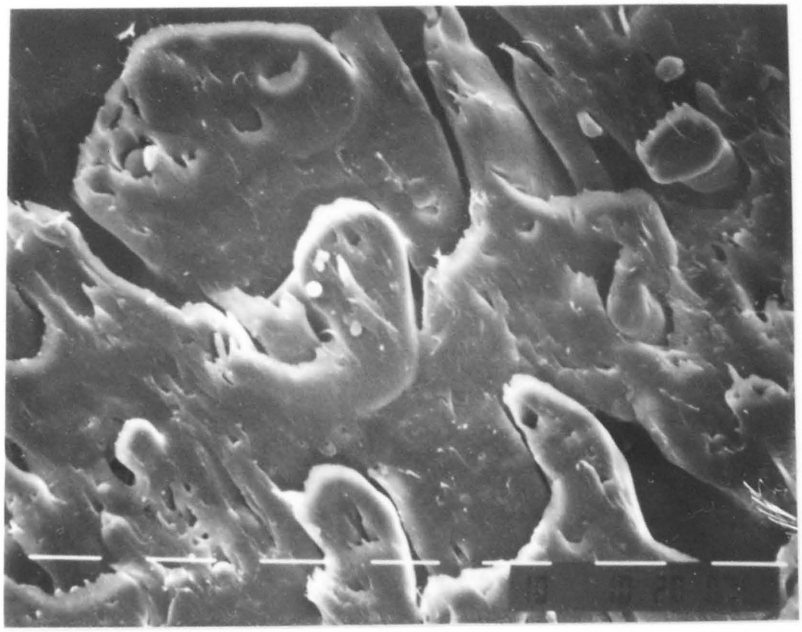

Picture 4.41 50% LDPE-1/50% R-PET-2

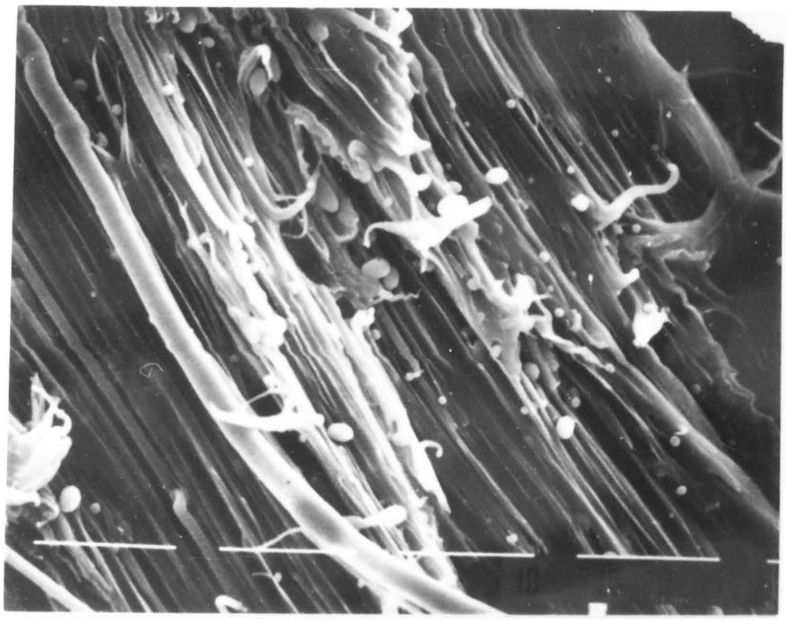

Picture 4.42 80% LDPE-1/20% R-PET-2

Pictures 4.43 - 4.45

Scanning electron micrographs (SEM) of fractured surfaces from tensile fractured specimens of LDPE/R-PET blends with AClyn ionomer A285.

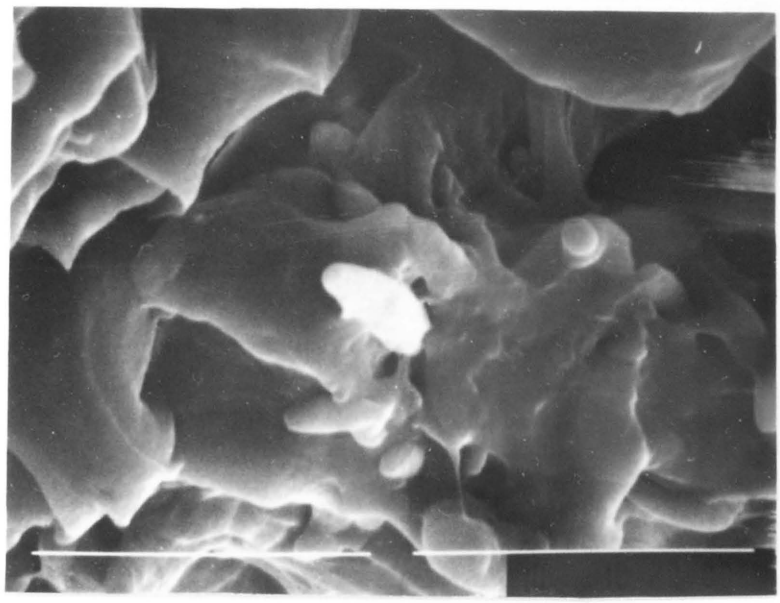

Picture 4.43 90% LDPE-2/10% R-PET-2 with 2% 285A

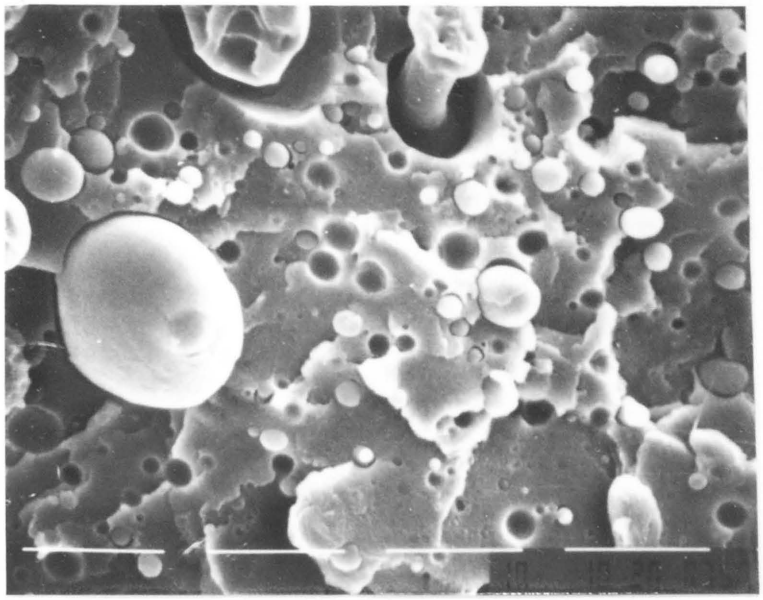

Picture 4.44 20% LDPE-1/80% R-PET-2 with 6% 285A

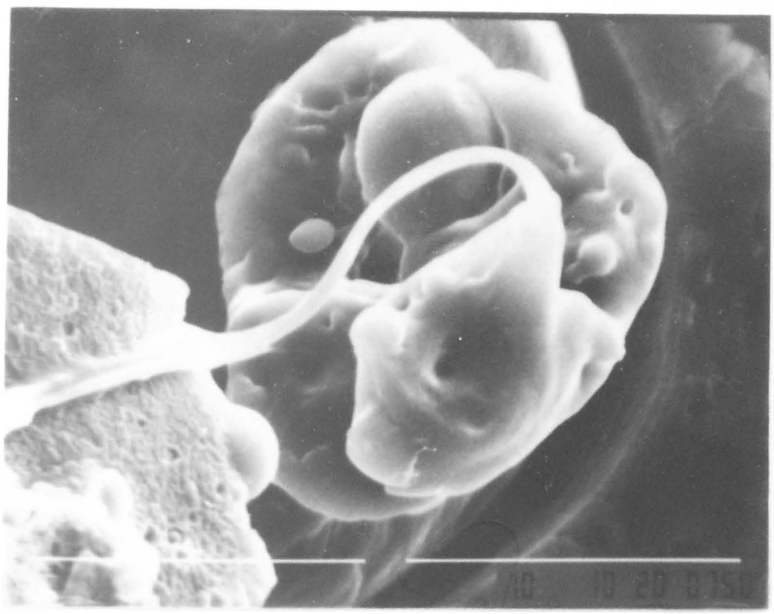

Picture 4.45 Magnification (detail) of a part of Picture 4.44

Pictures 4.46 - 4.48

Scanning electron micrographs (SEM) of fractured surfaces from tensile fractured specimens of LDPE/R-PET blends with Surlyn ionomer.

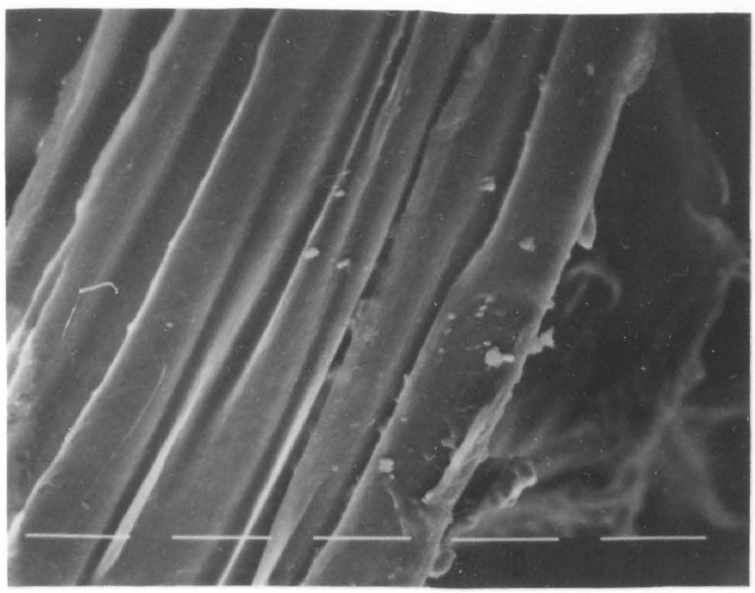

Picture 4.46 90% LDPE-2/10% R-PET-1 with 2% S8920

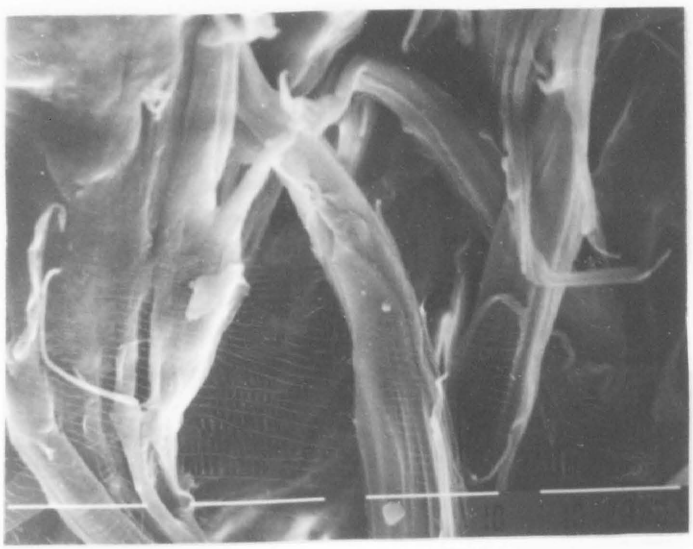

Picture 4.47 50% LDPE-2/50% R-PET-1 with 2% S8920

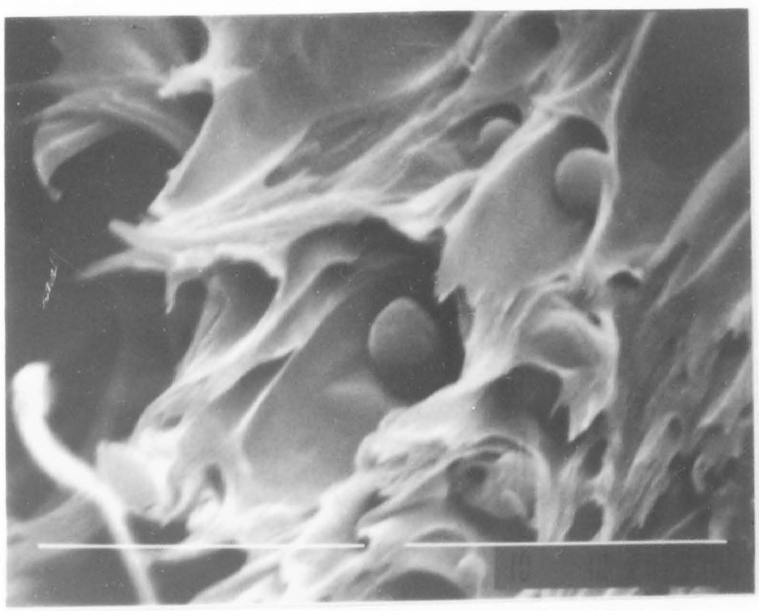

Picture 4.48 20% LDPE-1/80% R-PET-2 with 6% S8527